MRI METHODS FOR PREDICTING RESPONSE TO CARDIAC RESYNCHRONIZATION THERAPY

A Thesis
Presented to
The Academic Faculty

by

Jonathan D. Suever

In Partial Fulfillment
of the Requirements for the Degree
Doctor of Philosophy in the
Bioengineering Program and Department of Biomedical Engineering

Georgia Institute of Technology
December 2013

MRI METHODS FOR PREDICTING RESPONSE TO CARDIAC RESYNCHRONIZATION THERAPY

Approved by:

John N. Oshinski, Advisor
Department of Radiology and Imaging Sciences
Emory University School of Medicine

Ioannis Sechopoulos
Department of Radiology and Imaging Sciences
Emory University School of Medicine

Marijn E. Brummer
Departments of Pediatrics and Radiology
Emory University School of Medicine

Xiangyang Tang
Department of Radiology and Imaging Sciences
Emory University School of Medicine

Michael S. Lloyd
Department of Cardiac Electrophysiology
Emory University School of Medicine

Anthony J. Yezzi
Department of Electrical and Computer Engineering
Georgia Institute of Technology

Date Approved: July 12, 2013

ACKNOWLEDGEMENTS

Successful research can never be completed without the help of others and my thesis research was no exception. The work contained herein was made possible by the hard work and contributions of a multitude of individuals. Although there is no way to properly recognize everyone who helped along the way, there are a few individuals that require special thanks.

First and foremost I would like to thank my Ph.D. advisor, John Oshinski, for his unwavering support and patience. During the summer prior to my enrollment at Georgia Tech, I did a research rotation with John. I immediately appreciated his attention to detail, scientific rigor, and passion for clinical research. He provided me the unique opportunity of directly applying my very technical image processing knowledge to real clinical problems. Over the five years of my graduate career, John served as both an academic mentor and a personal role model. He demonstrated to me that one can successfully balance and excel at both their professional and personal lives.

I truly believe that the enjoyment you get from the work you do is as much a function of those who surround you as the actual work you're doing. I have sincerely enjoyed my time as a member of the Oshinski lab. We found a way to have a great time whether it was a "three-martini" lunch, pulling a marathon-like data mining session, or socializing on John's deck. Upon first joining the lab, Brandon and Jana helped me to find my niche and did a lot of the preliminary work on my project. Bill, Ian, Luke, Lizz, and Adrian were always willing to sacrifice time on their own projects to let me bounce ideas off of them and complain about the existence of the for loop. Throughout my grad career, I had the pleasure of mentoring a number of undergraduate students. I learned more from them than they ever did from me and their hard work was crucial to the completion of this research project.

Next I would like to thank my thesis committee for their support, availability, and valuable input throughout my entire graduate career. Specifically, I would like to thank

Dr. Lloyd for acquiring the majority of our clinical data and providing a great deal of insight into the electrophysiological aspects of our research. The expertise of Dr. Tang and Dr. Sechopoulus augmented our own lab's experience with MRI and enabled a lot of the multi-modal analysis. Drawing upon his years of experience with cardiac MR image analysis, Dr. Brummer was able to provide input regarding both the image processing and clinical application. Dr. Yezzi used his ability to meld theory and practice to help develop critical methodology that was used throughout this research.

In clinical research, the constant challenge is to successfully bridge the gap between the lab and the clinic. Thankfully, Emory has the infrastructure and personnel necessary to make this possible. This work relied on the medical and administrative expertise from many research nurses, clinical scientists, physicians, and MR technicians at both the main and Midtown campuses of Emory University Hospital.

Although the majority of the Ph.D. experience is spent in the lab, I learned a tremendous amount from my coursework, specifically those classes taught by Dr. Anthony Yezzi and Dr. Oskar Skrinjar. I left their classes every day excited by how what I'd learned that day could be applied to my own work. Anyone who thinks that math is boring has never had a teacher like these.

I had the pleasure of working closely with Prof. Franklin Bost as a teaching assistant for the Capstone Design course. I admire how he selflessly worked to convey his love of design to his students and teaching assistants. Thanks to my two semesters working with Franklin, I was able to develop a critical eye and an appreciation for detail.

I have received financial support through a National Institutes of Health Training Grant as well as a National Science Foundation Graduate Research Fellowship. Their support has allowed me to further my education, my research skills, and the field as a whole.

Of course in addition to all of my professional help, I couldn't have gotten to where I am today without my friends and family. I have had the pleasure of getting to know many bright and passionate people during my time in Atlanta. I look forward to seeing where life takes them all and hope our paths cross along the way.

TABLE OF CONTENTS

LIST OF TABLES

LIST OF FIGURES

LIST OF SYMBOLS OR ABBREVIATIONS

3D	Three-Dimensional.
6MWD	Six-Minute Walk Distance.
ABS	Acrylonitrile Butadiene Styrene.
ACE	Angiotensin-Converting Enzyme.
AHA	American Heart Association.
aLBBB	Atypical Left Bundle Branch Block.
AP	Anterior Posterior.
AV	Atrio-Ventricular.
CAD	Coronary Artery Disease.
CAU	Caudal.
CDC	Centers for Disease Control and Prevention.
CMR	Cardiovascular Magnetic Resonance.
CNR	Contrast to Noise Ratio.
CRA	Cranial.
CRT	Cardiac Resynchronization Therapy.
CS	Coronary Sinus.
CT	Computed Tomography.
CTA	Computed Tomography Angiogram.
CXR	Chest X-ray.
DCM	Dilated Cardiomyopathy.
DENSE	Displacement Encoding with Stimulated Echoes.
DICOM	Digital Image Communications in Medicine.
EAM	Electroanatomical Mapping.
EF	Ejection Fraction.
EGM	Electrogram.
EKG	Electrocardiogram.
EMD	Electro-mechanical Delay.

FDM	Fused Deposition Modeling.
FOV	Field of View.
Gd	Gadolinium.
HF	Heart Failure.
HLA	Horizontal Long Axis.
ICD	Implantable Cardioverter-Defibrillator.
IR	Inversion Recovery.
IRB	Institutional Review Board.
IVCD	Inter-ventricular Conduction Delay.
LAO	Left Anterior Oblique.
LBBB	Left Bundle Branch Block.
LGE	Late Gadolinium Enhancement.
LPEI	Left Ventricular Pre-Ejection Interval.
LV	Left Ventricle.
LVAD	Left Ventricular Assist Device.
LVEDV	Left Ventricular End Diastolic Volume.
LVEF	Left Ventricular Ejection Fraction.
LVESV	Left Ventricular End Systolic Volume.
MI	Myocardial Infarction.
MLHFQ	Minnesota Living With Heart Failure Questionnaire.
MR	Magnetic Resonance.
MRA	Magnetic Resonance Angiography.
MRCV	Magnetic Resonance Coronary Venogram.
MRI	Magnetic Resonance Imaging.
MTC	Magnetization Transfer Contrast.
NCC	Normalized Cross Correlation.
NYHA	New York Heart Association.
PCMR	Phase Contrast Magnetic Resonance.
PET	Positron Emission Tomography.

QoL	Quality of Life.
QT	Quality Threshold.
RAO	Right Anterior Oblique.
RBBB	Right Bundle Branch Block.
RDC	Radial Displacement Curve.
RF	Radio Frequency.
RMSE	Root Mean Squared Error.
RV	Right Ventricle.
SENC	Strain Encoding.
SLD	Septal-Lateral Delay.
SNR	Signal to Noise Ratio.
SPAMM	Spatial Modulation of Magnetization.
SPECT	Single-Photon Emission Computed Tomography.
SPWMD	Spetal-to-Posterior Wall Motion Delay.
SSFP	Steady State Free Precession.
STL	Stereo Lithography.
SV	Stroke Volume.
TDI	Tissue Doppler Imaging.
TE	Echo Time.
TI	Inversion Time.
TR	Repetition Time.
TSI	Tissue Synchronization Index.
TVM	Tissue Velocity Mapping.
VLA	Vertical Long Axis.

SUMMARY

Cardiac Resynchronization Therapy (CRT) is a treatment option for heart failure patients with ventricular dyssynchrony. CRT corrects for dyssynchrony by electrically stimulating the septal and lateral walls of the left ventricle (LV), forcing synchronous contraction and improving cardiac output. Current selection criteria for CRT rely upon the QRS duration, measured from a surface electrocardiogram (EKG), as a marker of electrical dyssynchrony. Unfortunately, 30-40% of patients undergoing CRT fail to benefit from the treatment. A multitude of studies have shown that presence of mechanical dyssynchrony in the LV is an important factor in determining if a patient will benefit from CRT. Furthermore, recent evidence suggests that patient response can be improved by placing the LV pacing lead in the most dyssynchronous or latest contracting segment. The overall goal of this project was to develop methods that allow for accurate assessment and display of regional mechanical dyssynchrony throughout the LV and at the site of the LV pacing lead. To accomplish this goal, we developed a method for quantifying regional dyssynchrony from standard short-axis cine magnetic resonance (MR) images. To assess the effects of LV lead placement, we developed a registration method that allows us to project the LV lead location from dual-plane fluoroscopy onto MR measurements of cardiac function. By applying these techniques in patients undergoing CRT, we were able to investigate the relationship between regional dyssynchrony, LV pacing lead location, and CRT response.

Specific Aim 1 demonstrated that it is possible to derive regional dyssynchrony information from standard cine MR images, which can then be mapped to the American Heart Association (AHA) 17-segment model to identify the latest contracting segment. We used these regional dyssynchrony maps to characterize normal and dyssynchronous contraction and determine the relationship between electrical and mechanical dyssynchrony.

In Specific Aim 2 we developed a technique to determine the location of the LV pacing lead relative to MR-based regional dyssynchrony measurements. By reconstructing the

coronary veins from a contrast-enhanced MR acquisition and registering them to dual-plane venograms and imaging of the lead location, we determined the spatial correspondence between the two modalities. By back-projecting the lead onto the MR data, we were able to determine the lead position in 3D and map it onto the AHA 17-segment model. We validated our methodology using a coronary vein phantom and found the accuracy of our lead localization to be superior to existing techniques.

Specific Aim 3 applied the regional dyssynchrony technique from Aim 1 and the LV lead localization method from Aim 2 in nine patients undergoing CRT. By following these patients for six months, we were able to determine the effect of pacing at or near the latest contracting segment on patient response to CRT. In this small patient group, we found that no mechanical dyssynchrony parameter was able to discriminate between patients who responded to CRT and those who did not.

In summary, we developed techniques that allow for more accurate assessment of regional dyssynchrony and LV lead location. Using these techniques, we can study a variety of factors and their effect on CRT response. With the successful identification of these factors, it may be possible to improve the current non-response rate in CRT patients.

CHAPTER I

BACKGROUND & INTRODUCTION

1.1 Heart Failure

Heart failure (HF) is the name given to a combination of symptoms that limit the ability of the heart to meet the metabolic needs of the body. As cardiac function decreases, blood pressure drops and the vital organs do not receive necessary nutrients. Consequently, Heart failure patients exhibit exercise intolerance, shortness of breath, and worsened prognosis [1]. By increasing blood pressure, heart rate, ventricular volumes, and arterial stiffness, the body is able to compensate for the failing heart. Although these compensatory mechanisms may initially improve the patient's condition, they can significantly impact the long-term prognosis of heart failure patients [1–3].

Statistics from the American Heart Association (AHA) and the Centers for Disease Control and Prevention (CDC) indicate that more than five million individuals in the United States are living with chronic heart failure [4]. Heart failure accounts for approximately 20% of all hospital admissions for patients over the age of 65 [5].

1.1.1 Ventricular Remodeling

Heart failure symptoms include changes to ventricular size and function due to both chemical and mechanical factors [5]. Remodeling occurs in response to myocardial infarction, cardiomyopathy, hypertension, or valvular heart disease [6, 7].

If a patient had a myocardial infarction (MI), where a major vessel supplying blood the myocardium is blocked; the downstream myocardium supplied by the blocked vessel undergoes necrosis and is replaced over time by fibrotic tissue in an attempt to heal the infarct [8]. The fibrous tissue has different mechanical and contractile properties than healthy myocardium, so an MI often leads to abnormal loading conditions throughout the ventricle resulting in dilatation and hypertrophy; increasing end diastolic volumes and limiting the ability of the heart to pump effectively [7, 9].

1.1.2 Effects of Ventricular Remodeling

As the left ventricle (LV) dilates, it not only increases in volume, but also becomes more spherical. Both of these morphological changes inhibit proper operation of the mitral valve. The diameter of the valve annulus increases in response to the dilatation but the size of the leaflets and their orientation relative to the papillary muscles remains unchanged [10, 11]. This mismatch can result in mitral valve regurgitation, characterized by the transfer of blood back into the left atrium during systole. Mitral regurgitation increases the load of the left ventricle and promotes additional remodeling [5].

Changes to the ventricular wall as a result of remodeling can also disrupt the electrical activation network within the heart. These disruptions can result in atrial fibrillation or irregular ventricular activation and contraction [5, 12]. Underlying electrical conduction issues manifest themselves as changes in the contraction timing of the heart, which decreases the ejection fraction (EF) and further diminishes the pumping efficiency of the heart [13–15].

1.2 Cardiac Dyssynchrony

Although heart failure can manifest itself in a variety of ways, cardiac dyssynchrony affects 30 to 50% of heart failure patients [13, 14, 16]. Dyssynchrony is indicative of a disruption in the conduction pathway of the heart caused by ischemia, inflammation, fibrosis, and aging [5]. These disruptions cause different parts of the heart to be activated at different times. Because mechanical contraction requires electrical activation, irregular electrical activation leads to discoordinate mechanical contraction of the heart. We refer to the differences in electrical activation as electrical dyssynchrony, and the associated difference in contraction times as mechanical dyssynchrony. Dyssynchronous contraction of the ventricle is much less efficient than a synchronous heart because blood is transferred within the ventricle rather than being ejected [17,18]. There is a direct relationship between dyssynchrony and ejection fraction [13–15]. This increases the energy demand on the heart and worsens the prognosis for heart failure patients with dyssynchrony.

1.2.1 Electrical Dyssynchrony

The normal conduction pattern of the ventricles of the heart begins at the atrio-ventricular (AV) node, and then travels through the bundle of His along either the right or left bundle branches. The right branch travels through the septum and finally connects to the Purkinje fibers, which can then stimulate the myocardium. In the left bundle, the electrical impulse travels to either the mid-LV septum, or the anterior and posterior fascicles where it connects to the Purkinje fibers and can then reach the myocardium [19]. In the LV, the stimulation of myocytes starts at the endocardium of the apex of the heart and travels to the epicardium. In a healthy individual, the time required for the both ventricles to be activated is between 50 and 80 ms [20].

1.2.1.1 Causes of Electrical Dyssynchrony

It is possible to have a disruption in the conduction pathway of the heart, called a block, which causes the propagation of the activation front to be altered or slowed. There are a variety of pathologies that can alter the conduction properties of the myocardium and affect the activation of the left ventricle.

In the case of an MI, the conductivity of the fibrotic region is impaired compared to healthy myocardium; effectively blocking electrical conduction. To compensate, the activation front has to circumvent the infarcted region. Another pathology that can drastically alter the electrical conduction system of the heart is dilated cardiomyopathy (DCM). DCM is typically associated with an AV conduction block resulting in delayed contraction of the ventricles relative to atria, thereby shortening the diastolic filling time which can have adverse effects on mitral regurgitation [19]. It was found that conduction velocities were decreased due to dysfunctional gap-junction communication caused by the phosphorylation of Cx43, a member of the connexin family [21,22]. This abnormality causes dyssynchronous electrical activation of the heart [23].

1.2.1.2 Bundle Branch Block

Regardless of the cause of the conduction block, the location of the block has the largest effect on the electrical activation pattern of the heart. Left bundle branch block (LBBB) is the most frequent electrical conduction abnormality amongst heart failure patients. LBBB worsens a patient's prognosis, and has been shown to be a strong predictor of sudden death [19,24]. In LBBB, the electrical activation front is unable to travel via the left bundle of His and therefore the impulse travels instead from myocyte to myocyte via cell-to-cell coupling. As a compensatory mechanism, the expression of connexins (Cx), primarily Cx43, is altered resulting in slower conduction velocities [23, 25, 26]. This slower conduction can result in large regional differences in electrical activation throughout the LV. Typically, LBBB results in early septal activation and late electrical activation of the basal postero-lateral wall [19,27]; however, recent multi-center studies have demonstrated that the site of the latest activated region is heterogeneous among heart failure patients [28].

Similar to LBBB, right bundle branch block (RBBB) is a disruption within the right bundle of His which can cause delayed activation of the basolateral portion of the right ventricle (RV). RBBB rarely has an impact on LV electrical activation patterns [19].

1.2.1.3 Measurement of Electrical Dyssynchrony

There are several methods available to detect and quantify electrical dyssynchrony. A physician can use a surface electrocardiogram (EKG) to diagnose a conduction block. The EKG measures the vector sum of the electrical stimulations throughout the entire heart [29]. The QRS complex of an EKG trace represents the electrical depolarization of the ventricles. In the case of a conduction block, the activation front is slowed; extending the time it takes for the entire ventricle to contract. On the EKG trace, this conduction block manifests itself as an elongation of the QRS complex. Several large studies have found that a QRS duration > 120 ms is associated with increased patient mortality even after accounting for other clinical factors [30,31]. In addition to the global EKG, the signal for each electrode in a 12-lead EKG can be examined to differentiate between LBBB, RBBB, and an interventricular conduction delay (IVCD) [32].

To obtain more focal information regarding electrical activation of the heart, it is necessary to employ more invasive techniques than a surface EKG. Electrodes can be placed on a catheter tip and inserted either into the cavities of the heart to make endocardial recordings. Similarly, a catheter can be placed in the coronaries to obtain epicardial measurements. These local recordings, electrograms (EGMs), are a measurement of the electrical potential of the myocytes at the location of the electrode tip [33]. The main limitation of this technique is the difficulty in localizing the measurement location and targeting the desired measurement site [34, 35]. Often, landmarks such as ribs and other vessels have to be used to register and guide the catheter [35]. It is possible to obtain multiple simultaneous recordings using either epicardial socks or endocardial balloons, although these techniques are much more invasive procedures than a single catheter [36, 37].

Three-dimensional electroanatomical mapping (EAM) systems have been developed to improve the localization of EGM measurements. In these systems, the catheter is fitted with a coil in addition to the EGM electrode. Three magnetic field generators are placed under the patient, and three different fields are generated at different positions. The catheter coil can detect the strength of each of the magnetic fields. The strength of the magnetic field at the coil is inversely proportional to the distance from the magnetic field generator to the coil. Because there are three magnetic field generators, triangulation can be used to determine the 3D position of the catheter tip and the EGM recording [35, 38]. The user can acquire measurements at many sites within the ventricle cavity to obtain a map of electrical activation [34]. Unfortunately, the trade-off is that EAM requires special hardware only available at specialty institutions.

1.2.2 Mechanical Dyssynchrony

Mechanical dyssynchrony is when regions of the heart contract at different times. There are several general types of mechanical dyssynchrony. Inter-ventricular dyssynchrony is a difference in contraction times between the left and right ventricles. Atrio-ventricular mechanical dyssynchrony is characterized by an abnormal delay between atrial and ventricular activation, which can result in a shortened diastolic filling period and a decreased stroke

volume. Of particular interest in heart failure patients is intra-ventricular dyssynchrony, the discoordinate mechanical contraction of different regions within the same ventricle [29].

1.2.2.1 Causes of Mechanical Dyssynchrony

As mentioned previously, a region that experiences delayed electrical activation should also experience delayed mechanical contraction, since myocytes require electrical activation to contract. All of the causes of electrical dyssynchrony, including DCM and a previous MI, also contribute to mechanical dyssynchrony.

It is possible to have mechanical dyssynchrony without underlying electrical dyssynchrony. The most common example of abnormal wall motion without electrical dysfunction is in the case of myocardial infarction [39, 40]. Infarcted tissue is, fibrous, non-conductive, and non-contractile because there are no myocytes in the infarcted region. Therefore, when the electrical activation arrives at the infarcted region (on time), the infarct does not contract. Instead, the regions proximal to the infarcted region contract normally and "pull" the infarcted region. Because the region is not actively contracting, abnormal motion may be observed despite the synchronous electrical activation [29].

1.2.2.2 Bundle Branch Block

As mentioned earlier, LBBB results in early septal and late lateral wall activation and subsequent contraction. In these patients, the blood is being transferred from the early contracting septum to the lateral wall and then transferred back to the septal wall when the lateral wall finally contracts. As a result of this "sloshing", mechanical dyssynchrony is often accompanied by a decrease in EF [19]. The systolic function of the heart is impaired because the delayed regions have to overcome the higher pressures inside the ventricle caused by the earlier-contracting regions. A decrease in EF means that the heart has to work even harder to meet the metabolic needs of the body [18, 41].

1.2.2.3 Measuring Mechanical Dyssynchrony

Clinically, ultrasound is the most common modality used to assess mechanical dyssynchrony of the heart.

1.2.2.3.1 M-mode Echocardiography M-mode echocardiography is a standard technique for visualizing wall motion in the heart. By imaging wall motion over the cardiac cycle, the contraction times of opposite segments of the heart can be determined and the delay between the regions can be computed. The most frequent use of M-mode imaging is to determine septal-to-posterior wall motion delay (SPWMD). A SPWMD greater than 130 ms is associated with intraventricular mechanical dyssynchrony [42, 43]. The primary limitation of SPWMD is that it only considers one location; therefore there is only data from two segments rather than segments throughout the LV. In patients with LBBB, the septal and lateral walls would be the most disparate and this is not detected in SPWMD.

1.2.2.3.2 Doppler Echocardiography Conventional Doppler echocardiography can be used to obtain Doppler flow velocity data from the ascending aorta. By comparing the onset of the QRS complex with the beginning of aortic flow, the left ventricular pre-ejection interval (LPEI) can be computed [44]. LPEI values exceeding 140 ms are typically associated with intraventricular dyssynchrony [44, 45]. This method is only useful for determining global dyssynchrony, as it cannot discern between the effects of different LV regions on the observed delay.

1.2.2.3.3 Tissue Doppler Imaging Instead of imaging the velocity of blood flow or wall motion, tissue Doppler imaging (TDI) is used to measure the velocity of the myocardium. By obtaining data from multiple views, it is possible to determine the velocity throughout much of the heart. Septal-to-lateral delay (SLD) can be computed by taking the difference in the time-to-peak systolic myocardial velocity profiles for the septal and lateral walls of the LV. In a similar fashion, the maximum delay between any two segments in the LV can be computed and is referred to as the maximum difference [46]. TDI can also be used to compute a more global measure of mechanical dyssynchrony. Tissue velocity curves from 12 different left ventricular segments can be acquired and the time between the QRS complex and the maximum myocardial velocity is determined for each segment. The standard deviation of these delays provides a measure of dyssynchrony, referred to as

the Yu index [47]. To improve the delay estimates between tissue velocity curves, more advanced analysis methods such as cross-correlation analysis have been employed to replace time-to-peak measurements [48]. The primary limitations of TDI dyssynchrony analysis are that the velocity measurements are sensitive to the incident angle of the ultrasound and only one location can be analyzed at a time. This is an issue if there are large beat-to-beat variations as there often are in heart failure patients with dyssynchrony [29].

1.2.2.3.4 Speckle Tracking Speckle tracking is a technique that can derive strain and strain rate data from echocardiographic images. Speckle tracking detects and follows the position of natural acoustic markers over the cardiac cycle. From the position of each marker relative to another, it is possible to derive both strain and strain rate values throughout the myocardium. The advantage of using strain data, is that it can distinguish between actively contracting myocardium and infarcted regions that are "pulled" by the healthy surrounding myocardium [29]. Unfortunately, the frame rate of speckle tracking is only 60 frames per second compared to 180 for TDI [49]. There is some initial work on expanding speckle tracking to three dimensions to be able to derive all three principal strain directions simultaneously [50].

1.2.2.3.5 Single-Photon Emission Computed Tomography Utilizing an EKG-gated single-photon emission computed tomography (SPECT) acquisition, it is possible to estimate myocardial wall thickness based upon the number of counts from a particular region of the LV [51]. Through phase-analysis of myocardial thickening, the delay of each region can be determined and regional dyssynchrony can be assessed [52].

1.2.3 Relationship of Electrical and Mechanical Dyssynchrony

The exact relationship between electrical and mechanical dyssynchrony is not well understood. In canine models, it has been shown that a small electrical delay between two regions can have a much more pronounced mechanical delay [53, 54]. The accentuated mechanical delay is thought to be due to the fact that in order to see mechanical contraction of a portion of the ventricle, it must first overcome the pressure within the ventricle. As such, the later

the electrical activation in a region, the higher the pressure in the ventricle and therefore the longer the delay between electrical and mechanical activation, the electromechanical delay (EMD). Additionally, there have been instances where there is no underlying electrical dyssynchrony, but there is a delay in mechanical contraction [39, 40]. The distinction between electrical and mechanical dyssynchrony is important when developing techniques for correcting dyssynchrony. Some treatment options aim to correct electrical dyssynchrony while others focus on mechanical dyssynchrony.

1.3 Treatment Options for Heart Failure

Heart failure can result from a wide range of pathologies, therefore a variety of treatment options are available to improve patient quality of life.

Due to low cost and ease of administration, pharmacological treatments are the ideal therapeutic approach to mitigate compensatory remodeling. Angiotensin-converting-enzyme (ACE) inhibitors are traditionally prescribed as a treatment for high blood pressure; however, ACE inhibitors have also been shown to improve survival in heart failure patients by lowering patient heart rate [2, 55, 56]. In the failing heart, epinephrine and norepinephrine increase the heart rate to compensate for impaired cardiac function [3]. β-blockers inhibit the binding to β adreno-receptors and therefore prevent the excessive stimulation of the myocardium, slowing patient heart rate [2]. In addition to treating the symptoms of heart failure, it is possible to prescribe treatments that treat the underlying causes of heart failure. Specifically, treating hypertension and hyperlipidemia has been shown to be effective at preventing the onset of heart failure symptoms [57]. Overall, these pharmacological treatments improve exercise tolerance and patient survival; however it may not be sufficient for patients with advanced heart failure [2, 55, 56, 58].

In cases of severe heart failure, left ventricular assist devices (LVADs) can be implanted to pump blood more efficiently to the rest of the body. Although this is typically a short-term treatment option for heart failure patients awaiting a heart transplant, continuous flow devices have been used recently for long-term cardiac support [59–62].

In heart failure patients with arrhythmias or other conduction abnormalities, an implantable cardioverter-defibrillator (ICD) can be implanted. The purpose of the ICD is to provide a strong electrical stimulation to terminate the arrhythmias. It has been shown that ICD implantation decreases mortality in heart failure populations, specifically patients with LBBB [24, 63–65].

Cardiac resynchronization therapy (CRT) is a treatment option for heart failure patients with cardiac dyssynchrony. Approximately 30% of heart failure patients suffer from dyssynchrony, which is associated with a decrease in ejection fraction and worsened prognosis [13–16]. As discussed earlier, electrical dyssynchrony typically results from a conduction block that causes a delay between the activation of different sections of the ventricle. CRT utilizes a biventricular pacemaker to electrically stimulate the myocardium in an effort to restore synchronous electrical activation and improve cardiac output.

Advanced heart failure patients that fail to respond to either pharmacological or device-based therapies are referred for a heart transplant. Unfortunately the cost and the need for a donor do not make transplantation readily accessible [59, 64, 66].

1.4 Cardiac Resynchronization Therapy

Cardiac resynchronization therapy utilizes a biventricular pacemaker to resynchronize left ventricular contraction in heart failure patients with dyssynchrony. CRT utilizes three leads: an atrial sensing lead and two pacing leads; one in the RV and one in the LV. The CRT device senses the arrival of the electrical excitation in the right atrium with the atrial lead, and after a pre-programmed AV delay, initiates ventricular contraction. The RV pacing lead is placed into the apex of the RV cavity and serves to stimulate the apex of the RV as well as the interventricular septum. The LV pacing lead is implanted into the coronary veins in order to stimulate the epicardial surface of the free wall of the left ventricular. Normal electrical activation is restored by simultaneously stimulating the septal and free wall of the LV.

Due to the overlap between patients with cardiac dyssynchrony, LBBB, and a higher risk of sudden cardiac death, most CRT devices also serve as an ICD (CRT-D) [19, 24]. In

this configuration, the atrial sensing lead is used to detect the onset of atrial fibrillation or ventricular tachycardia and the RV pacing lead is used to supply the ICD electrical pulse.

Currently, there are four major criteria that must be met for a patient to qualify for CRT implantation [67]:

- **QRS Duration > 120 ms**

  QRS duration is a measure of the electrical dyssynchrony of the heart. Without electrical dyssynchrony, the simultaneous stimulation of the septal and lateral walls of the LV will have no effect.

- **Ejection Fraction < 35%**

  A healthy ejection fraction is greater than 50%. A low EF is indicative of inefficient cardiac function.

- **NYHA HF Functional Class III-IV**

  The New York Heart Association (NYHA) functional classification serves to determine the effect that heart failure has on patient activity and comfort (Table 1.1). Patients classified as Class III-IV are considered to have moderate to severe heart failure.

- **Optimal Medical Therapy for at least 3 Months**

  Before resorting to an implantable device, it is necessary to ensure that the patient cannot benefit from guided pharmacological treatments.

Several large, randomized, and controlled trials have been conducted and demonstrate the efficacy, safety and long-term beneficial effects of CRT. Compared to patients receiving optimal pharmacologic therapy, patients undergoing CRT showed significant improvements in exercise tolerance, quality of life, and overall cardiac function [68–70]. Additionally, CRT reduces left ventricular end-systolic volume (LVESV) and increases LV ejection fraction, indicating reverse remodeling [69, 71–79].

1.4.1 Response to Cardiac Resynchronization Therapy

Response is a commonly used term that refers to the improvement in a patient's condition following cardiac resynchronization therapy. There are a vast number of ways to classify a

Table 1.1: Description of New York Heart Association Functional Classes

NYHA Class	Functional Capacity
I	The patient has cardiac disease but there are no limitations on physical activity. Ordinary physical activity does not cause fatigue, palpitation, dyspnea or angina pain
II	The patient is slightly limited with respect to physical activity. They are comfortable at rest; however, ordinary physical activity results in fatigue, palpitation, dyspnea or angina pain.
III	Patients suffer from significant limitation of physical activity. Although the patient is comfortable at rest, less than ordinary activity causes fatigue, palpitation, dyspnea or angina pain
IV	Patients cannot carry on any physical activity without discomfort. Symptoms of heart failure may be present even at rest. Discomfort increases with any physical activity.

Classification of severity of heart failure based upon the effect of heart failure symptoms on patients' lives and physical activity [67].

patient's response. Currently, there are 17 widely used definitions of response to CRT [80]. The major two categories of response criteria are clinical response and quantitative response. In this study, we will utilize clinical response criteria for two reasons. First, the reduction of symptoms and improvement in quality of life (QoL) of the patient is a more direct benefit to the patient than a change in a functional parameter that may have little or no impact on patient ability or comfort. Second, quantitative response criteria require a six-month follow-up echocardiogram, whereas clinical metrics only require simple tests and questionnaires. In an effort to maximize the number of patients included in this work, we will not utilize quantitative response criteria, as they were not available for all patients.

1.4.1.1 Clinical Response Criteria

Clinical response criteria focus on detecting improvement of symptoms in heart failure patients. Below are the most commonly used clinical response criteria. Often several criteria are used in combination to define CRT response [80].

- **New York Heart Association Functional Classification**

  The New York Heart Association (NYHA) functional classification attempts to assess

how diagnosed heart failure affects an individual's physical ability (Table 1.1). Based upon NYHA classification, a responder to CRT is a patient who improves by at least one heart failure class six months after device implantation [80]. NYHA classification is performed by the physician at both the time of implantation and the six month follow-up time point using the standard guidelines [67].

- **Minnesota Living with Heart Failure Questionnaire**

  The Minnesota Living with Heart Failure Questionnaire (MLHFQ) attempts to assess the quality of life of the patient. The questionnaire consists of 21 questions covering a wide range of daily activities to determine the effect of heart failure symptoms on the patient's daily routine. All questions are answered on a scale of 0 to 5 where larger scores indicate a larger negative effect [81]. CRT response is typically considered to be a decrease of at least 15 points compared to the baseline survey [82].

- **Six-minute Hall Walk Distance**

  Similar to the NYHA functional class, the six-minute walk distance (6MWD) is a measure of how heart failure affects an individual's susceptibility to fatigue due to physical activity [83]. The metric measures the distance that can be travelled by the patient in a six-minute interval. CRT response, as determined by 6MWD, is marked by an increase of between 10 and 25% [46, 84].

1.4.1.2 Quantitative Response Criteria

In addition to clinical criteria, there are a variety of quantitative measures that have been used in the literature to classify patients as responders or non-responders to CRT. Quantitative measures typically identify signs of reverse remodeling including improved cardiac output and decreased cardiac volumes. A brief list is provided in Table 1.2 [80]:

Although both MRI and echocardiography can be used to measure these response metrics, it is not possible to perform a post-implant MRI due to artifacts caused by the CRT device as well as interference with the CRT. Therefore, it is necessary to use a follow-up echocardiogram to obtain these values.

Table 1.2: Quantitative CRT Response Criteria

Metric	Response Cutoff
LV Ejection Fraction (LVEF)	Increased by at least 5% (absolute) or 15%
LV End Systolic Volume (LVESV)	Decreased by at least 10% - 15%
LV End Diastolic Volume (LVEDV)	Decreased by 15% or more
Stroke Volume (SV)	Increased by at least 15%

Quantitative values and the associated values that are used to determine whether a patient responded to cardiac resynchronization therapy.

1.4.2 Non-Response to Cardiac Resynchronization Therapy

There have been a large number of randomized clinical trials that demonstrate the efficacy of CRT; however, at least 30% of patients undergoing CRT do not benefit from the treatment [68–70, 85]. The ability to identify candidates who will respond positively to CRT is critically needed to prevent the unnecessary expenditure of approximately $60,000 for a device that is not improving their condition [66, 86].

1.4.3 Factors Influencing Response to Cardiac Resynchronization Therapy

The current selection criteria are not comprehensive as evidenced by the $> 30\%$ non-response rate. There must be additional factors that contribute to an individual's response to CRT. It is thought that the presence of mechanical dyssynchrony, the amount and location of myocardial scar, and coronary vein anatomy all play a role in a patient's response to CRT [87].

1.4.3.1 Presence and Location of Mechanical Dyssynchrony

CRT aims to improve cardiac output by correcting intraventricular dyssynchrony through the electrical stimulation of the myocardial muscle, forcing the ventricle to contraction synchronously [88, 89]. If there were no electrical or mechanical dyssynchrony present, then pacing the ventricle synchronously would not improve cardiac function. Studies that incorporated mechanical dyssynchrony into CRT patient selection demonstrated superior sensitivities and specificities [46, 90–92]; however, specificity ranged from 33% to 96% [46, 47, 82, 92]. This indicates that a single factor is unlikely to predict a patient's response to CRT.

1.4.3.2 Myocardial Scar Burden and Location

A number of studies have shown that the overall size and location of myocardial scar tissue plays a role in patient response to CRT [40,93–99]. The fibrous tissue composing the infarct is much less conductive than inter-myocyte gap junctions [100]. If the LV pacing lead were to be inserted into a scarred region of the myocardium, the applied electrical stimulus will not stimulate myocardial contraction, and resynchronization is unlikely to occur. Additionally, because of the lack of contractility in scar tissue, if there is too much scar present within the LV, then the ability of the heart to pump is inhibited.

1.4.3.3 Left Ventricular Lead Placement and Coronary Vein Anatomy

The left ventricular pacing lead is positioned within the coronary veins and makes contact with the epicardial surface of the lateral wall of the left ventricle. It is generally accepted in the electrophysiology community that optimal response can be obtained by targeting the lateral, posterolateral, or anterolateral cardiac vein [101]. An acceptable target vein is visualized and identified using contrast-enhanced coronary venograms obtained at the beginning of the procedure. If necessary, coronary venoplasty or stenting can used to access the target site [102, 103]. The target vessel must be small enough to allow the LV pacing lead to be wedged into place for stability [104]. The lead must also avoid stimulation of the phrenic nerve, which has branches that run along the lateral wall of the LV. If nerve stimulation occurs, then another branch of the coronary sinus must be used [105]. Final lead placement and pacemaker delay settings are then optimized based on an intra-procedural echo exam [106].

In addition to the currently employed factors we have just discussed, the ideal LV pacing site is thought to be located in the most dyssynchronous region [16]. Placement of the LV lead in a region remote to the most dyssynchronous region was indicative of non-response in as many as 21% of patients [107]. However, currently no information regarding the location of myocardial infarction or dyssynchronous regions is taken into account prior to lead placement. In order to properly target this area, the distribution of dyssynchrony within the LV must be known before the implantation procedure. Due to the fact that the

LV pacing lead is placed in the coronary sinus, access to the most dyssynchronous region with the LV pacing lead is constrained by the coronary vein anatomy [85, 108, 109]. By determining both the ideal pacing site as well as the coronary vein anatomy, it would be possible to determine a patient's suitability for CRT prior to implantation.

1.4.4 MRI Assessment of Factors Influencing Response to CRT

Magnetic resonance imaging (MRI) can be used to assess all of these factors within a single pre-implantation session. MRI can assess mechanical dyssynchrony, determine the presence and distribution of myocardial scar tissue, and discern the coronary vein anatomy, making MRI a potentially powerful tool for CRT patient selection.

1.4.4.1 MRI Assessment of Mechanical Dyssynchrony

The identification and quantification of mechanical dyssynchrony is important in a variety of pathologies including dilated cardiomyopathy, tetralogy of Fallot, and CRT. For this reason, a number of techniques have been developed to assess mechanical dyssynchrony using MRI. Unlike echocardiographic imaging techniques, MRI is not limited by the echocardiographic windows of the torso, and is therefore able to acquire images throughout the entire myocardium, thus dyssynchrony can be detected at *any* location in the heart. Several MRI-based techniques have been employed to detect mechanical dyssynchrony including myocardial tagging, phase contrast tissue velocity mapping (TVM), displacement imaging, and cine wall motion assessment.

The most basic way to assess mechanical dyssynchrony using MRI is to utilize steady state free precession (SSFP) cine imaging. One of the primary benefits of cine wall motion analysis techniques is that SSFP cines are part of a standard cardiac MRI exam. Because of routine use, cine SSFP sequences have been optimized to show myocardial motion at both high temporal and spatial resolution. As a result, many groups have attempted to devise methods to quantify the mechanical dyssynchrony that is easily identified upon visual assessment. These methods utilize myocardial wall motion, wall thickening, and three-dimensional deformation in an attempt to quantify mechanical dyssynchrony [110–113]. All of these methods either provide a global measure of dyssynchrony or make assumptions

about the contraction [114, 115]. To determine the most dyssynchronous region in CRT patients, it is necessary to have a method that both provides regional dyssynchrony information and works in moderate to severe heart failure patients with impaired LV function and abnormal LV contraction.

In myocardial tagging, spatial modulation of magnetization (SPAMM) is used to create a grid of non-invasive markers (or tags) on the tissues within the imaging plane [116]. These tags persist throughout a cine acquisition of the slice. By studying the deformation of these tags over the cardiac cycle, it is possible to derive displacement and strain information within the myocardium. Unfortunately, due to the low spatial frequency of the tags, there are usually only 1-2 tags through the thickness of the myocardium, resulting in coarse spatial resolution of the derived strain values. Additionally, the analysis has to be performed in the frequency domain and is often difficult and requires specialized software [117].

Tissue velocity mapping is another approach to quantify dyssynchrony with MRI. This approach is very similar to TDI analysis in echocardiography. Phase-contrast MRI (PCMR) utilizes paired bipolar gradients to estimate the velocity of a pixel. Tissue that moves along the direction of the encoding gradient receives a phase shift proportional to its velocity. By performing PCMR in a short-axis image, the velocity of the myocardium can be determined in a given direction. Using two acquisitions, the x and y components of the velocity can be used to construct the magnitude of the in-plane velocity over the cardiac cycle. Furthermore, tissue velocity can be encoded in all three dimensions to track circumferential, longitudinal, and radial motion of the myocardium. The velocity at two different locations can be compared to determine the temporal lag between the two regions [118, 119]. Unlike myocardial tagging, the spatial resolution of TVM is limited by the pixel dimensions of the acquisition. Unfortunately, acquisition times for complete TVM datasets are long due to the need for reference and velocity-encoded images as well as the requirement to use both respiratory and cardiac gated acquisitions.

Displacement of the myocardium can be measured directly using a technique called displacement encoding with stimulated echoes (DENSE) [120]. With DENSE, the goal is to encode positional information into the phase of the pixels in the image. The spatial

resolution of DENSE is only limited to the dimensions of a pixel unlike tagging which is dependent upon tag density. The disadvantage to utilizing DENSE is that the sequence is still in the research stage and is only available at a small number of research institutions. As a result, it cannot be employed in large multi-center dyssynchrony studies.

The goal of our work is to develop a method to detect dyssynchrony that is regional, high-resolution, simple, amenable to heart failure patients, and utilizes standard cardiac MR images. For this reason, we want to perform wall motion analysis on short-axis cine SSFP images.

1.4.4.2 MRI Assessment of Scar Burden and Location

Late Gadolinium Enhancement (LGE) imaging is an off-label use of an extracellular Gadolinium (Gd) chelate-based contrast agent for the imaging of myocardial infarction [121]. The contrast agent is injected intravenously as a bolus (0.1 mmol/kg) and diffuses into the interstitial space. In healthy myocardium, there is little intercellular space (a low extracellular volume fraction) and the extracellular contrast agent cannot pass through the cell membranes of the myocytes. In a chronic myocardial infarction, the effective extracellular volume fraction is much larger and more contrast can diffuse into the region [122]. Approximately 10 minutes after contrast injection, an inversion recovery (IR) sequence is used to acquire an image of myocardial infarction. An inversion time (TI) is selected to effectively null the signal from the myocardium. The T1-shortening characteristics of gadolinium cause the signal from the infarcted region to be much greater than that of the nulled myocardium [123]. Due to the bright blood pool (also full of Gd), it is easy to segment the endocardial and epicardial boundaries, as well as visualize the location of the myocardial infarction. In this way, scar transmurality can be assessed throughout the ventricle by performing a series of LGE scans. Many groups have successfully performed LGE imaging in patients scheduled for CRT [98, 99, 124].

1.4.4.3 MRI Assessment of Coronary Vein Imaging

Magnetic resonance angiography (MRA) has focused on imaging the coronary arteries; however, MR imaging technology has reached a point where visualization of the coronary veins

has become feasible. A number of studies have employed both contrast and non-contrast techniques to successfully visualize the coronary venous anatomy prior to CRT device implantation [125]. Using either a magnetization transfer contrast (MTC) preparatory pulse in combination with a 3D gradient echo sequence or a slow infusion of a Gd-chelate-based contrast agent plus a 3D whole heart sequence, good image contrast can be achieved between the coronary veins and the surrounding myocardial tissue [126–130]. It has been shown, however, that contrast-based methods provide better signal-to-noise (SNR) and contrast-to-noise (CNR) than non-contrast techniques [128]. In cases where the patient is already being administered a Gd-based contrast agent, it is beneficial to obtain a contrast-enhanced coronary vein scan.

Extracellular contrast agents quickly diffuse into the extracellular space shortly after injection, thereby limiting the time during which they are effective for vessel enhancement [131]. Additionally, the contrast diffuses into the myocardium, enhancing both the myocardium and the coronaries, effectively decreasing the contrast between the two. It is possible to use an intravascular contrast agent to improve the contrast of the coronary veins. Some intravascular contrast agents bind to albumin in the blood, and therefore do not diffuse out of the vessel before it is filtered out of the blood [132–134]. For this reason, the concentration in the blood remains elevated relative to the myocardium for significantly longer than extravascular contrast agents [135]. Unfortunately, this class of contrast agent is not optimal for LGE imaging because LGE relies upon the differential diffusion of Gd into the infarcted and normal myocardium. If both LGE and coronary vein imaging are to be performed in the same scan, this type of contrast agent is not feasible.

Instead of using an intravascular contrast agent, it is possible to achieve extended periods of elevated Gd contrast using a slow infusion of contrast agent [125, 136, 137]. This slow infusion replenishes any contrast that may have diffused from the blood into the surrounding tissue. Eventually this will create a steady state of contrast agent concentration, yielding a constant concentration of Gd in the vasculature. As long as contrast is being injected, this level will remain relatively constant. Coronary vein imaging can be performed during this contrast "plateau" to achieve maximal contrast between the coronary veins and the

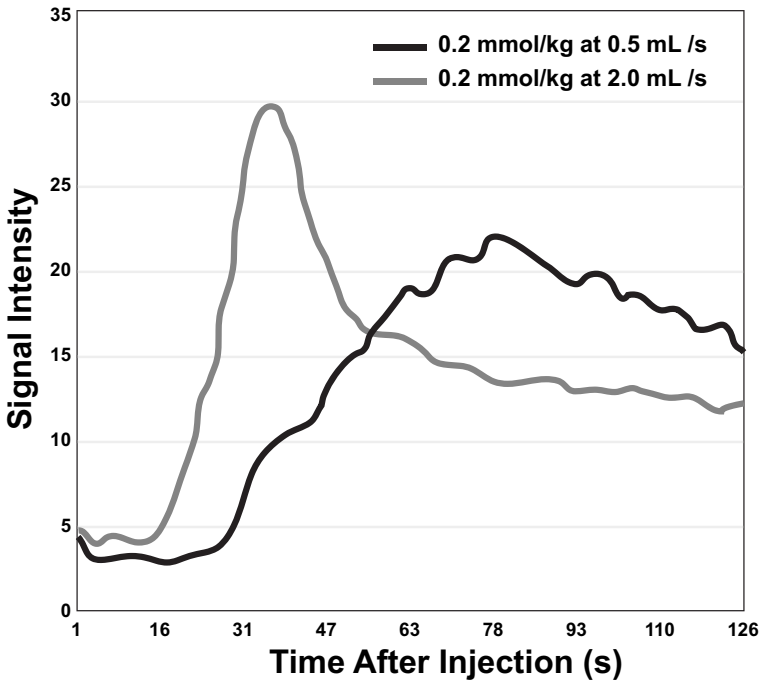

Figure 1.1: Data for the signal intensity of the vasculature following injection of extracellular Gd-chelate contrast agent. Note the lower initial intensity but longer and higher intensity plateau resulting from slow infusion of contrast agent [138].

surrounding tissue The total concentration in the blood is lower than if a standard bolus were to be used, but with a bolus, the concentration of Gd in the blood falls off quickly as the contrast agent diffuses into the tissue (Figure 1.1).

1.4.4.4 Inability of Magnetic Resonance Imaging to Assess LV Lead Placement

Ideally, we would like to be able to determine the final location of the left ventricular pacing lead and its position relative to dyssynchronous and infarcted regions. With the development of MRI-compatible pacemakers, ICDs, and CRT devices, it is possible to perform a post-implant MRI; however there are many required precautions. First, the device is often disabled to prevent errant pacing rates as well as inadvertent ICD activation, and as a result, an electrophysiologist or cardiologist must be present during the imaging procedure [139, 140]. Additionally, the deposition of energy by the radiofrequency (RF) pulses can warm the lead tip and potentially cause harm to the surrounding tissue, especially when imaging at the location of the lead tip [141, 142]. Although it may be technically possible to obtain LV lead location from a post-implant MRI, it would require an additional MR

procedure as well as specialized personnel and extra precautions. It is ideal to use existing imaging data to discern LV lead position relative to pre-implant MR-derived assessment of myocardial scar and mechanical dyssynchrony.

The LV pacing lead is readily visible in x-ray imaging, which is part of the standard CRT device implantation procedure. For this reason, it would be ideal to use intra-procedural fluoroscopic imaging to localize the position of the LV lead relative to pre-implant MR-derived parameters. It would prevent the need for extra imaging procedures and allow the data to be obtained at any institution without extra precautions and specialized training.

1.5 X-ray Fluoroscopic Imaging

CRT device and transcatheter lead implantation are performed under fluoroscopic guidance. Intra-procedural contrast-enhanced coronary venograms are acquired to survey the coronary vein anatomy and identify the target for the LV pacing lead. Similarly, post-implant x-ray images can clearly show the location of both the RV and LV pacing leads. It would be ideal to be able to use intra-procedural x-ray imaging to determine the LV pacing lead location relative to regional dyssynchrony information derived from MRI.

1.5.1 X-ray System Geometry

The most basic x-ray system consists of two components: an x-ray source and a detector. The source can focus x-rays at the detector in a variety of shapes including a fan, cone, or parallel beams [143]. A more flexible system is required to guide catheter-based interventions, such as CRT device implantation.

The typical electrophysiological procedure room contains a C-arm x-ray fluoroscopy system. The source and detector are mounted at opposite ends of a C-shaped track facing each other. The C-arm can be rotated about its center (Figure 1.2B), or translate along its own path (Figure 1.2A). The projections utilized in this work include the following:

- **Right Anterior Oblique**

  Right anterior oblique (RAO) images involve positioning the detector over the patient's right chest and directed toward the source located behind the patient's left

back (Figure 1.2A). The primary angle of the source is 30° off-vertical. The secondary angle is near zero.

- **Left Anterior Oblique**

  Left anterior oblique (LAO) images are the opposite; detector over the patient's left chest and the source behind the patient's right back. The primary angle is once again 30°.

- **Anterior-Posterior**

  An anterior-posterior (AP) image is acquired by setting all angles to zero and projecting x-rays from the patient's back to their chest.

When we refer to dual-plane imaging, we are referring to imaging an object using both RAO and LAO projections. A true biplane x-ray system has two detectors, capable of obtaining both views simultaneously.

1.5.2 Retrograde Coronary Venography

Visualization of the coronary sinus and its tributaries is necessary to identify the target vein for implantation of the LV pacing lead. A balloon catheter is inserted into the ostium of the coronary sinus and inflated to completely occlude the coronary sinus. An iodinated contrast agent is injected retrograde into the coronary veins, opacifying all potential target veins. By acquiring cine images at 30° LAO and 30° RAO during contrast injection, it is possible to use the venogram as a reference for positioning the LV lead [105]. It is important to note that the contrast is only present in the coronary veins, thus it is not possible to simultaneously visualize either the coronary arteries or the cardiac chambers.

1.5.3 Left Ventricular Lead Localization

To compare the position of the LV pacing lead to parameters derived from other modalities, such as MRI, it is necessary to discern the position of the LV pacing lead relative to the left ventricle. After successful implantation of the atrial sensing lead, and RV and LV pacing leads, dual-plane radiographs can be acquired to visualize the final position of the leads.

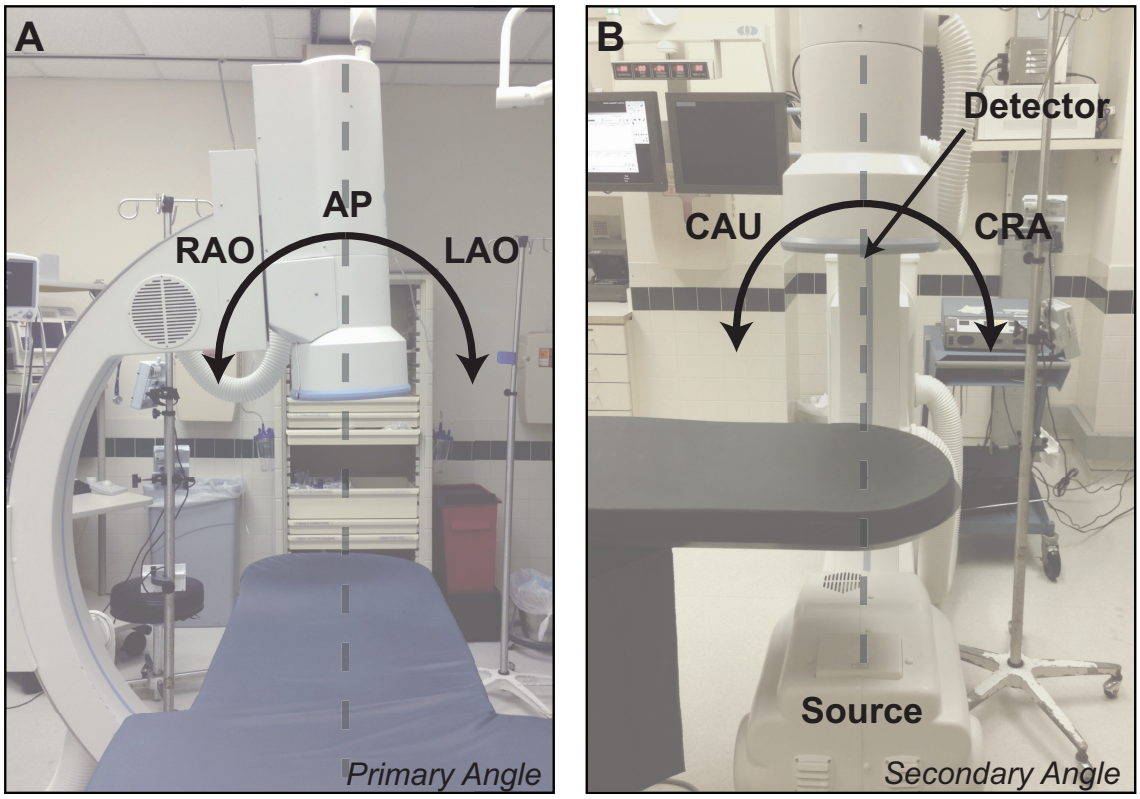

Figure 1.2: A c-arm fluoroscopy imaging system is capable of acquiring projections from a variety of angles. By rotating along the c-arm, right anterior oblique (RAO), left anterior oblique (LAO), and anterior posterior (AP) projections can be obtained (A). Rotating about the center of the c-arm, it is possible to obtain cranial (CRA) and caudal (CAU) projections (B). Any combination of these two angles can be used to obtain a double oblique image. Note that the c-arm can be positioned at the head of the table as opposed to the patient's side shown here.

There are several methods that are frequently used to determine the position of the pacing lead relative to the LV from fluoroscopic images.

1.5.3.1 Mortensen's o'clock

Mortensen's o'clock refers to a commonly used technique that determines LV pacing lead location from dual-plane lead position angiograms. Using 30° LAO and 30° RAO views, one can estimate the circumferential and longitudinal position of the LV pacing lead. The LAO image roughly corresponds to a short-axis view of the LV, and therefore can be used to identify the circumferential position of the lead (Figure 1.3 A and C). The longitudinal information can be obtained from the RAO image, which is similar to a long axis view of the ventricle (Figure 1.3 B and D) [144].

The advantages of Mortensen's o'clock method are its simplicity as well as the utilization of images acquired during the standard CRT device implantation procedure. However, the primary drawback is that it is incapable of accounting for a wide range of ventricle orientations seen in the general population, and specifically seen in heart failure patients. The position of the LV can vary from vertical to almost horizontal in the chest cavity depending on patient size and weight [145]. In these instances, the LAO and RAO no longer correspond to the short and long-axis views of the LV and it is difficult to accurately determine the LV pacing lead location using Mortensen's o'clock.

1.5.3.2 Chest X-ray

Another post-implantation method to determine lead placement is from routine posteroanterior and lateral chest x-ray (CXR). In this method, two planar x-ray scans are performed. The first is posteroanterior (i.e. front to back). This provides information regarding the lead position in the vertical axis of the heart and can be used to determine the longitudinal position of the lead. The source and detector and are then rotated to obtain a lateral CXR which can be used to determine whether the lead is on the anterior or posterior wall of the LV [145].

The disadvantage of CXR for lead localization is that it provides information about the lead position only in two dimensions, specifically the horizontal and vertical axis of the heart.

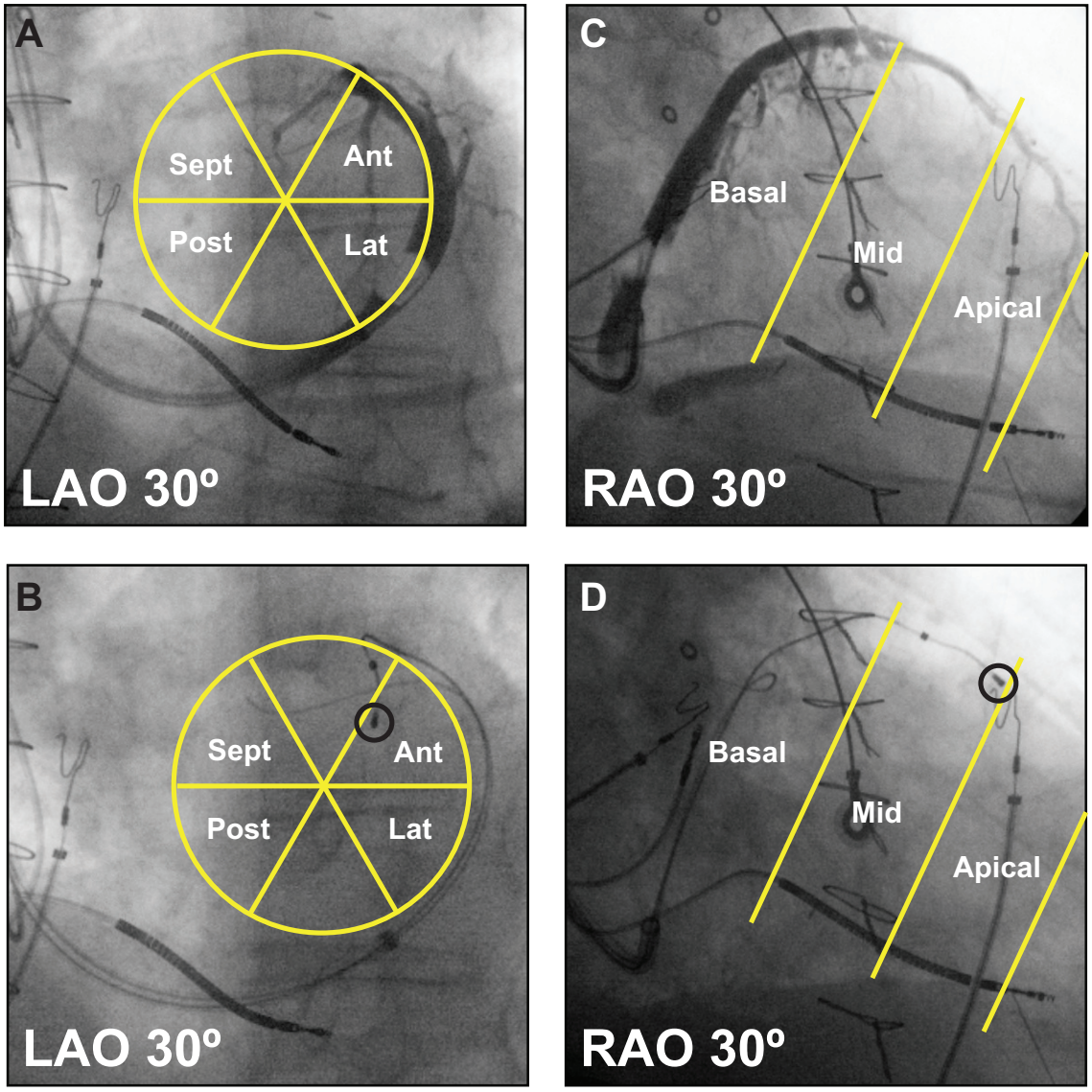

Figure 1.3: In Mortensen's o'clock LV lead localization method, the circumferential position is determined from the LAO coronary venogram (A) and lead localizer (B) and the longitudinal position is derived from the RAO coronary venogram (C) and lead localizer (D). LV pacing lead locations are marked with black circles in B and D.

There is no information available in the septal to lateral direction. Additionally, Kumar et al., found that CXR resulted in 73.4% misclassification of LV lead tip position [146].

1.5.3.3 Computed Tomography

Computed Tomography (CT) is an excellent method for determining final LV lead location. By combining the innate ability of x-ray-based imaging modalities to visualize metal components based on their high attenuation, with the ability of CT to obtain a three-dimensional volume, it is possible to determine the exact position of the LV pacing lead relative to the coronary veins and the cardiac chambers. Additionally, CT is able to accurately depict the LV lead location regardless of the orientation of the heart within the chest cavity.

Although the use of CT lead localization would provide ideal results, it requires additional imaging procedures, resulting in a radiation dose to the patient and increased cost of the procedure. For this reason, it is desirable to have a lead localizing technique that relies upon images typically acquired during the implantation procedure and provides accurate results in a wide range of patients.

1.5.3.4 Limitations of Current Techniques

Mortensen's o'clock and chest radiographs are the most widely applied techniques for determining lead location due to the reliance upon routinely acquired images. They do, however, sacrifice true three-dimensional localization of the LV pacing lead because of their simplicity. Often, they can only characterize the position of the LV lead in terms of anterior, lateral, posterior, and inferior. Although CT can provide a high-resolution and accurate location of the pacing lead, the additional radiation, money, and time required for the scan results in limited applicability. Our goal is to develop a method that combines pre-implant MRI data with dual-plane x-ray imaging to determine the true location of the LV pacing lead in three dimensions. The benefit is that it will provide a 3D location (similar to that of CT) without any additional imaging or radiation exposure.

1.6 Predicting Response to Cardiac Resynchronization Therapy

As we have discussed, non-response to CRT is a multi-factorial problem. To better understand how mechanical dyssynchrony, myocardial infarction, and coronary vein anatomy affect patient response to CRT, we need to retrospectively assess each of these factors at the location of the LV pacing lead in both responders and non-responders. After determining the significance of each of these factors, it is possible to provide a protocol for screening patients for CRT and provide pre-operative guidance for LV lead placement. To this end, it is important to display all regional dyssynchrony, myocardial infarction, and coronary vein anatomical information in a format that is both familiar and functional for physicians.

1.6.1 American Heart Association 17-Segment Model

The AHA has developed a segmented model of the LV for improving communication between imaging modalities for research and clinical purposes. The segment model is applicable for MRI, CT, positron emission tomography (PET), coronary angiography, and echocardiography [147]. The AHA segment modal is a polar plot where data from each slice is represented as a concentric ring with apical slices located at the center of the plot while the most-basal slice is on the outside (Figure 1.4).

1.6.2 Mapping Regional Dyssynchrony Data to the AHA 17-Segment Model

As part of our work, we aim to measure the dyssynchrony present at various points within the LV. This data is derived from short-axis cine SSFP images to not only allow for finer resolution analysis of wall motion, but to allow for easy adaptation to the AHA 17-segment model. Regional delay times are computed at 100 locations circumferentially for each slice. As such, it is possible to map these delay times directly to the AHA 17-segment model to create a mechanical activation delay visualization.

1.6.3 Mapping Coronary Vein Anatomy to the AHA 17-Segment Model

In this work, we determine the anatomy of the coronary sinus and its tributaries using MRI. By segmenting the coronary veins in each image, we can utilize the position information stored in the DICOM header to compute the 3D location of the coronary veins

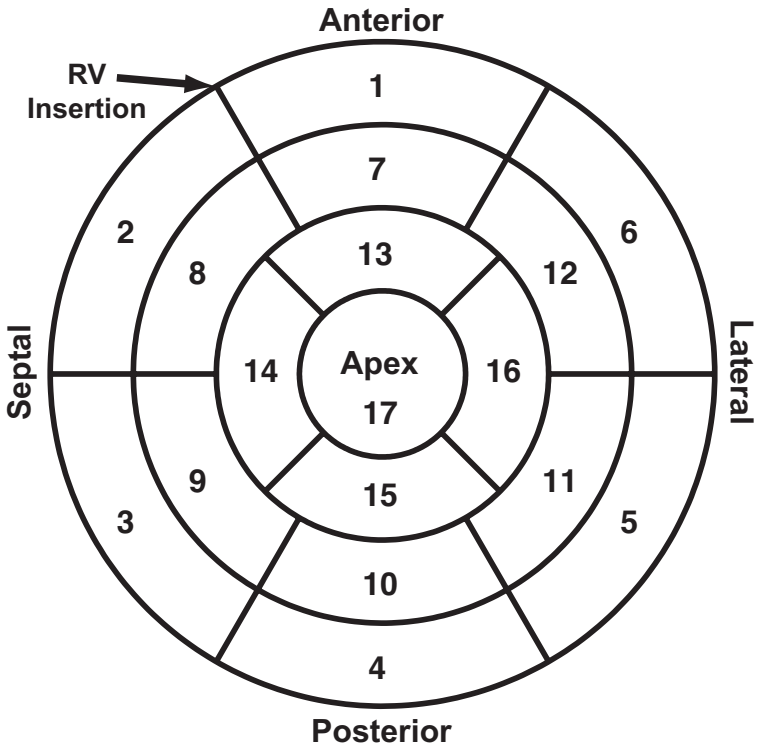

Figure 1.4: The AHA 17-segment model of the left ventricle displays circumferential slice information in concentric circles starting at the apex in the middle and reaching the base on the outside.

(Appendix C). After the 3D location of all vein points are computed, they can be projected onto the AHA 17-segment model (Appendix A). By superimposing this information with maps of regional dyssynchrony, it is not only possible to determine the latest contracting region (the ideal pacing site), but determine if this site is even accessible via the coronary veins.

1.6.4 Mapping LV Lead Location to the AHA 17-Segment Model

Ultimately, we want to determine the role that mechanical dyssynchrony plays in predicting response to CRT. To do so, we need to superimpose the final LV pacing lead location onto the regional dyssynchrony data. We will use dual-plane x-ray images to obtain the position of the LV pacing lead in 3D space. We can then map this 3D lead location onto the AHA model (Appendix A) to determine the mechanical activation delay times at and around the LV pacing site. It is then possible to study the relationship between regional dyssynchrony and CRT response.

1.7 Summary

By synergizing maps of regional dyssynchrony, coronary vein anatomy, and final LV lead location; we can determine the effect that regional mechanical dyssynchrony has on a patient's response to CRT. Additionally, by providing a standard way to visualize regional delay distributions, myocardium viability, and coronary vein anatomy, we are able to provide a prospective tool for assessing the suitability of a patient for cardiac resynchronization therapy, and determining the ideal pacing site prior to device implantation.

CHAPTER II

HYPOTHESIS & SPECIFIC AIMS

2.1 Central Hypothesis

We hypothesize that magnetic resonance imaging can be used to detect and display regional dyssynchrony in the left ventricle and this data can be combined with left ventricular lead positions, obtained from dual-plane x-ray imaging, to study the effect of lead placement on cardiac resynchronization therapy response.

2.2 Approach

Using magnetic resonance imaging, we obtained short-axis cine images of the left ventricle. We utilized the endocardial boundary in these images to compute the radial displacement of sections of the ventricle over the cardiac cycle. By comparing the delay between these regions, we were able to determine the relative mechanical contraction times throughout the left ventricle and characterize dyssynchronous contraction. These mechanical delay times were compared to local electrograms to study the unclear relationship between electrical and mechanical dyssynchrony. In order to understand the effect of pacing in the latest-contracting segment of the ventricle on patient response to cardiac resynchronization therapy, we used post-implant dual-plane x-ray data to determine the position of the left ventricular pacing lead. By combining the lead position with regional dyssynchrony information, it was possible for us investigate the relationship between dyssynchrony at the lead tip and cardiac resynchronization therapy response. To achieve these goals, we investigated the following specific aims:

2.3 Aim 1: Quantifying Regional Left Ventricular Mechanical Dyssynchrony

Develop a method to quantify regional left ventricular mechanical dyssynchrony and compare regional mechanical delay times with electrical delay times at various points within the left

ventricle.

We proposed that we would develop a method for quantifying and displaying regional dyssynchrony. This data must be able to be mapped to the AHA 17-segment model, a standard method for displaying data over the left ventricle, to allow for comparison with other metrics such as myocardial scar distributions for multi-factorial assessment of potential response to CRT.

Our goal was to generate a high-resolution map of regional dyssynchrony that can be used to identify regions of latest contraction that can be targeted as lead placement sites that would maximize the likelihood of patient response to CRT. We compared these late contracting regions with the latest activated regions (electrically) to understand the relationship between electrical and mechanical dyssynchrony. This work was broken into two sub-aims:

2.3.1 Aim 1a: Regional Dyssynchrony from Short Axis Magnetic Resonance Images

Generate a regional map of left ventricular mechanical dyssynchrony and identify the regions of delayed mechanical activation.

In order to locate the most dyssynchronous region of the LV, a high-resolution measure of regional dyssynchrony is needed. Additionally, it is desirable to obtain dyssynchrony maps using magnetic resonance imaging so that all pre-implant imaging is performed using a single modality. This method must also be able to be applied easily at a wide range of medical facilities to assist in the creation of multi-center studies researching the effects of dyssynchrony on CRT response.

There are many techniques for detecting LV dyssynchrony but they involve either complicated post-processing or MR protocols that are only available at pioneering research institutions. Short-axis steady state free precession (SSFP) images are a standard part of any cardiac MRI (CMR) examination. Additionally, due to their widespread use, SSFP images have been optimized to be high temporal and spatial resolution. By using these images, we determined the timing of mechanical activation throughout the left ventricle based upon cross correlation analysis of radial displacements of the endocardial surface.

The specific hypothesis was: Magnetic resonance cine images can be used to derive regional displacement curves to determine the mechanical activation delay at any point within the left ventricle.

To fulfill this aim, we computed radial displacements of the endocardial wall over the cardiac cycle. Using these radial displacement curves (RDCs), we clustered them into regions with similar contraction patterns. By averaging the largest of these clusters, we obtained a patient-specific reference RDC to which all other RDCs could be compared. Cross-correlation was used to determine the delay between any RDC and the reference. These delay times were then mapped directly to the AHA 17-segment model of the LV.

2.3.2 Aim 1b: Comparing Mechanical and Electrical Delay Times in the LV

Investigate the relationship between mechanical activation delay from our magnetic resonance imaging-based method and electrical activation delays from local electrogram data.

The current clinical eligibility criteria for CRT include a QRS duration that exceeds 120 ms. This elongated QRS duration is indicative of prolonged electrical activation in the LV resulting from electrical dyssynchrony. Several studies have shown that placing the LV pacing lead in the latest-activated region improves patient response to CRT. There have, however, been just as many studies showing no significant gains in patient response. Still other groups have shown that it is mechanical dyssynchrony that is important, not the electrical dyssynchrony. Studies in canine and computational models have come up with conflicting findings regarding the effect of pacing at the latest contracting segment on CRT response. Due to the fact that these studies were not performed in a human population, our goal is to obtain electrical and mechanical delay times at potential pacing sites and observe the relationship between the two.

The specific hypothesis was that the observed regional mechanical dyssynchrony would correlate with the underlying electrical dyssynchrony.

To research this aim, we combined MR-derived regional dyssynchrony information from Aim 1a with electrical delay times obtained from local electrograms. Using intra-operative electrograms, we were able to determine the electrical delay between several pacing sites

throughout the coronary veins and a reference electrode located in the apex of the RV. To compare mechanical delay times in the region surrounding the pacing lead, the locations of the electrical measurements were mapped to the AHA 17-segment model and compared directly to mechanical delay times

2.4 Aim 2: Localizing the Left Ventricular Pacing Lead on Magnetic Resonance Images

Develop a method for localization of the cardiac resynchronization therapy left ventricular pacing lead on magnetic resonance images.

To evaluate the importance of lead placement on response to CRT, we must register the LV lead position from dual-plane x-ray images with MR images of the coronary veins and with the display of regional dyssynchrony. We accomplish this with the following sub-aims:

2.4.1 Aim 2a: Coronary Venous Anatomy using Magnetic Resonance Imaging

Perform a three-dimensional reconstruction from magnetic resonance images of the coronary veins and project the venous anatomy onto a display of regional mechanical dyssynchrony (from Aim 1a).

In order to test the hypothesis that lead position affects CRT response and to potentially use the methodology for treatment (lead placement) planning, we need to map the coronary vein anatomy onto the AHA 17-segment model showing regional dyssynchrony information.

Our specific hypothesis was that a method to generate a three-dimensional reconstruction and a projection onto the AHA 17-segment model of the coronary veins from contrast-enhanced MR data can be developed.

To achieve this aim, we studied the motion and cross-sectional area of the coronary sinus over the cardiac cycle to identify the ideal coronary vein imaging period for CRT patients. By acquiring image data during this period and employing a slow injection of gadolinium, we were able to obtain a three-dimensional image of the coronary sinus and its tributaries. From this data, we created a mesh around points identified to be within the coronary veins. This mesh could then be projected onto the AHA 17-segment model. This allows for the visualization of coronary venous anatomy relative to measures of dyssynchrony and/or

myocardial scar tissue.

2.4.2 Aim 2b: Registration of Dual-Plane X-ray Images and Magnetic Resonance Data

Register x-ray-based dual-plane venograms to the magnetic resonance representation of the coronary veins and use post-implant dual-plane images to determine lead location and map the lead location onto the magnetic resonance data.

It is thought that placing the LV pacing lead in the latest-activated (most-dyssynchronous) region will lead to improved response to CRT. In order to evaluate the effect that lead placement has on response, it is necessary to project the actual LV pacing lead location onto the AHA 17-segment model (from Aim 1) that contains dyssynchrony information. Due to the fact that a patient is unable to receive an MRI after device implantation, we must determine the lead position via dual-plane x-ray images. This lead location can then later be mapped back to the MR data using the coronary vein anatomy from both MR and fluoroscopy to perform registration.

Our hypothesis was: Lead localizing dual-plane images can be used to accurately map the lead location from the x-ray images into the MR coordinate system, and subsequently be projected onto the AHA 17-segment model containing regional dyssynchrony information.

We accomplished this aim by acquiring dual-plane images of both contrast-enhanced coronary vein anatomy and the LV lead location. By registering these two sets of dual-plane images, we were able to identify the position of the LV pacing lead in each of the dual-plane venograms. The 3D reconstruction of the coronary veins from the magnetic resonance coronary vein (MRCV) scan was projected onto each of the venograms and corresponding branch-points were used to correct for possible scaling and translation caused by patient table motion. After correcting for these parameters, the position of the lead could then be projected back to the source to determine the position of the LV pacing lead in 3D. This position was then mapped onto the AHA 17-segment model.

2.4.3 Aim 2c: Registration Verification and Validation

Create magnetic resonance / x-ray coronary vein phantom for method development and technique validation. Compare the LV lead position from our new method with previously proposed methods.

In order to develop and test our method for mapping the x-ray lead position to the MR data, we need to have a way to visualize the lead location in both the MRI and x-ray imaging systems. To this end, we had to develop an imaging phantom of the coronary vein anatomy with pacing leads that could be visualized with both modalities. The accuracy of our registration method in Sub aim 3b, can be determined by measuring the distance between the registered lead positions and the actual lead locations as visualized by MRI.

We hypothesized that our pacing lead location technique would be more accurate than existing techniques.

To fulfill this aim, we obtained a CT angiogram (CTA) of the coronary veins using an iodinated contrast agent. The coronary venous anatomy and cardiac chambers were segmented out and a negative phantom was created using 3D printing techniques. The phantom was able to be filled with iodinated contrast agent for x-ray imaging and a gadolinium-based contrast agent for MR imaging. Markers that could be filled with the appropriate contrast agents represented six pacing lead locations. In this way, we were able to directly compare the actual lead location to the registered lead position using our technique.

2.5 Aim 3: Quantifying the Effect of Mechanical Dyssynchrony on CRT Response

Quantify the effect of mechanical dyssynchrony (Aim 1a) at the site of the left ventricular pacing lead (Aim 2) on response to cardiac resynchronization therapy.

In order to show the utility of the methods developed in this thesis, and determine the importance of regional dyssynchrony, we need to apply the techniques in a group of patients who have been selected for CRT. We followed nine patients for six months after device implantation to determine if they benefitted from the therapy or not. We analyzed the regional dyssynchrony maps, coronary vein anatomy, and LV lead locations to determine

the effect on patient response.

We hypothesized that patients will not respond to CRT according to clinical response criteria if the LV pacing lead is not located in the latest contracting segment.

To study the effect of dyssynchrony and coronary vein anatomy on patient response, we studied nine patients that were selected to receive CRT via standard enrollment criteria. We were successfully able to apply the developed techniques in all patients to successfully compute regional dyssynchrony, coronary vein overlays, and determine the location of the LV lead. We compared the response rate of patients in which the pacing lead was placed in the latest contracting segment with those where it was in a neighboring segment or a remote segment.

2.6 Significance and Innovation

There have been several techniques developed to assess regional dyssynchrony in the LV; however, they either involve complicated post-processing or specialized MR protocols, only available to specialized research institutions. Our method is intended to be both straightforward and applicable in any clinical settings. The method and imaging can therefore be easily incorporated into multi-center studies to answer questions regarding regional dyssynchrony.

Several groups have studied mechanical dyssynchrony and its electrical substrate; however, these studies were performed using either animal or computational models. Our approach utilizes data not only obtained from patients, but electrical and mechanical activation data at *only* possible pacing sites, rather than throughout the entire LV.

Currently, there is no method used to register coronary anatomy from dual-plane x-ray data to MR data. This is an important step in order to characterize the tissue, electrical, and mechanical properties at the site of the pacing lead. The most commonly employed techniques to perform this task are a subjective estimation using Mortensen's o'clock or obtaining a post-implant CT scan. Our method allows the use of already available imaging data and can be expanded to work with a variety of imaging modalities including CT.

There is a vast amount of literature that attempts to tease out the effect that factors such as mechanical dyssynchrony, scar burden, and lead position have on patient response

to CRT. The goal of our work, is not to prove that pacing at the latest contracting region of the LV improves patient response. Rather, we would like to demonstrate that using the methodology developed in this thesis, it is possible to determine the relationship between MR-derived metrics and LV lead position. For this reason, we will demonstrate its utility in a number of patients and provide some initial indication of the importance of mechanical dyssynchrony at the LV pacing location.

The goal of this thesis is to provide the methodology necessary to better understand the relationship between mechanical dyssynchrony, coronary vein anatomy, left ventricular pacing location, and patient response to CRT.

CHAPTER III

REGIONAL DYSSYNCHRONY ASSESSMENT FROM SHORT-AXIS CINE IMAGES

Adapted from "A Method to Create Regional Mechanical Dyssynchrony Maps from Short-Axis Cine Steady State Free Precession Images" by Jonathan D. Suever, Brandon K. Fornwalt, Lee R. Neuman, Jana G. Delfino, Michael S. Lloyd, John N. Oshinski. J Magn Reson Imaging (in press).

The purpose of this work was to develop a method to generate high-resolution maps of regional dyssynchrony from magnetic resonance short-axis images to identify regions of latest contraction. In this chapter we detail the determination of regional delay times from the radial displacement of the endocardium. By mapping this information onto the AHA 17-segment model, the results can be used to identify LV lead placement sites that maximize the likelihood of patient response to CRT.

3.1 Introduction

Intra-ventricular mechanical dyssynchrony results from a dis-coordinate timing of contraction between segments of the LV. This LV dyssynchrony is present in approximately 30% of patients with heart failure, particularly those with dilated cardiomyopathy and LBBB [24, 27]. CRT is an effective treatment for patients with heart failure and evidence of electrical dyssynchrony on a surface electrocardiogram. In CRT using bi-ventricular pacing, one lead is placed through the RV into the septal wall and a second lead is placed through the coronary sinus into the lateral wall of the LV. Simultaneous pacing of the leads stimulates coordinated contraction of the septal and lateral regions of the LV to restore synchrony. Although CRT increases survival and improves quality of life in specific heart failure populations [70], 30% of appropriately selected candidates for CRT do not

have measureable improvement in symptoms 6 months after CRT implantation (so-called "non-responders") [148, 149].

The role of mechanical dyssynchrony as a predictive tool for CRT response is not well understood. Mechanical dyssynchrony is usually not currently considered during patient selection despite some evidence showing its ability to select patients who will have a positive response to CRT [108]. Echocardiographic techniques such as tissue Doppler imaging (TDI) have been utilized to assess LV mechanical dyssynchrony [88,150]. These methods are operator-dependent, require an acoustic window, and exhibit poor reproducibility [151]. In large international multi-center trials, echocardiographic measures of dyssynchrony failed to significantly improve CRT patient selection over standard echocardiographic parameters [152].

Placement of the LV lead in the region of latest contraction may have a role in response to CRT. Retrospective studies have shown that patient response to CRT is greatest when the LV pacing lead is placed in the most dyssynchronous or latest-contracting segment [101,153]. To discern the relationship between regional mechanical dyssynchrony, lead position, and CRT response, a method to determine regional mechanical dyssynchrony over the LV that can be applied in large multi-center studies must first be developed. A regional map of dyssynchrony could also be used as a tool to plan lead placement.

Several MRI-based methods have been developed in order to provide an assessment of mechanical dyssynchrony. Myocardial tagging can be used for assessing dyssynchrony [154]. However, tagging requires specialized acquisition sequences and significant post-processing [117, 155] to determine regional dyssynchrony. A number of groups have utilized advanced phase-based techniques such as DENSE [120, 156, 157], TVM [118], and strain-encoding (SENC) [158]. These techniques can obtain regional dyssynchrony information based on either strain or displacements; however, only specialized centers are capable of performing and analyzing these scans, limiting the feasibility of using these techniques in multi-center dyssynchrony studies.

In contrast to tagging, DENSE, TVM, and SENC, SSFP cine images are part of nearly all standard CMR examinations, and SSFP is optimized for both high temporal and spatial

resolution acquisitions. SSFP-based methods have been developed to derive regional and global LV motion information from cine images. Previous techniques developed to quantify dyssynchrony are either global measures [114, 115], assume that the contraction follows an idealized motion pattern [114], use time-to-peak based measurements reliant on user identification of the end systolic time point [159], or involve complicated post-processing or large training sets [160]. Thus these existing techniques are difficult to use for accurate and reproducible regional dyssynchrony analysis.

The goal of this study was to develop a method that utilized SSFP cine images to create regional maps of mechanical dyssynchrony. The method obtains radial displacement curves (RDCs) from short axis cine images, determines the mechanical activation delay at any location within the left ventricle relative to a patient-specific reference using cross-correlation, and displays this information on a standard AHA 17-segment model for visualization. By utilizing a patient-specific reference, it is possible to determine which regions contract early and late in each patient. The resultant maps show regional distributions of LV motion and could be used as a guide for lead placement. We applied the method in a study group of subjects with clinical evidence of LV dyssynchrony and compared the measurements to a group of healthy controls.

3.2 Methods

3.2.1 Study Subjects

This study included 10 control subjects with no history of cardiovascular disease, a normal EKG, and no evidence of electrical dyssynchrony (QRS duration $<$ 120 ms on a 12-Lead EKG), and 10 patients who met accepted clinical criteria for CRT: NYHA Class III or IV heart failure, LV Ejection Fraction (LVEF) $<$ 35%, QRS Duration $>$ 120 ms, and optimal medical therapy for at least one month. All patients used in this study had a QRS duration $>$ 150 ms (evidence of electrical dyssynchrony) and were responders to CRT as determined by a 15% decrease in LV end systolic volume (LVESV) at 3 months post-implantation. Emory University's Institutional Review Board approved this study.

3.2.2 Image Acquisition

Steady-state free-precession (SSFP) short-axis images were acquired during end-expiration 8–12 second breath holds using a 1.5T Philips Intera scanner and a five-element phase array cardiac coil (Philips Medical Systems, Best, Netherlands). EKG triggering was used to obtain 20 frames per cardiac cycle (reconstructed temporal resolution: 32.6 – 58.8 ms). Eight-millimeter thick slices were acquired with no slice-gap to ensure coverage of the entire left ventricle. Acquisition parameters were: acquired matrix size = 192 x 256, reconstructed matrix size = 256 x 256, field of view (FOV) = 370 mm, flip angle = 65°, TR = 4 ms, and TE = 2 ms. Vertical long-axis (two-chamber, VLA) and horizontal long-axis (four-chamber, HLA) SSFP cine images were also acquired using the same acquisition parameters.

3.2.3 Post-processing

All processing was performed in Matlab (The MathWorks, Natick, MA, USA). The endocardial border on all short-axis and long-axis images was delineated using an active appearance model-based technique with manual corrections [161,162] (Figure 3.1A). Each contour was sampled at 100 equally spaced points radially starting at the anterior insertion of the right ventricle. The distance from any point relative to the centroid of the left ventricle was computed over time to obtain an RDC at each point throughout the LV. Each RDC was up-sampled by a factor of 10 using Fourier interpolation and a Gaussian smoothing filter with a width of 12.5% of the time series was applied to the data to minimize the effects of frame-to-frame discrepancies in the endocardial contour. The mechanical delay time relative to a reference RDC was determined for each of these RDCs. These mechanical delay times were then mapped onto the standard AHA 17-segment model (Figure 3.1E).

3.2.4 Determination of LV Centroid

The location of the central axis of the LV is known to change over the cardiac cycle. Thus in order to obtain an accurate assessment of regional wall motion, it is necessary to track the central axis of the LV over the cardiac cycle. If a stationary centroid is used, simple translation of the heart within the chest cavity will result in erroneous radial displacement

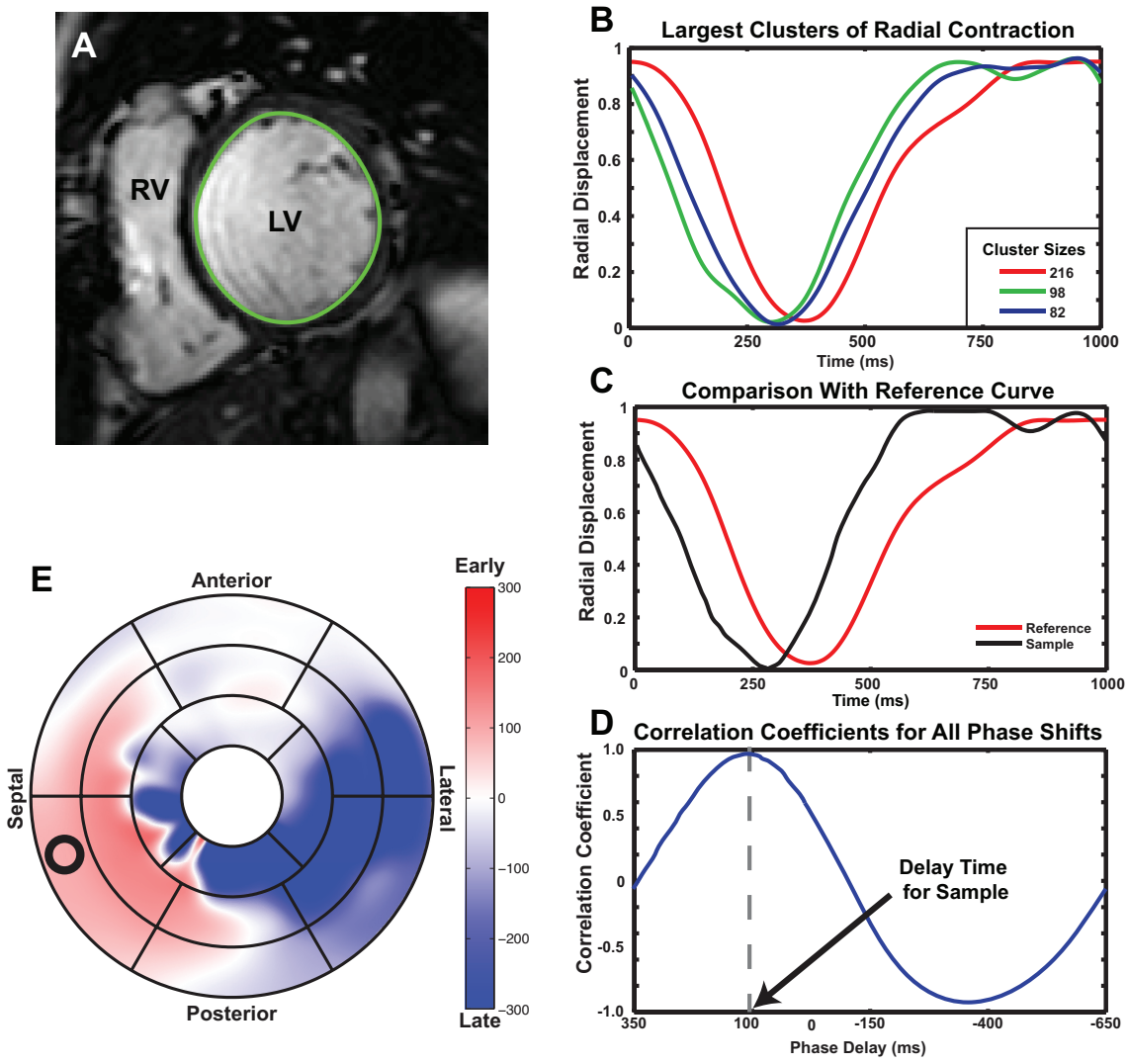

Figure 3.1: Using endocardial borders (A), RDCs were computed and clustered using QT clustering (B). The largest cluster was considered to be the patient-specific reference to which all other RDCs were compared (C). The delay time between any RDC and the reference was computed using cross-correlation (D). The delay times throughout the LV were then mapped to the standard AHA bullseye (E).

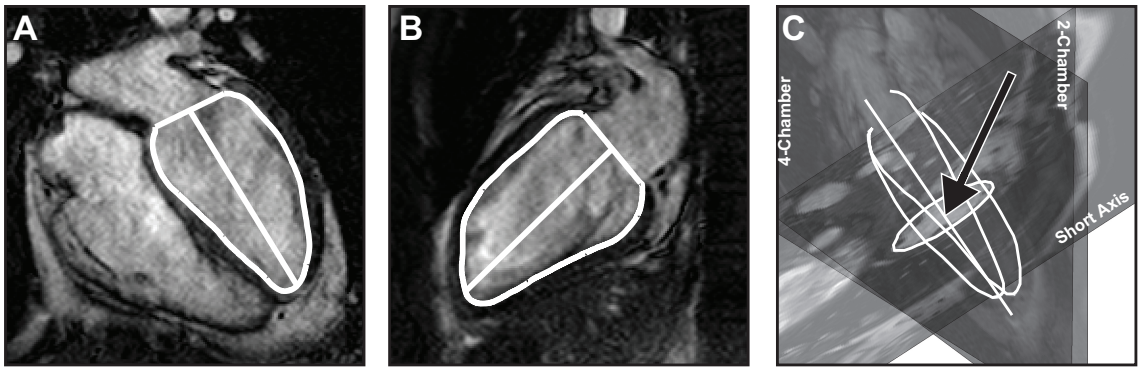

Figure 3.2: The location of the mitral valve plane and the central axis of the left ventricle were defined in the four-chamber (A) and two-chamber (B) image planes. Using position information from the DICOM header, this data was projected into three-dimensional space (C) and the intersection of the central axis with the short-axis image plane was defined as the centroid for that particular slice and phase (black arrow).

estimations [163,164]. To determine the central axis, endocardial boundaries were traced on the two-chamber and four-chamber long axis images. The mitral valve plane was identified in each long axis view by manual selection of the mitral valve annulus. The apex was determined as the centroid of the bottom 15% of the LV. A line extending from the midpoint of the valve plane to the apex of the left ventricle served as the central axis in the imaging plane of the two-chamber and four-chamber views (Figure 3.2A-B). Utilizing 3D position information from the DICOM header, the central axis in each view was converted to a plane normal to the imaging plane. The intersection of the planes in 3D space was used as the central axis of the LV. The intersection of this central axis with each short-axis imaging plane for each phase of the cardiac cycle was used as the centroid for that particular slice and phase (Figure 3.2C).

3.2.5 Reference RDC Determination

To determine whether a given region contracts early or late, the RDC in this region must be compared to a reference ("normal") RDC. This reference RDC could be obtained by taking the global average of all RDCs for each individual. However, a global average includes data from early, normal, and late-contracting segments. This can lead to distortions of the reference RDC, especially in patients with large dyssynchronous regions. Therefore, we used a patient-specific reference that preserves as much detail as possible to ensure proper delay

time estimation. Additionally, in order to accurately determine regional delay times using cross-correlation, it is assumed that the two samples being compared have similar shape. By using a patient-specific reference, rather than a reference RDC derived from healthy individuals, we can account for inter-patient variability of radial contraction patterns.

To determine the reference RDC in this study, quality threshold (QT) clustering [165] using root-mean-square error (RMSE) was used to cluster all RDCs into groups with similar contraction patterns (Figure 3.1 B). In this application, the RMSE is a measure of how similar two RDCs are, which is indicative of the similarity of the contraction of the two regions represented by the RDCs. RMSE was computed as shown in Equation 3.1 where N is the number of samples in each radial displacement curve, and f and g are the RDCs being compared.

$$RMSE = \sqrt{\frac{\sum_{i=1}^{N}(f_i - g_i)^2}{N}} \tag{3.1}$$

In order to perform QT clustering, it is necessary to define a minimum quality for the members of each cluster. To determine an acceptable quality threshold, we utilized the RDCs obtained from 10 normal subjects. The RMSE between all RDCs in the normal subjects were computed. A quality threshold was selected so that 95% of "normal" RDCs would be clustered into the same group. Theoretically this quality threshold would allow members of a single cluster to vary within the range observed in a healthy left ventricle. A cutoff value of 33% was determined to be representative of the variation seen in the healthy population (Figure 3.3).

All clusters were then constrained to have a maximum RMSE of 33% between any two RDCs in the group. We then assume the largest cluster in each patient is representative of "dysynchronous" contraction of the LV. By averaging all RDCs in this largest cluster, we obtain a patient-specific reference RDC that preserves as much detail as possible (Appendix D.1).

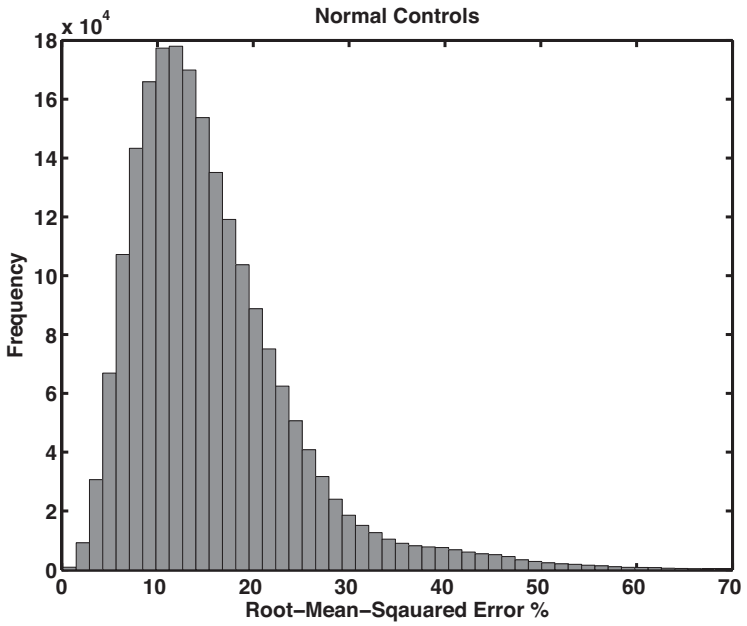

Figure 3.3: The distribution of RMSE values observed in healthy subjects. It was found that a RMSE of 33% allowed for 95% of all healthy RDCs to be clustered together.

3.2.6 Mechanical Activation Delay

Normalized cross-correlation analysis (Appendix B.1) was used to determine the delay time between RDCs throughout the LV and the patient-specific reference RDC. In the cross-correlation analysis, each RDC was shifted in time relative to the reference RDC. At each time shift, correlation with the reference was computed [166]. The shift yielding the highest correlation value with the reference was the delay time for that particular RDC (Figure 3.1D). Due to the cyclic nature of the data, periodicity was assumed for cross-correlation (Appendix B.2). This process was repeated for all RDCs throughout the LV. It is important to note that because the patient-specific reference is an average of many RDCs, the delay time computed for the RDCs used to compute the reference is often non-zero.

3.2.7 Creation of Regional Maps

To create a display of the spatial distribution of mechanical contraction delay times throughout the LV, we used a polar plot with a superimposed 17-segment AHA model [147]. The apical (17th) segment was omitted in our work due to the lack of clear endocardial boundaries at the most apical short-axis slice. Delay times were computed for 100 locations in

each slice throughout the LV and mapped to the polar plot with a delay time of 0 (white) indicating synchronous contraction, a positive delay (red) indicating early contraction, and a negative delay (blue) representing a late-contracting segment (Figure 3.1E).

3.2.8 Characterization of Normal Contraction and Identification of Size and Location of Dyssynchronous Regions

We also investigated the range of mechanical activation times observed in a healthy population. For this sub-study, we acquired and analyzed high temporal resolution MR images in 10 healthy volunteers with no evidence of electrical dyssynchrony (QRS < 120 ms). We were able to acquire short-axis cine images at 60 frames per cardiac cycle yielding an effective temporal resolution of 17 ms. By computing the delay times throughout the LV for each of the normal volunteers, we were able to use the 95% confidence interval to define what range of delay times constitutes "normal" contraction. By applying these cutoff values to 27 patients enrolled for CRT, we were able to classify each RDC as either synchronous or dyssynchronous. From this, we could compute the size of the dyssynchronous region as a percentage of the LV.

3.2.9 Dyssynchrony Parameters

Average delay times and the average absolute value of the delay times were computed throughout the LV for all patients. In order to compare our maps to previous parameters, we calculated several commonly used dyssynchrony measures.

The Yu Index

The Yu index, is a method that is typically applied to data acquired with TDI. It measures the dispersion of delay times throughout the ventricle. The left ventricle is segmented into 12 regions and the average delay time within each segment is computed [89]. The Yu index is then equal to the standard deviation of the average delay times. A larger value is indicative of a more dyssynchronous left ventricle. To compute this value in our data, we divided our data into basal and mid sections with 6 segments per section.

Tissue Synchronization Index

Tissue Synchronization Index (CMR-TSI) is a parameter that was applied by Chalil et

al to MRI-derived regional contraction times. Similar to the Yu index, it is the standard deviation of regional delay times. Due to the fact that MR can better resolve the entire left ventricle, it utilizes delay times from 16 AHA segments [114].

3.2.10 Reproducibility

Inter-observer reproducibility was assessed in five of the normal subjects and five of the patients. Two observers provided unique contours for all three views (short axis, two-chamber, and four-chamber) and average delay times were computed for each AHA segment. Bland Altman analysis was used to determine the agreement between the AHA segment averages [167]. Because a primary benefit of a regional measure of mechanical dyssynchrony in patients undergoing CRT is the ability to identify the latest contracting segment, the two observers' contours were used to create regional dyssynchrony maps and determine the latest contracting segment in each of the subjects. Cohen's κ-coefficient, a measure of agreement which accounts for agreement by chance, was used to assess agreement between the observers [168]. Equation 3.2 shows the calculation of κ where $\Pr(e)$ is the probability that the observers agree by chance and $\Pr(a)$ is the observed agreement between the observers.

$$\kappa = \frac{\Pr(a) - \Pr(e)}{1 - \Pr(e)} \tag{3.2}$$

For the reproducibility analysis, it is necessary to exclude akinetic regions. For this reason, only regions where the radial displacement exceeded 2 mm (greater than one pixel) were considered.

3.3 Results

Regional activation maps were generated for all ten normal subjects and in all ten patients. Representative regional dyssynchrony maps are shown in Figure 3.4. The absolute values of the delay times were 23.9 $\pm$ 33.8 ms and 93.1 $\pm$ 99.9 ms ($p < 0.001$) in normal and patients, respectively (Figure 3.5A). The larger value for the patients indicated that they have a wider range of delays over the LV.

Delay times were extracted using the time shift that yielded the largest correlation coefficient between an RDC and the patient-specific reference RDC. These coefficients were

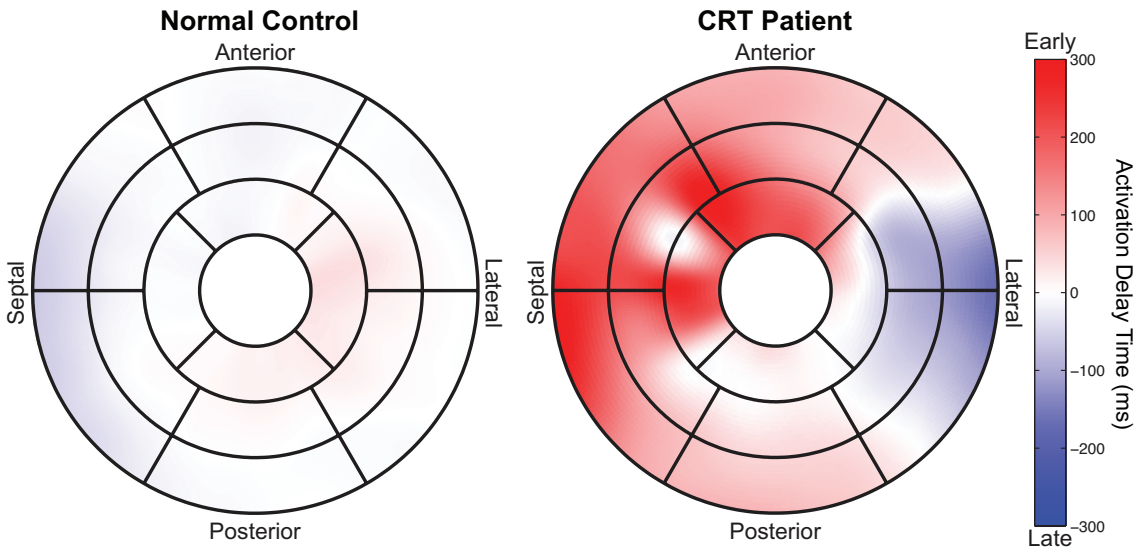

Figure 3.4: Representative AHA 17-Segment Models of regional delay times for both normal controls (left) and patients undergoing CRT (right)

Table 3.1: Mechanical Dyssynchrony in Patients and Normals

	Normals (n = 10)	Patients (n = 10)	p-value
Delay Times (ms)	23.9 ± 33.8	93.1 ± 99.9	< 0.001
Correlation (R^2)	0.95 ± 0.1	0.88 ± 0.1	< 0.001
Yu Index (ms)	28.9 ± 15.6	76.1 ± 23.6	< 0.001
CMR-TSI (ms)	27.1 ± 12.8	76.7 ± 25.0	< 0.001

Comparison of delay times and mechanical dyssynchrony parameters in CRT patients and healthy individuals.

0.95 ± 0.07 (Range: 0.27 – 1.00) for normal subjects and 0.88 ± 0.12 (Range: 0.19 – 1.00) for patients enrolled for CRT (Figure 3.5B). These correlation values indicate acceptable confidence in the estimated delay times.

The Yu index was found to be 28.9 ± 15.6 ms in normals compared to 76.1 ± 23.6 ms in patients undergoing CRT ($p < 0.001$), and the CMR-TSI parameter was 27.1 ± 12.8 ms in normals and 76.7 ± 25.0 ms in patients ($p < 0.001$). All metrics were determined to be significantly different between patients and normal subjects.

Averaging delay times over AHA segments, it was possible to identify the latest-contracting segment in all patients undergoing CRT. The latest-contracting segment varied among the study patients (antero-lateral segment in 5 patients, postero-lateral segment in 3 patients,

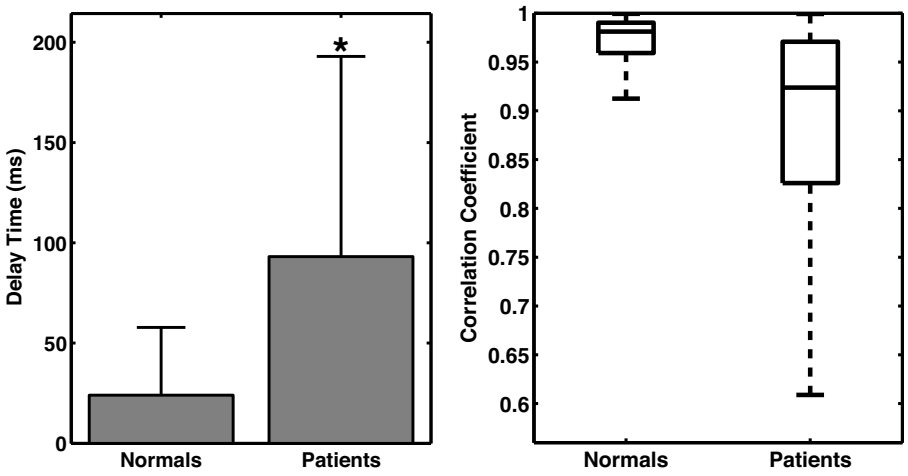

Figure 3.5: Average absolute delay times in normals and patients (left) were significantly different ($p < 0.001$). Normalized cross-correlation coefficients computed between the RDCs and the patient-specific reference RDCs.

and septal segment in 2 patients).

In the reproducibility analysis, segment delays for two observers differed by 6.8 ± 39.3 ms (Bias: 6.8; CI: 77.1). The latest contracting segment was determined to be the same in all but three patients (kappa: 0.64). In two of the patients where the disagreement occurred, the segments selected by the two observers were neighboring lateral wall segments.

3.3.1 Characterization of Normal Contraction

In order to determine the normal range of LV contraction timing, we computed the 95% confidence interval of the contraction times seen in normal subjects. We utilized data obtained from 10 normal subjects with no evidence of electrical dyssynchrony (QRS duration < 120 ms). The delay times seen in this normal population were -10.8 ± 47.4 ms. Using the 95% confidence interval, normal contraction times were found to be between -103.7 and 82.1 ms (Figure 3.6).

Regional delay times were computed in a total of 27 patients enrolled for CRT that met standard enrollment criteria. In these patients, delay times were found to be -34.4 ± 121.7 ms. The total number of dyssynchronous AHA segments using a 16-segment AHA model was 2.4 ± 3.6. Additionally, the size of the dyssynchronous region was $36.4 \pm 11.9\%$ of the left ventricle (Figure 3.7).

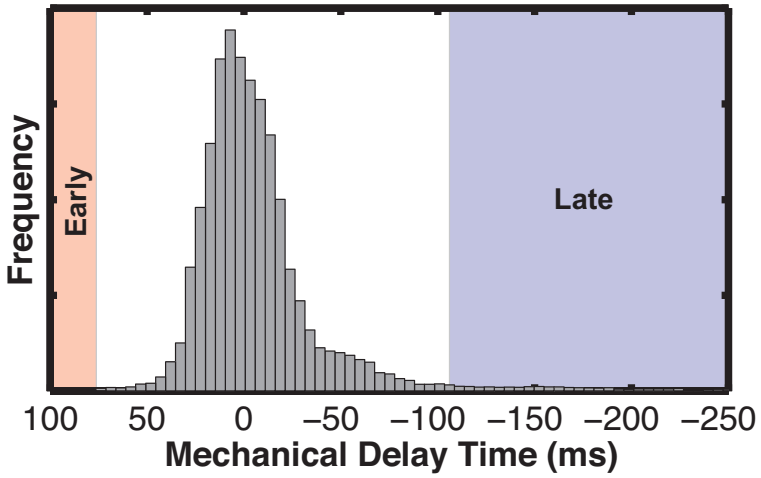

Figure 3.6: Histogram of combined contraction times from healthy subjects with no evidence of dyssynchrony. The cutoff region for late contraction (shaded blue) was found to be 103.7 ms and the cutoff for early contraction (shaded red) was 82.1 ms.

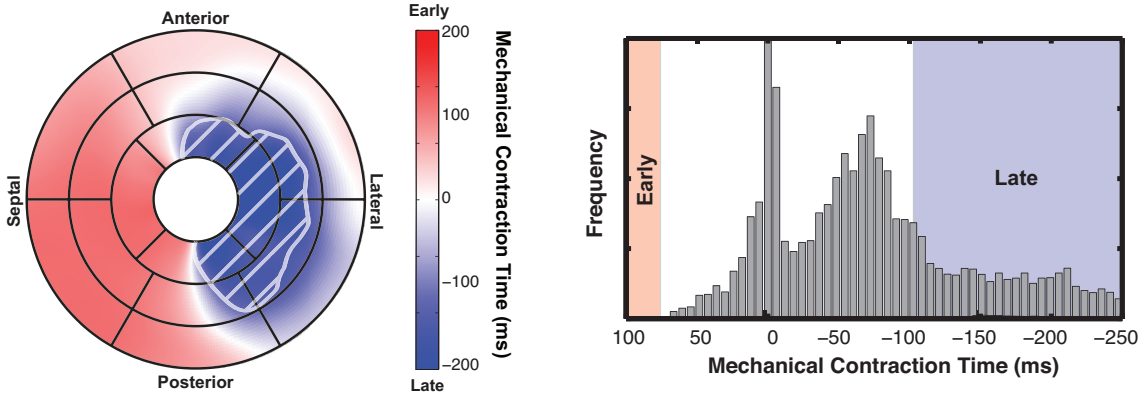

Figure 3.7: Representative patient regional dyssynchrony bullseye and corresponding delay time histogram. The late-contracting dyssynchronous region is highlighted in white on the segment model.

3.4 Discussion

This study describes a new method for assessing and displaying regional mechanical dyssynchrony from standard cine CMR images. The method is suitable for widespread use due to reliance on SSFP images present in all standard CMR exams. The absolute value of the delay times in patients was significantly greater than delay times in normal subjects. Additionally, both patients and normal subjects had high correlation coefficients when determining the regional delay times between each regional RDC and the reference RDC indicating confidence in the similarities of the RDCs when shifted in time.

3.4.1 Comparison with Previous Methods

The delay times obtained in this study agree with published contraction timings obtained with various modalities and methodologies. The CMR-TSI values derived from our regional dyssynchrony data agreed with previous studies by Chalil et al. (27 ± 13 ms vs. 21 ± 8 ms and 77 ± 25 ms vs. 106 ± 55.8 ms for normal subjects and patients, respectively). [114] The Yu index of 76.1 ± 23.6 ms in this study was slightly lower than those previously presented found using 3D speckle tracking (124 ± 88 ms) [169]. This discrepancy could be due to the lower temporal resolution data provided by MRI compared to that of echocardiography. Higher frame-rate cines could be employed to further explore this discrepancy.

In our study cohort, the location of the latest contracting segment of the left ventricle varied widely. Prior studies have reported conflicting results when identifying the region of the LV most commonly associated with late contraction [169–171]. Although our dataset is small, it agrees with more recent data from the MADIT-CRT study which showed widely varying regions of latest delay across study populations [28]. In our group, two patients were shown to have the latest contracting segment in the septum, which appears paradoxic to what is typically expected in LBBB patients. In these two patients, there was a very early inward motion of the septum, known as septal flash which is often presented in patients with LBBB [172]. In a patient with septal flash, the septal segments undergo two separate displacements during systole. The first results in a small, very early displacement of the septum (prior to myocardial thickening) followed by a much larger displacement when the

rest of the ventricle contracts. Due to the nature of our method, in these individuals, the early displacement was not seen by the cross-correlation algorithm as early contraction and thus the second, later inward motion of the septal segments were labeled as late contraction. Based on our convention, it appears that those with the "septal flash" or "septal bounce" phenomenon truly have late septal, rather than lateral, thickening and contraction.

We cannot compare the reproducibility of our method to existing MR or echocardiographic techniques due to the lack of reproducibility information from other studies. To understand how the reproducibility of our method compares to these other methods, we could have two observers analyze our data using these other methods, and then compute inter-observer reproducibility. In our study, the inter-observer reproducibility between the two observers was 6.8 $\pm$ 39.3 ms (Bias: 6.8; CI: 77.1). The bias is very close to zero indicating good agreement. The fairly large confidence interval is due to the variability in the segment delays seen across patients and normal subjects and is on the order of the temporal resolution of the data ($\sim$50 ms). Higher temporal resolution scans should be utilized to further improve the reproducibility of these scans. The exact same AHA segment was identified as the latest contracting segment in all but three of the patients, and in two of those patients, the neighboring lateral segment was selected. Previous studies have shown that LV leads placed in segments adjacent to the most-delayed segment demonstrated improved response [173]. The high reproducibility of this method in determining the latest-contracting segment is necessary for utilizing regional dyssynchrony information for LV lead placement planning.

3.4.2 Correction for Gross Translation

We utilized a floating centroid based upon endocardial contours on two and four-chamber images in order to compensate for translational motion of the LV. The floating centroid is a well-known issue for LV dyssynchrony assessment [174–176]. Without compensation, translation of the heart will result in apparent relaxation of one side of the ventricle (translation away from the centroid), while the other side of the ventricle will appear to exhibit strong contraction (translate toward the centroid). This will produce irregular RDCs, which could

result in false delay detection. Various methods have been used in CT [177] and echocardiography [164] to deal with the floating centroid; however, no one has utilized long axis cine information as presented in this study. Due to the fact that the short-axis and long-axis images are acquired at different times, patient movement and respiration can potentially cause misalignment between these images. In this study, no such error was present, but if necessary, the endocardial contour of the two-chamber image and short-axis images could be registered to account for respiratory motion.

3.4.3 Patient-Specific Reference RDC

Chalil, et al. have previously used the earliest contracting RDC as a reference [114]. Using the earliest contracting RDC has several potential drawbacks including the reliance on a single RDC, and the use of a potentially irregular reference. Using a single RDC can result in poor reproducibility due to the fact that two observers could produce very different reference RDCs, which are then used directly to compute all delays [112]. Another danger of using the earliest contracting RDC is that it could possibly be an irregular curve as is often the case in patients undergoing CRT (e.g. in a patient with septal flash). It is difficult to do any meaningful comparison with such an RDC because cross-correlation analysis assumes that the shape of the RDCs is relatively similar. In our method, we combine the detail-preserving power of clustering and the smoothing effect of averaging the largest cluster. Using our method, one can discern early and late contraction from normal contraction, such as is present in patients with septal flash or post-systolic contraction [172, 178]. Our clustering technique ensures that the reference RDC is representative of the majority of the left ventricle.

3.4.4 Detection of Akinetic Segments

One of the primary limitations of displacement-based methods utilizing endocardial boundaries on short-axis cines (as opposed to strain-based methods) is the inability to identify akinetic regions. Active myocardium surrounding the affected region may cause the endocardial border segment to move, resulting in an RDC regardless of the viability of the tissue. Using cross-correlation to determine delay times, however, enables us to not only obtain a

time delay between two RDCs, but also provides a correlation value that is indicative of similarity. In akinetic segments, the correlation would be computed between the reference RDC and essentially a flat line, but the corresponding correlation would be low compared to correlations of other RDCs. As expected, the correlations were lower in patients due to the complexity of the RDCs as well as the influence of potentially akinetic regions.

3.4.5 Future Directions and Applications

By displaying the regional dyssynchrony information onto a polar (bullseye) map and on the standard AHA 17-segment model, dyssynchrony information can be superimposed with other regional measures of cardiac function or tissue characteristics such as scar or edema. Therefore, one could correlate akinetic or late-contracting segments with scar transmurality information from late gadolinium enhancement MRI [179].

Higher frame-rate imaging could be employed to obtain finer resolution of mechanical delay times.

Although this study utilized 2D radial displacement information, it could easily be applied to three-dimensional data. The extension of this research to 3D data would allow for the detection of both radial and longitudinal dyssynchrony.

3.4.6 Limitations

Since we use short-axis images for dyssynchrony analysis, we are only making a radial dyssynchrony map, and longitudinal, through-plane, and torsional motion are not considered. The lack of longitudinal dyssynchrony detection is not a large limitation due to the fact that other studies have not observed significant changes in longitudinal dyssynchrony after CRT device implantation. [180, 181] Additionally, by expanding this method to 3D, it could potentially be used to detect both longitudinal and radial dyssynchrony.

Our utilization of a patient-specific reference RDC assumes that the patient has some synchronous contraction remaining in the left ventricle. We believe that this is a valid assumption since any dyssynchronous RDCs will have a wide variance of contraction patterns, while the normal RDCs, even if small in number, will be more similar to each other, and will thus be clustered effectively.

This study did not utilize age-matched controls and as a result, age-based differences could be a factor in the differences observed between patients and normal subjects.

3.5 Conclusions

We have presented a method to create regional mechanical activation maps by analyzing RDCs from cine SSFP images using a moving centroid and cross-correlation analysis. This method shows significant differences in measures of dyssynchrony in those with clinical evidence of dyssynchrony compared to controls. Our data supports this method as a potentially useful pre-operative tool to guide LV lead placement for CRT.

3.6 Major Findings

- We developed a reproducible method to assess regional dyssynchrony from short-axis cine MR images
- Normal contraction times were found to be between -103.7 and 82 ms
- Regional delay times were significantly higher in patients undergoing CRT compared to healthy controls
- The location of the latest-contracting AHA segment was heterogenous amongst CRT patients

CHAPTER IV

RELATIONSHIP BETWEEN MECHANICAL AND ELECTRICAL DYSSYNCHRONY IN CRT PATIENTS

The purpose of this work was to determine the relationship between electrical and mechanical dyssynchrony at potential pacing sites throughout the coronary sinus. Previous studies are conflicted on whether pacing at the latest electrically activated segment or latest contracting segment results in improved response to CRT. In an effort to understand this relationship, we compared regional delay times obtained from a pre-implant MRI with electrical delay times from intra-procedural electrogram measurements.

4.1 Introduction

Intraventricular dyssynchrony results from the dis-coordinate contraction of the ventricular walls, and the presence of dyssynchrony is associated with increased mortality in heart failure patients [24]. CRT is a treatment option for drug-refractory heart failure patients with low ejection fraction and evidence of LV electrical dyssynchrony. Currently, the primary marker for LV electrical dyssynchrony is QRS duration. A QRS duration of 120 ms or greater is indicative of delayed electrical activation within the ventricles and is an independent predictor of mortality and sudden death in heart failure patients [16]. However, at least 30% of patients fail to improve after CRT device implantation despite appropriate patient selection [108]. One reason for this non-response may be attributed to a difference between electrical and mechanical dyssynchrony. QRS duration is a measure of electrical dyssynchrony and may not accurately reflect the degree of mechanical dyssynchrony seen in imaging techniques such as MRI or echocardiography [152]. Currently, it is not clear if the presence of electrical and mechanical dyssynchrony are equivalent in determining patient response to CRT.

There are two reasons that the relationship of electrical and mechanical dyssynchrony is important in CRT. First, the effect of LV lead position has been studied extensively

in an attempt to explain poor response to CRT. Several groups have shown that pacing the LV in the latest contracting segment (greatest mechanical dyssynchrony) results in improved response to CRT [46, 90–92]. However, other groups have demonstrated that pacing in the most delayed region does not result in better response [182]. Similarly, canine and human studies have seen varied results when pacing at the latest electrically activated region [183, 184]. These contradictory findings may be a result of the complex interaction between electrical and mechanical dyssynchrony.

Second, many groups have shown that the time to mechanical activation in a region is longer than the underlying electrical activation time [53,185]. This delay is often termed the electromechanical delay (EMD), and it is the delay between electrical activation and onset of shortening. EMD has been shown to vary regionally within the LV as well as vary between individuals [186]. Therefore, any relationship between electrical and mechanical activation times may not be applicable across a range of patients. EMD is often accentuated in late-contracting regions due to the larger dP/dt within the LV caused by the early-contracting segments. The larger EMD is a result of the increased force required to generate shortening within the late activated region [185]. Interestingly, there can even be a mechanical delay without any evidence of electrical activation delay [187]. Most of these studies, however, have been conducted in canine models of LBBB and it is uncertain how this relationship manifests in patients undergoing CRT.

The purpose of this study was to combine regional mechanical contraction timing information throughout the LV derived from MRI with measures of electrical activation delay derived from local electrograms (EGMs) acquired at several locations in the LV from within the coronary veins. After registering EGM measurements to the MR-derived maps of regional dyssynchrony, we compared electrical and mechanical delay times at potential LV pacing locations to evaluate how electrical and mechanical timing varies by location in the LV and between individuals.

4.2 Methods

This study was conducted in 10 patients enrolled for CRT based upon current guidelines (QRS Duration < 120 ms, Ejection Fraction < 35%, and NYHA Heart Failure Class III-IV despite optimal medical therapy). Twelve-lead EKGs were used to classify all patients based upon their QRS morphology. Left bundle branch block was defined as a QS or rS complex in V1 and/or V2; monophasic R wave in I, aVL, V5, and V6; and mid QRS notching or slurring in >2 of I, aVL, V1, V2, V5 or V6. Right bundle branch block was defined as R, rR', rsR', or rSR' complexes in V1 and slurred S wave in I and V6 [188]. Interventricular conduction delay (IVCD) included those that did not meet any of the above criteria. Emory University's Institutional Review Board (IRB) approved this study and all patients gave written informed consent.

4.2.1 Magnetic Resonance Imaging Acquisition

Patients were placed in a 1.5T Siemens Avanto (Siemens Healthcare, Erlangen, Germany) scanner and were imaged using a 5-element phased array coil. EKG triggering was used to obtain 60 frames per cardiac cycle yielding an effective temporal resolution of 13.7 ± 3.3 ms (Range: 8.9 – 19.6 ms). SSFP short-axis images were acquired parallel to the mitral valve plane to cover the entire length of the LV at a slice thickness of 7 mm and no slice gap. Two- and three-chamber cine images were also acquired. Acquisition parameters: acquired matrix size = 192x192, reconstructed matrix size = 192x192, FOV = 275x275 mm, flip angle = 67°, TR = 4 ms, TE = 1.3 ms.

4.2.2 Regional Mechanical Delay Maps

To determine the mechanical delay times throughout the LV, we used the method discussed in Chapter 3 [189]. Briefly, endocardial boundaries were semi-automatically traced on all of the short-axis images (Figure 4.1A). Radial displacement curves (RDCs) were generated by computing the distance of the endocardial contour relative to the centroid of the LV at 100 circumferentially spaced points (Figure 4.1B). To account for translation of the LV over the cardiac cycle, the centroid was determined from the location of the mitral valve

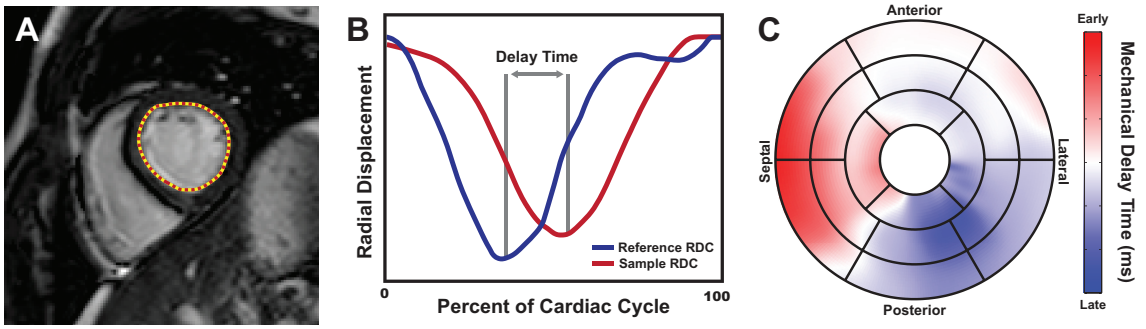

Figure 4.1: Endocardial contours are traced on short-axis cine SSFP images (A) and the distance relative to the centroid is computed (B; red). Each regional RDC is compared to a patient-specific reference (B; blue) to determine the mechanical delay time. These delay times are then mapped to the standard AHA 17 segment model (C).

annulus and apex of the LV in the two and three-chamber views. RDCs were sorted into similarly-contracting groups using QT clustering [165] and a patient-specific reference RDC was obtained by averaging all members of the largest cluster (Appendix D.1). Normalized cross-correlation [166] was then used to determine the temporal delay between each RDC throughout the LV and the reference RDC (Figure 4.1B) (Appendix B.2). After mechanical delay times had been computed throughout the entire LV, the delay times were then mapped to a polar map and the standard AHA 17-segment model was superimposed [147] to facilitate comparison between electrical and mechanical delay times (Figure 4.1C).

4.2.3 Electrogram Acquisition

One of several models of approved passive fixation LV leads was used to obtain local EGMs during the CRT device implantation procedure. The RV pacing lead was inserted into the apex of the RV near the apical septal wall of the LV. After coronary sinus venography, the LV lead was directed to various achievable locations throughout the coronary venous system. Although the implanted pacing leads had multiple electrodes, we used a unipolar configuration in which only one electrode was used for recording local EGMs. EGMs were simultaneously recorded from the RV and LV leads at a sampling frequency of 500 Hz (2 ms temporal resolution).

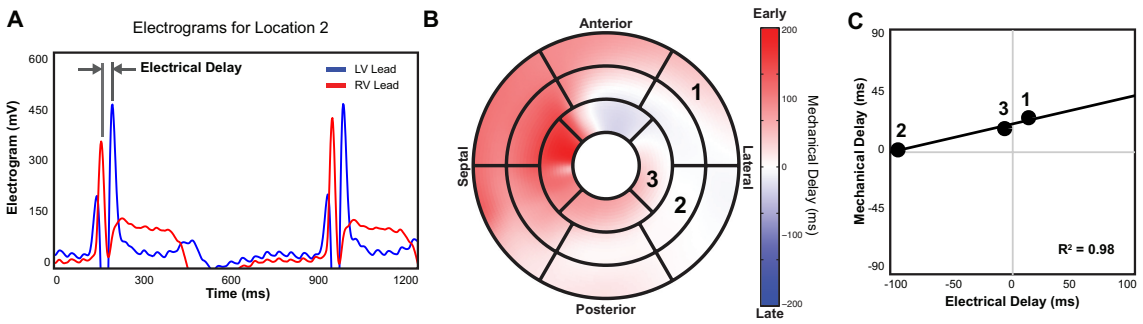

Figure 4.2: Electrical delay times at each lead location were determined by comparing the LV EGM with the RV EGM (A). Using the mapped lead positions, mechanical delay times could be sampled from the regional dyssynchrony map (B) and compared directly to the electrical delay times (C).

4.2.4 Regional Electrical Delay

Electrical delay times were assessed as the delay between the RV and LV EGMs as determined using in-house software written in Matlab (The MathWorks, Natick, MA). Each EGM was first filtered using a band-pass filter. Low frequencies were removed to eliminate baseline drift that could occur over the course of the 5 sec measurement duration. Additionally, an upper limit was selected to eliminate high-frequency noise from the signal.

LV EGMs were super-imposed on the RV reference EGM for each location. A blinded experienced observer selected corresponding peaks of the two signals (the arrival of electrical activation at each site). The peak-to-peak time difference was computed from these user-defined points to obtain the electrical delay time at each sampling location (Figure 4.2A).

This study utilized the convention that a positive electrical delay time indicated that the lateral wall was activated prior to the septal wall, whereas a negative electrical delay time indicated that the activation was delayed in the lateral wall relative to the septal wall.

4.2.5 Coronary Venous Imaging

Venous imaging in the electrophysiology lab was performed using standard procedures. Briefly, prior to any EGM measurements, a balloon catheter was inflated to occlude the proximal coronary sinus and iodinated contrast agent (Visipaque, GE Healthcare, Waukesha, WI) was injected retrograde into the coronary veins. During contrast injection, coronary venograms were acquired at the following views: 30° RAO, AP, and 30° LAO (Figure 4.3,

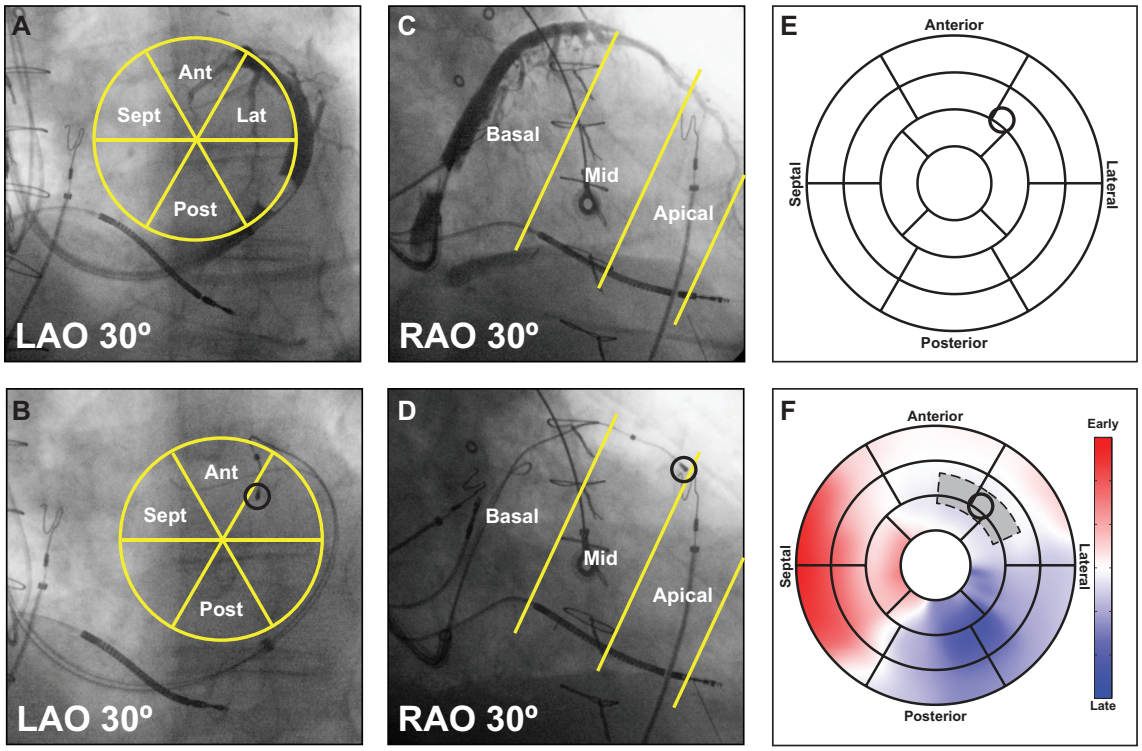

Figure 4.3: Dual-plane venograms (A, C) and lead localizing x-ray images (B, D) were used to map LV pacing lead locations (black circle) onto the AHA 17-segment model (E). LAO images were used to determine the circumferential location while RAO images were used for longitudinal position. Mechanical delay times in a region surrounding the lead location (shaded region) can be determined directly from the 17-segment model (F).

top row). Each LV EGM recording site was recorded fluoroscopically in 30° RAO and LAO positions (Figure 4.3, bottom row).

4.2.6 Registration of Lead Position to Regional Mechanical Delay Maps

To determine the mechanical delay corresponding to each of the locations where the EGM was measured, it was necessary to map the lead location from the angiographic images to the MR imaging domain. An experienced observer used dual-plane venograms and lead localizing dual-plane images to determine the location of the LV pacing lead on the AHA 17-segment model (Figure 4.3). The RAO image was used to determine the longitudinal position of the lead, while the LAO image was used to determine the circumferential position. Lead positions were determined for all coronary vein EGM recording sites.

4.2.7 Corresponding Electrical and Mechanical Delay Times

Since the MR-derived mechanical delay times are already projected onto the AHA 17-segment model, it is possible to directly compare the mechanical and electrical delay times at each location (Figure 4.3F). Due to the lower spatial resolution of the local EGM, and to reduce sensitivity to possible errors in lead localization, mechanical delay times within a region the size of an AHA segment, but centered about the lead location, were averaged to obtain the mechanical delay time corresponding to each lead position (Figure 4.2B). The mechanical and electrical delay times obtained at each location were then compared (Figure 4.2C).

4.2.8 Comparison of Electrical and Mechanical Delays

Pearson's correlation coefficient was computed between the electrical and mechanical delay times observed for each patient. The location (AHA segment number) of the latest electrical activation and latest mechanical contraction were determined in each patient.

The MR-derived regional mechanical delay times were computed *relative to a patient-specific reference curve*. The EGM-derived electrical delay times in the LV were computed *relative to the electrogram obtained at the apex of the RV*. The different references for the electrical and mechanical measurements mean that: 1) the exact numerical values of the electrical and mechanical delay measurements at a single location cannot be compared, and 2) each patient has a different reference, so mechanical (or electrical) measurements cannot be compared between patients. As a result, the correlations between electrical and mechanical delays were performed in each patient individually.

4.2.9 Reproducibility of Electrical Delay Times

To evaluate how robust our methodology is, we assessed inter-observer reproducibility of the methods used. We have previously computed the inter-observer reproducibility of our MR-based method in Chapter 3. To determine the reproducibility of our method used to derive electrical delay times from local EGMs, we had two blinded observers identify the peak-to-peak differences between the RV and LV EGMs. We computed the correlation

Table 4.1: Relationship Between Electrical and Mechanical Delay Times

	Patients	**Correlation (R^2)**	**Correlation Range**	**Trendline Slope**
LBBB	7	0.83 ± 0.25	0.35 – 1.00	1.35 ± 1.22
IVCD	2	0.88 ± 0.03	0.86 – 0.91	1.51 ± 0.43
RBBB	1	0.95	N/A	4.11

Patient-specific correlation values between electrical and mechanical delay times for various QRS morphologies.

between the two observations as well as performed Bland Altman analysis [167].

4.3 Results

Ten consecutive patients enrolled for CRT underwent a CMR examination and multi-site EGM acquisition during the CRT device implantation procedure. Seven patients presented with left bundle branch block (LBBB), two with inter-ventricular conduction delay (IVCD), and one with right bundle branch block (RBBB). Mechanical and electrical delay times were sampled at a total of 35 potential pacing sites (14 anterolateral, 11 posterolateral, and 10 anterior) within the coronary veins of the ten patients. All patients had at least 3 locations measured.

Correlation values (R^2) between electrical and mechanical delay times on a per-patient basis were 0.85 ± 0.21 (0.35 – 1.00). Correlation values for all QRS morphologies can be seen in Table 4.1.

There was a strong linear relationship between electrical and mechanical delay times in all patients. The positive slope of this best-fit line for all patients indicated that as electrical delay increases, the mechanical delay also increases. However the slope and hence the magnitude of this relationship varies from patient to patient (Figure 4.4). The slope of the trendline was 1.66 ± 1.33, indicating that, on average, mechanical delay was greater than electrical delay.

Among the LV EGM sites measured, the segment that had the largest electrical delay also had the largest mechanical delay in all 10 patients. The latest segment was posterolateral in 3 patients, anterolateral in 6 patients, and anterior in 1 patient.

From our reproducibility analysis of our method for measuring electrical delay times,

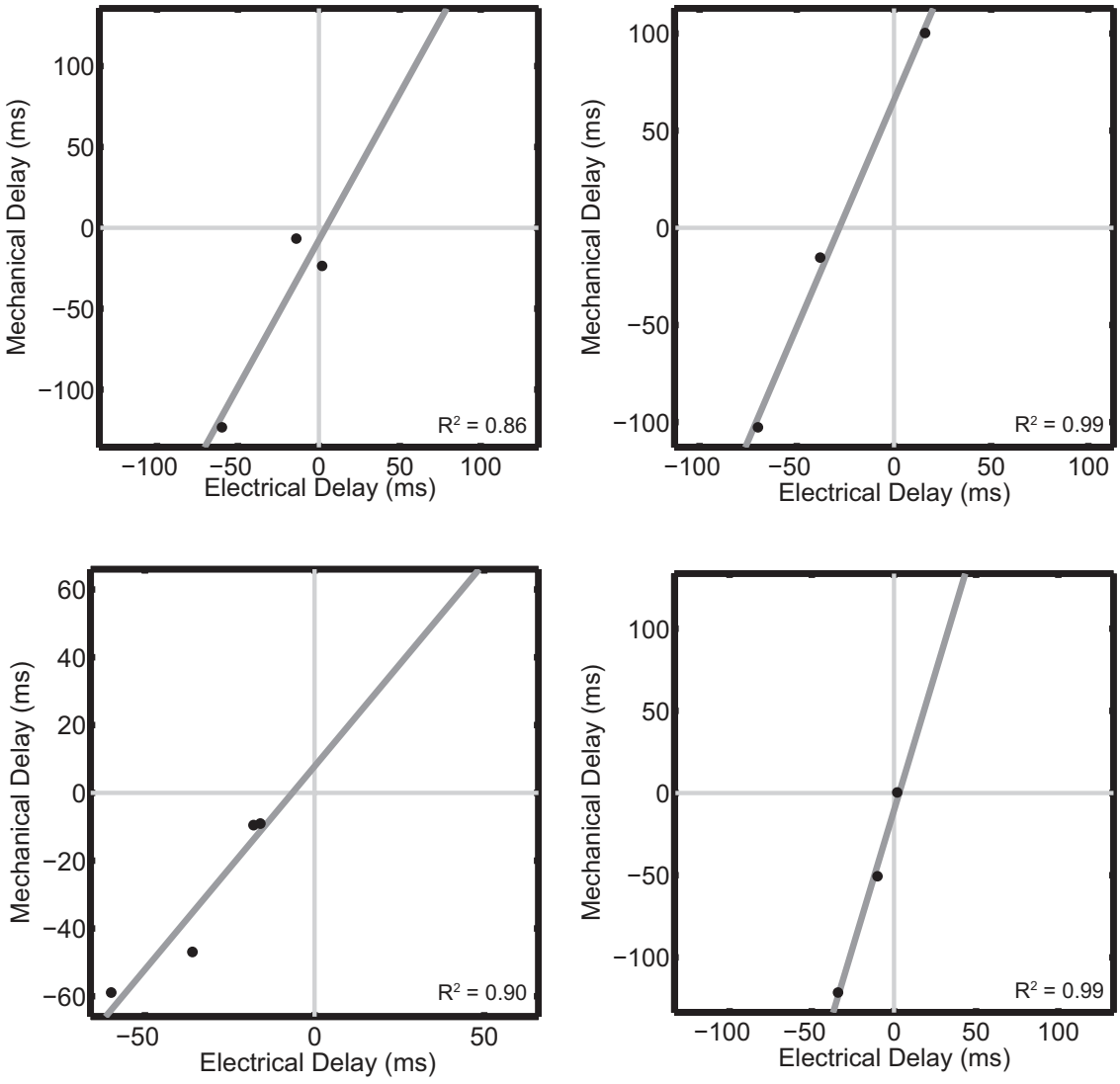

Figure 4.4: Linear trendlines between electrical and mechanical delay times in representative patients. All trendlines exhibited high and positive correlation values.

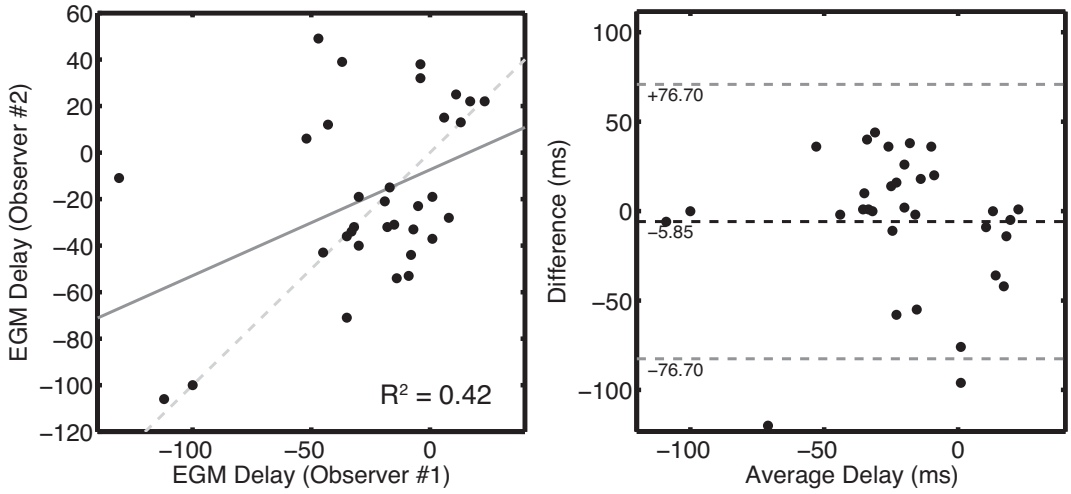

Figure 4.5: Inter-observer agreement for determining the electrical delay time between EGMs obtained at LV and RV pacing sites. Correlation between observers (left) and Bland Altman analysis (right) were computed for all electrical delay times across all patients.

we found the correlation between observers to be R = 0.65. Additionally, there was a bias of -5.85 ms with a confidence interval of -82.6 – 70.9 ms. (Figure 4.5).

4.4 Discussion

The main findings of this study were: 1) there was a strong correlation between electrical and mechanical delay times measured at potential pacing locations within the coronary veins; 2) the relationship between electrical and mechanical dyssynchrony varied greatly between patients, but was always positive; 3) the site with the largest electrical delay was the same site with the largest mechanical delay in all patients; and 4) the latest activated and contracting site is often not the posterolateral wall.

4.4.1 Previous Studies

A number of studies have measured the electromechanical delay in the LV, however, most have utilized animal or computational models for their analysis [184–186,190,191]. Regional analysis has shown that the temporal delay between electrical activation and the onset of shortening varies depending upon location in the LV [186]. In a computational model of the canine heart, Usyk et al. found that there was no direct correlation between electrical activation time and the onset of shortening. There were several cases where the EMD

was positive, indicating that mechanical contraction actually occurred prior to electrical activation [191]. Other canine studies have also shown that mechanical activation follows electrical activation with a non-fixed delay which could result in a poor correlation between the two variables [185, 186]. In models of LBBB, this variation in electromechanical delay is attributed to the requirement that the late lateral wall has to overcome the higher dP/dt values due to early septal contraction [185]. Biventricular pacing results in a decreased and more consistent EMD, but this is not always accompanied by acute improvement in LV ejection fraction or QRS duration [184].

4.4.2 Correlation between Electrical and Mechanical Delays

Our study showed a strong correlation between electrical and mechanical delay times at different sites within the LV. We employed a method that utilized the entire radial contraction curve in an attempt to characterize LV dyssynchrony rather than just using a single time point measuring the onset of shortening to determine mechanical contraction time. Additionally, we only utilized potential pacing sites located throughout the coronary sinus. Had we considered locations within the septum, it is possible these data points would not agree with the previously-stated trend.

The slope of the fit to the plot of mechanical vs. electrical delay time provides a measure of the type of relationship between the two. Not only was there a strong linear relationship between electrical and mechanical delay times at the sampling locations, but the relationship was always positive, indicating increasing electrical delay results in an increased mechanical delay. A larger slope indicates a longer mechanical delay for a small electrical delay whereas a slope less than one implies that even large electrical delays do not result in substantial mechanical delays. Delay times were only compared between sites within each patient. It is important to note that although there was a consistent positive relationship between the two, the slope values were 1.6 ± 1.3 (Range: 0.06 – 4.11) therefore the relationship between electrical and mechanical delay times was very dependent upon the individual.

Previous studies have come to a wide range of conclusions regarding whether pacing the latest electrical or mechanical activated site improves response to CRT [46, 91, 183, 184]. A

variety of modalities have been used to assess both electrical and mechanical dyssynchrony in the LV. Several studies have demonstrated that pacing in the latest contracting segment results in improved CRT response [46, 90–92] by employing electro-anatomical mapping of the left ventricle to measure endocardial electrical activation throughout the entire LV [183, 185]. Tse et al. found that pacing at the latest activated region in the posterior and lateral wall of the LV resulted in improved acute global response [183]. In Russell's canine study, however, electrical activation patterns and QRS duration correlated poorly with global measures of LV function [184]. The mixed results from these previous studies could be accounted for by the heterogeneity amongst individuals that we observed in this study.

In our current study, only epicardial electrical activation was measured with the LV pacing lead. The current approach for LV lead placement involves epicardial placement of the lead via the coronary veins, therefore identification of the latest electrical region in the entire LV is not as important as finding the latest site that is accessible via the coronary sinus and its tributaries, unless surgical epicardial lead placement is being considered. Our analysis showed very good agreement between the latest electrically activated site measured by EGM and the MR-derived mechanical data. Therefore, either electrical or mechanical delay times can be used for optimizing CRT LV lead placement. We found that by analyzing only potential pacing sites, there is a strong correlation between electrical and mechanical delay times.

4.4.3 Patients with Little to No Dyssynchrony

In several patients, both electrical and mechanical delay times were very small indicating no dyssynchrony. This may mean we did not acquire an EGM in an area with delayed electrical or mechanical activation. For example, in one LBBB patient who had a particularly poor correlation value ($R^2 = 0.35$), there were 3 sampling sites located in posterolateral, anterolateral, and anterior segments. The mechanical delay times amongst these sites ranged from -2 to 26 ms, while the electrical delay times ranged from -2 to 6 ms. Both of these ranges are small relative to the temporal resolution of either modality, therefore resulting in a potentially inaccurate correlation between the two measurements. If you exclude this

patient from analysis, the average correlation value for LBBB patients rises to 0.91.

4.4.4 Reproducibility of Electrical Delay Times

Reproducibility analysis showed that there was a correlation (R) of 0.65 between the electrical delay times obtained by two independent observers. There was a negligible bias between the two observers and 95% confidence interval was within an acceptable range, as the range of electrical delays was larger than the width of the confidence interval. There are several potential reasons for the poor correlation between the two observers. First, the EGM was acquired over 20 heartbeats, and the electrical delay time often changed with every beat. The representative delay was chosen by the observers; however, this adds some subjectivity to the measurement. Another potential source of error is that with the time-to-peak method used to assess electrical delay, the activation spike must be visible in both EGMs. In some cases there were multiple peaks, or the measurement was too noisy to correctly identify the peak corresponding to the electrical activation.

4.4.5 Unexpected Results

There were two patients with very low slope values (0.07 and 0.23) but with good correlation values (0.83 and 0.98, respectively). In these patients, a large electrical delay time yielded relatively constant mechanical delay times (Figure 4.6). Using computation models, it has been reported that mechanical contraction can occur prior to epicardial breakthrough of the electrical activation front [191]. This phenomenon would manifest itself as a small mechanical delay time for a large electrical delay since we are measuring electrical activation at the epicardial surface.

4.4.6 Limitations

Instead of measuring onset of shortening, our method computes the mechanical delay by comparing the entire radial contraction curve of a segment to the patient-specific reference. This means that a patient may have a slow radial contraction of the myocardium in a particular region despite having an early onset. The advantage of this method is that we can determine the timing of the true contraction of the segment relative to the rest of the

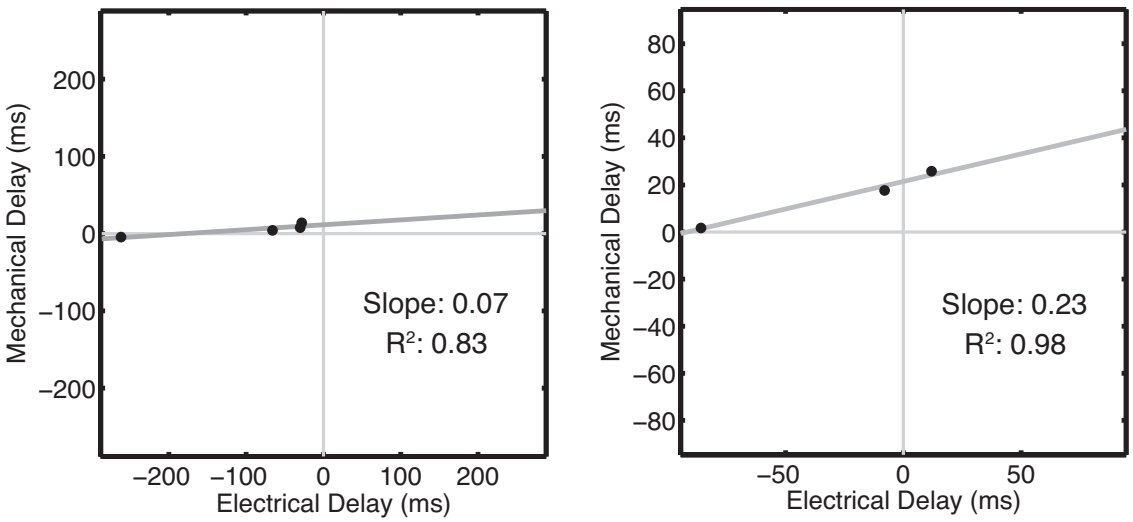

Figure 4.6: In several instances, very large electrical delays were measured; however, the mechanical dyssynchrony measured by MRI was only affected slightly.

LV; however, our method may be incapable of detecting early inward motion of the septum but rather identifies the later thickening of the septal wall.

We only have an average of 3.5 measurement locations per patient, resulting in an obviously low sampling density. This would be difficult to improve due to extra time and radiation required for additional data points. Effort was made to sample a wide range of regions in each patient to compensate for this limitation.

4.5 Conclusion

In this study, we found that there is a strong positive correlation between electrical and mechanical delay times in the LV pacing sites accessible via the coronary veins. Although the latest electrical region always corresponded with the latest mechanical region, the relationship between electrical and mechanical delay times throughout the coronary sinus varied greatly among patients. This study provides initial evidence that pacing guided by non-invasive mechanical activation patterns targets the electromechanical substrate of intraventricular dyssynchrony

4.6 Major Findings

- There was a strong correlation between electrical and mechanical delay times measured at potential pacing sites within the coronary veins
- The relationship between electrical and mechanical activation varied greatly between patients
- The latest contracting segment always corresponded to the latest activated segment

CHAPTER V

MAGNETIC RESONANCE IMAGING AND RECONSTRUCTION OF THE CORONARY VEINS

Adapted from "Time-Resolved Analysis of Coronary Vein Motion and Cross-Sectional Area," by Jonathan D. Suever, Pierre J. Watson, Stamatios Lerakis, Robert E. O'Donnell, and John N. Oshinski. 2011, J Magn. Reson. Imaging, Vol. 34(4), pp. 811-5.

The purpose of this work was to create a method to reconstruct the coronary vein anatomy from a 3D whole heart MR coronary vein scan. By overlaying coronary vein anatomy with measures of regional mechanical dyssynchrony and myocardial infarction, it is possible to determine the ideal LV pacing site prior to CRT device implantation. We were able to successfully image the coronary veins using a slow infusion of Gadolinium and the quality was sufficient to successfully create 3D reconstructions of the coronary vein anatomy.

5.1 Introduction

Coronary vein anatomy plays a critical role in planning treatment for patients undergoing cardiac resynchronization therapy (CRT). The LV pacing lead is placed within the coronary sinus and its tributaries and paces the epicardial surface of the lateral wall of the left ventricle. Traditionally, implanting electrophysiologists have favored the lateral, posterolateral, or anterolateral cardiac vein based on positive response observed in large patient cohorts [101]. In addition to targeting a specific region, the final LV pacing site is selected to prevent phrenic nerve stimulation and allow for lead stabilization [104, 105].

There is a growing amount of research suggesting that both the degree of mechanical dyssynchrony and amount of myocardial scar at the LV pacing site affects a patient's response to CRT [16, 40, 87, 93, 96–99, 192, 193]. Currently, the potential pacing sites for a

patient are not assessed prior to a contrast-enhanced coronary venous angiogram obtained at the beginning of the implantation procedure. Pre-implantation assessment of coronary vein anatomy, mechanical dyssynchrony, and myocardial scar, would allow the clinician to determine the possible target veins and effectiveness of these sites prior to device implantation. All of these factors can be assessed using MRI.

Traditionally, magnetic resonance angiography (MRA) has focused on imaging of the coronary arteries; however, interest in improving CRT response has encouraged the development of new techniques for visualizing the coronary veins [127]. Magnetic resonance coronary venograms (MRCV) are often 3D whole heart scans to provide complete visualization of the coronary sinus and its tributaries. This amount of data cannot be obtained within a single breath hold, so they must utilize both respiratory and cardiac gating [194]. Navigator-echo based respiratory gating allows free breathing during acquisition, but at the penalty of lengthening the total acquisition time. As a result, a 3D whole heart coronary vein acquisition can take up to 10 minutes. Acquisition time often increases in patients with breathing difficulties such as those with advanced heart failure.

There are two primary techniques for imaging the coronary veins: non-contrast and contrast-enhanced MRCV. Similar to a method used to image the coronary arteries, a non-exogenous contrast imaging sequence utilizing magnetization transfer contrast (MTC) can be used to image the coronary veins [127]. MTC takes advantage of the transfer of magnetization between water and protons located within the myocardium [195, 196]. By saturating the myocardial protons, it is possible to null the signal from the myocardium, while the signal from the blood pool, and thus the coronary veins, remains unchanged. Combining the MTC preparatory sequence with a 3D gradient echo protocol yields the best visualization of the coronary vein anatomy [127].

Another approach to coronary vein imaging is to utilize a Gd-chelate-based T1-shortening contrast agent. After injection of the contrast agent, the concentration in the blood remains higher than that in the myocardium, providing contrast between the coronary veins and the myocardium. Ideally, an intravascular contrast agent is used to provide maximum

myocardial/blood contrast throughout the duration of the lengthy whole-heart acquisition [132–134]. For patients requiring LGE imaging, however, an extracellular contrast agent must be used to allow contrast to leave the vasculature and diffuse into the myocardium and infarct. Consequently, the contrast between the myocardium and blood is decreased, diminishing the visibility of the coronary veins. Several groups have compensated for this limitation by performing a slow infusion of extracellular contrast agent resulting in extended periods of elevated gadolinium contrast [125,136,137]. This plateau of heightened contrast improves coronary vein visibility in whole heart acquisitions. In general, it is best to use contrast-based methods of coronary visualization because they yield better SNR and CNR compared to non-contrast techniques [128].

Another challenge when imaging the coronary vessels is that they are directly affected by cardiac motion. To reduce the effects of cardiac motion on these coronary vein scans, it is desirable to acquire image data only during periods of low vessel motion, typically assumed to be during mid-diastole [197–199]. Using the temporal low motion period, the trigger delay can be set for MRCV acquisitions, and the duration of the low motion period can be used to set the width of the acquisition window. By determining the location and duration of the quiescent period of the coronary veins in CRT patients, it is possible to minimize coronary vein acquisition times and reduce artifacts from cardiac motion.

By utilizing slow contrast injection and characterizing the motion of the coronary veins in CRT patients, we aim to develop an acquisition protocol that minimizes acquisition time and maximizes the SNR of the coronary veins. Additionally, by developing a means to visualize the position of the coronary veins relative to relevant dyssynchrony and scar information, it is possible to provide electrophysiologists with a tool to determine the ideal LV pacing site prior to device implantation.

The purpose of this chapter was to understand coronary vein motion to improve MR imaging of the coronary veins and allow for 3D reconstruction of the coronary vein tree, which could assist with treatment planning for CRT patients. The study consisted of two parts. The first part of this study determined the location and duration of the stationary period of the coronary veins in CRT patients to improve MRCV. The displacement of the

coronary veins was compared to patients with coronary artery disease (CAD). The second part applied the MRCV technique in a group of patients undergoing CRT and reconstructed the coronary vein anatomy.

5.2 Methods

5.2.1 Coronary Vein Motion Analysis

5.2.1.1 Patients

Thirty-three patients in two separate groups were studied. Twenty of the 33 patients had coronary artery disease (CAD) with a documented myocardial infarction (MI) at least 6 months prior to exam (age: 56.2 ± 12.2 years). These represent those typically included in coronary artery motion studies. Thirteen patients (age: 60.9 ± 12.2 years) were scheduled for CRT, having been classified as New York Heart Association (NYHA) Class III heart failure with QRS duration > 120 ms and ejection fraction (EF) < 35%.

5.2.1.2 Coronary Vein Motion Analysis Image Acquisition

For this study, all subjects underwent a complete cardiac MR exam. Motion analysis was performed on SSFP cine images acquired in the vertical long-axis (two-chamber) orientation with 30 frames over the cardiac cycle (R-R interval) on a Siemens Avanto 1.5T Scanner (Siemens Medical Solutions, Erlangen, Germany) or a Philips Intera 1.5T Scanner (Philips Medical Systems, Best, The Netherlands) (Figure 5.1). Retrospective EKG gating was used in all acquisitions. Acquisition parameters were: acquired matrix size = 192 x 156 to 256 x 195, reconstructed matrix size = 192 x 156 to 256 x 256, FOV = 300 x 244 to 48 x 418 mm, flip angle = 65–67, TR = 2.5 – 3.4 ms, and TE = 1.25 – 1.7 ms.

5.2.1.3 Coronary Sinus Tracking

The coronary sinus was tracked under the assumption that its movement is an indicator of overall coronary vein motion [126, 177, 200]. The cross-sectional area and centroid of the coronary sinus were computed for each frame by manual tracing of each vein using in-house software developed in Matlab (The MathWorks, Natick, MA).

To determine low-motion periods, a variant of the quality threshold (QT) clustering

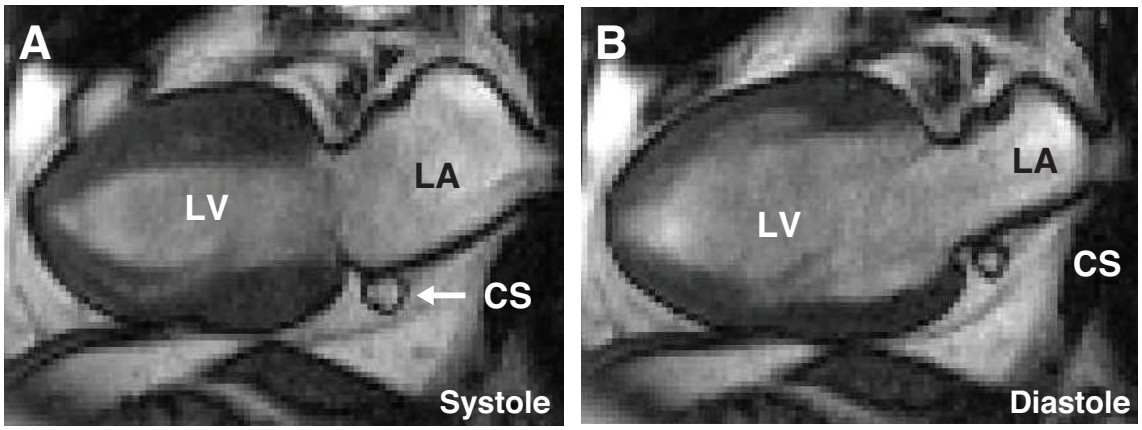

Figure 5.1: Two-chamber (VLA) images of the left ventricle where the position and size of the coronary sinus are easily discernible

algorithm was employed (Appendix D) [165]. In this analysis, the location of the centroid of the coronary sinus was compared across all phases of the cardiac cycle. Consecutive time points were concatenated until the cluster exceeded the pre-defined maximum diameter threshold. For our analysis, we used a cutoff of 0.67 mm, the pixel spacing used in our whole-heart coronary vein scan. Using this approach, we were able to identify periods over which the vessel translated less than a pixel in any given direction (Figure 5.2).

5.2.1.4 Coronary Vein Motion Classification

The temporal location and duration of the periods of low motion were determined as a percent of the cardiac cycle (%CC). The low motion periods were classified as either systolic or diastolic low motion periods based on their temporal location. Systolic low motion periods were defined as any low motion period that began before the onset of left ventricular relaxation. Diastolic low motion periods were defined as any low motion period that began after the smallest left ventricular volume was reached. Each patient was classified into either systolic dominant or diastolic dominant based on the ratio of each patient's systolic to diastolic low motion period duration. Patients with a ratio greater than or equal to one (systolic low motion period duration $\geq$ diastolic low motion period duration) were classified as systolic dominant and those with a ratio less than one were classified as diastolic dominant. The ejection fractions of the systolic and diastolic dominant groups were compared using a two-sample, unequal variance t-test. The temporal location for both the low motion

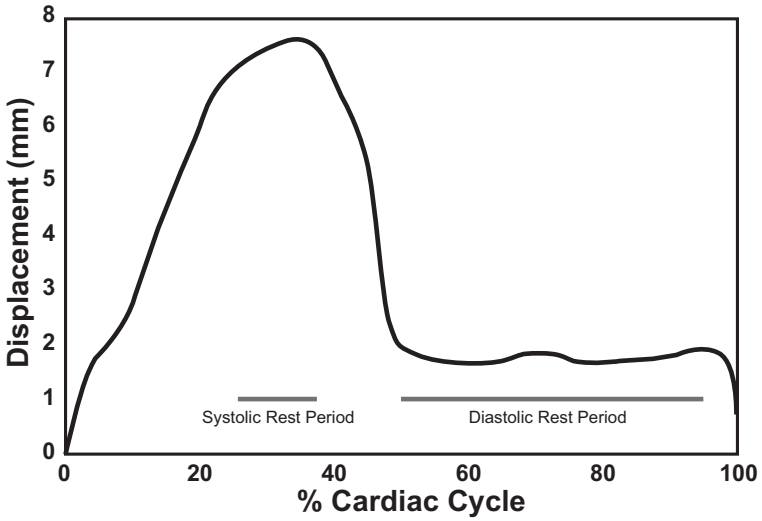

Figure 5.2: The coronary sinus can displace significantly over the cardiac cycle. In a healthy subject, there are low periods of motion during both systole and diastole during which MRCV imaging can be performed.

periods was calculated to determine the variability in onset times and duration for the two periods.

The average cross-sectional area of the coronary sinus over the cardiac cycle was determined. The difference in cross-sectional area between systolic low motion and diastolic low motion was compared for each vessel using a paired t-test to determine whether cross-sectional area was significantly larger in either low motion period. A larger cross-sectional area of the coronary sinus would result in increased coronary vein visibility.

5.2.2 Coronary Vein Imaging

The second part of this study used the data regarding the location and duration of the stationary period of the coronary sinus in CRT patients to specify parameters for coronary vein imaging.

5.2.2.1 Magnetic Resonance Coronary Venography

Coronary Vein imaging was performed in a total of nine patients who were enrolled for CRT and met the standard criteria (NYHA HF class III-IV, QRS Duration > 120 ms, EF $< 35\%$, optimal medical therapy for 3 months).

Imaging was performed on a combination of 1.5T and 3T systems (Siemens Medical

Solutions, Erlangen, Germany; Philips Medical Systems, Best, The Netherlands). A 3D whole-heart contrast-enhanced scan was used to visualize coronary vein anatomy. After a standard set of localizers in three principal planes, coronary vein images were acquired in the transverse plane, as opposed to the short-axis orientation, due to the improved ability to track the coronary vein branch points.

5.2.2.2 Contrast Injection Scheme

A double dose (0.2 mmol/kg body mass) of extracellular Gd-chelate contrast agent, Gadobenate dimeglumine ($[\text{Gd-BOPTA}]^{2-}$, MultiHance; Bracco Imaging SpA, Milan, Italy), was administered intravenously. Instead of the typical bolus injection, Gd-BOPTA was injected at a rate of 0.3 mL/s followed by the injection of 20 mL of saline at the same rate. The whole heart MRCV protocol was initiated 15 seconds after injection began [125, 136].

5.2.2.3 MRCV Pulse Sequence

For our coronary vein imaging protocol, we employed a 3D whole-heart Turbo Fast and Low Angle Shot (TurboFLASH) sequence, which has been applied successfully in coronary artery imaging [136]. This is a fast gradient echo sequence that utilizes an inversion-recovery (IR) 180° pre-pulse to effectively null the signal from the myocardium, increasing the contrast between the coronary veins and the surrounding myocardium. An inversion time of 200 ms was selected based on the approximate T1 value of the myocardium throughout the duration of the scan. Fat saturation was used to further improve coronary vein SNR. Centric-ordered k-space sampling was used to acquire central k-space data during the highest intravascular contrast seen following injection. Additional imaging parameters were: TE = 1.5 ms, FOV = 247 x 330 mm, acquisition matrix = 173 x 256, slice thickness = 0.75 mm, flip angle = 15°.

5.2.2.4 Respiratory Gating

Due to the long acquisition time, free breathing was required so the 3D whole-heart scan used a navigator-echo for respiratory gating. Briefly, a navigator-echo is a one-dimensional MR acquisition positioned at the interface between the diaphragm and the lung using a 2D

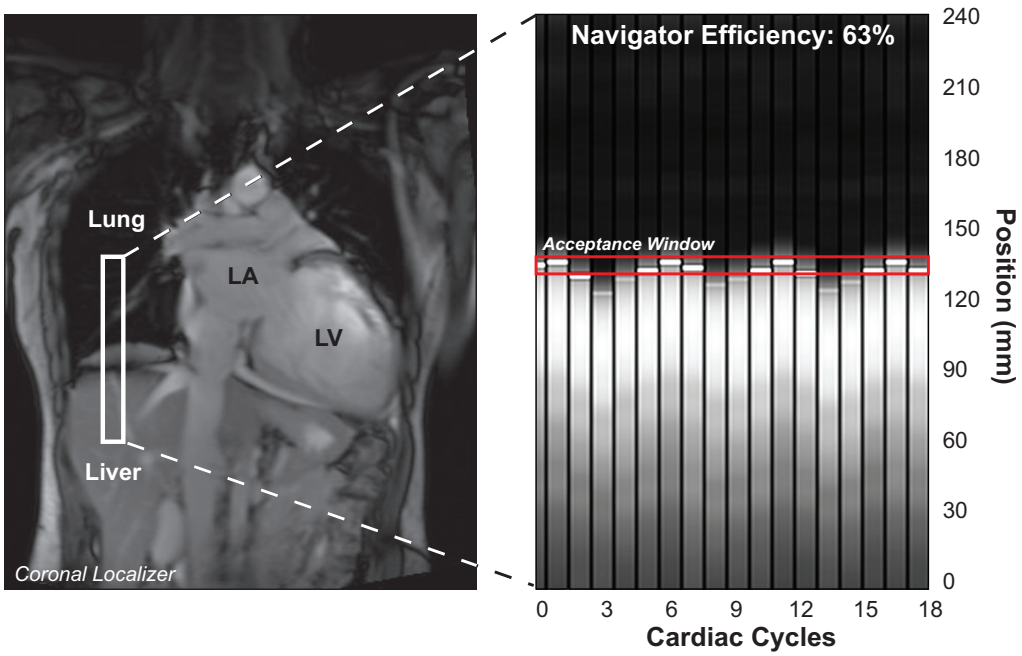

Figure 5.3: A Navigator echo is a selective pulse that images the interface of the liver and lung (left). Images are only acquired if the diaphragm is within the prescribed 5 mm acceptance window (right).

selective RF pulse (Figure 5.3) [201]. By tracking the location of this interface, it is possible to estimate foot-head motion during the course of a cardiovascular MRI acquisition [202]. By applying this navigator-echo with each TR, it is possible to ensure that all data is acquired during the same respiratory phase. For our imaging, we specified a 5 mm acceptance window to obtain reasonable navigator efficiency and good image quality (Figure 5.3).

5.2.2.5 Cardiac Gating

As with any cardiac scan, EKG gating is necessary to prevent motion artifacts arising from cardiac motion. Retrospective cardiac gating was used for all coronary vein imaging. A trigger delay was set based on our findings regarding coronary vein motion over the cardiac cycle. The acquisition period was adjusted for patients based on the length of their quiescent period (Figure 5.4).

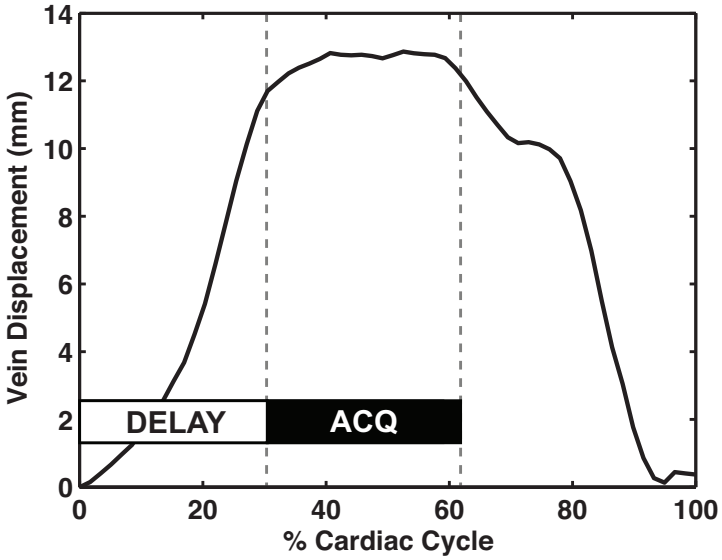

Figure 5.4: Images are only acquired during the stationary period of the coronary veins. The start of the acquisition window (DELAY) and the length of the acquisition window (ACQ) are determined by the location and duration of the rest period.

5.2.2.6 Coronary Vein Segmentation

Images were exported from the MR scanner as DICOMs and imported into custom software written using Matlab (The Mathworks, Natick, MA). The coronary sinus was identified using the connection with the right atrium at the coronary sinus orifice (Figure 5.5 A). From this point, the user placed seed points located within the coronary sinus (Figure 5.5 C). The user identified the coronary sinus and its branching vessels throughout the image stack (Figure 5.5 D). Care was taken to ensure that the selected vessels were the coronary veins and not the neighboring coronary arteries.

5.2.2.7 Three-Dimensional Coronary Vein Anatomy Reconstruction

The user-selected seed points were transformed for each image into 3D coordinates using orientation information stored in the DICOM header (Appendix C), resulting in a cloud of 3D points (Figure 5.5 E). To create a mesh from the 3D point cloud, we generated an alpha-shape (α-shape) (Appendix F) of all the selected vein points (Figure 5.6). Briefly, an α-shape creates a shape from a cloud of points using a constrained Delaunay triangulation.

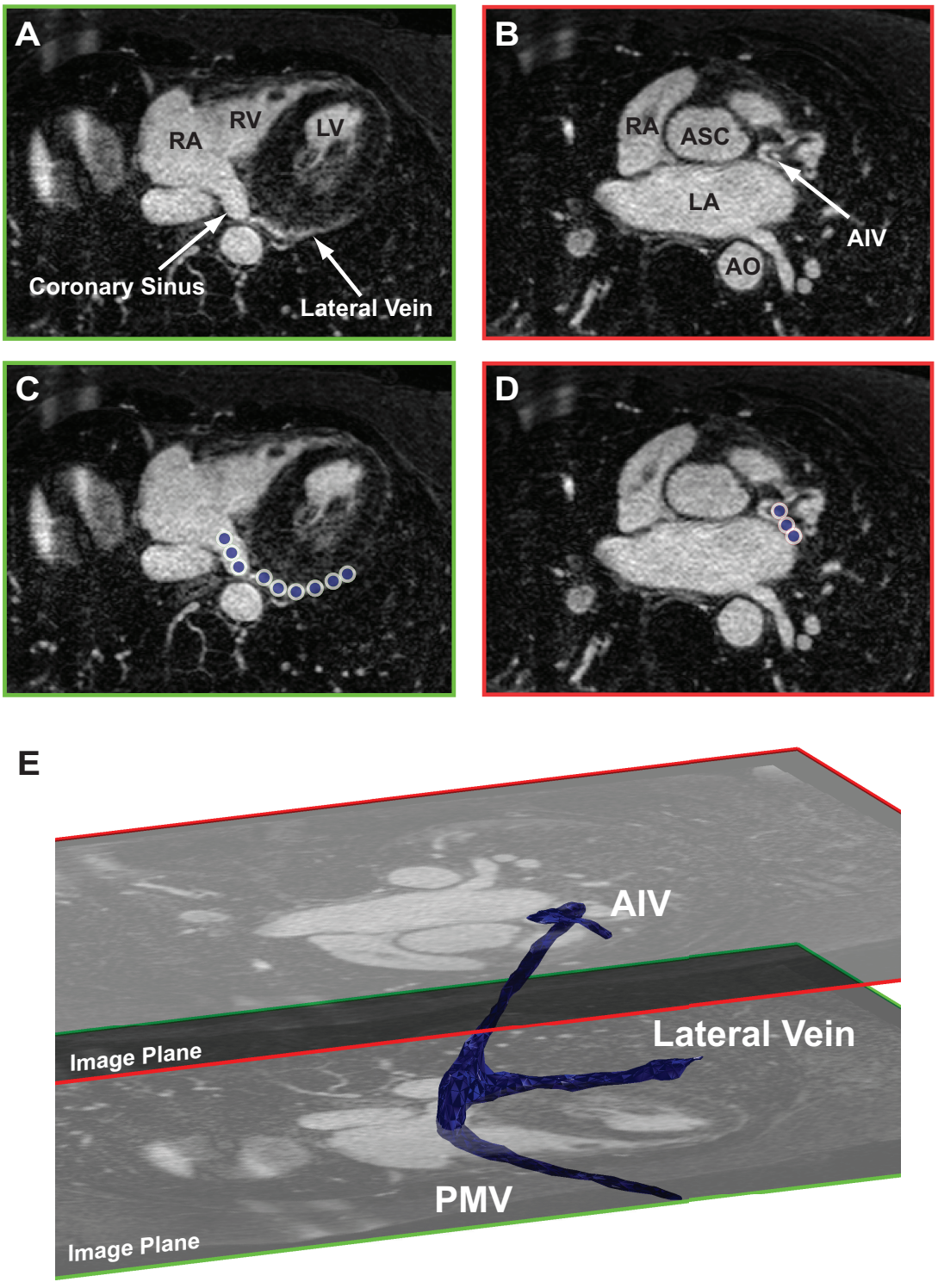

Figure 5.5: Due to the high contrast of the coronary veins, the coronary sinus is readily identified by the ostium (A) and the location of the coronary veins can be followed as they branch off of the great cardiac vein (B). Veins are identified by user-defined points (C and D), which can then be mapped to three-dimensions (E) using DICOM position information.

The constraint, α, is a limitation on the size of each face of the solution. Using this method, it is possible to generate complex three-dimensional reconstructions from point clouds [203]. For this work, a default α value of 4 mm was selected based on the slice thickness as well as expected coronary vein radius. The resulting triangulation was smoothed using a curvature flow-based method [204].

5.2.2.8 Coronary Vein Anatomy Display

Using the 3D mesh of the coronary veins obtained from the α-shape analysis, it is possible to display the vein reconstruction alongside 3D reconstructions of the endocardial and epicardial surfaces (Figure 5.7). Additionally, using the central axis of the left ventricle (Section 3.2.4), it is possible to project this 3D mesh onto the AHA 17-segment model. As we have shown previously, the AHA 17-segment model can be used to display regional functional measures of cardiac function including mechanical dyssynchrony and myocardial infarction. In this way, it is possible to visualize the location of the coronary veins relative to the dyssynchronous regions and infarct distributions (Figure 5.8).

5.3 Results

5.3.1 Coronary Vein Motion

The coronary sinus was well visualized in the two-chamber vertical long-axis cine images in all patients. Nineteen of the 32 patients (59%) were classified as systolic dominant and 13 (41%) were diastolic dominant. All 13 CRT-scheduled patients (100%) were systolic dominant. Thirteen of the 19 (68%) CAD patients were diastolic dominant. Typical displacement curves for the systolic dominant CRT patients and diastolic dominant CAD patients can be seen in Figure 5.9. In the systolic dominant group, the center of systolic low motion occurred at 46.6 ± 8.2 %CC with a duration of 12.6 ± 5.4 %CC (98.7 ± 41.1 ms). Six of the 19 (32%) systolic dominant patients had no separate diastolic low motion period. Either the diastolic low motion period was completely absent or combined with the systolic low motion period. The diastolic dominant group had a diastolic period of low motion located at 73.1 ± 3.9 %CC with a duration of 20.0 ± 4.9 %CC (168.3 ± 48.7 ms). The systolic low motion occurred at 35.6 ± 5.2%CC with a duration of 7.6 ± 1.6 %CC (62.6 ± 12.2 ms).

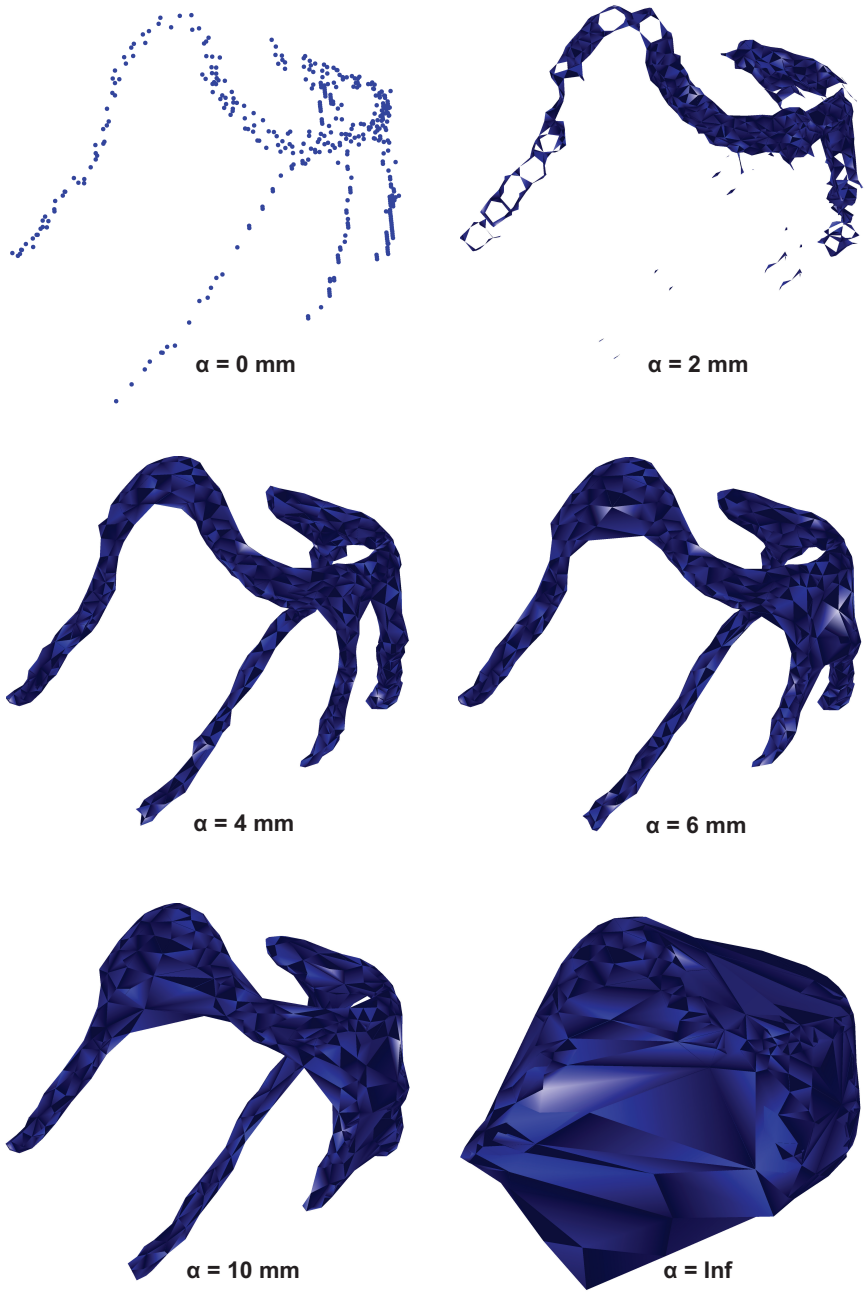

Figure 5.6: Alpha shapes generate a three dimensional mesh from a cloud of points using a constraint (α) on the size of a face in the Delaunay triangulation of the point-cloud. Small alpha values preserve local detail while no constraint (Inf) leads to a convex hull. We selected an alpha value of 4 mm.

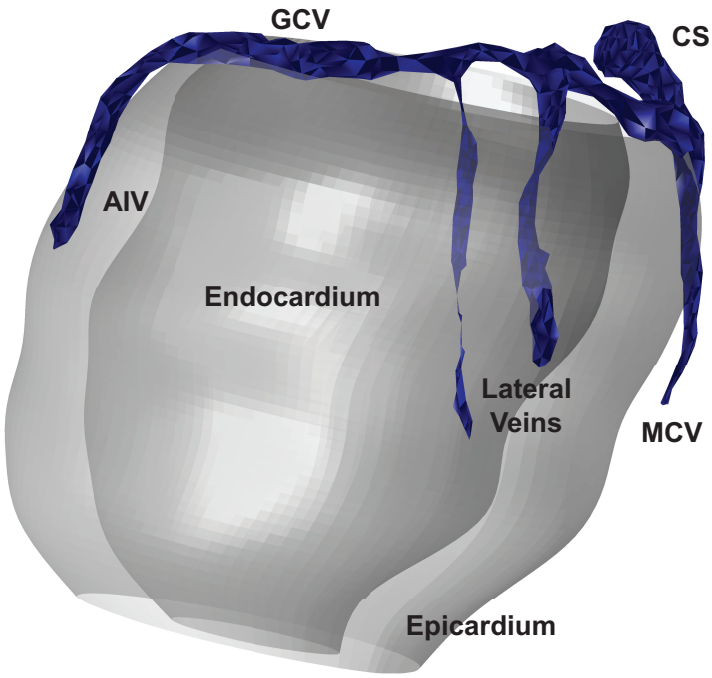

Figure 5.7: Due to the use of a single imaging session for assessment of all factors, the 3D reconstruction of the coronary veins can be combined with geometry and functional data.

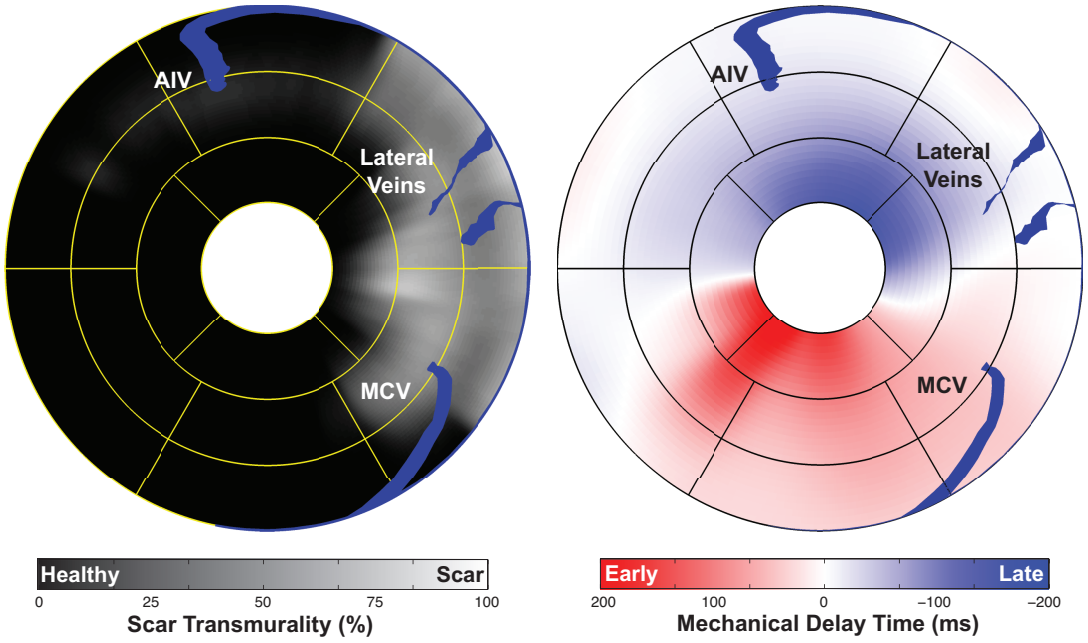

Figure 5.8: Using the central axis of the left ventricle, it is possible to project the coronary vein reconstruction onto the AHA 17-segment model and maps of myocardial infarction (left) and regional dyssynchrony (right).

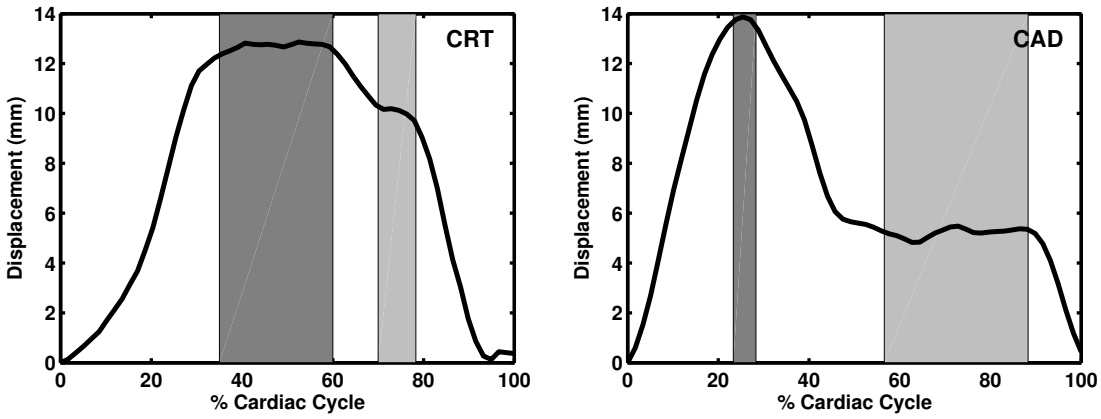

Figure 5.9: Representative displacement of the coronary sinus over the cardiac cycle in CRT (left) and CAD (right) patients. Coronary vein rest periods are denoted by the shaded regions. Note the long systolic rest period in CRT patients and the long diastolic rest period in the CAD patient.

All (100%) patients with an EF less than 35% were systolic dominant and all (100%) patients with an EF greater than 35% were diastolic dominant ($p < 0.001$) (Figure 5.10). The EFs for the systolic dominant group were $21.7 \pm 7.8\%$ and for the diastolic group were 53.6 ± 10.8 % ($p < 0.001$). The heart rates were 76.9 ± 11.4 beats per minute (bpm) for the systolic group and 72.5 ± 7.3 bpm for the diastolic groups ($p = 0.2$). Therefore, cardiac cycle length was not significantly different between the two groups.

5.3.2 Coronary Sinus Cross-Sectional Area

Six of the 19 systolic dominant patients (32%) had no diastolic low motion period and were therefore excluded from the percent change in cross-sectional area calculations. In 20 of the 26 patients (77%) with both systolic and diastolic rest periods, the cross-sectional area was larger during the systolic low motion period than during the diastolic low motion period (60.1 ± 21.5 mm^2 vs. 43.7 ± 22.6 mm^2, $p < 0.001$). Three of the diastolic dominant patients (23%) and 3 of the systolic dominant patients (16%) had a smaller coronary sinus diameter in systole compared to diastole. Of the 13 systolic dominant patients, the area change was 18.6 ± 16.2 % with 3 having larger area during diastole than during systole. The diastolic dominant group showed significantly more change (46.8 ± 29.6 %) in cross-sectional area ($p = 0.006$) (Figure 5.11).

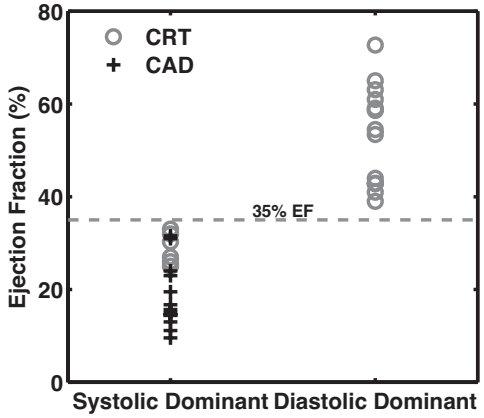

Figure 5.10: Patients were classified as either systolic or diastolic dominant based upon which rest period had a longer duration. It was found that an EF less than 35% had 100% specificity for identifying patients with a systolic rest period, regardless of etiology.

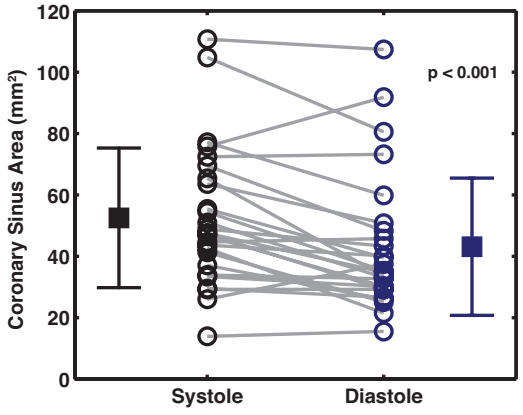

Figure 5.11: Area of the coronary sinus during the systolic and diastolic rest periods in all patients. There was a slightly larger CS area during the systolic rest period.

5.3.3 MRCV Image Acquisition in CRT Patients

Three-dimensional whole-heart coronary vein scans were acquired in nine patients. Acquisition delay times were set to coincide with the systolic rest period as determined in the previous part of this work. The length of the acquisition window was manually defined for each patient by looking at the motion of the coronary sinus in the VLA images.

5.3.4 Three-dimensional Reconstruction of Coronary Vein Anatomy

Three-dimensional reconstructions were successfully created for 9 patients. An α value of 4 mm was determined to be ideal to create acceptable reconstructions across all patients. Representative coronary vein reconstructions are shown in Figure 5.12.

5.4 Discussion

The major findings of this study were: 1) 100% of patients scheduled for CRT had a longer systolic rest period, 2) 100% of patients with an EF less than 35% were systolic dominant, 3) In 77% of subjects, the cross-sectional area of the coronary sinus is larger in systole than in diastole, 4) It was possible to identify the coronary veins using the slow infusion of contrast and the appropriate quiescent period, 5) A three-dimensional mesh could be generated and mapped to the AHA 17-segment model in CRT patient.

5.4.1 Coronary Vein Motion

Despite previous studies stating that scanning during diastolic low motion is most beneficial for imaging coronary vasculature [199], all of the subjects scheduled for CRT were systolic dominant and therefore scanning them during diastole would result in more motion artifacts or smaller optimal acquisition windows. For the systolic dominant patients, beginning a scan during systole instead of during diastole would allow a longer temporal window with low motion and would allow a reduced scan time. However, there was a large variability in systolic duration between patients particularly in the systolic dominant group.

The EF of patients was observed to be a significant predictor ($p < 0.001$) of their low motion period classification. All of the CRT scheduled patients had an EF less than 35% as required for this treatment, and all of them were classified as systolic dominant. The only

Figure 5.12: Coronary vein anatomy from nine patients using user-defined points and α-shapes for 3D reconstruction.

CAD patient with an EF less than 35% was classified as systolic dominant. A patient's EF could potentially be used to determine which low motion period should be used for minimal motion artifacts.

The large variability in the length and position of the low motion periods in this patient population suggests that each patient should be imaged to determine a patient-specific window position and length for MRCV. Of the systolic dominant patients, 21% did not have clearly defined diastolic low motion periods. The subjects without separate diastolic low motion periods typically had very long systolic low motion periods that continued into diastole. These periods were technically both systolic and diastolic low motion because they occurred during both parts of the cardiac cycle but were defined as systolic low motion based on the temporal starting location of the low motion period as mentioned previously.

Analysis of the cross-sectional area difference showed that 93% of subjects had a larger area during systole than during diastole presumably due to increased coronary venous pressure. The coronary sinus is the largest of the coronary veins and collects blood from the ventricular veins during systole and empties into the right atrium causing the vessel to contract during systole and dilate during diastole [205]. Increased atrial and ventricular pressure in end systole at the end of left ventricular ejection causes dilation of the vessel [206, 207].

When analyzing cross-sectional area between the systolic and diastolic dominant groups, it was observed that the diastolic dominant group showed significantly larger percent changes in area over the cardiac cycle than the systolic dominant group. Two of the systolic dominant subjects had larger cross-sectional area during diastole. The combination of larger vessel areas during the systolic low motion periods and the fact that all of the pre-CRT patients had longer systolic low motion periods suggest that systolic imaging would be preferable in obtaining MRCV in pre-CRT patients. Increased cross-sectional areas during systole would improve visualization of the vessel due to its larger size.

5.4.2 Coronary Vein Imaging and 3D Reconstruction

By utilizing the slow injection of gadolinium for coronary vein imaging, we were able to obtain adequate contrast between the coronary veins and myocardium. Unfortunately, due to the proximity of the veins to the coronary arteries and the insufficient contrast between veins and arteries, we were unable to utilize an automated approach for coronary vein segmentation. Manual identification of the coronary veins allows for an accurate representation of true coronary vein anatomy.

We were able to generate 3D coronary vein anatomy from all patients and superimpose this information onto the AHA 17-segment model. Using previously developed methods to detect regional dyssynchrony and myocardial scar distributions within the LV, these factors that affect CRT response can also be mapped to the AHA 17-segment model. With this combined display, it is possible to identify an LV pacing site that has low scar burden, high regional dyssynchrony, and is accessible via the coronary veins.

5.4.3 Limitations

A limitation of this study is that the coronary sinus moves in all three dimensions during the cardiac cycle and therefore the cross-sectional area changes might be due not only to vessel dilation but also to different slice alignments over the cardiac cycle with respect to the vessel. Changes in vessel diameter over the vessel length could be misinterpreted as cross-sectional area changes if the slice plane moves perpendicularly to the vessel.

For coronary vein reconstruction, manual segmentation is time-consuming and requires an expert observer. An automated technique would be ideal. Although the contrast between the coronary veins and myocardium is relatively high utilizing the current imaging sequence, it is not sufficient for automatic segmentation. Additionally, the proximity of the enhanced coronary arteries to the coronary veins could potentially lead to an erroneous inclusion of the arteries in the segmentation result.

α-shapes utilize a global α value, which can limit the ability to detect local features of the point cloud. Ideally, a smaller α value would be employed at more distal regions of the coronary veins while a larger α value would be used for the coronary sinus. Although an

adaptive (or conformal) α-shape, may result in a more-detailed reconstruction, the spatial resolution is not necessary for visualizing the position of coronary veins relative to infarct and dyssynchrony [208].

5.5 Conclusion

The movement of the coronary sinus can be used to classify patients as either systolic dominant or diastolic dominant based on the location of their periods of low motion within the cardiac cycle. All the patients scheduled for CRT and one CAD patient (with an EF $< 35\%$) were classified as systolic dominant and a period of diastolic low motion was not present in several of these patients. The cross-sectional area was observed to be significantly larger during systole than during diastole leading to improved image resolution of the vessel during systole. The temporal imaging location should be not assumed to be during diastole and each patient's low motion periods should be categorized before imaging the coronary veins to ensure the correct period is being utilized to minimize motion artifacts. By utilizing the systolic rest period, we were able to obtain good SNR and sufficient contrast to be able to perform a 3D reconstruction of the coronary veins for display with other MR-derived parameters of cardiac function and viability.

5.6 Major Findings

- The low motion period of the coronary veins in CRT patients with an EF less than 35% always occurred during systole.
- 32% of patients did not actually have a diastolic coronary vein rest period.
- Using a respiratory and EKG-gated contrast-enhanced inversion recovery sequence, we were able to visualize the coronary veins
- Using user-defined seed points, we created a 3D reconstruction of the coronary veins which was projected onto the AHA 17-segment model to assist with CRT treatment planning

CHAPTER VI

DETERMINING LEFT VENTRICULAR PACING LEAD LOCATION

In this chapter, we will develop a method for determining the spatial correspondence between MR and fluoroscopic data. By applying this transformation to post-implant dual-plane images of LV lead location, we can assess MR-derived measurements of mechanical dyssynchrony at the LV pacing lead tip.

6.1 Introduction

Although CRT has been shown to improve quality of life and improve CRT patient prognosis, approximately 30% of patients fail to respond to the treatment [70, 209–211]. In an effort to understand what factors affect an individual's response to CRT and contribute to the 30% non-response rate, an increasing number of studies have concentrated on regional metrics. For example, in some patient groups total scar burden in the LV fails to predict patient response, but the location of the infarcted myocardium within the ventricle does predict response [98, 172, 192]. Specifically, it is thought that the presence of myocardial scar at the location of either RV or LV pacing site results in a worsened prognosis for CRT recipients [172,212]. Similarly, many echocardiographic studies have demonstrated that the suitability of the LV pacing site is dependent upon the degree of regional dyssynchrony at that location [150, 213]. To perform retrospective studies, it is necessary to have an accurate method for mapping the pacing lead location to distributions of dyssynchrony and scar created in other imaging modalities.

Currently, there are several methods used to determine the position of the ventricular pacing leads from radiographic and CT data. The most commonly employed method is Mortensen's o'clock, which uses x-ray projections acquired in RAO and LAO views. The LAO image is assumed to be the short-axis view of the LV while the RAO image is the longitudinal projection. Using these images, the circumferential and longitudinal position of the lead can be determined and then mapped to the AHA 17-segment model (Figure 6.1) [144].

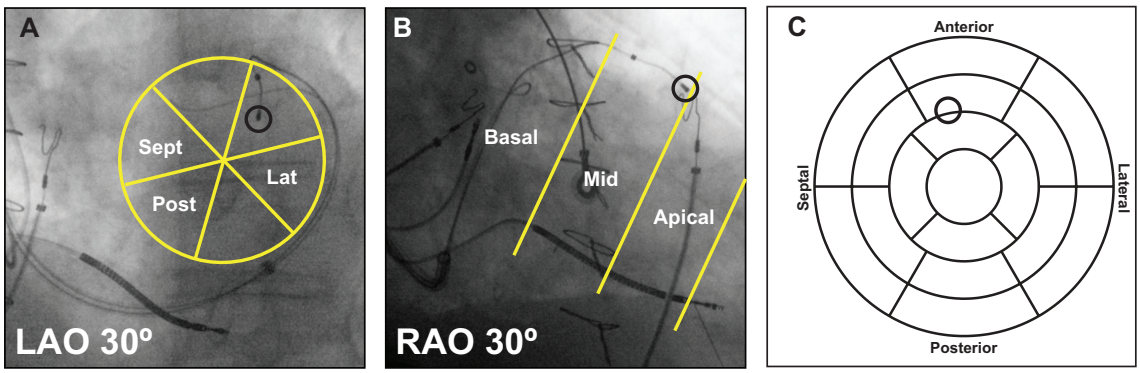

Figure 6.1: Using the Mortensen's o'clock technique, the LAO projection (A) is used to determine the circumferential position of the LV lead and the RAO projection (B) provides an estimate of longitudinal position. With these two values, it is possible to project the LV lead location onto the AHA 17-segment model (C).

Similarly, posteroanterior and lateral chest x-ray (CXR) has been used to estimate the pacing site [214]. These projection-based methods do not determine the true 3D position of the pacing lead, but rather map it onto the AHA 17-segment model for further analysis. Additionally, they assume a typical orientation of the heart within the chest cavity, and the axis of the heart often varies in heart failure patients [214]. CT can be used to accurately localize the position of the pacing lead via a post-implant scan, however, this requires an additional imaging session and results in extra radiation dosage [212]. Based upon these limitations, it is apparent that there is a need for an accurate lead localizing method that utilizes images acquired as part of the standard implantation procedure to limit imaging time and radiation exposure.

As we have shown in the preceding chapters (Chapters 1 and 3), it is possible to use MRI to detect regional dyssynchrony distributions throughout the LV [110–113]. To perform retrospective analysis on the effect of lead placement, it is necessary to determine the position of the pacing lead relative to the MR dataset. Unfortunately, MRI cannot be used to image the final position of the CRT pacing leads. With recent advances in CRT device design, MR-compatible devices have been developed. These devices are effective if patients need to receive an MRI for non-cardiac diagnosis, but there are still artifacts present near the pacing control module and the lead tips. Because of these distortions

in the image, it is difficult to do any cardiac analysis even with an MR-compatible CRT device [215]. Additionally, potential lead tip heating and the need for an electrophysiologist or cardiologist to supervise each scan renders MR imaging of the lead location unrealistic for routine use [139–142].

The goal of this aim was to develop a technique to determine the position of the CRT pacing leads relative to a pre-implant MRI. We registered MRCV data to dual-plane venograms obtained during the implantation procedure to compute the spatial correspondence between the two modalities, allowing us to transfer the lead position from the x-ray images to the MR images.

6.2 Methods

6.2.1 Overview

Prior to CRT device implantation, our 3D contrast-enhanced whole-heart MRCV scan, combined with our reconstruction algorithm (Chapter 5), was used to generate coronary vein geometry for each patient. During the implantation procedure, venograms were acquired while injecting contrast retrograde into the coronary sinus and its tributaries. By projecting the MR reconstruction back onto these imaging planes, it is possible to select corresponding branch points to estimate patient position, and thus determine spatial correspondence between the dual-plane venograms and the MR dataset. To determine the location of the LV pacing lead, post-implant dual-plane x-ray images of the lead position were acquired using the same image acquisition geometry and orientation as the venogram. By registering these lead-localizing dual-planes to the venograms, we could then infer the three-dimensional location of the LV pacing lead and analyze its position relative to MR-derived metrics of cardiac function (Figure 6.2).

6.2.2 Magnetic Resonance Image Acquisition and Reconstruction

As detailed in Chapter 5, we were able to determine the geometry of the coronary veins from a pre-implant MRCV scan. By employing a slow infusion of gadolinium-based contrast agent, it was possible to obtain a high spatial resolution stack of images of the coronary veins. Using user-defined seed points within the coronary sinus and its tributaries, and

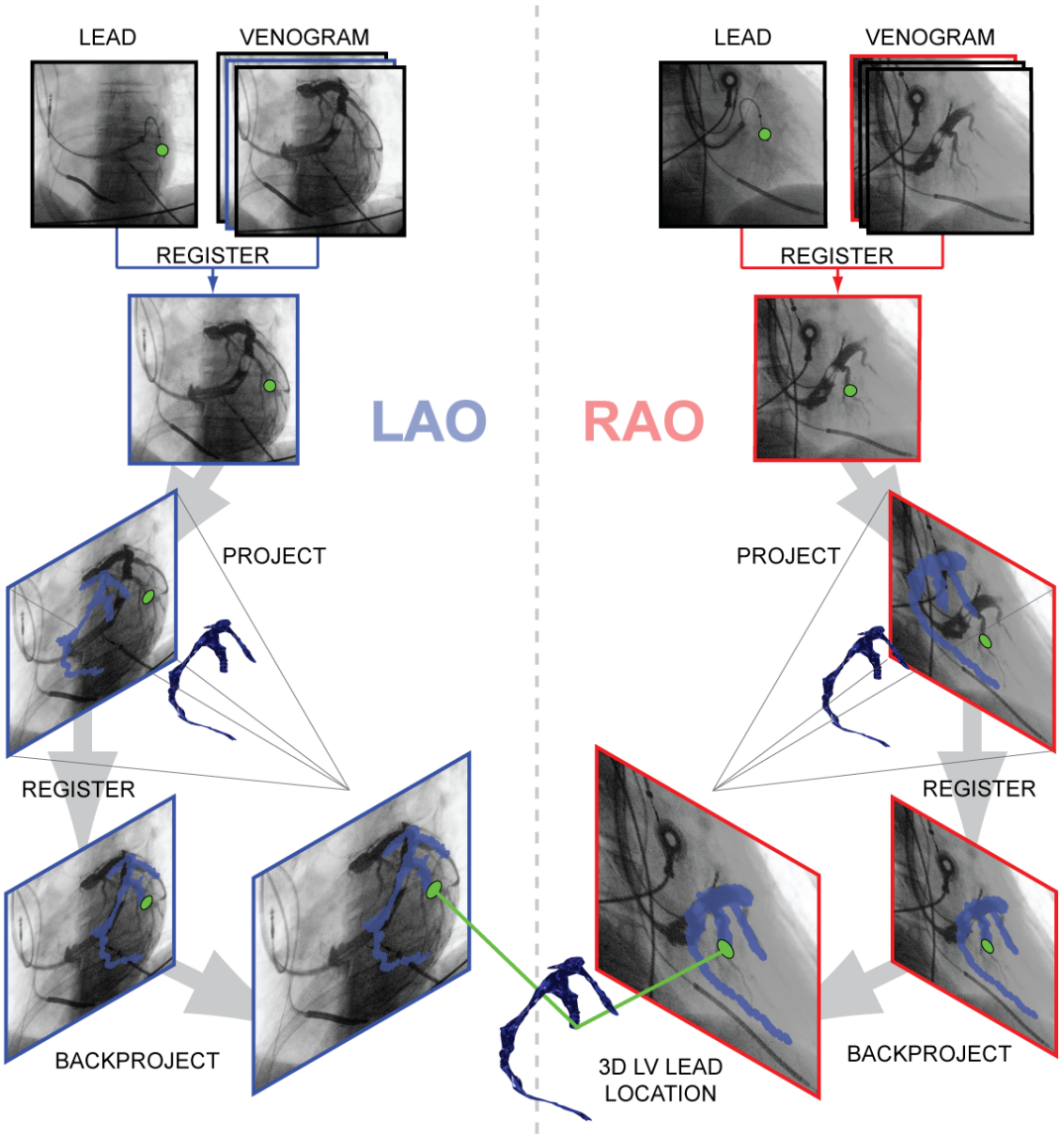

Figure 6.2: During the CRT implantation procedure, venograms are obtained at 30° RAO and 30° LAO during retrograde contrast injection. After LV lead implantation dual-plane lead localizers are obtained at the same angulation as the venograms. By registering these two, we can obtain the lead position relative to the venogram frame that best corresponds to the respiratory and cardiac phase of the lead localizer. By projecting the 3D reconstruction of the MR coronary vein scan onto each of the x-ray projections, we can use corresponding branch points to adjust the dual-plane geometry to compensate for patient motion. After both LAO and RAO dual-planes are properly registered to the MR projection, the lead locations in each image can then be backprojected to the x-ray source locations, and the intersection of these projections yields the true 3D LV lead location.

position information from the DICOM header, we generated a 3D mesh representing the coronary venous tree (Appendix C).

6.2.3 CRT Device Implantation Procedure

To understand our methodology for lead registration, it is advantageous to have an overview of the CRT procedure.

6.2.3.1 Right Ventricular Pacing Lead Placement

Typically, the CRT leads were implanted using a transcatheter approach in which a guidewire was fed into the subclavian vein and a sheath for lead insertion was slid over the guidewire. The right atrial sensing lead and RV pacing lead were then guided through the sheath to their desired locations. The RV pacing lead was placed in the apex of the right ventricular cavity and positioned against the endocardium of the septal wall [105]. The purpose was to electrically stimulate the septal wall of the left ventricle.

6.2.3.2 Coronary Venogram Acquisition

To assess patient venous anatomy and determine the LV pacing target, a retrograde coronary venogram was performed. A balloon catheter was inserted into the proximal coronary sinus and inflated against the walls to prevent the flow of blood to the coronary sinus (Figure 6.3). An iodinated contrast agent (Visipaque, GE Healthcare, Buckinghamshire, UK) was injected retrograde into the coronary veins [105]. X-ray cine venograms were acquired at 30° LAO and 30° RAO (Figure 6.3). Typically, an AP venogram was also acquired. The cine venogram acquisition duration was approximately 5 seconds starting simultaneously with contrast injection. This duration was chosen to ensure that venograms were acquired at all permutations of respiratory and cardiac motion. Additionally, it guarantees sufficient contrast between the coronary veins and the background. Fresh contrast was injected for each of the three projections to ensure maximum contrast of the vasculature.

6.2.3.3 Left Ventricular Pacing Lead Placement

A lateral or posterolateral vein small enough to stabilize the pacing lead was targeted for LV pacing lead placement [101]. Care was taken to ensure that pacing at the target

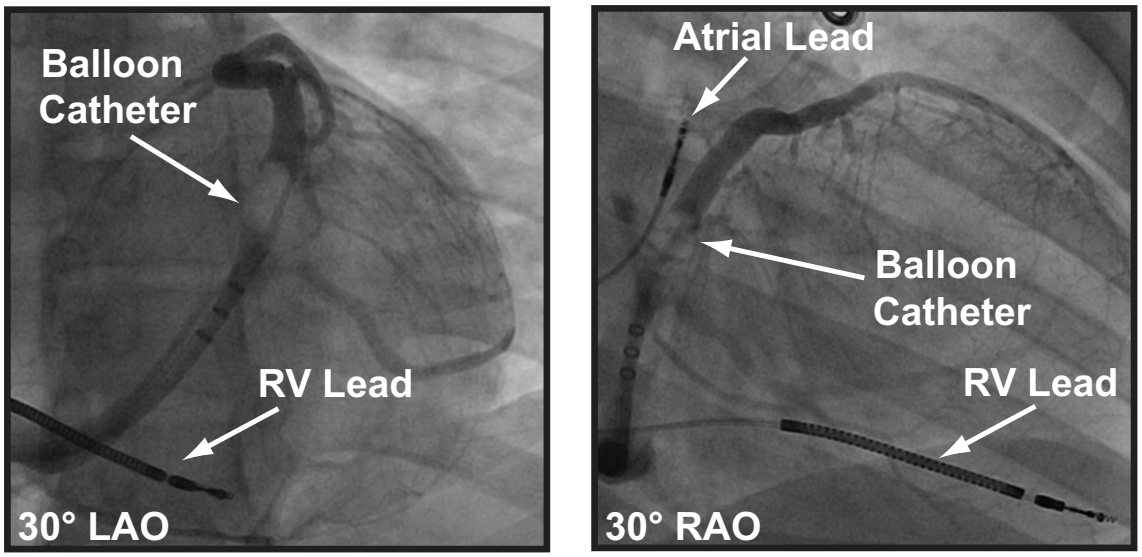

Figure 6.3: After RV and atrial sensing lead implantation, a balloon catheter is inflated in the proximal coronary sinus and iodinated contrast agent is injected retrograde into the coronary veins to obtain venograms to visualize potential targets for LV lead placement.

vein did not result in phrenic nerve stimulation and that appropriate capture thresholds were obtained [216, 217]. To adhere to current clinical practice, no information regarding mechanical dyssynchrony or myocardial scar was considered when selecting the LV pacing location [104].

6.2.3.4 Left Ventricular Lead Localizing Dual-Plane Acquisition

After the sheath used to introduce the pacing lead to the coronary sinus was withdrawn, two non-contrast images were acquired to document the LV lead position. These images were acquired in the same orientation (30° LAO and RAO) and with the same geometric position as the pre-implant dual-plane venograms (Figure 6.4). The duration of the lead localizing image acquisition was only a single frame. Regardless of the cardiac or respiratory phase of the acquisition, it should correspond to one of the venograms acquired over the 5-second cine.

6.2.4 Registration of Lead Localizers and X-Ray Venogram

In our LV lead placement technique, both the MR coronary vein geometry and LV lead localizer dual-plane images are registered to the venograms. The first step was to determine

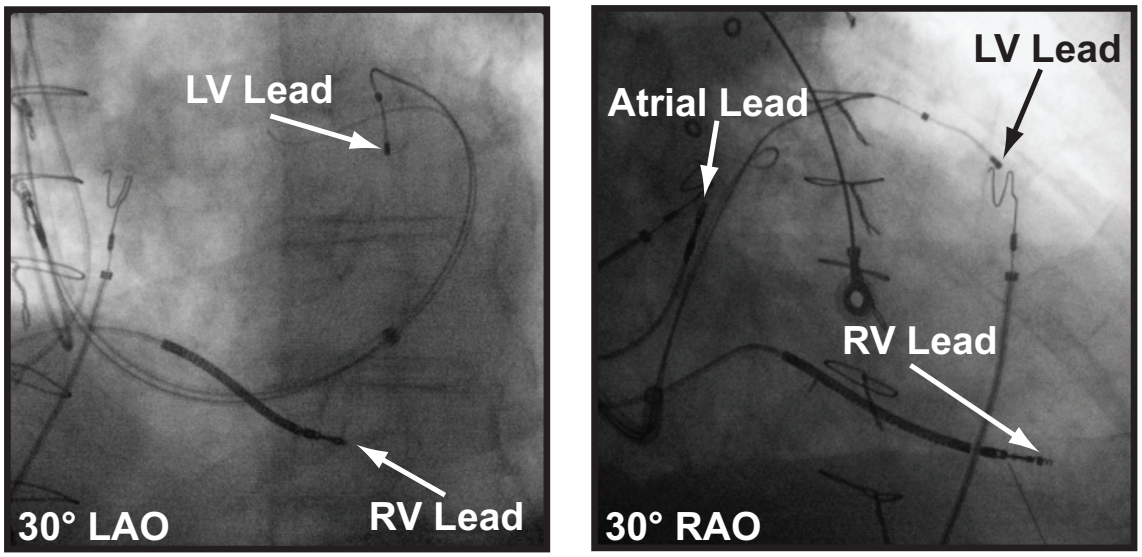

Figure 6.4: After LV lead implantation, non-contrast dual-plane images are acquired to visualize the final lead location. These images are in the same orientation as the venograms.

the lead location on the coronary venous anatomy obtained from the dual-plane venogram. As mentioned previously, every effort was made to acquire the lead localizers in the exact same position as the venograms; however, the patient table is free to move during the implantation procedure so it is possible that the position of the patient table was altered between the two acquisitions. Additionally, both cardiac beating and respiration shift the position of the heart over the course of the acquisition. It is necessary to find the venogram image that best matches the respiratory and cardiac phase of the lead localizer and estimate the offset that will correct for any table movement between the two images.

6.2.4.1 Vessel Enhancement Filter

In addition to the objects of interest in the fluoroscopic images that move with patient and physiologic motion (i.e. the LV and RV leads, and coronary venous anatomy), there are many objects present in the image that are not vessels. These include sternal fixation wires from a previous surgery, EKG electrodes on the surface of the chest, and clasps and tools placed on top of the surgical drapes. The displacement of these extraneous objects between the acquisitions represents patient and table motion but not changes in cardiac or respiratory phase between frames. Because we must identify the frame of the venogram that

best corresponds to the respiratory and cardiac phase of the lead localizer, we must disregard these objects and consider only the objects affected by physiologic motion. To prevent these objects from interfering with our analysis, we utilized a vesselness filter developed by Frangi et al. to help consider only the relevant portions of the image [218].

Briefly, the vesselness filter combines analysis of the Hessian of the image with multi-scale analysis to detect vessel-like objects in an image. At each scale, analysis of the eigenvalues of the Hessian is performed to determine the likelihood of a given pixel belonging to a vessel. With the multi-scale analysis, it is possible to fine-tune the filtering to detect only vessels within a certain range of sizes. In the Frangi implantation, vessels were assumed to have a Gaussian intensity profile across the vessel, therefore the scale is defined by the standard deviation of the Gaussian (σ) that would best describe the vessel [218]. To ignore sternal wires and other objects, σ values between 5 and 8 were used. This was too large of a scale to detect sternal wires and too small to detect larger objects lying on top of the patient. The result of the vesselness filter is a probability image where values close to 1 indicate that there is a very high probability that that pixel belongs to a vessel, whereas pixel values close to 0 indicate that the pixel is most likely background tissue or another non-vessel. More information on the implementation of the Frangi vesselness filter can be found in Appendix E.

In our analysis, instead of using raw pixel values directly to register the lead localizer images with the venograms, we registered the respective vesselness images. To do this, we applied the vesselness filter to the single localizer from each projection as well as all frames of the venogram acquisitions (Figure 6.5).

6.2.4.2 Registration of Filtered Lead Location and Venograms

To determine the translation of the lead localizer that yields the best agreement with each frame of the venograms, we used 2D normalized cross-correlation of the vesselness images [166] (Appendix B.3). For each view (LAO or RAO), we shifted the Frangi filtered lead localizer over the filtered version of the first frame of the venogram and computed the correlation between the two images at each shift. The 2D shift that yielded the highest

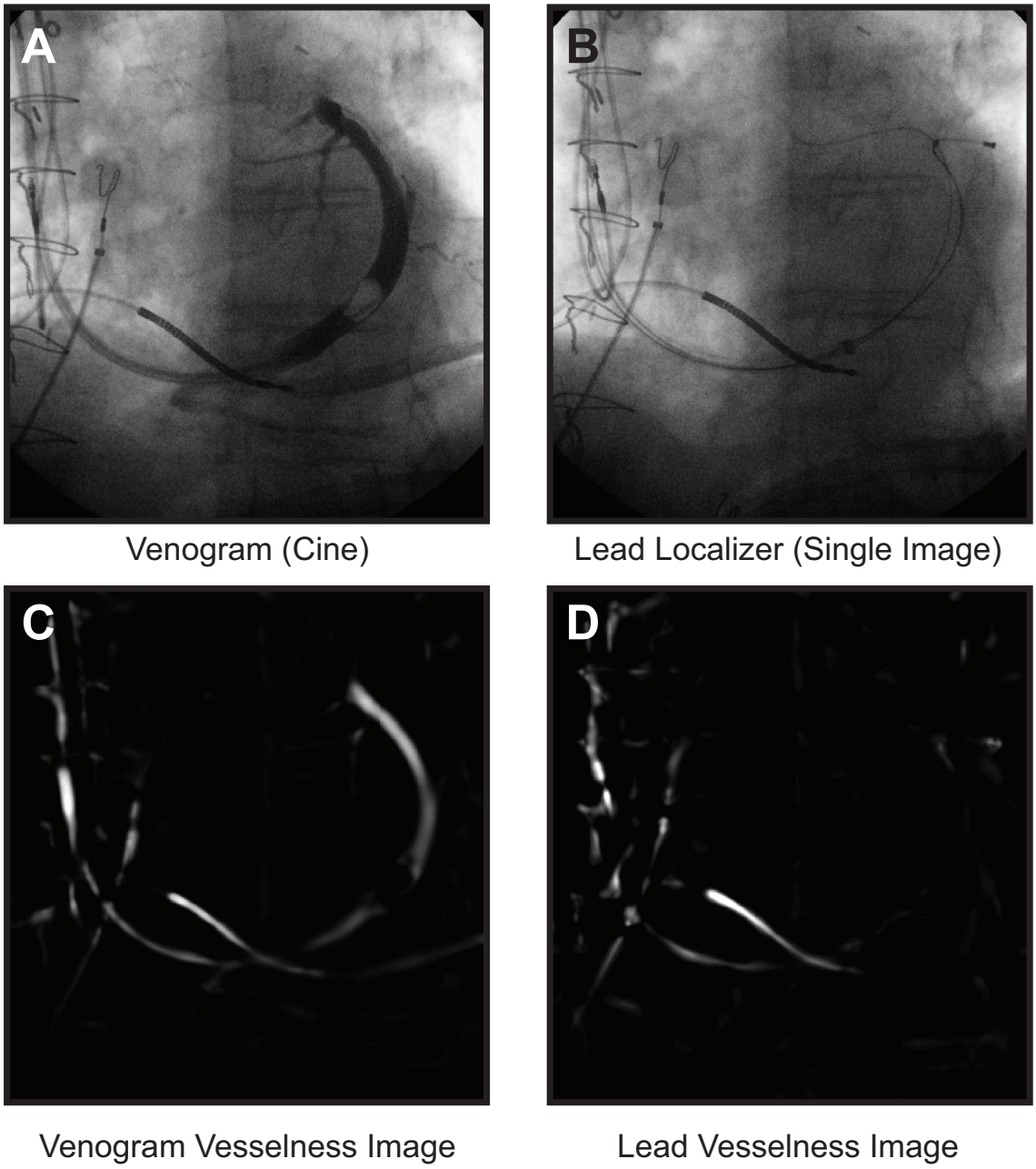

Figure 6.5: A Frangi vesselness filter was applied to the venogram and lead localizing dual-plane images to remove intensity changes across the images and unwanted objects such as sternal fixation wires. Shown here are a representative frame from the LAO cine venogram (A), lead localizer (B) and filtered versions (C and D).

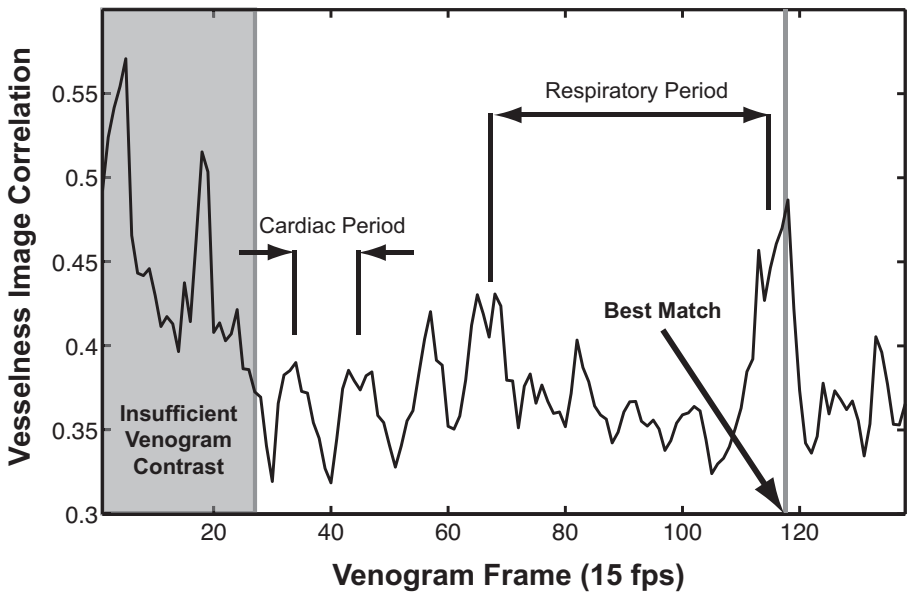

Figure 6.6: Using normalized cross correlation; each frame of the venogram was registered with the lead localizer images. The maximum correlation across all frames was determined to be the best match in respiratory and cardiac phase. Only correlations after sufficient venogram contrast were considered.

correlation was stored as the shift for that particular venogram frame. This was repeated for all frames of the venogram cine acquired over the 5-second period. For each venogram frame, we then have a correlation value and a corresponding displacement (Figure 6.6). By finding the maximum correlation value over *all* frames of the venogram, we have identified the venogram that has both a similar cardiac and respiratory phase and we can register the lead location image to this particular venogram frame using the displacement computed from 2D cross correlation (Figure 6.7). Registration was only performed for frames after which the contrast was injected. Using this information, we can determine the position of the LV lead in the venograms.

In a true biplane angiographic setup, there are two detectors that are capable of imaging the same geometry simultaneously [219]. In the electrophysiology suites at Emory University Hospital and many other institutions, only a single image can be acquired at a time. Therefore, the LAO and RAO images of the coronary veins or lead positions are acquired at different cardiac and respiratory phases. To account for this difference, registration between the venograms and lead localizers were *performed for each of the views independently.*

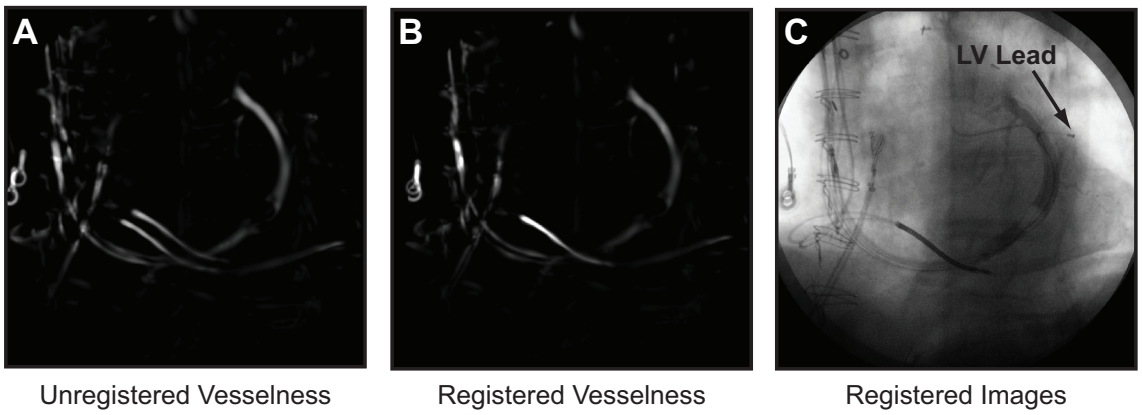

Figure 6.7: Overlays of vesselness filtered LAO venogram and lead localizer showing the unregistered version (A) and registered result (B). By registering the filtered images, we obtain an acceptable registration of the venogram and lead localizer dual-planes (C).

6.2.5 Registration of MR Coronary Vein Reconstruction and Dual-Plane Venograms

After determining the position of the LV pacing lead in the venograms, the next step was to obtain the spatial relationship between the venograms and the MR-derived coronary vein anatomy. Due to differences between the two imaging modalities and the movable patient table of the fluoroscopy system, the venograms correspond to translated and scaled projections of the MR reconstruction of the coronary veins. Below we describe the methodology to estimate the scaling and translation required to match the MR geometry to the venograms.

6.2.5.1 Projection of Magnetic Resonance Coronary Vein Anatomy

Using the techniques developed previously (Chapter 5), we obtained a 3D mesh representing the pre-implant anatomy of the coronary veins. Using position information contained in the DICOM headers of both the MR and x-ray angiographic data, each point in the 3D mesh of the coronary venous anatomy from MRI can be projected onto both the LAO and RAO venogram imaging planes (Figure 6.8 A). The patients were supine during both MR acquisition and CRT device implantation, therefore no corrections had to be made to perform the initial projection onto the venograms.

6.2.5.2 Coronary Vein Projection Mask

To assist with registering the projection of the MR coronary veins with the venogram, we need to create a pixel-based representation of the projection of the MR coronary veins.

To determine a pixel-based representation of the coronary vein mesh within each of the projections, all vertices of the 3D coronary vein mesh were projected back onto both the LAO and RAO image planes and converted to image coordinates (Figure 6.8 A). A binary mask the size of the angiographic image was created in such a way that only the pixels at the locations of the projected vertices were assigned a value of 1 (Figure 6.8 B). Using a circular mask, image dilation was performed on this "projection mask" until all projection points were merged into a single object, providing a binary representation of the projected MR-derived coronary vein anatomy (Figure 6.8 C and 6.9 A).

6.2.5.3 Selection of Corresponding Branch Points

To estimate the scaling and translation that must be applied to calibrate the venograms with the MR data, it is necessary to identify at least two corresponding sets of points in the MR and venograms. The most readily identifiable features in both the MR projections and the angiographic images are the vessel branch points.

To assist with identification of branch points in the binary "projection mask", the mask was skeletonized to provide a binary representation of the centerline of the projection of the MR-derived coronary vein anatomy (Figure 6.9 B).

For each view (LAO or RAO), the user selected at least two corresponding branch points in both the skeletonized MR vein projection ($x_{mri},\ y_{mri}$) and the venogram image ($x_{veno},\ y_{veno}$) (Figure 6.9 B and C). If possible, the user selected as many corresponding branch points as possible. This allowed for a better approximation of scaling and translation parameters and decreased sensitivity to small errors in corresponding point placement.

It is important to note that we are registering the projections to the venograms *independently* for the two views. Therefore, the corresponding branch points selected for the LAO projection do not have to be the same branch points in the RAO image. The corresponding points will likely change between the two views due to variability in contrast injection

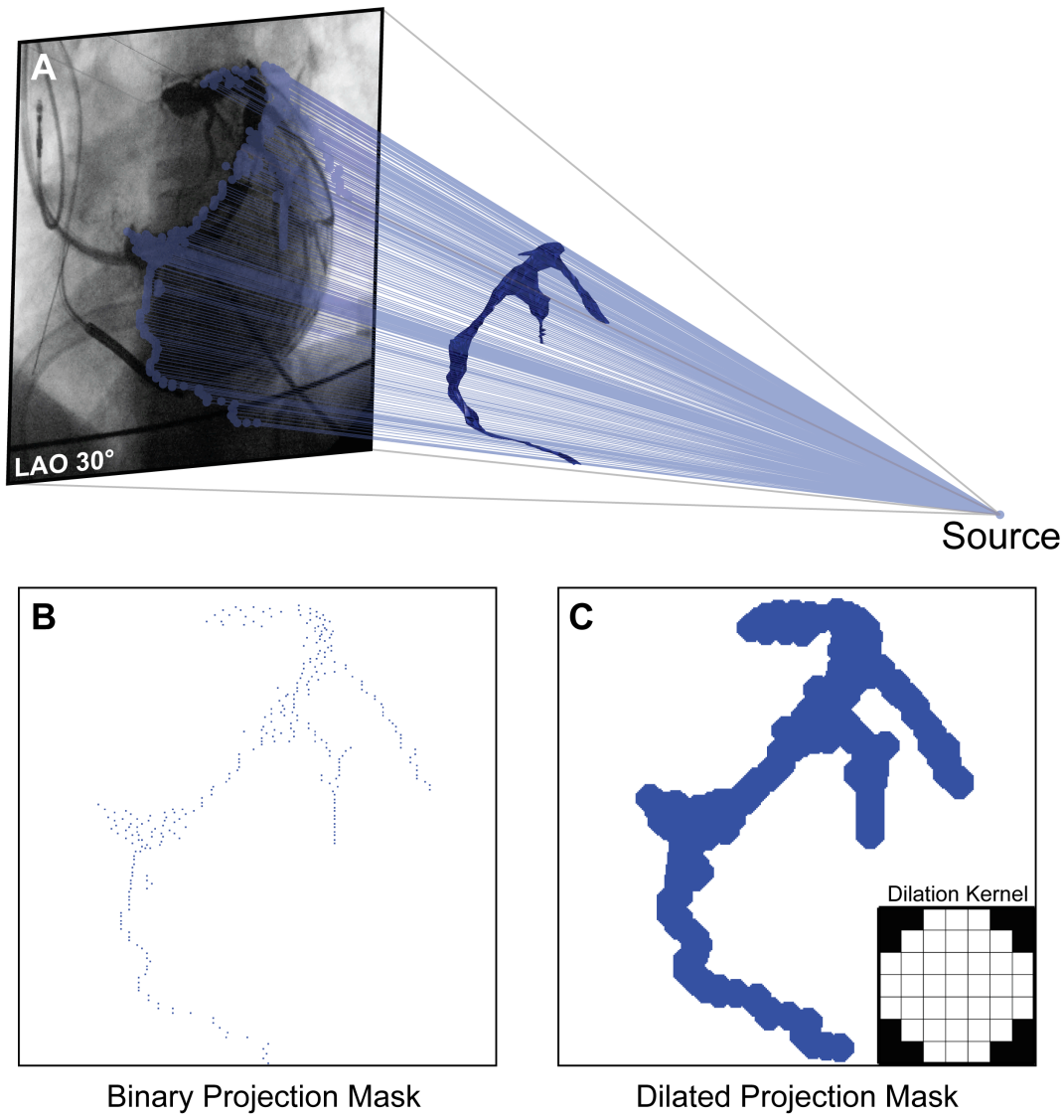

Figure 6.8: Using the coronary vein reconstruction from the MR coronary vein scan, we project the vertices of the mesh onto the venogram imaging plane (A). We create a mask the size of the venogram where the intersection of the projections results in a value of one (B). The mask is dilated with a circular kernel until it is a single object (C).

which can cause different veins to be visible in the two views. Additionally, the respiratory and cardiac phase is not the same between the RAO and LAO images, as they were each selected to match their corresponding lead localizer.

6.2.5.4 Approximation of Scaling and Translation

Using the user-selected corresponding points in the MRI projection ($x_{mri},\ y_{mri}$) and the venogram ($x_{veno},\ y_{veno}$), we want to figure out the transformation to apply to the venogram to align it with the MR projection.

The general transformation between the two sets of corresponding points is shown in Equation 6.1, where x_{mri} and y_{mri} are the user-selected branch points in the MR projection, x_{veno} and y_{veno} are the user-selected branch points in the venogram, α is the angle of rotation applied to the venogram points, S_x and S_y are the scaling in the x and y directions, and t_x and t_y are translations of the venogram points in the x and y directions, respectively.

$$\begin{bmatrix} x_{mri} \\ y_{mri} \end{bmatrix} = \begin{bmatrix} S_x & 0 \\ 0 & S_y \end{bmatrix} \begin{bmatrix} cos(\alpha) & -sin(\alpha) \\ sin(\alpha) & cos(\alpha) \end{bmatrix} \begin{bmatrix} x_{veno} \\ y_{veno} \end{bmatrix} + \begin{bmatrix} t_x \\ t_y \end{bmatrix} \tag{6.1}$$

In this work, we assumed that there was no rotation applied to the images. A non-zero rotation would indicate the patient was rotated to be non-parallel with the patient table. It is unlikely that there is a large rotation due to the narrow patient table and the fact that the patient would be extending over the edge of the table if significant rotation were to be applied. For this reason, Equation 6.1 simplifies to the following:

$$\begin{bmatrix} x_{mri} \\ y_{mri} \end{bmatrix} = \begin{bmatrix} S_x & 0 \\ 0 & S_y \end{bmatrix} \begin{bmatrix} x_{veno} \\ y_{veno} \end{bmatrix} + \begin{bmatrix} t_x \\ t_y \end{bmatrix} \tag{6.2}$$

Additionally, we know that the scaling will be uniform in the x and y directions because the imaging system geometry does not vary across the field of view. Because of this, S_x and S_y are equal and the matrix becomes a scalar (S) times the identify matrix (Equation 6.3).

$$\begin{bmatrix} x_{mri} \\ y_{mri} \end{bmatrix} = S \begin{bmatrix} 1 & 0 \\ 0 & 1 \end{bmatrix} \begin{bmatrix} x_{veno} \\ y_{veno} \end{bmatrix} + \begin{bmatrix} t_x \\ t_y \end{bmatrix} \tag{6.3}$$

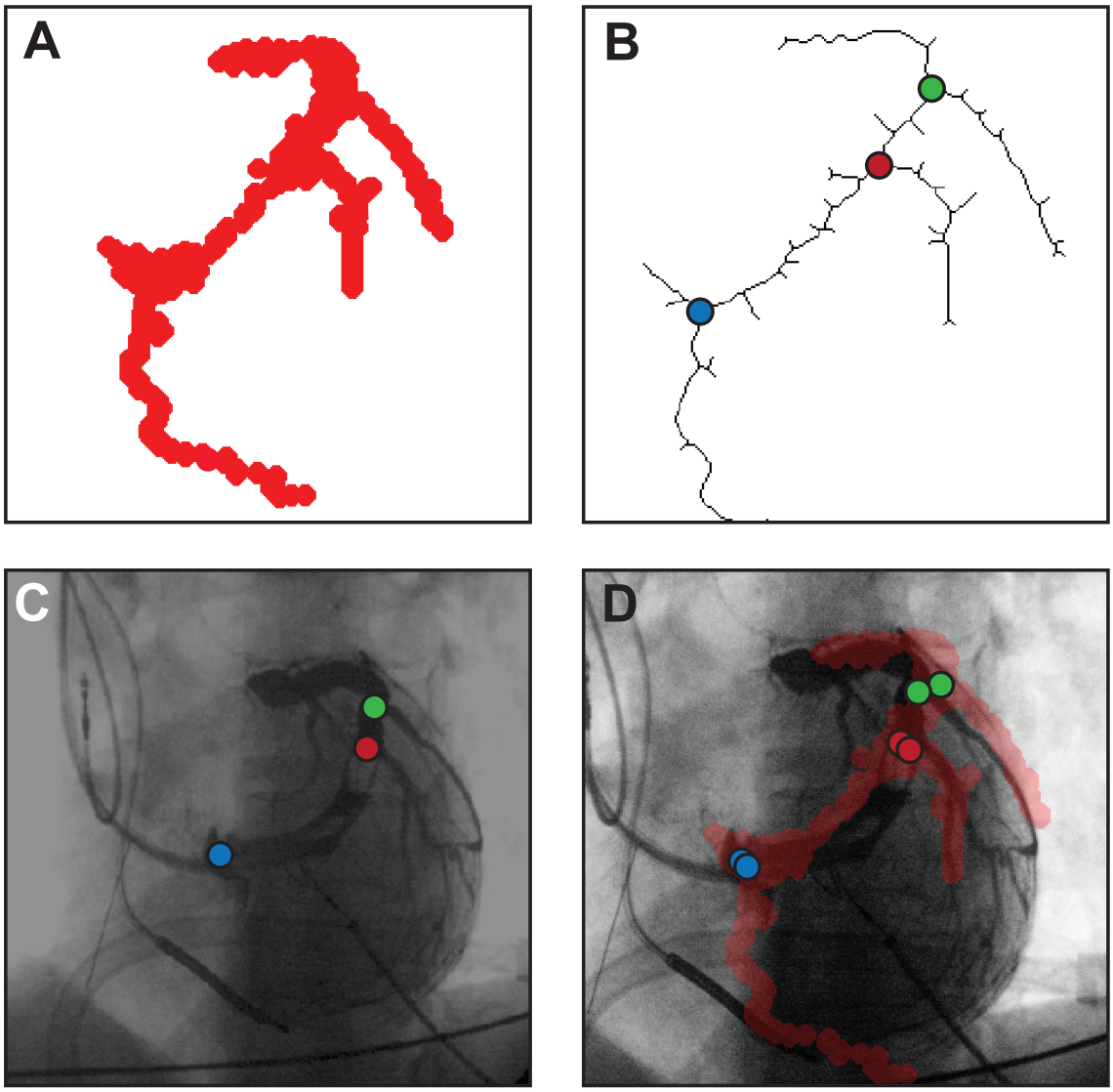

Figure 6.9: The reconstructed MRCV geometry is projected onto the venogram image plane as a binary mask and dilated to create a single entity (A). The dilated mask is then skeletonized to assist in identifying branch points (B). By selecting corresponding branch points in the skeleton (B) and venogram (C), the venogram can be calibrated to correspond to the MR imaging coordinates (D).

which simplifies to:

$$\begin{bmatrix} x_{mri} \\ y_{mri} \end{bmatrix} = S \begin{bmatrix} x_{veno} \\ y_{veno} \end{bmatrix} + \begin{bmatrix} t_x \\ t_y \end{bmatrix} \tag{6.4}$$

This leaves us with three unknown parameters: scaling (S), translation in the x direction (t_x), and translation in the y direction (t_y). Our goal is to determine the value of these parameters that yields the best match between the two sets of corresponding points.

If we have n sets of corresponding points, we can rewrite our transformation in the form $A\boldsymbol{\theta} = \boldsymbol{b}$, where:

$$A = \begin{bmatrix} x_{veno_1} & 1 & 0 \\ \vdots & \vdots & \vdots \\ x_{mri_n} & 1 & 0 \\ y_{veno_1} & 0 & 1 \\ \vdots & \vdots & \vdots \\ y_{veno_n} & 0 & 1 \end{bmatrix}, \quad \boldsymbol{\theta} = \begin{bmatrix} S \\ t_x \\ t_y \end{bmatrix}, \quad \boldsymbol{b} = \begin{bmatrix} x_{mri_1} \\ \vdots \\ x_{mri_n} \\ y_{mri_1} \\ \vdots \\ y_{mri_n} \end{bmatrix} \tag{6.5}$$

For any given rotation and translation, $\boldsymbol{\theta}$, we can compute the error between the MR points and the transformed venogram points (Equation 6.6). Our goal is to select the set of parameters, $\boldsymbol{\theta}$, that minimizes this error.

$$\boldsymbol{e} = ||A\boldsymbol{\theta} - \boldsymbol{b}||^2 \tag{6.6}$$

The error is minimized when:

$$A\boldsymbol{\theta} = \boldsymbol{b} \tag{6.7}$$

Alternately:

$$\boldsymbol{\theta} = A^{-1}\boldsymbol{b} \tag{6.8}$$

In our system, if the user selects two points, then we have an over-determined system with four equations and three unknowns. In this case, we must find the least-squares solution to the system of equations, where $\hat{\boldsymbol{\theta}}$ is the best estimate of the scaling and translation

between the projection and the venogram (Equation 6.9). This solution works if the user selects more than two corresponding points.

$$\hat{\boldsymbol{\theta}} = (A^T A)^{-1} A^T \boldsymbol{b} \tag{6.9}$$

By solving Equation 6.9 based on the user-defined corresponding points, we obtain the translations, $\hat{t}_x$ and $\hat{t}_y$, and scaling $\hat{S}$ that we need to apply to the x-ray imaging system to register the venograms to the projected MRI geometry. The next sections will detail how we actually apply these parameters to our data.

6.2.5.5 Correction of Scaling Factor

To scale the venogram by $\hat{S}$ to match the MR data, we must first understand how the magnification of the x-ray system is determined.

In an x-ray-based system, the scaling of an object is determined by the ratio of the source-to-detector distance (d_D) to the source-to-patient distance (d_P) (Figure 6.10). Equation 6.10 shows the radius of the projection (R) of an object with actual radius r, where d_P is the distance of the object from the x-ray source and d_D is the distance between the source and detector .

$$R = \frac{d_D}{d_P} r \tag{6.10}$$

A scaling factor of 1 would be obtained by imaging an object as it sits on the detector ($d_D = d_P$). If the object is midway between the source and detector, then the projection is scaled by a factor of two.

To ensure that our venogram has the scaling, $\hat{S}$, required to match it to the MR data, we need to ensure that $\frac{d_D}{d_P}$ is equal to $\hat{S}$. Most imaging systems provide the source-to-detector distance (d_D); therefore we can manually specify the source-to-patient distance (d_P) to correct for any scaling difference between the MR and venogram data (Equation 6.11).

$$d_P = \frac{d_D}{\hat{S}} \tag{6.11}$$

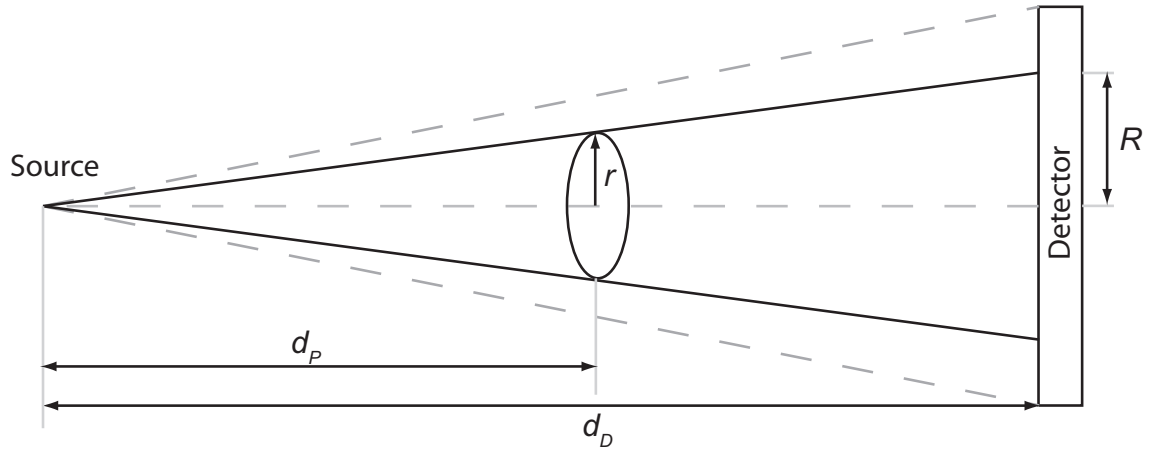

Figure 6.10: The scaling of an object in an x-ray system is dependent upon the distance of the source from both the detector and the object. An object of radius r will projection onto the imaging plane and have radius R. The scaling factor ($\frac{R}{r}$) is equal to the ratio of the distance from the source to detector (d_D) and the source to patient distance (d_P).

The scaling factor is computed separately for both the RAO and LAO views because they were acquired at different times and can therefore require different scaling corrections.

6.2.5.6 Correction of Translation

Now that we have corrected for the scaling, we need to translate the venogram to match the MRI projection. Using the corresponding points, we already found that x and y displacements of t_x and t_y, respectively, will register the two geometries. We convert these translations to a 3D displacement vector $\boldsymbol{\delta}$ using the DICOM position information (Figure 6.11 B) (Appendix C).

$$\boldsymbol{\delta} = \begin{bmatrix} \delta_x & \delta_y & \delta_z \end{bmatrix} \tag{6.12}$$

To register the MR projection and venogram, we need to apply a shift to the x-ray geometry.

When we apply a displacement ($\boldsymbol{\delta}_S$) to the x-ray imaging system, it is applied to the x-ray source and detector equally, shifting the entire system (Figure 6.11 C).

When we shift the detector, any point within the venogram shifts with the imaging system, therefore the displacement of the venogram is equal to the displacement applied to the system (Equation 6.13):

$$\boldsymbol{\delta}_{veno} = \boldsymbol{\delta}_S \tag{6.13}$$

The MR coronary vein reconstruction is fixed in space and therefore is not translated with the x-ray system; however, the *projection* shifts in the opposite direction. Additionally, because of the scaling factor, the displacement of the displacement is exaggerated. The displacement is shown in Equation 6.14, where $\boldsymbol{\delta}_{mri}$ is the displacement of the MRI projection, $\boldsymbol{\delta}_S$ is the displacement of the x-ray system (source and detector), and S is the scaling factor of the x-ray system.

$$\boldsymbol{\delta}_{mri} = -\boldsymbol{\delta}_S \cdot (S - 1) \tag{6.14}$$

To determine the $\boldsymbol{\delta}_S$ that will result in the displacement $\boldsymbol{\delta}$ computed by our registration, we use the following equation:

$$\boldsymbol{\delta} = \boldsymbol{\delta}_{veno} - \boldsymbol{\delta}_{mri} \tag{6.15}$$

By substitution in Equations 6.13 and 6.14, we get:

$$\boldsymbol{\delta} = \boldsymbol{\delta}_S + \boldsymbol{\delta}_S S - \boldsymbol{\delta}_S \tag{6.16}$$

$$\boldsymbol{\delta} = \boldsymbol{\delta}_S S \tag{6.17}$$

Therefore, to properly register the MR projection and the venogram we need to displace the x-ray system by:

$$\boldsymbol{\delta}_S = \frac{\boldsymbol{\delta}}{S} \tag{6.18}$$

The displacements are computed and applied separately to the LAO and RAO views because the images were not acquired at the same time, and the patient table could have been moved between the two acquisitions.

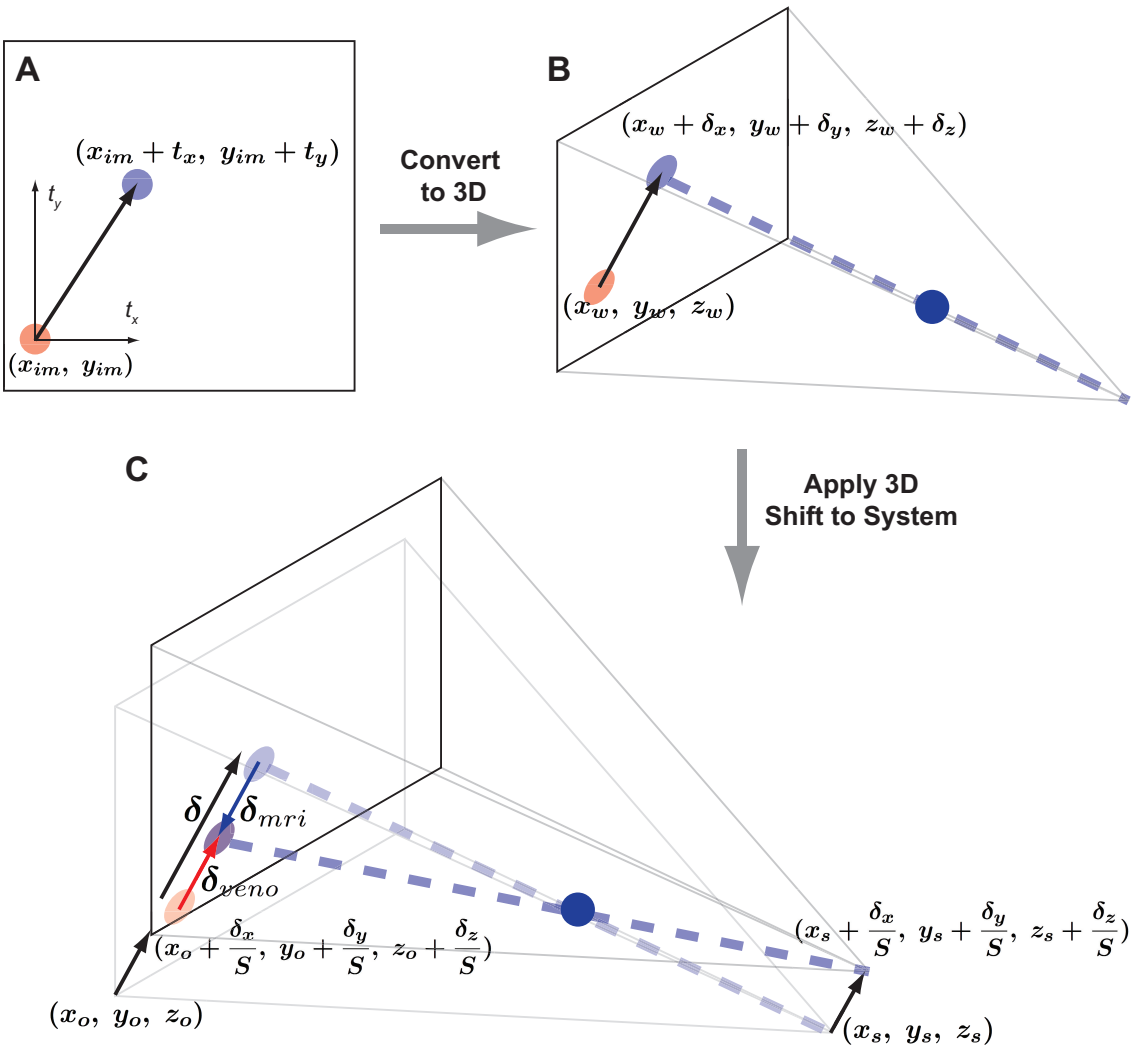

Figure 6.11: To align the venogram with the MR projection of the coronary veins, we first computed the translations, t_x and t_y, that would align the venogram (red) with the MR projection (blue) (A). To correct for the translation, the displacement in the image domain must first be converted to 3D displacements (δ_x, δ_y, and δ_z) using DICOM orientation information (Appendix C) (B). By shifting the x-ray source and detector orientations by $\frac{\delta_x}{S}$, $\frac{\delta_y}{S}$, and $\frac{\delta_z}{S}$, the projection of the MR and the venogram will be aligned (purple) (C).

6.2.6 Calculation of Three-Dimensional Lead Position

Now that we have registered both the RAO and LAO venograms to the MR geometry and we know the position of the LV lead in each of the venograms, we have all the information required to determine the true 3D position of the LV lead. To determine where this point lies in the 3D shared coordinate system, we projected a line back from the lead position to the source for each of the views (Green lines in Figure 6.12 A). In theory, these two lines would intersect at a point in 3D, and this point would correspond to the position of the LV pacing lead in 3D. In practice, due a variety of sources for error, the projections come close to crossing but rarely actually cross. For this reason, we compute the shortest line connecting the two projections. This line is known to be perpendicular to both lines. The midpoint of this line is used as the intersection of the two projections, and therefore corresponds to the 3D lead position (Figure 6.12 A). Because we calibrated the venograms to the MR anatomy, this 3D position is already in the MR coordinate system and can then be used for analysis (Figure 6.12 B).

6.2.7 Projection of Left Ventricular Pacing Lead onto AHA 17-segment Model

In this work, we have used the AHA 17-segment model to display LV regional information on a polar plot. The radial dimension is collapsed and only the circumferential and longitudinal position relative to the central axis of the LV are considered (Appendix A). Using the central axis obtained from the regional dyssynchrony analysis (Chapter 3), we projected the 3D lead location onto the AHA 17-segment model. This information could then be overlaid with displays of regional dyssynchrony or myocardial scar distribution (Figure 6.12 C).

6.3 Results

This method was successfully applied in 9 patients undergoing CRT at Emory University Hospital.

6.3.1 Lead Localizer and Venogram Registration

When registering the lead localizer and dual-plane venograms, we had to determine the best match in respiratory and cardiac phase based on the maximum correlation value. In this

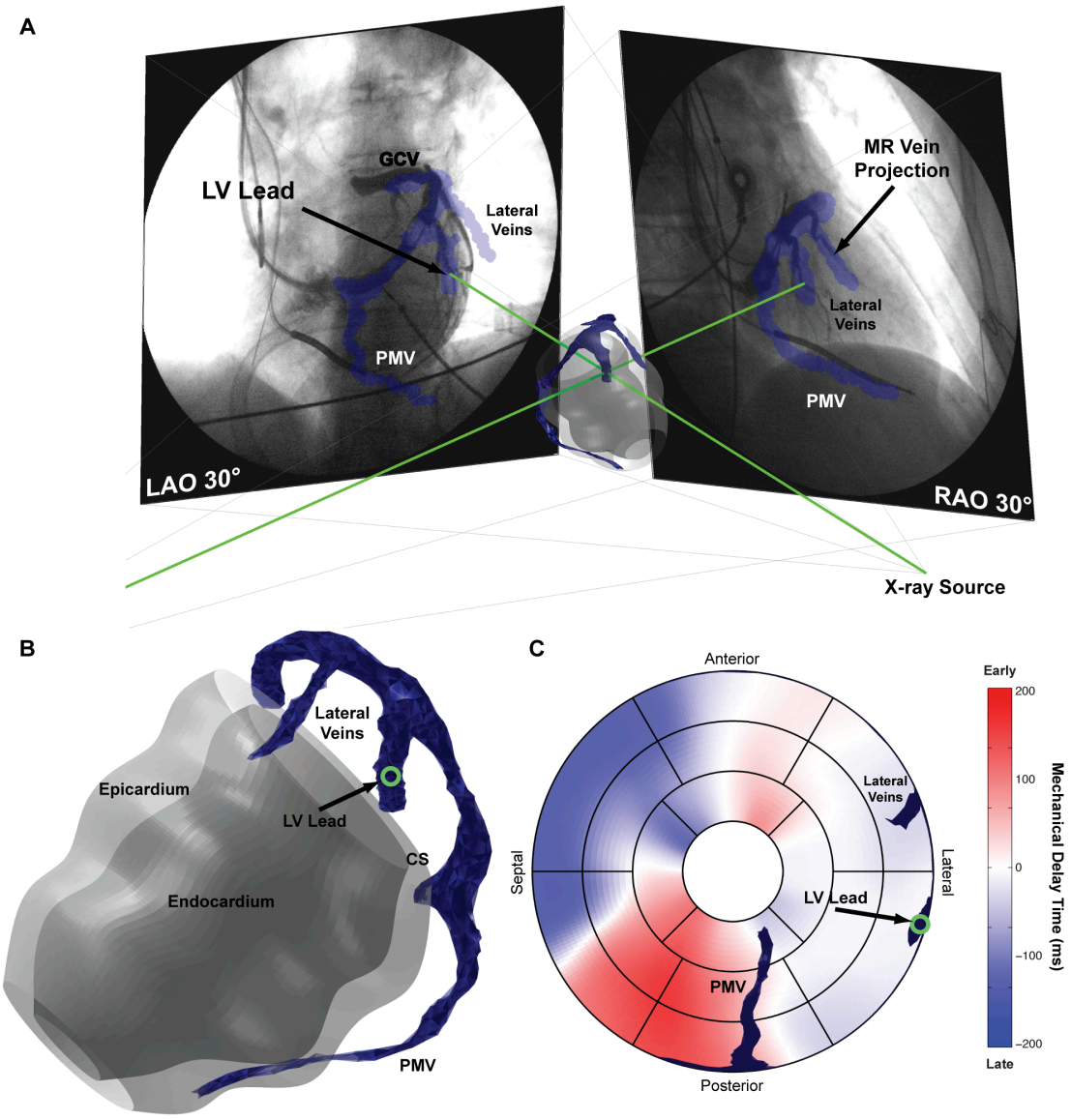

Figure 6.12: After registering the projection of the MR-derived coronary vein anatomy with the venograms, the lead position is projected back (green lines) to the source (A) and the intersection of these two projections is the lead location in 3D (B). This position can then be mapped to the AHA 17-segment model and displays of regional dyssynchrony or myocardial infarction (C).

group of patients, the maximum correlation values were 0.44 ± 0.17 (Range: 0.23 – 0.97). On average, the lead localizers had to be shifted by 23.0 ± 27.7 mm (Range: 0.0 – 106.1 mm) to align properly with the venograms.

6.3.2 MR Geometry and Venogram Registration

We had to correct for differences between the MR and x-ray angiography system by applying a scaling factor as well as a displacement to the imaging system. A scaling factor of 1.54 ± 0.31 (Range: 1.13 – 2.13) was needed across all patients, while an average offset of 50.5 ± 31.5 mm (Range: 9.9 – 113.3 mm) had to be applied to the x-ray geometry.

6.3.3 Three-Dimensional Lead Position

To determine the position of the LV lead in 3D, we back projected the lead location from the dual-plane venograms and found the intersection of the two lines in 3D. As mentioned, the intersection was defined as the midpoint of the shortest line connecting the two projections. The length of that line was 9.78 ± 5.99 mm (Range: 1.56 – 19.22 mm) in our patient population.

6.3.4 Projection of Left Ventricular Pacing Lead onto AHA 17-segment Model

The lead location was successfully mapped to the AHA 17-segment model in all patients (Figure 6.13). The lead location was lateral in 8 (88.9%) patients and anterior in one patient (11.1%).

6.4 Discussion

We have developed a method for mapping the position of the LV pacing lead from post-implant dual-plane fluoroscopic images to pre-implant MR image data. This methodology is important for retrospective studies attempting to assess scar and dyssynchrony distributions at the location of the LV pacing lead, and determining the effect of lead placement on patient response to CRT.

Currently, the relationship between myocardial scar, mechanical dyssynchrony, LV lead placement, and CRT response remains unclear as studies have shown inconclusive or disparate results. This lack of a consensus on lead placement and response could be partially

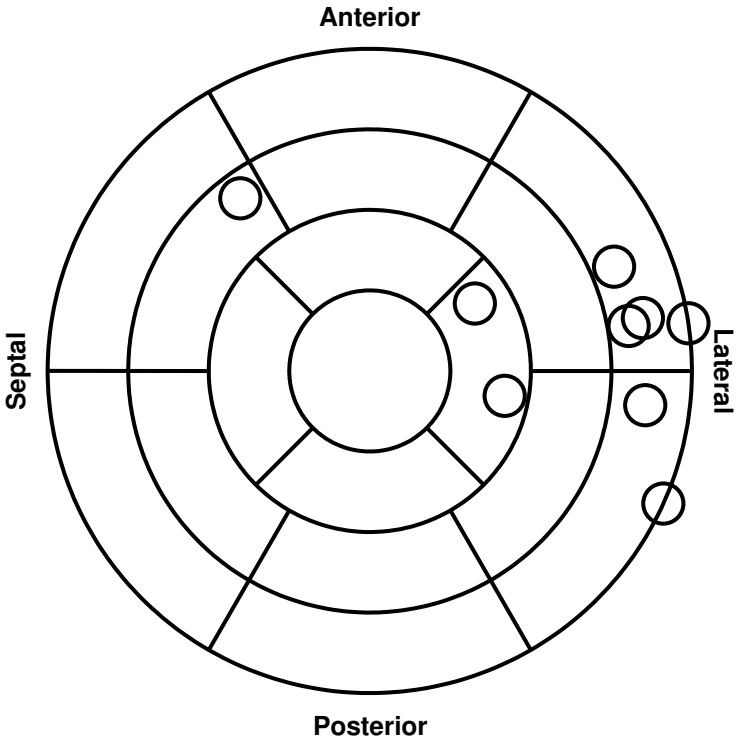

Figure 6.13: We applied our lead mapping technique in 9 patients receiving CRT devices. We were able to successfully map the lead location to the AHA 17-segment model in all patients.

attributed to the limitations of the techniques used to estimate the final position of the LV pacing lead [144, 212, 220]. For example, Mortensen's o'clock and similar methods make assumptions about the shape of the LV as well as its orientation within the chest cavity which may not be true in heart failure populations [144, 221]. Our method makes no assumptions regarding patient anatomy except that there is no significant change between the pre-implant MRI and CRT device implantation procedure.

Although we developed this method to determine the position of the LV pacing lead, it can be employed to find the position of the RV pacing lead as well, as we determine the spatial correspondence between the *complete* lead localizing images and the MR dataset. As a result, we can map *any* point in the localizers (or venograms) into MR coordinates, including the RV pacing lead tip. This could be useful, as a number of recent studies have shown that myocardial scar distributions at the site of the RV pacing lead can affect patient response to CRT [172, 212].

Due to the ability to image many factors that have been shown to affect response to CRT, we have elected to use MRI for pre-implant imaging. It is possible to use other modalities including CT to assess a patient's suitability for CRT prior to device implantation [222]. CT, specifically, allows for excellent visualization of the coronary veins using an iodinated contrast agent [200, 223, 224]. Similar to the work we have presented, a reconstruction of the coronary veins can be generated from the CT data and the lead locations can be mapped into the CT coordinate system. This provides a means of determining final lead placement without the need to subject the patient to an additional CT scan and resulting radiation dose. More generally, our method can be used to find the true lead positions in *any* modality capable of providing a three-dimensional representation of the coronary veins.

A strength of our methodology is that it is only dependent upon the angulation of the c-arm gantry. As such, minimal orientation information can be provided within the fluoroscopic DICOM header without affecting the ability to place the LV lead. This allows us to apply our method on a wide range of imaging systems without degradation in accuracy. Furthermore, our method does not require the use of any external fiducial markers to register the two modalities. We found that significant modifications had to be made to the position

of both the lead localizers and dual-plane venograms to register them with the MRI coronary vein geometry. Our ability to detect and correct for these large modifications speaks to the flexibility of our technique.

6.4.1 Limitations

Manual identification of branch points is required in this method. The branches are readily visible in both the MR and the x-ray venograms. The main reason that we cannot easily apply an automated registration technique is because of the scaling factor. This would require exploration of an enormous parameter space and would require an exorbitant amount of time and it is much easier, and more accurate, for a user to manually identify corresponding locations. As mentioned, only two corresponding points are required for estimation of scaling and translation parameters. For each patient, that is a total of 4 points that must be identified.

To obtain an x-ray venogram, the coronary sinus must first be occluded with a balloon catheter. The balloon prevents the flow of contrast into the coronary sinus, but unfortunately also prevents contrast from entering the posterior coronary veins. The posterior veins exhibit the best visibility in MR and would therefore serve as a reliable reference for MR/x-ray registration if they were visible in the venograms. As a result, our registration must rely on the anterior vein and smaller lateral veins, which may not be visible if MRCV image quality is poor. In some cases, however, complete occlusion does not occur and we can use the faint outline of the middle cardiac vein for registration.

We assumed that there was no rotational registration required between the venogram and the MR data. As mentioned previously, in order for there to be significant rotation in the venogram, the patient would have to be rotated so that they are no longer parallel with the patient table. This is impractical in the clinical settings, and the small deviations that may occur would be insignificant compared to the scaling and translation that occurs. If rotation were ever found to be a significant issue, we would have four unknown parameters (rotation, scaling, and x and y translation) which could also be solved by the least-squares approach presented.

An additional assumption was that there was no scaling difference between the venograms and the lead localizers at each projection angle, only that there was translation of the patient table. This was due to the fact that the patient is mainly shifted in the x and y directions during the implantation procedure, not towards and away from the source. The scaling was most necessary for the venogram/MR registration because the MR coronary veins could be closer to, or further from, the location of the x-ray source in 3D because of the different coordinate system for the modalities. If this scaling were found to be significant for a patient, the scaling could be estimated using the size of the RV pacing lead which is visible in both the lead localizers and venograms.

6.5 Conclusions

We developed a method for mapping lead position from dual-plane fluoroscopic images into the MR images. The methodology can be used to assess the relationship between MR-derived factors at the site of the pacing lead and response to CRT.

6.6 Major Findings

- We developed a method to determine the spatial correspondence between dual single-plane fluoroscopic images and MR images and determine the lead location relative to MR data
- Lead locations can be mapped to the AHA 17-segment model for co-visualization with maps of regional dyssynchrony and myocardial infarction
- The technique can be applied on a wide range of imaging systems due to its flexibility

CHAPTER VII

VALIDATION OF LEAD LOCALIZATION TECHNIQUE

In this chapter, we describe a phantom that allows us to visualize lead positions and coronary vein anatomy with both modalities. By conducting a pre-implant MR and a CRT implantation procedure including x-ray fluoroscopy imaging in the phantom, we can assess the error between the actual lead positions in MR and the lead positions obtained with our registration technique.

7.1 Introduction

In Chapter 6, we developed a registration technique to determine the position of any point in dual-plane fluoroscopic images relative to the MR image coordinate system. This spatial mapping technique can be used to determine the position of the LV pacing lead in three dimensions and map it to the AHA 17-segment model.

Validation of our technique in patients is difficult because we are not able to perform a post-implant MRI of the coronary veins to discern the final lead location. Even if a patient has one of the newer MR-compatible CRT devices, the device and leads could produce susceptibility artifacts that will render the images unusable and would make lead identification difficult [215].

To validate our registration technique to localize the LV lead on the MRI data, it is necessary to develop a way to image the coronary veins with both MR and x-ray fluoroscopy, and also visualize the true pacing location in both modalities. To perform this validation, we developed a model of the coronary veins that mimicked the natural geometry and orientation of the vessels. By including markers that could be imaged with both MRI and x-ray angiography, it was possible to evaluate the performance of our MR/dual-plane fluoroscopy registration technique. We computed the error between the true and registered locations and compared this to the error using Mortensen's o'clock, the most commonly employed technique for LV lead location identification. By quantifying the registration error in our

phantom, we could determine the accuracy of our registration technique for identification of the LV pacing site.

7.2 Methods

7.2.1 Phantom Creation

To validate our registration technique, we used an anthropogenic phantom with a fixed geometry that can be imaged with both modalities: MRI and x-ray angiography. We created a phantom with characteristic coronary vein geometry and markers for targeting pacing sites, visible by both MRI and x-ray angiography. These markers can serve as a common reference point to assess the technique's accuracy.

7.2.1.1 Acquisition of Coronary Vein Anatomy

The coronary venous system represented by the phantom was obtained from a single subject undergoing a cardiac CT scan at Emory Clinic. Iodinated contrast agent was injected intravenously and a computed tomography angiogram (CTA) was acquired, covering the entire extent of the left ventricle. The high spatial resolution of CT and the presence of contrast agent within the blood, provided high contrast to noise ratio in the coronary veins [225].

7.2.1.2 Coronary Vein Anatomy Post-Processing

Segmentation of the coronary veins and both the right and left ventricles was performed using the freely available software, Segment version 1.9 R2035 (Medviso, Lund, Sweden) [226]. After providing the software with seed points within the coronaries and ventricles, an ultra fast 3D level set algorithm coupled with Bayesian modeling was used to obtain a binary mask (Figure 7.1 A) [226, 227]. This three-dimensional binary mask was converted to a 3D mesh and exported as a STereoLitography (STL) file. The generated mesh had rough edges due to the discrete slices in CT, so regularization of the mesh was performed using Geomagic Studio 11.0 (3D Systems, Rock Hill, S.C.). Additionally, smaller branches were pruned from the coronary sinus to leave just the major tributaries.

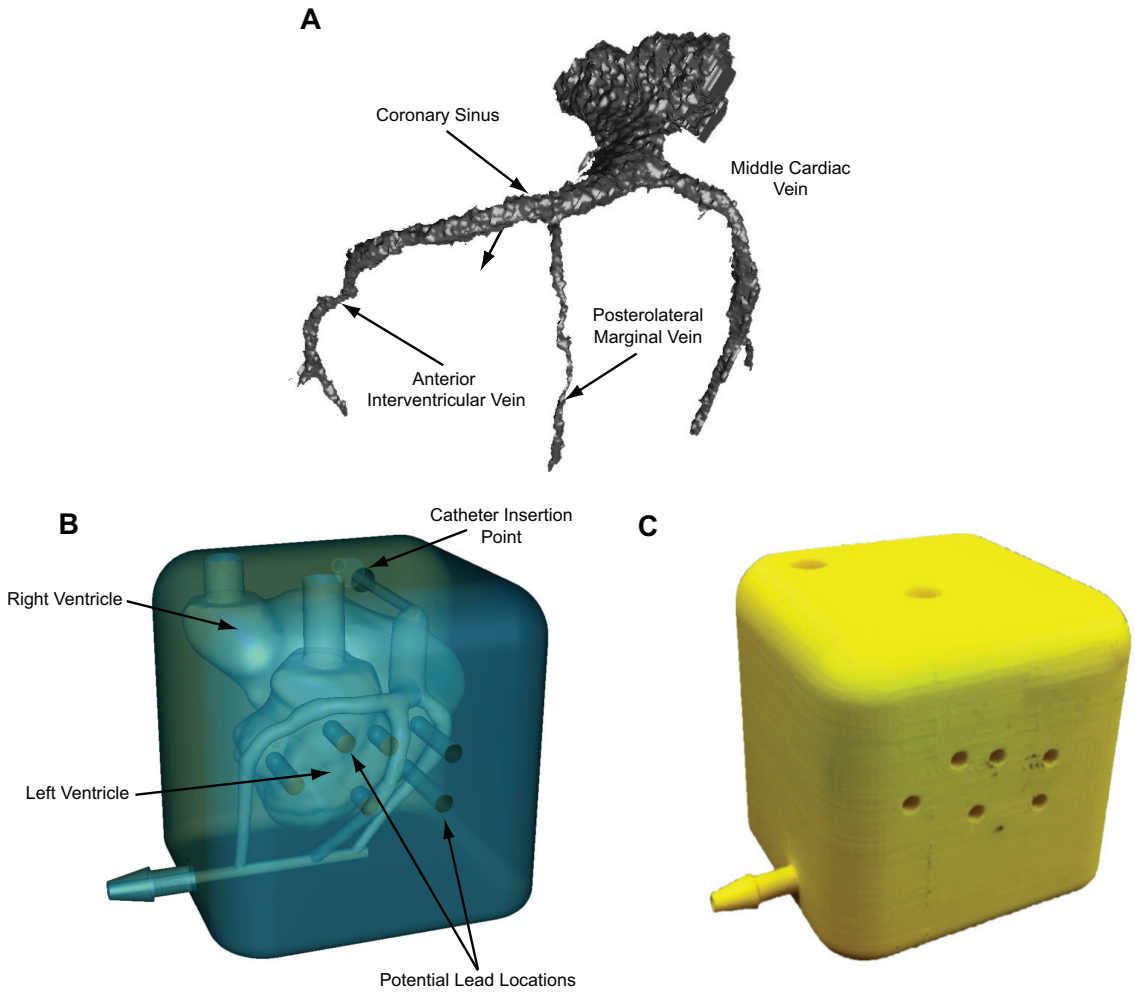

Figure 7.1: Computed tomography angiography (CTA) was used to obtain coronary vein anatomy from a volunteer (A). After segmentation of the cardiac chambers and coronary veins, a coronary vein phantom (B) was generated. In addition to cardiac anatomy, the phantom included six potential pacing sites to verify our registration technique. The phantom was 3D-printed using ABS plastic and an FDM rapid prototyping machine (C).

The optimized 3D meshes of the coronary veins and ventricles were imported into SolidWorks (Dassault Systémes SolidWorks Corp., Vélizy, France) to generate the overall phantom geometry. A solid 6 x 6 inch block was created, from which the ventricles and coronary veins were subtracted out as a negative. The coronary sinus was connected to the outside of the phantom via a channel to which external tubing could be connected. Additionally, the distal ends of the coronary veins were connected to a drain at the bottom of the phantom. Two ports were created for access to the ventricles (Figure 7.1 B). This series of channels and ports allowed the entire phantom to be filled with MR and X-ray contrast agents and flushed with water.

7.2.1.3 Pacing Site Identification

Target pacing locations were placed at six locations, proximal and distal locations for each of the major coronary veins visible in the model coronary venous anatomy. These pacing sites were bores from the side of the phantom block to within 2.5 mm of the coronary veins (Figure 7.1 B). By filling these channels with contrast agent, it was possible to visualize their location in both MR and fluoroscopy and have a marker for true lead position in MR.

7.2.1.4 Coronary Vein Phantom Fabrication

The STL files were exported from SolidWorks to a fused deposition modeling (FDM) rapid prototyping machine (Dimension SST 1200, Stratasys, Ltd., Edina, MN) at the Georgia Tech Biomedical Engineering machine shop. Due to the irregular geometry of the coronary veins, a lost wax technique was used in which a microcrystalline wax provided support for FDM and was later dissolved out of the printed model in a heated bath of sodium hydroxide. The material selected for the phantom creation was acrylonitrile butadiene styrene (ABS) plastic as it is commonly employed in rapid prototyping and was relatively radiolucent which allows for proper imaging under x-ray angiography. Additionally, ABS remains relatively invisible in clinical field-strength MRI (Figure 7.1 C).

7.2.2 Coronary Vein Phantom Imaging Protocol

7.2.2.1 X-ray Angiographic Imaging

The coronary vein phantom was placed into a custom-made foam base to ensure a consistent and realistic orientation of the heart between modalities. The phantom underwent imaging similar to what is done in a CRT procedure. Using 30° RAO images for guidance, a catheter was used to insert the LV pacing lead into the coronary veins. When the pacing lead reached each of the potential pacing sites (determined by the marker positions), images were acquired at 30° LAO and RAO. This process was repeated for all six potential pacing sites (Figure 7.2 C and D). This procedure generated six sets of dual-plane lead localizer images.

After all lead positions had been imaged; the coronary veins of the phantom were then filled with iodinated contrast agent (Visipaque, GE Healthcare, Buckinghamshire, UK) without changing the orientation of the phantom. Once the veins were filled with contrast agent, 30° LAO, 30° RAO, and AP images were acquired (Figure 7.2 A and B). This procedure generated the set of dual-plane venograms. Unlike during an actual patient scan, the acquisition of the venograms followed lead positioning to prevent the contrast from diffusing into the phantom prior to lead position imaging.

7.2.2.2 Magnetic Resonance Imaging Acquisition

All MR scanning was performed on a Siemens Trio 3T (Siemens Medical Solutions, Erlangen, Germany). Prior to being loaded into the MRI scanner, the ventricles, coronary veins, and pacing markers were filled with diluted gadobenate dimeglumine (Gd-BOPTA) contrast agent (MultiHance, Bracco Diagnostics, Princeton, NJ) and all ports were closed using rubber corks. The contrast agent simulated the signal intensity in the MR venogram images. The phantom was placed into the same foam base to ensure consistent anatomical positioning of the coronary vein anatomy. A multi-element phased-array chest coil, identical to that used for patients, was placed over the phantom and two saline phantoms.

An EKG simulator was set at 60 bpm to provide feedback for cardiac gating. After obtaining localizers, the navigator was positioned at the air/water boundary of one of the

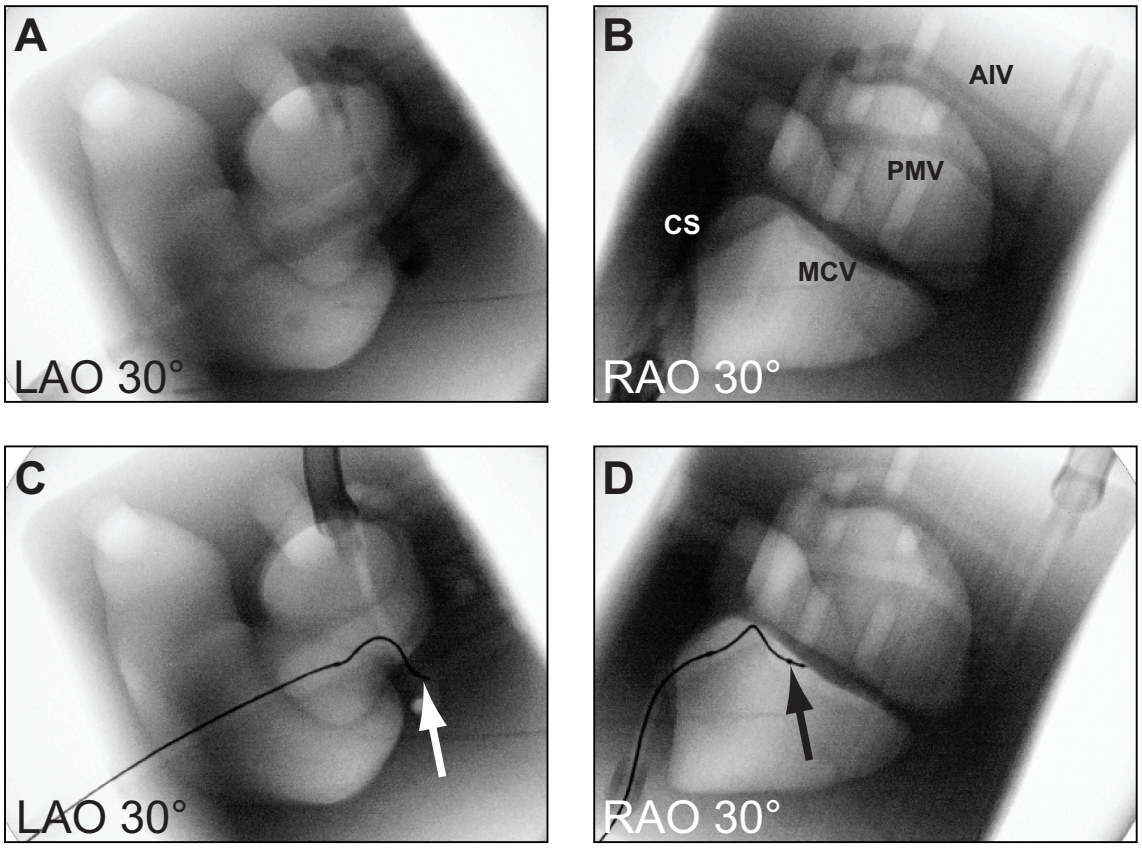

Figure 7.2: RAO and LAO 30° Angiographic images were acquired after contrast injection (A and B) and after LV pacing lead placement (C and D). The position of the LV lead is denoted with an arrow in C and D.

saline bottles, simulating a stationary diaphragm and 100% navigator efficiency. The 3D whole heart coronary vein scan sequence detailed in Chapter 5 was run with the following parameters: TE = 4.06 ms, FOV = 247 x 330 mm, acquisition matrix = 216 x 288, slice thickness = 2 mm, flip angle = 12°. MRCV of the coronary vein phantom required 4 minutes.

7.2.3 Validation of Lead Position

7.2.3.1 Comparison of Actual and Registered Lead Location

The LV lead mapping technique developed in Chapter 6 was used to map the LV lead position onto the AHA 17-segment model and into 3D MR coordinates [147]. The actual lead positions were determined in MR by finding the intersection of each marker and the coronary veins. Using the orientation and position information from the DICOM headers of the MR images, it was possible to map this position in image space to 3D world coordinates (Appendix C).

The error between the actual and registered lead locations was quantified using the root mean squared error (RMSE) between all six locations. RMSE was computed as shown in Equation 7.1, where n is the number of points (6), l represents the registered lead location and a represents that actual lead locations determined with MRI.

The lead positions were then mapped to the AHA 17-segment model and the error was computed as a percentage of an AHA segment in the longitudinal (radial) and circumferential directions.

$$RMSE = \sqrt{\frac{\sum_{i=1}^{n} ||l_i - a_i||^2}{n}} \tag{7.1}$$

7.2.3.2 Comparison with Mortensen's o'clock

An experienced observer was provided all angiographic images including dual-plane venograms and all six LV lead localizers. The RAO lead localizing image was used to estimate the longitudinal position of the pacing lead and the LAO lead localizer was used to estimate the circumferential position in each of the lead-localizing dual-plane images [144] (Figure 7.3).

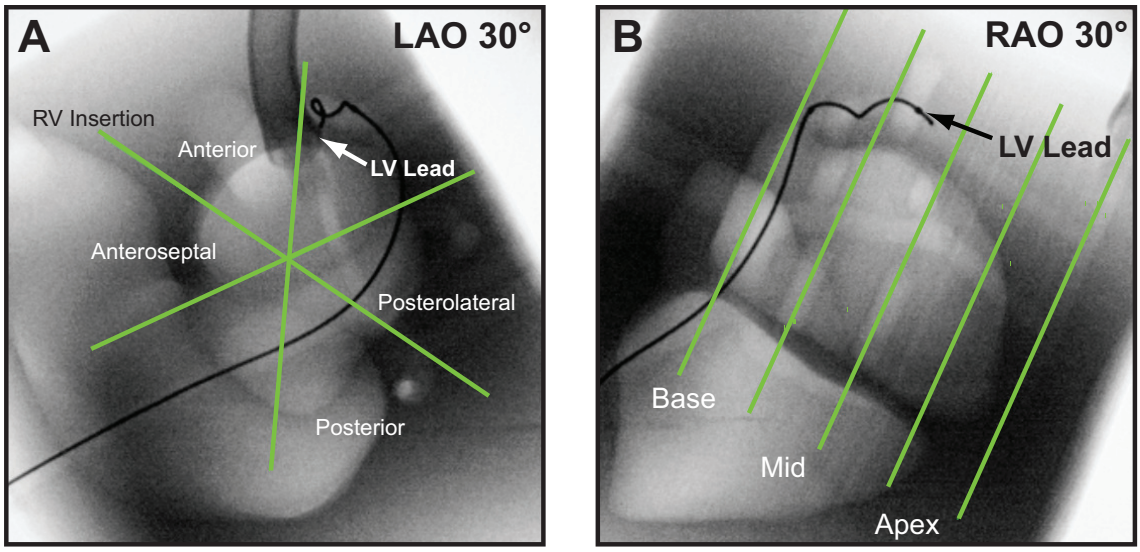

Figure 7.3: Dual-plane lead localizers were acquired after positioning the LV pacing lead at six potential pacing sites. The LAO image (A) was used to estimate the circumferential position of the lead and the RAO image (B) was used for the longitudinal position.

The estimated position of the LV pacing site was indicated on the AHA 17-segment model using custom-made software.

The projection of the actual pacing lead position onto the segment model was compared to the user-placed positions using Mortensen's o'clock. The error was computed as a percentage of an AHA segment in the longitudinal (radial) and circumferential directions. Three-dimensional error calculation cannot be performed because Mortensen's o'clock does not provide information in all three dimensions, only circumferential and longitudinal directions relative to the central axis of the LV.

7.3 Results

All images were successfully acquired for all six pacing sites with both modalities (Figure 7.2 and 7.4). In MRI, the contrast was sufficient to visualize all of the coronary veins, the ventricles, as well as all six potential pacing sites.

By comparing the actual position of the LV pacing lead in MRI to the registered lead location, we were able to compute the accuracy of our technique. The RMSE was found to be 4.27 mm between all six pacing sites (Figure 7.5 A).

Using the central axis of the LV, all 3D lead locations and coronary vein reconstruction

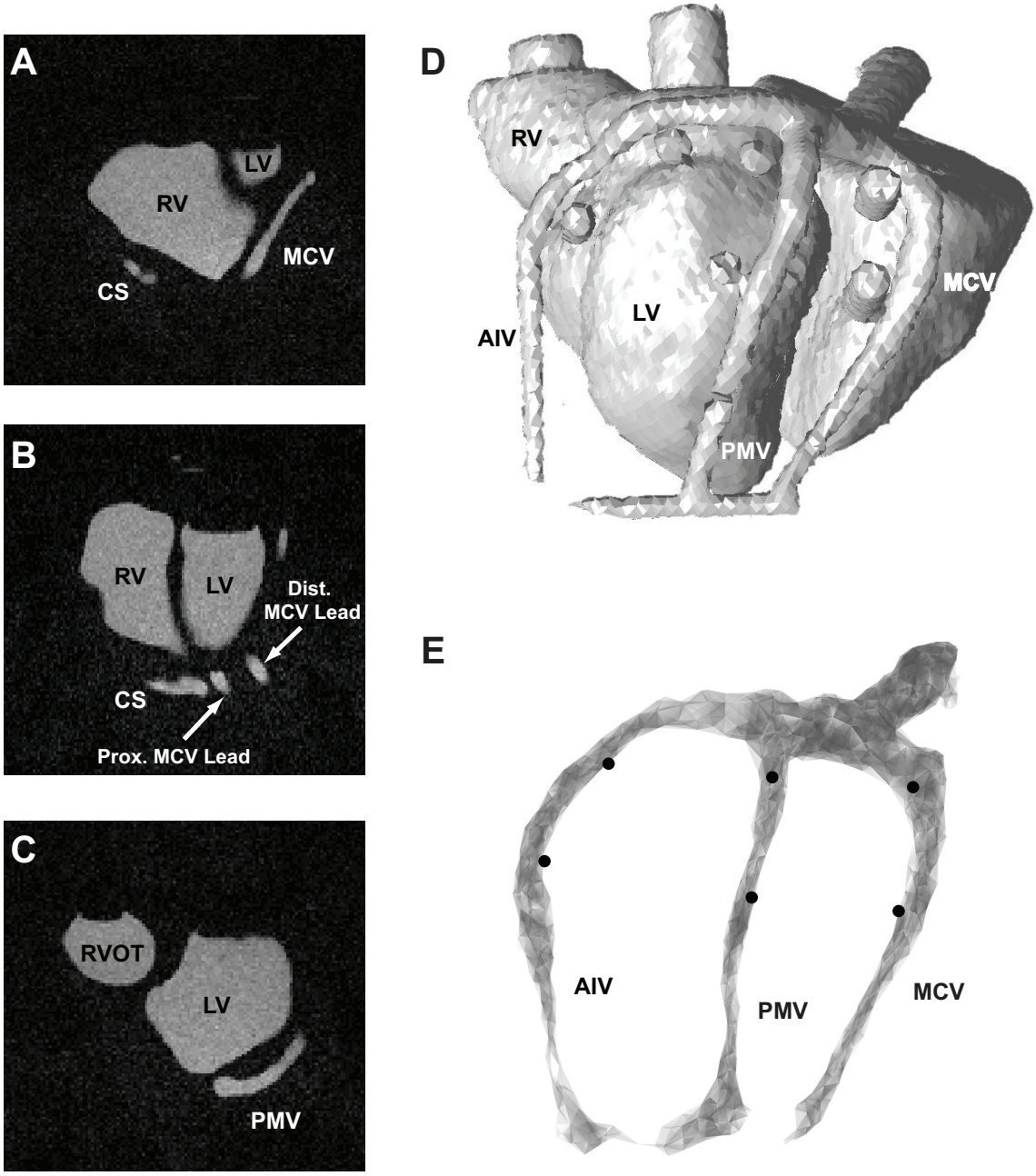

Figure 7.4: After filling the phantom with Gd-based contrast agent, transverse images were acquired of the coronary vein phantom to reveal the ventricles and coronary veins (A–C). An isosurface of the dataset shows that all vessels and potential pacing locations were sufficiently enhanced (D). Using user-selected points, the coronary veins were reconstructed and the pacing sites were identified (E).

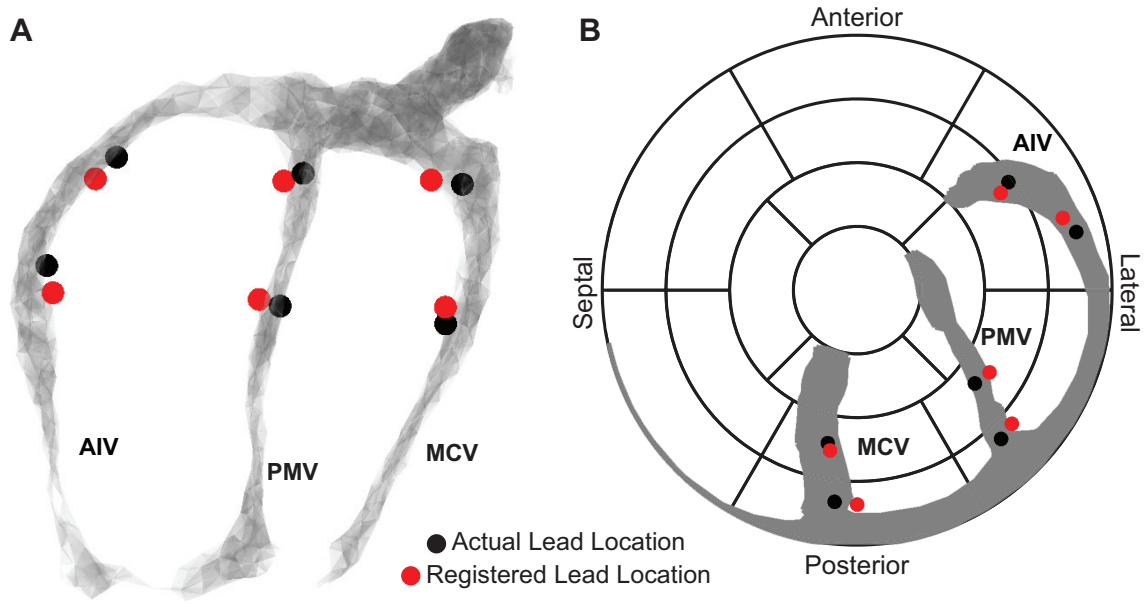

Figure 7.5: Pacing locations determined using our registration technique for dual-plane angiograms (red dots) were compared to actual pacing sites determined from MRI (black dots). Three-dimensional (A) and AHA 17-segment model (B) representations are shown.

were projected to the AHA 17-segment model. In all six cases, the actual and experimental pacing sites were within the same AHA segment (Figure 7.5 B). The average circumferential error was 4.17 ± 2.32° (Range: 1.26 – 6.53°) which was equivalent to 6.94 ± 3.87 % of an AHA segment (Range: 2.10 – 10.90%). The average longitudinal (radial) error was 13.36 ± 8.62% of an AHA segment (Range: 3.53 – 26.7%).

Using Mortensen's o'clock for localization of the LV pacing lead and comparing it to the actual lead location, the correct AHA segment was selected only twice (33%). The average circumferential error was 22.96 ± 10.15° (Range: 3.87 – 32.66°) which was equivalent to 38.27 ± 16.92% of an AHA segment (Range: 6.45 – 54.44%). The average longitudinal (radial) error was 57.82 ± 30.10% of an AHA segment (Range: 5.80 – 82.72%) (Figure 7.6).

7.4 Discussion

In this validation study, we found that our registration technique for localizing the LV pacing lead on MR data was more accurate than the Mortensen's o'clock method that has been used extensively in the literature. The RMSE between the actual and registered lead locations was 4.27 mm. When mapping LV lead location to the AHA 17-segment

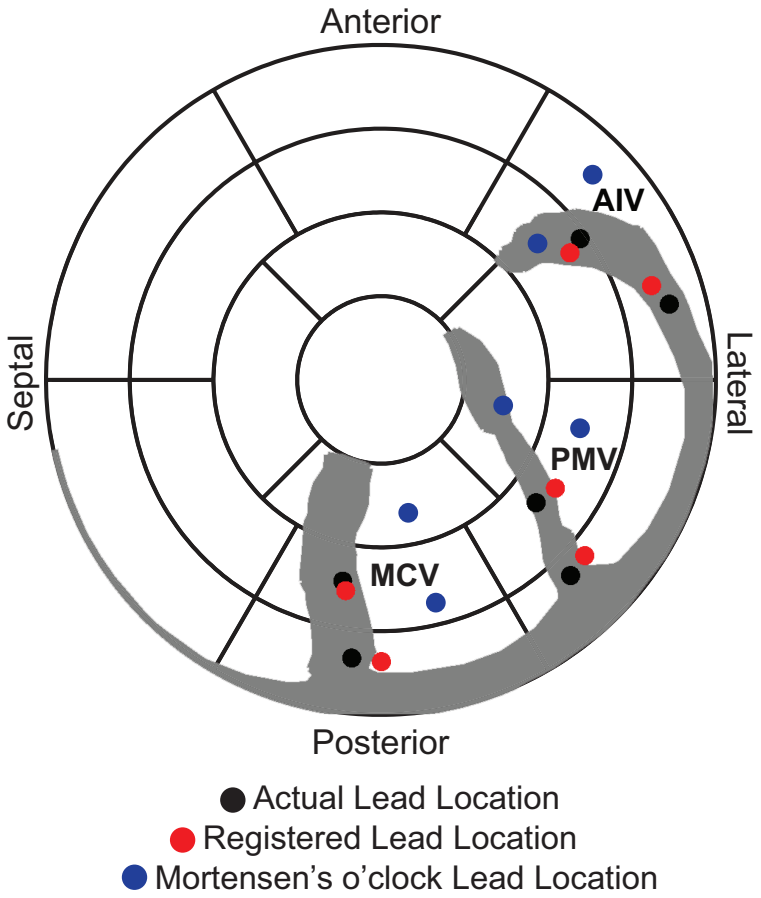

Figure 7.6: Six LV lead locations were determined using our registration technique (red) and the Mortensen's o'clock technique (blue). These lead positions were mapped onto the AHA 17-segment model alongside the actual lead positions (black).

model, our registration technique resulted in an error of 13.4% of an AHA segment in the longitudinal direction and 4.2% of an AHA segment in the circumferential direction. Conversely, Mortensen's o'clock mapping of the LV lead resulted in 57.8% of an AHA segment in the longitudinal direction and 38.3% of an AHA segment in the circumferential direction. Additionally, the registered lead positions were projected to the correct AHA segment 100% of the time with our methodology, while Mortensen's o'clock only had a 33% success rate.

Although the 4.27 mm RMSE between the actual lead locations and registered lead locations was non-zero, it was within an acceptable range. During phantom creation, the coronary vein segmentation from CTA was smoothed, resulting in relatively large diameters of the coronary veins (5.2 mm). Therefore, the RMSE was on the order of the vessel diameter of our phantom.

When comparing the placement of the LV pacing site on the AHA 17-segment model, we found that the actual and estimated pacing sites were within the same AHA segment in every case. Most analysis assesses the suitability of the LV pacing site based on a region the size of an AHA segment [30,87,104,228]. The longitudinal (radial) error found amongst our test sites was only 13.4% of an AHA segment and the circumferential error was 6.9% of an AHA segment. Therefore, a pacing site estimated using our technique would functionally correspond to the analysis using the actual pacing site.

When comparing our registration technique to Mortensen's o'clock we found that our error was significantly smaller. In this study, the use of Mortensen's o'clock was aided by the fact that the ventricles and coronary vasculature were somewhat visible in the dual-plane lead localizers due to the slight radio opacity of the phantom. As a result, the findings from this validation study are a "best-case scenario" for the Mortensen's o'clock method. Our registration technique relies upon the same imaging data that Mortensen's o'clock employs with the addition of the pre-implant MR coronary vein scan. As such, this technique could be suggested as a valid replacement as demonstrated by the superior accuracy and ability to obtain a true three-dimensional lead location.

7.4.1 Limitations

There are several potential sources of the error seen in this validation study. First, the channels representing our simulated pacing sites did not reach all the way to the coronary vein anatomy, but only came to within 2.5 mm of the vessels. Because of this, we had to estimate the intersection of the port and the coronary veins. This also affected guidance of the LV catheter during simulated LV lead implantation. The position of the pacing lead was guided primarily by fluoroscopy from the RAO projection. This projection only provides one angle of visualization, therefore positioning of the LV could potentially differ from the intended potential sites. Another source of the error is that the LV pacing lead, while being in the correct position longitudinally, may have been in different positions radially, such as against the vessel wall. MR-derived actual pacing sites were assumed to be at the center of the vessel. For this reason, it is possible that the positioning could theoretically be off by 2.5 mm (radius of the phantom vein) while still technically being in the correct location.

The current phantom was a simplified and ideal situation. There was no respiratory or cardiac motion applied to the phantom. Because of the lack of motion, it was guaranteed that the position of the lead localizers was the same as the venogram acquisition. This removes one potential source of error in the actual methodology.

7.5 Conclusions

By constructing a phantom model of the coronary veins and ventricles that could be imaged by both MR and x-ray angiography, we were able to assess the accuracy of our coronary vein registration technique. We found the error to be within a range that would have little effect on studies utilizing our registration technique to determine the suitability of an LV pacing site retrospectively.

7.6 Major Findings

- It was possible to view coronary vein anatomy and the position of the LV lead in both MRI and fluoroscopy using our coronary vein phantom

- The accuracy of our LV lead placement technique was 4 mm and within an AHA segment.
- Our methodology was more accurate than Mortensen's o'clock technique.

CHAPTER VIII

RELATIONSHIP BETWEEN REGIONAL DYSSYNCHRONY AND CRT RESPONSE

In this chapter, we apply our method of mapping regional LV contraction times (Chapter 3) in conjunction with our LV lead registration technique (Chapter 6) to determine contraction times at the site of the LV pacing lead. We performed a clinical assessment in CRT patients six months post-CRT to determine the relationship between mechanical contraction times at the site of the LV pacing lead and clinical response to CRT.

8.1 Introduction

Cardiac Resynchronization Therapy is a treatment option for heart failure patients with mechanical dyssynchrony [13–16]. Using current selection criteria (QRS duration $>$ 120 ms, EF $<$ 35%, NYHA Class III–IV, and optimal medical therapy for at least 1 month), approximately 30% of patients fail to benefit from CRT [69, 70, 85, 209]. Mechanical dyssynchrony is widely thought to be an important factor in determining if patients will responsd to CRT, the theory being that you cannot correct for dyssynchrony with biventricular pacing if no mechanical dyssynchrony is present [88, 89]. For this reason, many groups have sought to understand the relationship between the presence and location of mechanical dyssynchrony in the left ventricle and the ability of a patient to respond to CRT [46, 47, 90–92, 229, 230].

The majority of methods for detecting LV mechanical dyssynchrony are global metrics, characterizing the entirety of LV contraction with a single metric [89, 114, 115]. With the multi-center PROSPECT study, it was shown that no single echocardiographic mechanical dyssynchrony metric predicted CRT response [152]. There were several confounding factors with this study including poor reproducibility of the methods employed [231]. Additionally, the failure of the study may be at least partially attributed to the inability of echocardiography to image the entire LV. MRI suffers from fewer of these acquisition limitations, and as a result has been used to derive a number of measures of global dyssynchrony [114,115,124].

Some recent work suggests that it is not the global amount of dyssynchrony that is important, but also the location of the mechanically dyssynchronous regions [171, 232]. In the typical LBBB patient, the septal wall exhibits early mechanical contraction and the lateral wall contracts much later [19, 27]. To correct for this mechanical dyssynchrony within the ventricle through biventricular stimulation, it has been postulated that the LV pacing lead should be placed in the latest-contracting region of the lateral wall. Several studies have shown retrospectively that patients in which the pacing lead was placed in or near the latest contracting segment had superior outcomes compared to those in which pacing was remote to the late contracting segment [46, 90–92]. Other studies, however have demonstrated that a broad range of pacing locations within the lateral wall can result in successful resynchronization, and that lead position does not affect response rates [25, 233, 234]. These conflicting findings may be at least partially attributed to the unreliable methods for determining the LV pacing lead position in relation to the contraction times. In studies examining the relation of lead position and contraction time, the position of the LV lead was usually only classified as posterior, lateral, apical, basal, anterior. This classification does not allow for accurate lead localization and thus the analysis based on the pacing location is compromised.

In this dissertation, we have developed both a method to map regional contraction times within the left ventricle as well as a registration method for localizing pacing lead locations on these maps from intra-procedural fluoroscopic dual-plane images. By combining these methods, we can generate a high spatial resolution map of regional dyssynchrony and superimpose the exact location of the LV pacing lead. By applying this approach to patients undergoing CRT, we can better understand the relationship between mechanical dyssynchrony at the site of the LV pacing lead and CRT response.

The purpose of this study was to apply the developed methodology to determine: 1) the location of the latest contracting segment, 2) assess whether the latest segment was reachable via a coronary vein, 3) observe how often the LV pacing lead was placed in the latest contracting segment, and 4) determine if response to CRT was higher in patients in which the lead was placed in the latest contracting segment. We hypothesized that patients

in which the LV pacing lead is located in the latest contracting segment will have a higher response rate than those with the lead located in a remote location.

8.2 Methods

Nine consecutive patients that were referred to Emory University Hospital for CRT device implantation were enrolled in the study. All patients met current enrollment criteria for CRT (NYHA HF class II-IV, QRS duration $>$ 120 ms, EF $<$ 35%, and optimal medical therapy for 3 months). Four patients with lesser heart failure symptoms were included based on recent findings suggesting beneficial CRT device implantation in NYHA class II patients [64]. Patient selection was based on clinical factors and was not part of this study.

Twelve-lead EKGs were used to measure QRS duration and classify all patients based upon their QRS morphology. Left bundle branch block (LBBB) was defined as a QS or rS complex in V1 and/or V2; monophasic R wave in I, aVL, V5, and V6; and mid QRS notching or slurring in >2 of I, aVL, V1, V2, V5 or V6. Right bundle branch block was defined as R, rR', rsR', or rSR' complexes in V1 and slurred S wave in I and V6 [188]. Atypical LBBB (aLBBB) patients were characterized by a monophasic R wave in I, aVL, V5, and V6; but without the mid QRS notching or slurring in >2 of I, aVL, V1, V2, V5 or V6 seen in LBBB patients. Interventricular conduction delay (IVCD) included those that did not meet any of the above criteria.

This study was approved by the Emory Institutional Review Board.

8.2.1 Pre-Implant Magnetic Resonance Imaging

All patients received an MR examination prior to CRT device implantation (Figure 8.1). All imaging was performed on either a 1.5T or 3.0T Siemens Avanto system (Siemens Medical Solutions, Erlangen, Germany) using the protocol developed in Chapter 5. Briefly, localizers were acquired to determine initial patient anatomy. Two- and three-chamber (VLA and HLA) SSFP cines were acquired at 60 frames per cardiac cycle. Short-axis SSFP cines were acquired to span the entire ventricle. A Gd-chelate based contrast agent ($[\text{Gd-BOPTA}]^{2-}$, MultiHance; Bracco Imaging SpA, Milan, Italy) was injected intravenously at a rate of 0.3 mL/s. Acquisition of the respiratory and cardiac-gated 3D whole heart coronary vein scan

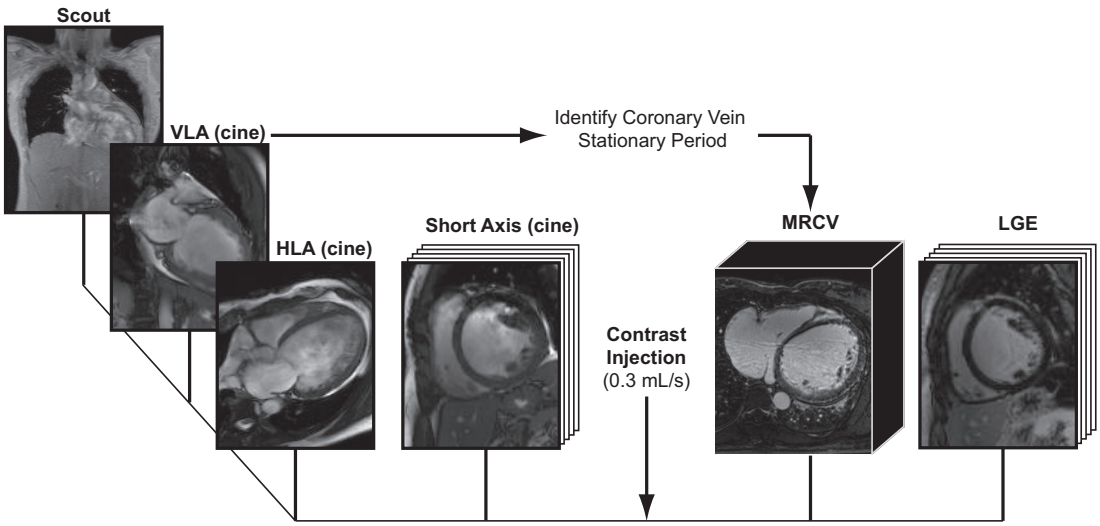

Figure 8.1: After obtaining localizers, horizontal and vertical long axis (HLA and VLA) cines were acquired with 60 frames per cardiac cycle. A stack of short axis cines were acquired to use for regional dyssynchrony detection. By identifying the stationary period of the coronary veins from the motion of the coronary sinus in the VLA image, we planned the coronary vein scan (MRCV). LGE imaging was performed immediately after the vein scan to detect myocardial infarction

was initiated 15 seconds after contrast injection was started [125, 136].

After completion of the coronary vein scan (approximately 12 minutes), late gadolinium enhancement (LGE) images were acquired. LGE imaging is an off-label use of Gd-chelate based contrast agent for imaging of myocardial infarction [121]. In a chronic myocardial infarction, the extracellular volume fraction is increased and more contrast can diffuse into the infarcted region than the healthy myocardium [122]. An inversion recovery (IR) sequence was used to obtain the image. An inversion time was selected to null the signal from the healthy myocardium. The contrast agent has a short T1, so the signal from the infarcted region is much brighter than the nulled healthy myocardium [123]. LGE images were obtained at the same locations as the SSFP cines to assess scar burden of the LV.

All images were exported from the scanner in the DICOM format.

8.2.2 Device Implantation and Imaging

All CRT device implantation procedures were performed at Emory University Hospital. The atrial sensing lead and RV pacing lead were first inserted via a transcatheter approach.

Prior to LV lead implantation, dual-plane venograms (30° RAO and LAO) were acquired with retrograde injection of iodinated contrast agent. LV pacing was targeted at the lateral or posterolateral region dependent upon venous access, lead stability, and absence of phrenic nerve stimulation [101, 216, 217]. Lead-localizing fluoroscopic images were then acquired at the same positions as the dual-plane venograms.

8.2.3 Regional Dyssynchrony Determination

Using the methodology developed in Chapter 3 and employing custom-written software, regional contraction timing maps were generated from radial displacement curves based on endocardial borders traced on high temporal resolution short-axis cine SSFP images. All contraction timing data was mapped to the standard AHA 17-segment model [147].

To determine the location of the latest contracting segment, we computed the average delay time within each segment of the AHA 17-segment model. To compute these averages, regional delay times throughout the LV were binned into AHA segments, and all delays within each segment were averaged. The latest AHA segment was identified as the segment with the latest mechanical contraction time.

8.2.4 Left Ventricular Lead Location Determination

The position of the LV pacing lead was determined using the registration methodology developed in Chapter 6. Briefly, by registering both the dual-plane (30° RAO and LAO) lead localizers and 3D MR reconstructed coronary vein anatomy to the dual-plane venograms, we were able to determine the spatial correspondence between the MR and x-ray coordinate systems. By selecting the location of the LV pacing lead in both lead localizers, we were able to determine the position of the LV pacing lead in 3D. This position was then mapped to the regional dyssynchrony AHA 17-segment model using the position of the central axis of the LV (Appendix A).

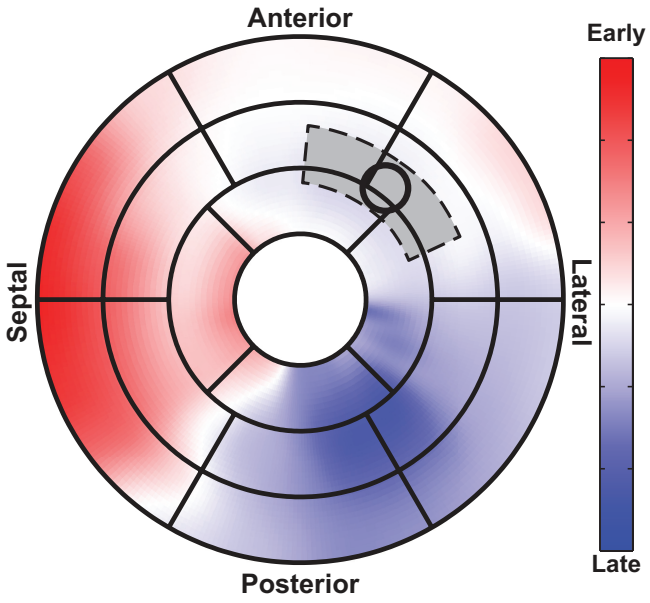

Figure 8.2: To compute the average delay time at the LV pacing site, mechanical contraction delay times in a region the size of an AHA segment (gray area) were averaged. The region was centered at the LV lead location (black circle).

8.2.5 Regional Dyssynchrony Determination

After the position of the LV pacing lead was projected onto the map of regional dyssynchrony, the contraction delay time in the region of the LV lead was determined. We considered the average delay time in a region the size of an AHA segment centered about the LV lead location (Figure 8.2).

To determine whether the LV lead was placed in the latest contracting AHA segment, the segment number in which the LV lead was implanted was compared directly to the latest contracting segment based on AHA segment averages. The LV pacing lead was considered to be adjacent to the latest contracting segment if it was implanted into any neighboring segment.

8.2.6 Patient Response

To determine patient response to CRT device implantation, a clinical assessment was performed 6 months post-implant. Each patient's clinical performance at this assessment was

compared to the baseline pre-implant evaluation. For this study, we utilized the following clinical criteria: NYHA heart failure classification, six-minute hall walk distance (6MWD), and Minnesota Living with Heart Failure Questionnaire (MLHFQ). We defined response the following ways:

- **NYHA Improvement ($\uparrow$ NYHA $\geq$ 1)** – The patient improved by at least one NYHA HF class [192, 235–237]
- **Increase in 6MWD ($\uparrow$ 6MWD $>$ 10%)** – Patient improved their 6MWD by at least 10% [84]
- **Composite ($\uparrow$ NYHA $\geq$ 1, $\uparrow$ 6MWD $>$ 50m, QoL $>$ 15)** – Required two of the following three parameters: NYHA improvement, increase in 6MWD of at least 50m, MLHFQ decrease of at least 15 points [229]

8.2.7 Statistics

Using the three different definitions of CRT response, we compared QRS duration between patients classified as responders and non-responders.

To determine if the delay time at the site of the LV pacing lead had any influence on CRT response, we compared the average delay times for a region the size of an AHA segment centered at the LV pacing site.

For all statistical analysis, a p-value < 0.05 was defined as statistically significant. All comparisons were performed using a two-tailed un-paired student's t-test.

8.3 Results

Imaging, post-processing, and follow-up assessments were successfully completed in 9 patients enrolled for CRT (Table 8.1). Only clinical baseline and 6-month follow-up data were obtained so all response metrics used in this study were based on clinical criteria.

Table 8.1: Patient Characteristics

Age (years)	61.9 ± 14.8
Male (%)	4 (44.4)
Ejection Fraction (%)	24.8 ± 10.4
QRS Duration (ms)	158.7 ± 14.6
Heart Failure Class	
II (%)	4 (44.4)
III (%)	5 (55.6)
QRS Morphology	
LBBB (%)	6 (66.7)
aLBBB (%)	2 (22.2)
IVCD (%)	1 (11.1)
Etiology	
Ischemic (%)	1 (11.1)
Non-Ischemic (%)	8 (88.9)

Table 8.2: Response Rates for Various Clinical Criteria

Response Criteria	**Non-Responders**	**Responders**
↑ NYHA ≥ 1	4 (44.4)	5 (55.5)
↑ 6MWD $> 10\%$	6 (66.7)	3 (33.3)
↑ NYHA ≥ 1, ↑ 6MWD > 50m, QoL > 15	5 (55.6)	4 (44.4)
All	3 (33.3)	2 (22.2)

8.3.1 Overall Response Rates

We classified all 9 patients as responders or non-responders using three common response criteria (Table 8.2). Based upon improvement in NYHA class, 56% (5/9) of patients responded. Sixty-seven percent (6/9) of patients responded according to improvement in their 6MWD, and 44% (4/9) responded when using a response criterion that considered all three clinical parameters. Overall there were three patients that failed to respond regardless of the response criteria and two patients who responded by all criteria.

8.3.2 Regional Dyssynchrony Maps

Using short-axis cine SSFP images, regional mechanical dyssynchrony maps of the LV were generated for all patients (Figure 8.3).

8.3.3 Location and Coronary Vein Access to the Latest Contracting

Using the maps of regional dyssynchrony derived from MRI short-axis images, we were able to determine average segment delay times (Figure 8.4) and identify the location of the latest contracting segment. The latest contracting segment was lateral in 2 patients, posterior in 2 patients, anterior in 2, and septal in 3. The longitudinal positions of the latest contracting segments were evenly distributed between basal, mid-basal and mid-apical locations (3 each). In all three of the patients with the latest contraction in the septum, we observed paradoxic motion of the septum in which there was early inward motion prior to systole followed by a larger displacement toward the end of systole [172, 238].

By projecting the MR coronary vein reconstruction onto the AHA 17-segment model, we were able to discern whether a coronary vein allowed access to the latest contracting segment. We found that in 6 patients (66.7%), there was a vein visible by MR that passed through the segment. In all patients in which there was not vein access to the latest-contracting segment, the late segment was located in the septum.

8.3.4 Effect of Pacing in the Latest Contracting Segment

Using our LV lead registration technique, we successfully determined the LV lead position in all 9 patients. The location of the LV pacing lead was lateral in 8 patients and anterior in 1 patient (Figure 8.5). The pacing lead was placed in a mid-apical segment in 2 patients, mid-basal in 1 patient, and basal in 6 patients.

To assess the effect of placing the LV pacing lead at the site of latest mechanical contraction, we analyzed the response rate when the pacing lead was placed in or near the latest contracting AHA segment. In this group of patients, the LV pacing lead was never placed in the latest contracting segment; however, there were four patients in which it was implanted into an adjacent segment. Table 8.3 shows the response rates for those patients in which the LV pacing lead was placed adjacent to the latest-contracting segment. The response rates in thing group ranged from 0 to 25% depending on response criteria used.

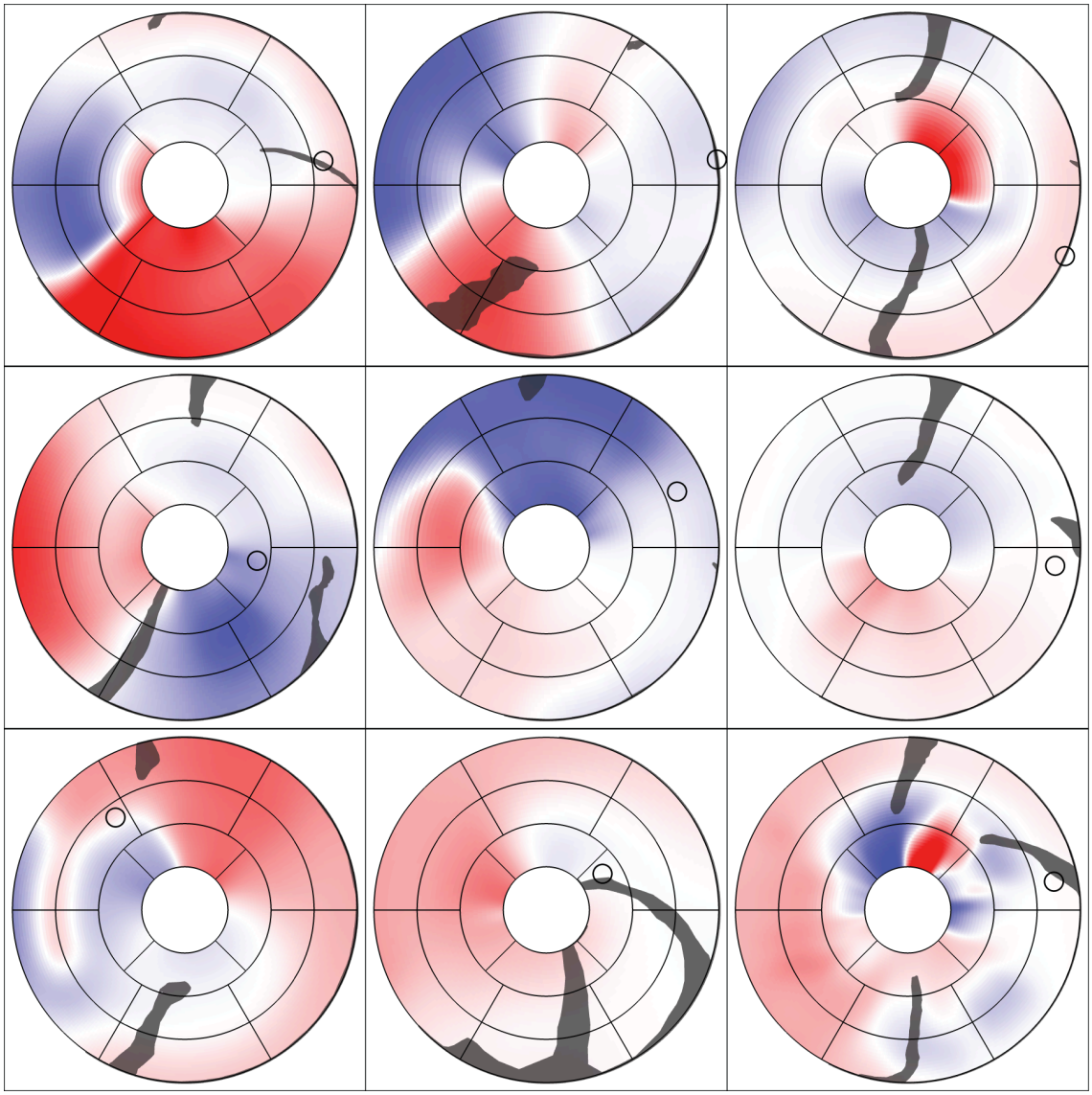

Figure 8.3: Dyssynchrony maps created using radial contraction curves from short-axis cine SSFP MR images. Red indicates early contraction, while blue represents late contracting regions. LV lead positions are shown with black circles and coronary veins from MRI are overlaid in gray.

Table 8.3: Response When Pacing Lead was In or Adjacent to Latest Contracting Segment

Response Criteria	Non-Responders	Responders
$\uparrow$ NYHA ≥ 1	3 (75)	1 (25)
$\uparrow$ 6MWD $> 10\%$	3 (75)	1 (25)
$\uparrow$ NYHA ≥ 1, $\uparrow$ 6MWD > 50m, QoL > 15	3 (75)	1 (25)
All	2 (100)	0 (0)

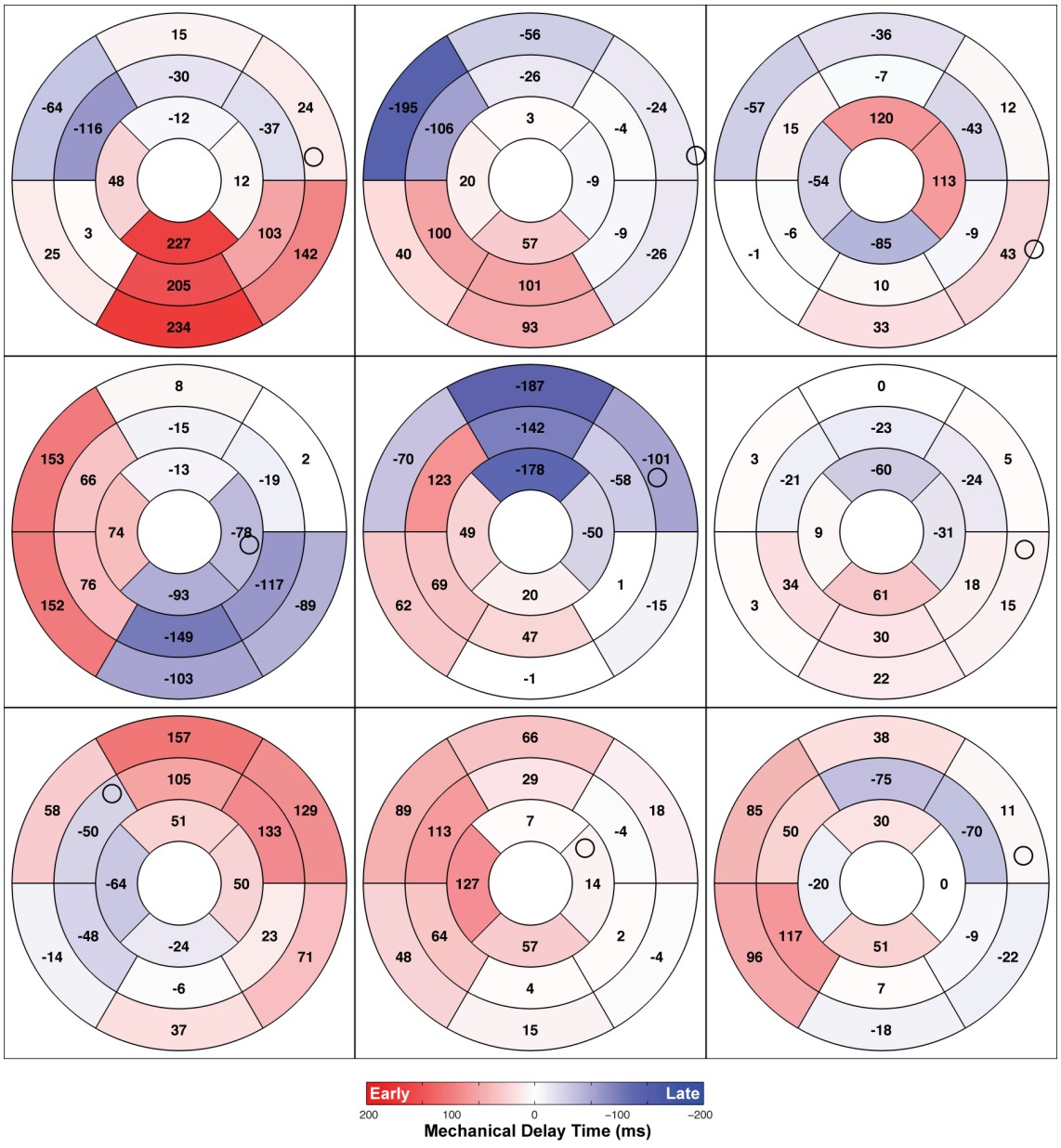

Figure 8.4: Regional delay times obtained from short-axis MR images were averaged within each segment of the AHA 17-segment model. The apex was excluded due to inability to properly contour the images from the apex. LV pacing locations are shown with black circles.

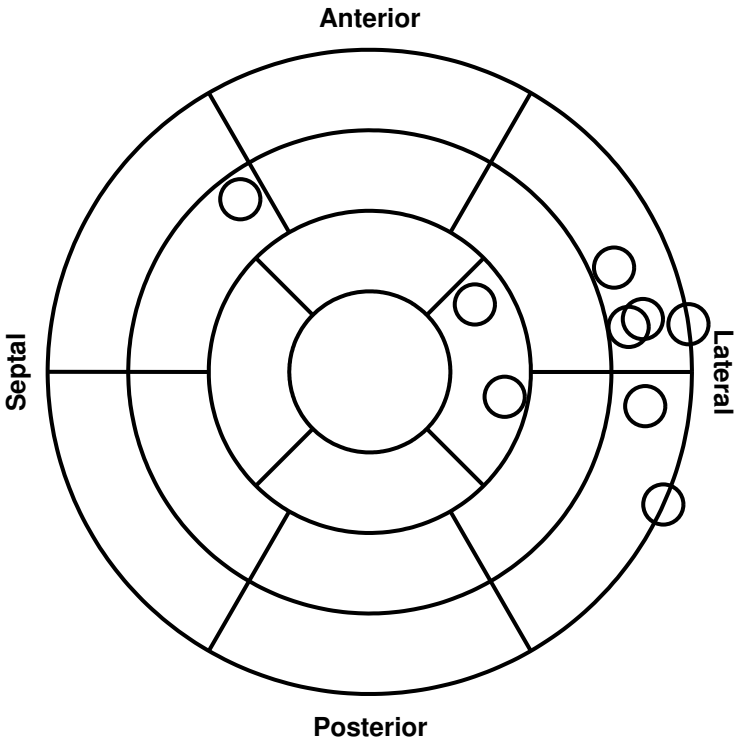

Figure 8.5: Localization of the left ventricular pacing lead on the AHA 17-segment model revealed that 8 (89%) of pacing leads were implanted in the lateral wall. There was a single lead implanted in the anterior interventricular vein. The LV pacing lead was placed in a mid-apical segment in 2 patients, mid-basal in 1 patient and basal in 6 patients.

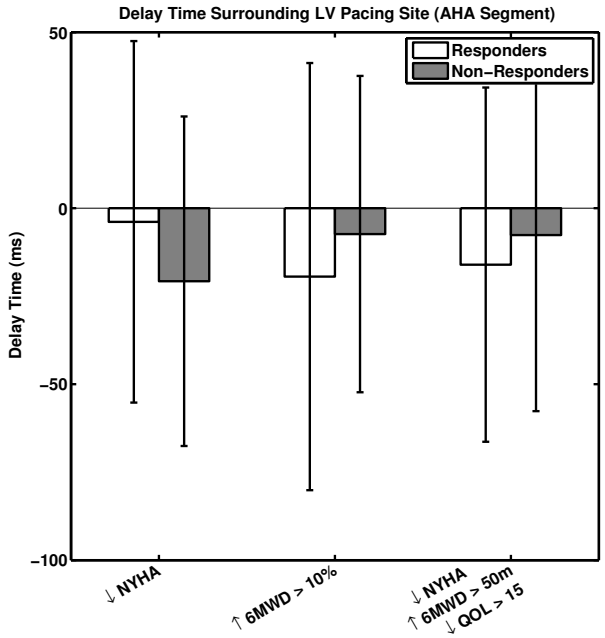

Figure 8.6: There was wide variability in the delay times in the AHA segment centered at the site of the LV pacing lead. There was no relationship between Segment delay time and patient response.

8.3.5 Relationship of Regional Mechanical Dyssynchrony and CRT Response

To look at the effect of regional dyssynchrony on CRT response, we assessed the mechanical delay time in a region the size of an AHA segment centered about the LV pacing site (Figure 8.6). There was no statistically significant difference between the mean delay times near the LV pacing lead in responders and non-responders.

8.3.6 Relationship of QRS and CRT Response

QRS Duration was compared between responders and non-responders to see if there was a relationship between global electrical dyssynchrony and response. There was no significant difference in the means of QRS duration between the two populations (Figure 8.7).

In this study, we had one patient with an interventricular conduction delay (IVCD) and two patients with atypical LBBB (aLBBB) as diagnosed from a 12-lead EKG. We assessed if QRS morphology affected response rates to CRT. Patients with aLBBB or IVCD failed to respond regardless of which response criterion was used. Response rates for LBBB patients ranged from 16.7 to 100% (Table 8.4).

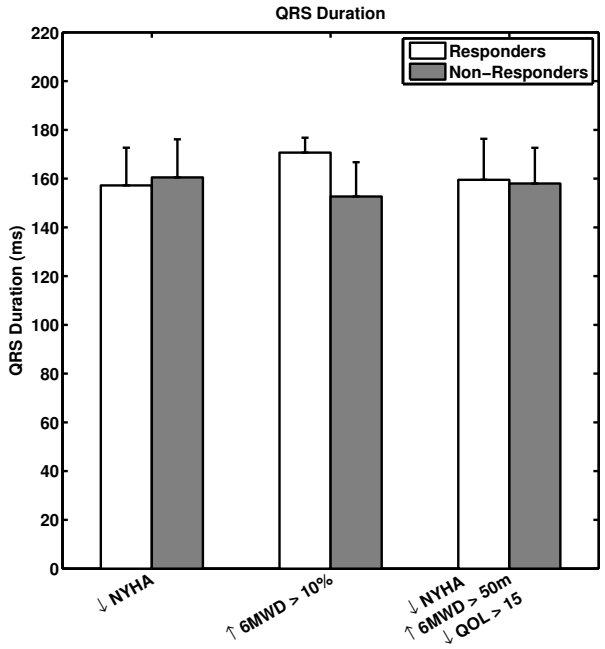

Figure 8.7: There was no statistically significant difference between QRS duration for responders and non-responders to CRT.

Table 8.4: Response Rates by QRS Morphology

Response Criteria	LBBB (n = 6)		aLBBB (n = 2)		IVCD (n = 1)	
	Non-Resp	**Resp**	**Non-Resp**	**Resp**	**Non-Resp**	**Resp**
↑ NYHA ≥ 1	1 (16.7)	5 (83.3)	2 (100)	0 (0)	1 (100)	0 (0)
↑ 6MWD $> 10\%$	3 (50.0)	3 (50.0)	2 (100)	0 (0)	1 (100)	0 (0)
↑ NYHA ≥ 1, ↑ 6MWD > 50m, ↓ QoL > 15	2 (33.3)	4 (66.7)	2 (100)	0 (0)	1 (100)	0 (0)
All	0 (0)	2 (100)	2 (100)	0 (0)	1 (100)	0 (0)

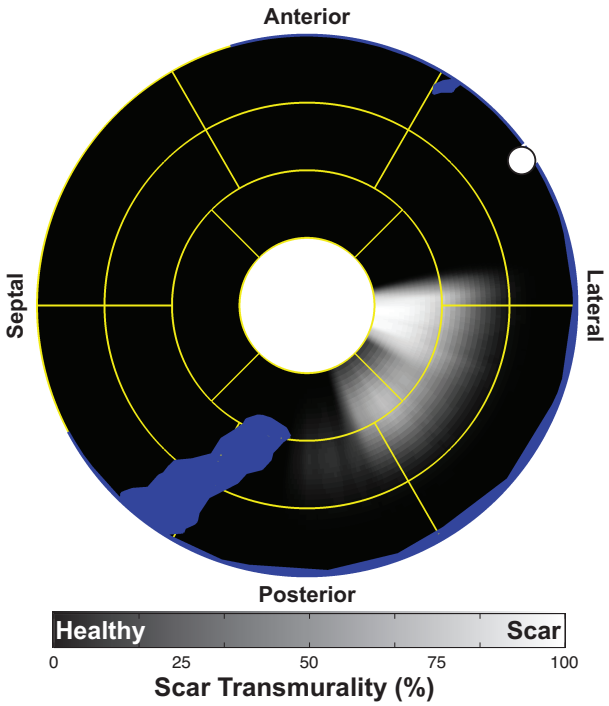

Figure 8.8: There was only one ischemic patient in our group of patients. The infarct was posterolateral while the pacing lead was placed anterolateral. This patient did not respond to CRT.

8.3.7 Relationship of Myocardial Infarction and CRT Response

We only had one ischemic patient in our patient population. From analysis of LGE MRI data, we determined that the LV had a total scar burden of 5.4% of LV mass (Figure 8.8). The LV pacing lead was placed in a basal anterolateral segment, which was remote from the infarct region. In addition to being ischemic, this patient was characterized as aLBBB. This patient failed to meet any of the criteria for patient response.

8.4 Discussion

In this study, we successfully applied the methodology developed for determining mechanical contraction delay and mapping of lead location to a group of patients undergoing CRT. The main findings of this study were: 1) in 67% of patients, the site of latest contraction could be reached by a coronary vein, 2) no patient had the lead placed in the latest contracting segment, 3) response rates were not different in patients with the lead implanted in the latest segment (or adjacent) compared to patients with a remote lead location.

8.4.1 Non-Response Rates

In our cohort of 9 CRT patients, we found non-response rates to be significantly higher than previously reported rates of 30% [69, 70, 85, 209]. Based on four different response criteria, our non-response rates ranged from 33 – 67%. Most likely this discrepancy is due to the small size of this study and the enrollment for patients with NYHA class II HF. Decreasing NYHA HF class from II to I is a major change. It is important to note, however, that although hard response cutoffs yielded low response rates, most patients improved to a lesser degree in all criteria. No patient deteriorated in NYHA heart failure classification, 89% of patients exhibited improved QoL, and 67% of patients improved their six-minute walk distance.

8.4.2 Effect of QRS Duration

Although QRS duration is used as a surrogate of electrical dyssynchrony for the selection of patients for CRT, it has been widely reported that QRS duration is a poor predictor of response in CRT patients [78, 85, 239]. Our findings agree with this previous work in that we saw no statistically significant difference in QRS duration between those who did and did not benefit from CRT.

8.4.3 Effect of Regional Mechanical Dyssynchrony

We were able to directly determine the mechanical contraction delay time at the location of the LV pacing lead using the methodology developed in this work. We failed to see a significant difference between absolute delay times at the site of the LV pacing lead in responders and non-responders. There was actually a large variation in the delay times at the pacing site (Range: -94.8 – 42.5 ms). For most response criteria, however, the trend was that responders had a larger mechanical delay at the site of the LV pacing lead but the value was not significant.

8.4.4 Effect of Pacing the Latest Contracting Segment

Current guidelines recommend pacing in a lateral or posterolateral vein; however, as we have shown in this study the position of the latest-contracting segment varies greatly, with

the most frequent delayed region being anterior. This heterogeneity of dyssynchrony agrees with data from the MADIT-CRT study in which the latest contracting segment was shown to vary from patient to patient [28]. Additionally, the TARGET study used echo speckle-tracking to show that the site of latest-contraction and ideal pacing site is very patient-specific [173]. In three patients, the latest contracting AHA segment was located in the septum. In all other patients, we were able to use MRI to visualize a vein from which the latest segment could be accessed. This indicates that our MRCV imaging protocol would be useful for determining if the latest contracting segment was accessible to the LV pacing lead.

Although we did not have any patients in whom the LV pacing lead was placed in the latest contracting segment, we did have four patients where it was implanted in a neighboring segment. In these four patients, the non-response rate ranged from 75 to 100%. This conflicts with some previous studies that have shown the benefit of pacing in the latest contracting segment. In this group of patients, our data suggest that pacing near the latest-activated region does not improve response.

8.4.5 Effect of QRS Morphology

Left bundle branch block (LBBB) results in a widened QRS complex and extended contraction times within the left ventricle. The conduction block typically causes early septal contraction followed by late contraction of the lateral wall. CRT theoretically corrects for this conduction block by electrically stimulating the lateral and septal walls of the LV to contract at the same time. CRT has been shown to be of little benefit to patients with IVCD or RBBB [240, 241]. In our study, we had three patients (33.3%) that had non-LBBB QRS morphology. All three of these patients failed to respond to CRT, regardless of which criteria was used to define response. While the presence of LBBB did not predict a patient's ability to respond (16.7 – 100% Non-response), it had a negative predictive value of 100%. Due to the small sample size of this study, this is by no means definitive, but remains a point of interest.

8.4.6 Effect of Myocardial Infarction on CRT Response

Only one patient (11.1%) suffered from ischemic cardiomyopathy. This patient presented with a previous posterior myocardial infarction. The LV pacing lead was placed in a basal anterolateral segment to obtain the necessary capture threshold. Because it was only a single patient, it was difficult to study the combined effect of regional scar and dyssynchrony distributions on CRT response. It is important to note, however, that this patient failed to respond according to any response criteria. Future studies should incorporate both myocardial scar distributions and regional dyssynchrony measurements to elucidate their combined effect on CRT response.

8.4.7 Effect of General Pacing Location

It has previously been shown that apical pacing negatively affects a patient's ability to respond to CRT [28, 242]. In this study, we had two patients in which the LV pacing lead was placed in a mid-apical lateral segment. One of these patients was the only patient that was considered a responder by all clinical criteria. The other patient was classified as a responder by all criteria except an improvement in 6MWD, although they did see an 8% improvement in 6MWD.

The only patient in whom the LV pacing lead was placed in anterior interventricular vein failed to respond to CRT by any metric. The latest contracting segment in this patient was in the anterior wall of the LV.

8.4.8 Limitations

The primary limitation of this work is that it only includes a cohort of 9 patients and therefore its not sufficiently powered to draw conclusions regarding the relationship between mechanical dyssynchrony, LV lead position, and CRT response. Rather, the goal of this study was to show that the methodology developed in this thesis could be applied to provide a more detailed analysis of the influence of a variety of factors on CRT response.

Another limitation is that only clinical response criteria were considered. Analysis of baseline and follow-up echocardiographic data is currently being performed and will

eventually be incorporated into this work to determine whether there is a relationship between dyssynchrony and quantitative response criteria.

Another major limitation is in the definition of CRT response. Fornwalt et al. analyzed response data for 426 patients from the PROSPECT trial using 15 metrics commonly employed to predict response [80]. They found that there was poor agreement between any of the parameters, implying that it is difficult to study how a factor such as mechanical dyssynchrony affects response when we do not truly know how to define response. In our study, the non-response rate ranged from 44 to 67% depending on the criteria used to determine response. For example, there was a patient that decreased heart failure class and increased their 6MWD by 37 meters (a responder by NYHA criteria); however, their MLHFQ score worsened by a total of 14 points. Conversely, there was a patient whose MLHFQ score improved from 72 to 15; however, their heart failure classification did not improve; therefore most criteria would characterize them as a non-responder. It is difficult to determine how certain factors affect response until a standard definition is developed.

8.5 Conclusions

We found no relationship between the amount of regional dyssynchrony present at the LV pacing site and response to CRT. Our study agrees with results from the MADIT-CRT study in which the location of the latest-contracting segment was heterogenous amongst CRT patients. The latest contracting segment was accessible via the coronary veins in 66% of patients. This study demonstrates that the techniques that we have developed can be used to study the relationship between mechanical contraction times, LV lead placement, and CRT response.

8.6 Major Findings

- It was possible to generate regional mechanical dyssynchrony maps and LV lead locations in CRT patient populations.
- Clinical response rates were low.

- The location of the latest contracting segment was heterogenous in our patient population.
- The latest contracting segment was accessible by a coronary vein in 67% of patients.

CHAPTER IX

CONCLUSIONS AND FUTURE WORK

9.1 Summary

The overall goal of this project was to develop the methodology necessary to assess mechanical contraction times at the site of left ventricular pacing lead in order to understand how regional dyssynchrony affects response to cardiac resynchronization therapy. We developed two new methods to achieve this goal. First, we created regional contraction timing maps from short-axis cine SSFP images, which improved upon global measures of dyssynchrony and did not rely on complicated methods for acquiring data to assess regional timing with MRI. The second method provides a way for us to map the final LV lead location, determined from dual single-plane fluoroscopy, onto the MR map of dyssynchrony. By combining these two techniques with clinical measures of response, it was possible to determine the relationship between dyssynchrony at the site of LV pacing and response to CRT.

The purpose of Specific Aim 1 was to develop a reproducible method for mapping regional contraction times and detecting regional left ventricular mechanical dyssynchrony. Many global metrics to detect dyssynchrony within the LV have been developed [46, 90–92]; however, recent studies suggest that the amount of dyssynchrony at the LV pacing site is more critical to a patients response to CRT [16, 107]. Some MR-based techniques for estimating LV regional dyssynchrony exist, but their utility is limited due to specialized acquisitions or complicated post-processing [117, 120]. We developed a method that uses high temporal resolution short-axis SSFP cine MR images to derive regional delay times from radial displacement of the myocardium. We demonstrated the performance and reproducibility of our methodology in a small patient population of patients enrolled for CRT.

First, we characterized normal delay times by applying our method in 10 healthy individuals and applied these limits on normal contraction to data from 27 CRT patients to compute the size and location of dyssynchronous regions. Second, we applied our method

in an effort to understand how mechanical dyssynchrony relates to underlying electrical activation delays. By comparing mechanical delay times using our regional dyssynchrony technique with electrical activation times from intra-procedural electrogram measurements, we were able to study the relationship between electrical and mechanical dyssynchrony at potential LV pacing sites within the coronary veins.

Overall, this aim demonstrated that regional dyssynchrony could be determined from short-axis cine MR images. By applying this regional dyssynchrony technique in CRT patients, we found that the location of the latest-contracting segment was heterogeneous amongst patients, and that there was a strong correlation between electrical and mechanical dyssynchrony in CRT patients.

The purpose of Specific Aim 2 was two-fold. First, we used data obtained from 3D whole-heart coronary vein scans to generate 3D reconstructions of the coronary sinus and its tributaries. By projecting this reconstruction onto the AHA 17-segment model, we were able to assess potential LV pacing sites relative to distributions of regional contraction timing and myocardial scar. This technique allows an electrophysiologist to determine the suitability of potential LV lead pacing sites prior to device implantation.

Using the coronary vein anatomy from MR, and dual-plane venograms and lead localizers, we developed a method to determine the position of the LV pacing lead with respect to the regional dyssynchrony maps created in Specific Aim 1. Our lead localization technique utilized images that can be part of the standard CRT implantation procedure: dual single-plane contrast-enhanced venograms, and biplane lead localizing radiographs. The fluoroscopic imaging system geometry was calibrated to correspond to the MR coordinate system using a projection of the coronary venous anatomy onto the biplane imaging planes. After accounting for cardiac and respiratory motion, the final LV lead location could be mapped directly from biplane images into 3D MR coordinates. The accuracy of our method was assessed using a coronary vein phantom in which the LV lead positions were capable of being imaged with both MR and fluoroscopy. The root mean squared error between our technique and the actual lead locations was 4.2 mm. This was a significant improvement over currently employed techniques for lead localization [144]. By accurately determining

the position of the LV lead post-implantation, we can more accurately assess the effect of a variety of factors on CRT response.

The purpose of Specific Aim 3 was to apply the methods we developed to determine the relationship between contraction timing at the LV pacing site and response to CRT. Several studies have found that pacing at the latest-contracting segment of the LV improves patient response [16, 87, 107]; however, their lead localization techniques were very coarse, potentially confounding their results. Using regional dyssynchrony measurements based on the methodology developed in Specific Aim 1, and final LV lead location computed based upon the techniques from Specific Aim 2, we were able to conduct a high-resolution analysis of the interaction of regional dyssynchrony and LV pacing site. In our small population of 9 patients enrolled for CRT, we found that no dyssynchrony metrics were statistically different between responders and non-responders and no dyssynchrony parameter was able to discriminate between responders and non-responders.

9.2 Potential Future Work

9.2.1 Detection of Akinetic Segments

Cross-correlation is a reliable way to determine regional delay times due to its utilization of the entire signal, rather than just the peak or upslope [48]. An additional benefit of cross correlation is that each delay is accompanied by a correlation value, which is indicative of the similarity of the radial contraction to the reference. In infarcted tissue of the heart, the healthy myocytes are replaced by non-contracting fibrous tissue and in hibernating tissue, function is down-regulated and contraction does not occur. Healthy myocardium surrounding the non-contracting tissue remains tethered and pulls the infarcted myocardium, causing a radial displacement [243, 244]. Theoretically, this displacement would look very different from active contraction and would therefore have a lower correlation value. A study could be conducted to determine the relationship between the correlation values obtained with our regional dyssynchrony method and the transmurality of the infarction at a particular location. If there was found to be a relationship, then our method could be used to not just detect regional dyssynchrony, but would allow for the identification of akinetic segment.

9.2.2 Paradoxic Septal Motion

When applying our regional contraction timing technique in a wide range of CRT patients, there were several cases in which the septum moved inward twice during the cardiac cycle. The radial displacement curve for this particular type of patient showed a small inward motion prior to systole followed by a larger displacement toward the end of systole. With our cross-correlation analysis of regional delay time, the larger of the two displacements was detected. It is important to understand if this early septal motion is the result of early electrical activation or is passive motion caused by higher right ventricular pressures. If it is active movement, our method needs to be able to detect this as the true delay for the region. To assess whether when the actual contraction of the septum occurs, the thickness of the myocardium can be determined over the cardiac cycle. The myocardium will not thicken unless active contraction is occurring. Using this methodology, we can determine which motion of the septum our method should detect, and also whether this motion should be considered dyssynchronous.

9.2.3 Relationship of Mechanical and Electrical Dyssynchrony During RV Pacing

In this study, we investigated the relationship between electrical and mechanical dyssynchrony under intrinsic rhythm, i.e. no external pacing. In 10 patients enrolled for CRT, we found a strong correlation between electrical and mechanical delay times at pacing locations within the coronary sinus. Additionally, we found that, at these sites, the latest mechanical location always corresponded to the latest electrical activation. From this, we were able to conclude that a map of regional dyssynchrony in the LV was useful for pre-operative planning of CRT lead placement. Unfortunately, this is only indicative of the situation during intrinsic rhythm. In CRT, there is an RV pacing lead in addition to the LV lead pacing the apical wall of the LV. It is unclear if the latest-contracting segment during intrinsic rhythm remains the same when RV pacing is applied. There need to be further studies to determine if the strong relationship between MR-derived mechanical delay times and local electrical

delay times remains even under RV pacing. If this correlation still holds, MR-derived regional dyssynchrony metrics can be used even more confidently for CRT LV lead placement planning.

9.2.4 Further Validation of Left Ventricular Lead Localization

To validate our lead localization methodology, we constructed and imaged a coronary vein phantom. Although it was based on actual anatomy, it cannot completely simulate a patient. Our registration methodology is designed to compensate for both respiratory and cardiac motion, neither of which the current phantom is able to recreate. It is possible to develop a more complicated phantom that can simulate patient motion; however, it would be ideal to be able to validate the lead position in actual patients. Three-dimensional coronary vein geometry can be generated from contrast-enhanced CT angiograms and can therefore be substituted for the MR-derived anatomy in our lead localization technique. Furthermore, CT is capable of imaging the position of the LV lead post-implantation and can therefore be used to image the actual lead location. By comparing the estimated and actual lead locations in a number of patients, the true accuracy of our technique could be assessed.

9.2.5 Effect of Myocardial Scar on Response

In this dissertation, we have provided a method for mapping LV lead position from dual single-plane fluoroscopy to the AHA 17-segment model to retrospectively assess the suitability of the LV pacing site. Using our method for detecting regional dyssynchrony, we assessed the degree of dyssynchrony present at the pacing site and its effect on CRT response. Several studies have shown that in addition to regional dyssynchrony, the amount of myocardial scar at the site of the LV pacing lead determines whether a patient will respond [40, 93, 94, 96–99, 192]. Our improved lead mapping technique can be applied in ischemic patients with a chronic MI to more accurately assess the effects of myocardial scar. In the current study we only had a single ischemic patient, therefore it is difficult to make generalizations based upon our observations.

9.2.6 Application of Regional Dyssynchrony Analysis to Other MR Sequences and Modalities

In this work, we computed the regional delay times between radial displacement curves obtained from short-axis cine MR images. The methodology is not limited to this type of data, but can be applied to data from a number of analysis and imaging techniques. For example, strains can be computed at locations throughout the myocardium over the cardiac cycle using an advanced imaging technology such as DENSE [245]. Similar to our analysis with radial displacement curves, strain data can be clustered to determine a reference, and cross-correlation can estimate a delay time between each curve and the reference. Future work could determine the suitability of our methodology for assessing regional delay times from different measurements of cardiac motion and contractility and various modalities including CT and SPECT.

9.2.7 CRT Response Prediction

We have presented initial findings regarding the relationship between regional dyssynchrony and CRT response. This study only consisted of 9 patients, and thus was not sufficiently powered to make any conclusions and generalize the results to all CRT patients. By increasing the number of patients, the study would be properly powered to detect the differences between responders and non-responders. By increasing the number of patients, and using our improved methods, future work can discern the relationship between regional dyssynchrony, myocardial infarction, and LV lead location and be used to improve patient response to CRT.

9.2.8 Utilization of Quantitative Echocardiographic CRT Response Criteria

In the current study, we relied upon clinical measures of response to CRT. Although these metrics are indicative of the effect that heart failure has on a patient's personal life, they are relatively subjective measures. In addition to clinical response criteria, future studies should incorporate quantitative echocardiographic measures of left ventricular reverse remodeling. By combining these two categories of response criteria, we would be able to better understand how and if a patient responded to the treatment.

9.2.9 Decrease Processing Time

Ideally, the methodology developed in this thesis could be used to pre-operatively plan the LV lead placement using the MR coronary vein scan and regional mechanical contraction maps. In the current implementation, the endocardial contours required for regional delay calculations are drawn semi-automatically. This process is slow due to the fact that we are acquiring data at 60 frames per cardiac cycle. If a patient has 10 short axis slices, that is 600 individual images that have to be contoured (takes 4 hours for an experienced user). An automated segmentation algorithm could considerably improve the processing time required to make this a feasible tool for lead placement planning.

9.3 Clinical Implications

The overall goal of this project was to develop techniques that allow us to more accurately assess the relationship between mechanical dyssynchrony, electrical dyssynchrony, LV pacing location, and response to CRT. This is important because currently, at least 30% of patients who receive CRT devices fail to respond to the treatment [69, 70, 108, 209]. Current CRT enrollment criteria consider cardiac output, and electrical dyssynchrony, but there is no pre-operative assessment of mechanical dyssynchrony [59, 246]. Unfortunately, when echocardiographic-based measures of mechanical dyssynchrony were considered for patient selection in a large multi-center trial (PROSPECT), there was no improvement in outcomes [152]. By using MRI for our dyssynchrony assessment, we can potentially overcome some of the reproducibility issues that plague echocardiography [29, 231]. Additionally, our regional dyssynchrony method improves upon current techniques by using standard images, which makes it feasible for use in future multi-center studies. Recently, focus has shifted to looking at the amount of mechanical dyssynchrony at the actual LV pacing lead, rather than across the entire LV. To properly study the effect of LV pacing lead location on response to CRT, it is essential to accurately determine the position of the lead. A reliable lead-mapping technique is needed because the current techniques have poor reproducibility and low accuracy. Our lead mapping technique was accurate to within several millimeters.

By combining this accurate lead-mapping technique with our high-resolution maps of regional dyssynchrony, we can determine the actual mechanical delay at the actual LV pacing site, and study the relationship. This work has a high impact because it is not limited to mechanical dyssynchrony assessment. Using our method, LV lead location can be mapped onto the AHA 17-segment model to be compared with any parameter. With the development of more accurate and reproducible techniques, we may be able to remove much of the variability that exists in the field and actually determine the factors that affect CRT response.

APPENDIX A

MAPPING THREE-DIMENSIONAL POINTS TO THE AHA 17-SEGMENT MODEL

The American Heart Association (AHA) 17-segment model is a segmented model of the left ventricle for improving communication between imaging modalities for research and clinical purposes [147]. It is a polar plot where data from each slice is represented as a concentric ring with apical slices located at the center of the plot while the most basal slice is on the outside.

The AHA 17-segment model only represents data from two dimensions relative to the central axis of the LV: longitudinal and circumferential. The procedure for mapping any point in 3D onto the AHA 17-segment model is detailed below.

A.1 Determination of the Left Ventricular Central Axis

To map points to the AHA 17-segment model, the position of the LV must be known in three dimensions. We determine the central axis of the LV from two- and four-chamber images. Endocardial contours are traced on the two- and four-chamber images long axis images. The mitral valve plane is identified in each view by manually selecting the edges of the annulus. The apex is defined as the centroid of the bottom 15% of the LV. A line extending from the midpoint of the valve plane to the apex of the LV served as the central axis within each image. Using 3D position information from the DICOM header, the central axis in each view was converted to a plane normal to the imaging plane. The intersection of these planes in 3D was used as the central axis of the LV.

For a given dataset, such as regional dyssynchrony analysis, information is only available for a finite number of slices, and analysis rarely considers the most basal and apical portions of the LV. To account for this, the basal end-point of the central axis (X_b, Y_b, Z_b) is the intersection of the central axis with the most-basal slice in which the analysis was performed.

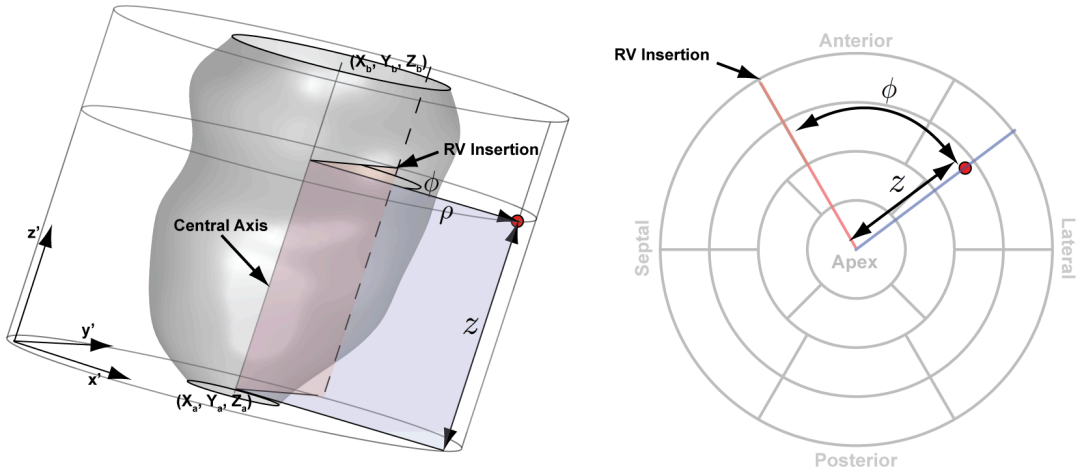

Figure A.1: Any point in 3D can be mapped to the AHA 17-segment model. After converting to an alternate coordinate system, the point can be converted to cylindrical coordinates. By discarding the radius value (ρ), we can then map the location directly to the AHA segment model

Similarly, the apical central axis endpoint (X_a, Y_a, Z_a) was the intersection of the central axis with the most apical slice plane.

A.2 Mapping 3D Point to AHA 17-Segment Model

To map any point in 3D to the AHA 17-segment model, we need to define an alternate coordinate system (x', y', z'), relative to the left ventricle. The z' axis points from the apex to the base and is scaled such that the origin is at (X_a, Y_a, Z_a) and a z' value of 1 corresponds to (X_b, Y_b, Z_b). The y' axis points at the anterior insertion of the right ventricle. The x' axis is orthogonal to the other axes.

To determine the position of a 3D point, the point must first be rotated into this alternate coordinate system from the standard (x, y, z) cartesian coordinate system. We then convert from (x', y', z') to a cylindrical coordinate system (ρ, ϕ, z), where ρ is the radius, or distance of the point from the central axis, ϕ is the angle between the RV insertion and the point, and z is the distance from the origin along the z' direction. In these cylindrical coordinates, ϕ represents the circumferential position and z represents the longitudinal position.

When mapping points to the AHA segment model, the radial position ρ is collapsed. By eliminating ρ, we can now convert to a polar coordinate system where the radial direction is

z and the angular direction is ϕ. We can then map this point *directly* to the AHA segment model.

By standard convention, we rotate the result so that the RV insertion is always located at $\frac{2\pi}{3}$.

APPENDIX B

CROSS CORRELATION ANALYSIS

Cross correlation is a commonly used signal processing technique for determining the phase difference between two discrete-time signals [166]. Unlike many techniques for determining the delay time between two signals, such as differences in time-to-peak, cross correlation utilizes the entire curve to estimate delay time. This results in a delay estimate that is less sensitive to noise.

B.1 One-Dimensional Cross Correlation

The basic premise is that one signal is shifted in time relative to another, and at each shift, the correlation between the shifted signal and the reference signal is computed. This correlation calculation is shown in Equation B.1, where R is the stationary reference signal, X is the shifted signal being compared to the reference, N is the number of data points in R and X, and τ is the shift applied to the signal. .

$$CC(\tau) = \frac{1}{N}\sum_{t=0}^{N-1}(X(t-\tau)R(t) \tag{B.1}$$

The result is an array of correlation values corresponding to shifts in time. The maximum correlation value corresponds to the true temporal delay between the two signals (Equation B.2).

$$\tau_{delay} = \underset{\tau}{\operatorname{argmax}}\, CC(\tau) \tag{B.2}$$

In cases where the two signals being compared may have different amplitudes, normalized cross correlation (NCC) can be used to compare the signals. NCC is a specific type of cross correlation wherein the mean of each of the signals ($\overline{X}$ and $\overline{R}$) is first subtracted, and each signal is divided by the standard deviation (σ_X and σ_R). This ensures that cross correlation analysis remains unaffected by differences in magnitude (Equation B.3).

$$NCC(\tau) = \frac{1}{N}\sum_{t=0}^{N-1}\frac{(X(t-\tau)-\overline{X})(R(t)-\overline{R})}{\sigma_X\sigma_R} \tag{B.3}$$

B.2 Circular Cross Correlation

When shifting one signal relative to another, it is possible that one signal extends beyond the extent of the other signal. Typically these values are ignored and correlation calculations only consider overlapping data points. If the two signals are periodic in time, and the data is obtained over a whole-number multiple of the period of the signal, it is possible to use periodicity when computing the correlation values. In this case, values beyond the signal duration are sampled from the far end of the periodic signal.

The 1D example of circular cross correlation is shown in Equation B.4, where X and R are the signals being compared, N is the number of samples in X and R, and τ is the shift being investigated. The modulo operator is used to sample the signal periodically.

$$CC(\tau) = \frac{1}{N}\sum_{t=0}^{N-1}(X((t-\tau) \bmod N)R(t) \tag{B.4}$$

B.3 Two-Dimensional Cross Correlation

In B.1, we presented the basic description of determining temporal delay between two 1D discrete-time signals [166]. The same concept can be expanded to higher dimensions (Equation B.5). In 2D, cross correlation is often employed to register two similar images to one another. By computing the correlation value for all shifts, i and j in the row and column directions, respectively, it is possible to determine the shift of one image that will yield the best match with the reference image. In equation B.5, A is the shifted image, B is the stationary reference image, M and N are the number of rows and columns in A.

$$CC(i,j) = \frac{1}{M \cdot N}\sum_{m=0}^{M-1}\sum_{n=0}^{N-1}A(m-i,n-j)B(m,n) \tag{B.5}$$

Similar to Equation B.2, the shifts (δy and δx) which yield the best match of the two images can be obtained by finding the maximum correlation value and it's corresponding shifts (Equation B.6).

$$(\delta y, \delta x) = \underset{i,j}{\operatorname{argmax}}\, CC(i,j) \tag{B.6}$$

To account for potential differences in intensity between the two images being registered, normalized 2D cross correlation is used. In Equation B.7, we can subtract the means of the two images ($\overline{A}$ and $\overline{B}$) and normalized to the standard deviations of each image, σ_A and σ_B.

$$NCC(i,j) = \frac{1}{M \cdot N} \sum_{m=0}^{M-1} \sum_{n=0}^{N-1} \frac{(A(m-i, n-j) - \overline{A})(B(m,n) - \overline{B})}{\sigma_A \sigma_B} \tag{B.7}$$

This same concept can be extended to higher dimensions.

APPENDIX C

THREE-DIMENSIONAL POSITION FROM DICOM IMAGES

DICOM images exported from magnetic resonance imaging systems contain application-specific information including the data necessary to map any point in the imaging plane to a three-dimensional point. This information is conveyed through three fields [247]:

1. **Image Position Patient** (0020,0032) – Specifies the x, y and z coordinates of the center of the upper left hand pixel in the image.

$$IPP = \begin{bmatrix} IPP_x \\ IPP_y \\ IPP_z \end{bmatrix} \tag{C.1}$$

2. **Image Orientation Patient** (0020,0037) – Provides the directional cosines of the rows and columns of the image, respectively. Directional cosines provide the weights for the components of a unit vector.

$$IOP = \begin{bmatrix} IOP_{r,x} & IOP_{c,x} \\ IOP_{r,y} & IOP_{c,y} \\ IOP_{r,z} & IOP_{c,z} \end{bmatrix} \tag{C.2}$$

3. **Pixel Spacing** (0020,0039) – Contains the distance between pixel centers for the rows and columns, respectively.

$$PS = \begin{bmatrix} PS_r & PS_c \end{bmatrix} \tag{C.3}$$

The following equation was used to determine the 3D position (x_w, y_w, z_w) of any point (r_i, c_i) in image space.

$$\begin{bmatrix} x_w \\ y_w \\ z_w \end{bmatrix} = IPP + IOP \begin{bmatrix} r_i \cdot PS_r \\ c_i \cdot PS_c \end{bmatrix} \tag{C.4}$$

Note: Zero-based indexing is assumed so image coordinates (r_i, c_i) of the upper left hand corner pixel center are (0,0)

APPENDIX D

QUALITY THRESHOLD CLUSTERING

Quality Threshold (QT) clustering is a technique that was initially developed for gene clustering [165]. Instead of specifying the number of desired clusters, the user provides a quality parameter that ensures members within a single cluster adhere to this quality. This quality value is based on any number of metrics including Euclidean distance and root mean squared error (RMSE). The advantage of QT clustering is that the quality of the resulting clusters is guaranteed; however, the algorithm is computationally expensive.

In our research, we utilize QT clustering for two purposes. First, we used it to cluster radial displacements of the endocardium throughout the left ventricle (LV) in order to identify a representative synchronous radial displacement. Second, we used a modified QT clustering approach to identify the frames of the cardiac cycle over which the position of the coronary sinus did not move more than a specified distance in an effort to identify ideal time periods for imaging the coronary veins with MRI.

D.1 QT Clustering for Reference Radial Displacement Curve

In our research, we utilize radial displacement of the endocardium to detect regional dyssynchrony. By sampling the endocardium at points throughout the entire left ventricle, we obtain radial displacement curves (RDCs). To determine the delay time of a particular RDC, it is necessary to compare it to a reference. By clustering the RDCs for each patient, we were able to identify the largest group of RDCs with a similar contraction pattern and these were considered to be representative of "synchronous" contraction for that particular patient. The root mean squared error (RMSE), was the metric used for QT clustering, and the quality threshold was defined to be 33% based upon studies in healthy controls. The implementation is shown in Algorithm 1.

Input: $RDCs$: Radial Displacement Curves

Output: C: Subset of $RDCs$ in the largest cluster

foreach *i in RDCs* **do**

    add i to its own new cluster A_i;

    $flag \leftarrow$ TRUE;

    while *(flag = TRUE) and* ($A_i \neq RDCs$) **do**

        /* Find the most similar member of $RDCs$ */

        find j in ($RDCs$ - A_i) such that RMSE($A_i \cup j$) is a minimum;

        /* Ensure RMSE between any two members does not exceed the threshold */

        if *RMSE*($A_i \cup j$) > *threshold* **then**

            $flag \leftarrow$ FALSE;

        else

            /* Add j to the current cluster */

            $A_i \leftarrow A_i \cup j$

        end

    end

end

/* Find cluster with the most members */

identify set $C \in \{A_1, A_2, ...\}$ with maximum cardinality;

return C;

Algorithm 1: QT Clustering of Radial Displacement Curves to Define Synchronous Contraction

After we have the subset of RDCs (C) that are all members of the largest cluster, we average these RDCs to obtain the patient-specific reference curve.

D.2 QT Clustering for Stationary Period Determination

In Chapter 5, we use a modified QT clustering algorithm to identify the stationary periods of the coronary sinus in vertical long axis (VLA) images. The goal is to identify consecutive frames over which the coronary sinus moves less than a specified distance cutoff (0.67 mm). Using the standard QT clustering technique, we could identify the frames during which the coronary sinus is within the specified distance; however, a stationary period *must* be consecutive frames, therefore we must have an additional constraint. The modified algorithm is shown in Algorithm 2.

Input: CS: Coronary Sinus centroids for all phases

Output: C: Consecutive subset of CS within the specified distance threshold

foreach *i in CS* **do**

add i to its own new cluster A_i;

$flag \leftarrow$ TRUE;

`/* Store the next position after` i `*/`

$j \leftarrow i$.next();

while *(flag = TRUE) and* $(A_i \neq CS)$ **do**

`/* Inspect the next element of` CS `to see if it exceeds the threshold */`

if *diameter(*$A_i \cup j$*) > threshold* **then**

$flag \leftarrow$ FALSE;

else

`/* Add` j `to the current cluster */`

$A_i \leftarrow A_i \cup j$;

`/* Move` j `to the next position */`

$j \leftarrow j$.next();

end

end

end

`/* Find cluster with the most members */`

identify set $C \in \{A_1, A_2, ...\}$ with maximum cardinality;

return C;

`/* Call using` $(CS - C)$ `as the input to get second largest cluster */`

Algorithm 2: QT Clustering of Coronary Sinus Displacement

The QT clustering was run once to determine the longest rest period, then re-run with the un-clustered time points to determine the location of the second longest rest period.

APPENDIX E

FRANGI VESSELNESS FILTER

The Frangi vesselness filter generates an image where the pixel values correspond to the likelihood that a given pixel belongs to a vessel or not. By computing the Hessian matrix and its eigenvalues, it is possible to obtain a description of the local second order structure of an image including: blob-like objects, constant background pixels, and pixels that belong to tubular structures [248, 249]. Frangi et al. determined the relationship between the eigenvalues of the Hessian that best provides a measure of "vesselness" [218]. Additionally, they developed a multi-scale approach wherein only vessels within the specified range are detected.

For our analysis, we utilized the Frangi vesselness filter to exclude unwanted objects from biplane venograms including sternal fixation wires, and tools placed on the patient's chest during the CRT implantation procedure.

In the multi-scale approach suggested by Frangi et al, the intensity profile of a vessel in a medical image is assumed to be Gaussian-like, therefore we can specify the scale of interest using σ, the standard deviation of the Gaussian. The equation of the 1D Gaussian is shown in Equation E.1, where μ is the center of the Gaussian, and σ is the standard deviation of the Guassian.

$$G(x) = \frac{1}{\sigma\sqrt{2\pi}} e^{-\frac{1}{2}\left(\frac{x-\mu}{\sigma}\right)^2} \tag{E.1}$$

The Hessian matrix is composed of the second order partial derivatives of an image. The partial derivatives are computed within the local neighborhood of a given pixel

$$H = \begin{bmatrix} \dfrac{\partial^2 I}{\partial x^2} & \dfrac{\partial^2 I}{\partial x \partial y} \\ \dfrac{\partial^2 I}{\partial x \partial y} & \dfrac{\partial^2 I}{\partial y^2} \end{bmatrix} \tag{E.2}$$

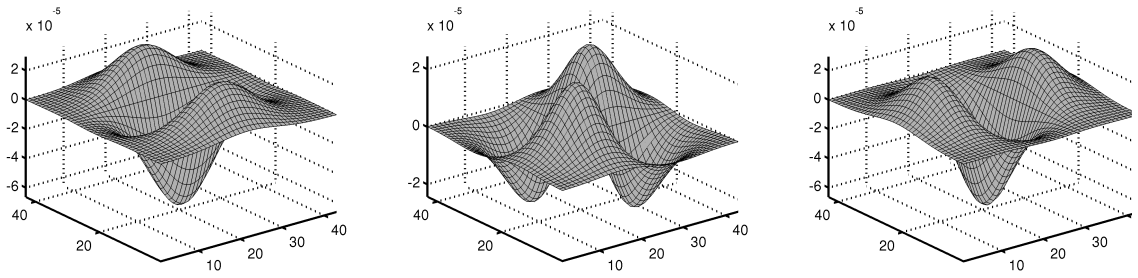

Figure E.1: Filter kernels to estimate the second derivatives of an image. The kernel on the left computes $\frac{\partial^2 I}{\partial x^2}$, the middle kernel is used to find $\frac{\partial^2 I}{\partial x \partial y}$, and the filter on the right yields $\frac{\partial^2 I}{\partial y^2}$. The kernels are computed by taking the second derivative of the Gaussian with the specified scale, σ. In this case, $\sigma = 5$.

To compute these second derivates of the image at the scale σ, we created a filtering kernel that is the second derivative of the Gaussian in the x, y, and diagonal directions (Figure E.1). By filtering the image with these kernels, we can populate the Hessian for each pixel in the image.

We perform eigenvalue decomposition on the Hessian and obtain two eigenvalues (λ_1 and λ_2) and their corresponding eigenvectors (v_1 and v_2). The eigenvalues are sorted in increasing absolute value (Equation E.3).

$$|\lambda_1| < |\lambda_2| \tag{E.3}$$

For a pixel lying within a vessel of scale σ, the largest change in curvature will be across the vessel boundary, therefore v_2 will be normal to (across) the vessel boundary. Because of the orthogonality of eigenvectors, v_1 will point along the vessel and will λ_1 will be close to 0 since the intensity along the vessel is relatively constant.

Therefore, eigenvalues of the Hessian for a pixel belonging to a vessel will typically be related in the following ways:

$$|\lambda_1| \approx 0 \tag{E.4}$$

$$|\lambda_1| \ll |\lambda_2| \tag{E.5}$$

It is possible that a pixel that belongs to the background may meet these criteria due to noise and local fluctuations in the image. Thankfully, the corresponding eigenvalues will be small due to the lack of a true second order structure in background noise. So we can add one more criteria for identifying vessels based on the magnitude of the eigenvalues:

$$S = \sqrt{\lambda_1^2 + \lambda_2^2} \gg 0 \tag{E.6}$$

With these three criteria (E.4, E.5, and E.6), the "vesselness" of a pixel can be computed as shown in Equation E.7, where β and c are weights that have to be assigned empirically.

$$V = \exp\left(-\frac{1}{2\beta^2}\left(\frac{\lambda_2}{\lambda_1}\right)^2\right)\left(1 - \exp\left(-\frac{S^2}{2c^2}\right)\right) \tag{E.7}$$

As per the recommendation of Frangi, et al., a β value of 0.5 was used. Based upon analysis of our biplane venogram images, a value of 15 was selected for c to properly suppress false positives in the background of the image.

APPENDIX F

ALPHA SHAPES

An alpha shape (α-shape) is a volumetric representation of a finite set of points in either $\mathbb{R}^2$ and $\mathbb{R}^3$. For our purposes, we will focus on the 3D representation. Our goal is to generate a 3D mesh that represents the geometry of the coronary veins using points defined in a 3D stack of MR images.

First, user-defined points within the coronary veins were selected throughout the entire 3D stack of MR images. These 2D image coordinates were converted to 3D coordinates, $\boldsymbol{P}$, using position information from the DICOM header (Appendix C).

To compute the α-shape for a set of points, we first have to compute the Delaunay triangulation [250]. Briefly, the Delaunay triangulation is a triangulation in which all of the original data points, $\boldsymbol{P}$, lie outside of the circumcircle of any triangular face of the resulting triangulation. The concept of a circumcircle is shown in Figure F.1. In our work, all Delaunay triangulations were computed using the built-in `delaunayn` routine in Matlab (The Mathworks, Natick, MA).

The Delaunay triangulation of a set of points, $\boldsymbol{P}$, results in a triangulation of the convex hull of those points. In our case, we are trying to reconstruct the coronary vein anatomy which has several branches, therefore the convex hull fails to capture these local features. An α-shape enables us to detect these local features by limiting the size of the faces of the triangulation.

An α-shape is achieved by placing a constraint (α) on the radius of the circumcircle for each face in the Delaunay triangulation. This constraint eliminates large faces that span the entire point cloud to create the convex hull. By decreasing α, it is possible to get more local features, although it can also result in unsuccessful triangulation if the original data points are too far apart [203].

In our implantation, we utilized `TriRep.circumcenters` in Matlab to compute the

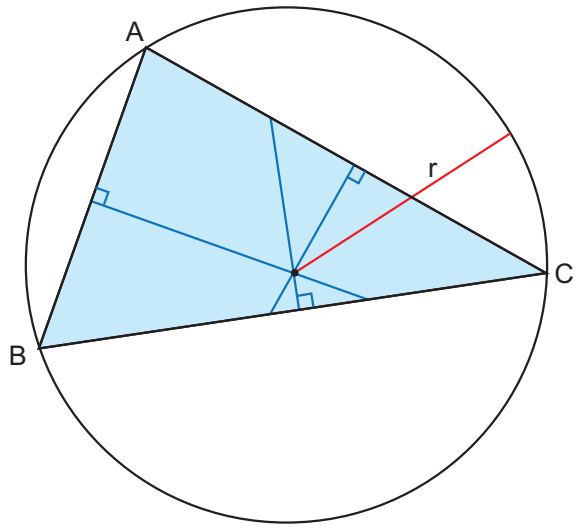

Figure F.1: The circumcircle of three points (A, B, and C) is the smallest circle with radius r that touches all three points.

radius of all circumcenters. Triangular faces with radii larger than the pre-determined cutoff were removed and the resulting α-shape was returned.

In our research, we needed to select an α value small enough to separate the coronary veins from one another but large enough to successfully connect points selected in two neighboring slices. We empirically determined that an α value of 4 mm created a successful 3D mesh of coronary vein anatomy.

REFERENCES

[1] Poole-Wilson, P. A., "History, definition and classification of heart failure," in *Heart Failure: Scientific Principles and Clinical Practice* (Poole-Wilson, P. A., Colucci, W., Massie, B., Chatterjee, K., and Coates, A., eds.), pp. 269–77, London: Churchill Livingstone, 1997.

[2] Lonn, E. and McKelvie, R., "Drug treatment in heart failure," *British Medical Journal*, vol. 320, no. 29, pp. 1188–92, 2000.

[3] Steeds, R. P. and Channer, K. S., "Drug treatment in heart failure.," *British Medical Journal (Clinical research ed.)*, vol. 316, pp. 567–8, Feb. 1998.

[4] Lloyd-Jones, D., Adams, R. J., Brown, T. M., Carnethon, M., Dai, S., De Simone, G., Ferguson, T. B., Ford, E., Furie, K., Gillespie, C., Go, A., Greenlund, K., Haase, N., Hailpern, S., Ho, P. M., Howard, V., Kissela, B., Kittner, S., Lackland, D., Lisabeth, L., Marelli, A., McDermott, M. M., Meigs, J., Mozaffarian, D., Mussolino, M., Nichol, G., Roger, V., Rosamond, W., Sacco, R., Sorlie, P., Stafford, R., Thom, T., Wasserthiel-Smoller, S., Wong, N. D., and Wylie-Rosett, J., "Heart Disease and Stroke Statistics–2010 Update. A Report From the American Heart Association.," *Circulation*, pp. 410–528, 2009.

[5] Jessup, M. and Brozena, S., "Heart failure.," *The New England Journal of Medicine*, vol. 348, pp. 2007–18, May 2003.

[6] Eichhorn, E. J. and Bristow, M. R., "Medical therapy can improve the biological properties of the chronically failing heart. A new era in the treatment of heart failure.," *Circulation*, vol. 94, pp. 2285–96, Nov. 1996.

[7] Sutton, M. G. and Sharpe, N., "Left ventricular remodeling after myocardial infarction: pathophysiology and therapy.," *Circulation*, vol. 101, pp. 2981–8, June 2000.

[8] van Nieuwenhoven, F. a. and Turner, N. a., "The role of cardiac fibroblasts in the transition from inflammation to fibrosis following myocardial infarction.," *Vascular Pharmacology*, vol. 58, pp. 182–8, Mar. 2013.

[9] Pfeffer, M. a. and Braunwald, E., "Ventricular remodeling after myocardial infarction. Experimental observations and clinical implications," *Circulation*, vol. 81, pp. 1161–1172, Apr. 1990.

[10] He, S., Fontaine, A. A., Schwammenthal, E., Yoganathan, A. P., and Levine, R. A., "Integrated mechanism for functional mitral regurgitation: leaflet restriction versus coapting force: in vitro studies.," *Circulation*, vol. 96, pp. 1826–34, Sept. 1997.

[11] Otsuji, Y., Gilon, D., Jiang, L., He, S., Leavitt, M., Roy, M. J., Birmingham, M. J., and Levine, R. A., "Restricted diastolic opening of the mitral leaflets in patients with left ventricular dysfunction: evidence for increased valve tethering.," *Journal of the American College of Cardiology*, vol. 32, pp. 398–404, Aug. 1998.

[12] Benjamin, E. J., Wolf, P. A., D'Agostino, R. B., Silbershatz, H., Kannel, W. B., and Levy, D., "Impact of atrial fibrillation on the risk of death: the Framingham Heart Study.," *Circulation*, vol. 98, pp. 946–52, Sept. 1998.

[13] McCullough, P. A., Hassan, S. A., Pallekonda, V., Sandberg, K. R., Nori, D. B., Soman, S. S., Bhatt, S., Hudson, M. P., and Weaver, W. D., "Bundle branch block patterns, age, renal dysfunction, and heart failure mortality.," *International Journal of Cardiology*, vol. 102, pp. 303–8, July 2005.

[14] Shenkman, H. J., Pampati, V., Khandelwal, A. K., McKinnon, J., Nori, D., Kaatz, S., Sandberg, K. R., and McCullough, P. A., "Congestive heart failure and QRS duration: establishing prognosis study.," *Chest*, vol. 122, pp. 528–34, Aug. 2002.

[15] Silvet, H., Amin, J., Padmanabhan, S., and Pai, R. G., "Prognostic implications of increased QRS duration in patients with moderate and severe left ventricular systolic dysfunction.," *The American Journal of Cardiology*, vol. 88, pp. 182–5, A6, July 2001.

[16] Iuliano, S., Fisher, S. G., Karasik, P. E., Fletcher, R. D., and Singh, S. N., "QRS duration and mortality in patients with congestive heart failure.," *American Heart Journal*, vol. 143, no. 6, pp. 1085–91, 2002.

[17] Kass, D. A., "Ventricular resynchronization: pathophysiology and identification of responders.," *Reviews in Cardiovascular Medicine*, vol. 4 Suppl 2, pp. S3–S13, 2003.

[18] Nelson, G. S., Berger, R. D., Fetics, B. J., Talbot, M., Spinelli, J. C., Hare, J. M., and Kass, D. A., "Left ventricular or biventricular pacing improves cardiac function at diminished energy cost in patients with dilated cardiomyopathy and left bundle-branch block.," *Circulation*, vol. 102, no. 25, pp. 3053–9, 2000.

[19] Bilchick, K. C., Helm, R. H., and Kass, D. a., "Physiology of biventricular pacing.," *Current Cardiology Reports*, vol. 9, pp. 358–65, Sept. 2007.

[20] Durrer, D., Van Dam, R. T., Freud, G. E., Janse, M. J., Meijler, F. L., and Arzbaecher, R. C., "Total Excitation of the Isolated Human Heart," *Circulation*, vol. 41, pp. 899–912, June 1970.

[21] Peters, N. S., "New insights into myocardial arrhythmogenesis: distribution of gap-junctional coupling in normal, ischaemic and hypertrophied human hearts.," *Clinical Science*, vol. 90, pp. 447–52, June 1996.

[22] Saffitz, J. E., Laing, J. G., and Yamada, K. A., "Connexin expression and turnover : implications for cardiac excitability.," *Circulation Research*, vol. 86, pp. 723–8, Apr. 2000.

[23] Akar, F. G., Spragg, D. D., Tunin, R. S., Kass, D. a., and Tomaselli, G. F., "Mechanisms underlying conduction slowing and arrhythmogenesis in nonischemic dilated cardiomyopathy.," *Circulation Research*, vol. 95, pp. 717–25, Oct. 2004.

[24] Baldasseroni, S., Opasich, C., Gorini, M., Lucci, D., Marchionni, N., Marini, M., Campana, C., Perini, G., Deorsola, A., Masotti, G., Tavazzi, L., and Maggioni, A. P., "Left bundle-branch block is associated with increased 1-year sudden and total mortality rate in 5517 outpatients with congestive heart failure: A report from the Italian network on congestive heart failure," *American Heart Journal*, vol. 143, pp. 398–405, Mar. 2002.

[25] Helm, R. H., Byrne, M., Helm, P. a., Daya, S. K., Osman, N. F., Tunin, R., Halperin, H. R., Berger, R. D., Kass, D. a., and Lardo, A. C., "Three-dimensional mapping of optimal left ventricular pacing site for cardiac resynchronization.," *Circulation*, vol. 115, pp. 953–61, Feb. 2007.

[26] Peters, N. S., Coromilas, J., Severs, N. J., and Wit, A. L., "Disturbed connexin43 gap junction distribution correlates with the location of reentrant circuits in the epicardial border zone of healing canine infarcts that cause ventricular tachycardia.," *Circulation*, vol. 95, pp. 988–96, Feb. 1997.

[27] Trautmann, S. I., Kloss, M., and Auricchio, A., "Cardiac resynchronization therapy.," *Current Cardiology Reports*, vol. 4, no. 5, pp. 371–8, 2002.

[28] Singh, J. P., Klein, H. U., Huang, D. T., Reek, S., Kuniss, M., Quesada, A., Barsheshet, A., Cannom, D., Goldenberg, I., McNitt, S., Daubert, J. P., Zareba, W., and Moss, A. J., "Left Ventricular Lead Position and Clinical Outcome in the Multicenter Automatic Defibrillator Implantation Trial-Cardiac Resynchronization Therapy (MADIT-CRT) Trial.," *Circulation*, vol. 123, pp. 1159–66, Mar. 2011.

[29] Hawkins, N. M., Petrie, M. C., MacDonald, M. R., Hogg, K. J., and McMurray, J. J. V., "Selecting patients for cardiac resynchronization therapy: electrical or mechanical dyssynchrony?," *European Heart Journal*, vol. 27, pp. 1270–81, June 2006.

[30] Elhendy, A., Hammill, S. C., Mahoney, D. W., and Pellikka, P. a., "Relation of QRS duration on the surface 12-lead electrocardiogram with mortality in patients with known or suspected coronary artery disease.," *The American Journal of Cardiology*, vol. 96, pp. 1082–8, Oct. 2005.

[31] Schinkel, A. F. L., Elhendy, A., van Domburg, R. T., Biagini, E., Rizzello, V., Veltman, C. E., Ten Kate, G. L., Sijbrands, E. J., Akkerhuis, K. M., Geleijnse, M. L., Ten Cate, F. J., Simoons, M. L., Bax, J. J., and Poldermans, D., "Prognostic significance of QRS duration in patients with suspected coronary artery disease referred for noninvasive evaluation of myocardial ischemia.," *The American Journal of Cardiology*, vol. 104, pp. 1490–3, Dec. 2009.

[32] Brenyo, A. and Zareba, W., "Prognostic significance of QRS duration and morphology.," *Cardiology Journal*, vol. 18, pp. 8–17, Jan. 2011.

[33] Venkatachalam, K. L., Herbrandson, J. E., and Asirvatham, S. J., "Signals and signal processing for the electrophysiologist: part I: electrogram acquisition.," *Circulation. Arrhythmia and Electrophysiology*, vol. 4, pp. 965–73, Dec. 2011.

[34] Bhakta, D. and Miller, J. M., "Principles of electroanatomic mapping.," *Indian Pacing and Electrophysiology Journal*, vol. 8, pp. 32–50, Jan. 2008.

[35] Gepstein, L. and Evans, S. J., "Electroanatomical mapping of the heart: basic concepts and implications for the treatment of cardiac arrhythmias.," *Pacing and Clinical Electrophysiology*, vol. 21, pp. 1268–78, June 1998.

[36] Hatala, R., Savard, P., Tremblay, G., Pagé, P., Cardinal, R., Molin, F., Kus, T., and Nadeau, R., "Three distinct patterns of ventricular activation in infarcted human hearts. An intraoperative cardiac mapping study during sinus rhythm.," *Circulation*, vol. 91, pp. 1480–94, Mar. 1995.

[37] Konings, K. T., Kirchhof, C. J., Smeets, J. R., Wellens, H. J., Penn, O. C., and Allessie, M. A., "High-density mapping of electrically induced atrial fibrillation in humans.," *Circulation*, vol. 89, pp. 1665–80, Apr. 1994.

[38] Gepstein, L., Hayam, G., and Ben-Haim, S. A., "A novel method for nonfluoroscopic catheter-based electroanatomical mapping of the heart. In vitro and in vivo accuracy results.," *Circulation*, vol. 95, pp. 1611–22, Mar. 1997.

[39] Bleeker, G. B., Schalij, M. J., Molhoek, S. G., Holman, E. R., Verwey, H. F., Steendijk, P., van der Wall, E. E., and Bax, J. J., "Frequency of left ventricular dyssynchrony in patients with heart failure and a narrow QRS complex.," *The American Journal of Cardiology*, vol. 95, pp. 140–2, Jan. 2005.

[40] Bleeker, G. B., Holman, E. R., Steendijk, P., Boersma, E., van der Wall, E. E., Schalij, M. J., and Bax, J. J., "Cardiac resynchronization therapy in patients with a narrow QRS complex.," *Journal of the American College of Cardiology*, vol. 48, pp. 2243–50, Dec. 2006.

[41] Sø gaard, P., Egeblad, H., Kim, W. Y., Jensen, H. K., Pedersen, A. K., Kristensen, B. O., and Mortensen, P. T., "Tissue Doppler imaging predicts improved systolic performance and reversed left ventricular remodeling during long-term cardiac resynchronization therapy.," *Journal of the American College of Cardiology*, vol. 40, no. 4, pp. 723–30, 2002.

[42] Pitzalis, M. V., Iacoviello, M., Romito, R., Massari, F., Rizzon, B., Luzzi, G., Guida, P., Andriani, A., Mastropasqua, F., and Rizzon, P., "Cardiac resynchronization therapy tailored by echocardiographic evaluation of ventricular asynchrony.," *Journal of the American College of Cardiology*, vol. 40, pp. 1615–22, Nov. 2002.

[43] Pitzalis, M. V., Iacoviello, M., Romito, R., Guida, P., De Tommasi, E., Luzzi, G., Anaclerio, M., Forleo, C., and Rizzon, P., "Ventricular asynchrony predicts a better outcome in patients with chronic heart failure receiving cardiac resynchronization therapy.," *Journal of the American College of Cardiology*, vol. 45, pp. 65–9, Jan. 2005.

[44] Cazeau, S., Bordachar, P., Jauvert, G., Lazarus, A., Alonso, C., Vandrell, M. C., Mugica, J., and Ritter, P., "Echocardiographic modeling of cardiac dyssynchrony before and during multisite stimulation: a prospective study.," *Pacing and Clinical Electrophysiology*, vol. 26, pp. 137–43, Jan. 2003.

[45] Cleland, J. G., Daubert, J. C., Erdmann, E., Freemantle, N., Gras, D., Kappenberger, L., Klein, W., and Tavazzi, L., "The CARE-HF study (CArdiac REsynchronisation in Heart Failure study): rationale, design and end-points.," *European Journal of Heart Failure*, vol. 3, pp. 481–9, Aug. 2001.

[46] Bax, J. J., Bleeker, G. B., Marwick, T. H., Molhoek, S. G., Boersma, E., Steendijk, P., van Der Wall, E. E., and Schalij, M. J., "Left ventricular dyssynchrony predicts response and prognosis after cardiac resynchronization therapy.," *Journal of the American College of Cardiology*, vol. 44, no. 9, pp. 1834–40, 2004.

[47] Yu, C.-M., Wing-Hong Fung, J., Zhang, Q., and Sanderson, J. E., "Understanding nonresponders of cardiac resynchronization therapy–current and future perspectives.," *Journal of Cardiovascular Electrophysiology*, vol. 16, pp. 1117–24, Oct. 2005.

[48] Fornwalt, B. K., Arita, T., Bhasin, M., Voulgaris, G., Merlino, J. D., León, A. R., Fyfe, D. a., and Oshinski, J. N., "Cross-correlation quantification of dyssynchrony: a new method for quantifying the synchrony of contraction and relaxation in the heart.," *Journal of the American Society of Echocardiography*, vol. 20, pp. 1330–1337.e1, Dec. 2007.

[49] Dandel, M., Lehmkuhl, H., Knosalla, C., Suramelashvili, N., and Hetzer, R., "Strain and strain rate imaging by echocardiography - basic concepts and clinical applicability.," *Current Cardiology Reviews*, vol. 5, pp. 133–48, May 2009.

[50] Nesser, H.-J., Mor-Avi, V., Gorissen, W., Weinert, L., Steringer-Mascherbauer, R., Niel, J., Sugeng, L., and Lang, R. M., "Quantification of left ventricular volumes using three-dimensional echocardiographic speckle tracking: comparison with MRI.," *European Heart Journal*, vol. 30, pp. 1565–73, July 2009.

[51] Galt, J. R., Garcia, E. V., and Robbins, W. L., "Effects of myocardial wall thickness on SPECT quantification.," *IEEE Transactions on Medical Imaging*, vol. 9, pp. 144–50, Jan. 1990.

[52] Chen, J., Garcia, E. V., Folks, R. D., Cooke, C. D., Faber, T. L., Tauxe, E. L., and Iskandrian, A. E., "Onset of left ventricular mechanical contraction as determined by phase analysis of ECG-gated myocardial perfusion SPECT imaging: development of a diagnostic tool for assessment of cardiac mechanical dyssynchrony.," *Journal of Nuclear Cardiology*, vol. 12, no. 6, pp. 687–95.

[53] Constantino, J., Hu, Y., and Trayanova, N. a., "A computational approach to understanding the cardiac electromechanical activation sequence in the normal and failing heart, with translation to the clinical practice of CRT.," *Progress in Biophysics and Molecular Biology*, vol. 110, pp. 372–9, Oct. 2012.

[54] Russell, K., Smiseth, O. a., Gjesdal, O., Qvigstad, E., Norseng, P. A., Sjaastad, I., Opdahl, A., Skulstad, H., Edvardsen, T., and Remme, E. W., "Mechanism of prolonged electromechanical delay in late activated myocardium during left bundle branch block.," *American Journal of Physiology. Heart and Circulatory Physiology*, vol. 301, pp. H2334–43, Dec. 2011.

[55] "Effects of enalapril on mortality in severe congestive heart failure. results of the cooperative north scandanavian enalapril survival study (consensus).," *The New England Journal of Medicine*, vol. 316, no. 23, pp. 1429–35, 1987.

[56] Foody, J. M., Farrell, M. H., and Krumholz, H. M., "beta-Blocker therapy in heart failure: scientific review.," *Journal of the American Medical Association*, vol. 287, pp. 883–9, Feb. 2002.

[57] "Prevention of stroke by antihypertensive drug treatment in older persons with isolated systolic hypertension. final results of the systolic hypertension in the elderly program (shep). shep cooperative research group.," *Journal of the American Medical Association*, vol. 265, no. 24, pp. 3255–64, 1991.

[58] "Effect of enalrapril on survival in patients with reduced left ventricular ejection fractions and congestive heart failure," *The New England Journal of Medicine*, vol. 325, no. 5, pp. 293–302, 1991.

[59] Jessup, M., Abraham, W. T., Casey, D. E., Feldman, A. M., Francis, G. S., Ganiats, T. G., Konstam, M. A., Mancini, D. M., Rahko, P. S., Silver, M. A., Stevenson, L. W., and Yancy, C. W., "2009 focused update: ACCF/AHA Guidelines for the Diagnosis and Management of Heart Failure in Adults: a report of the American College of Cardiology Foundation/American Heart Association Task Force on Practice Guidelines: developed in collaboration with t," *Circulation*, vol. 119, pp. 1977–2016, Apr. 2009.

[60] Rose, E. A., Gelijns, A. C., Moskowitz, A. J., Heitjan, D. F., Stevenson, L. W., Dembitsky, W., Long, J. W., Ascheim, D. D., Tierney, A. R., Levitan, R. G., Watson, J. T., Meier, P., Ronan, N. S., Shapiro, P. A., Lazar, R. M., Miller, L. W., Gupta, L., Frazier, O. H., Desvigne-Nickens, P., Oz, M. C., and Poirier, V. L., "Long-term use of a left ventricular assist device for end-stage heart failure.," *The New England Journal of Medicine*, vol. 345, pp. 1435–43, Nov. 2001.

[61] John, R., Kamdar, F., Liao, K., Colvin-Adams, M., Boyle, A., and Joyce, L., "Improved survival and decreasing incidence of adverse events with the HeartMate II left ventricular assist device as bridge-to-transplant therapy.," *The Annals of Thoracic Surgery*, vol. 86, pp. 1227–34; discussion 1234–5, Oct. 2008.

[62] Miller, L. W., Pagani, F. D., Russell, S. D., John, R., Boyle, A. J., Aaronson, K. D., Conte, J. V., Naka, Y., Mancini, D., Delgado, R. M., MacGillivray, T. E., Farrar, D. J., and Frazier, O. H., "Use of a continuous-flow device in patients awaiting heart transplantation.," *The New England Journal of Medicine*, vol. 357, pp. 885–96, Aug. 2007.

[63] Buxton, A. E., Lee, K. L., Fisher, J. D., Josephson, M. E., Prystowsky, E. N., and Hafley, G., "A randomized study of the prevention of sudden death in patients with coronary artery disease. Multicenter Unsustained Tachycardia Trial Investigators.," *The New England Journal of Medicine*, vol. 341, pp. 1882–90, Dec. 1999.

[64] McMurray, J. J. V., Adamopoulos, S., Anker, S. D., Auricchio, A., Böhm, M., Dickstein, K., Falk, V., Filippatos, G., Fonseca, C., Gomez-Sanchez, M. A., Jaarsma, T., Kø ber, L., Lip, G. Y. H., Maggioni, A. P., Parkhomenko, A., Pieske, B. M., Popescu, B. A., Rø nnevik, P. K., Rutten, F. H., Schwitter, J., Seferovic, P., Stepinska, J., Trindade, P. T., Voors, A. A., Zannad, F., and Zeiher, A., "ESC Guidelines for the diagnosis and treatment of acute and chronic heart failure 2012: The Task Force for the Diagnosis and Treatment of Acute and Chronic Heart Failure 2012 of the European Society of Cardiology. Developed in collaboration with the Heart," *European Heart Journal*, vol. 33, pp. 1787–847, July 2012.

[65] Moss, A. J., Hall, W. J., Cannom, D. S., Daubert, J. P., Higgins, S. L., Klein, H., Levine, J. H., Saksena, S., Waldo, A. L., Wilber, D., Brown, M. W., and Heo, M., "Improved survival with an implanted defibrillator in patients with coronary disease at high risk for ventricular arrhythmia. Multicenter Automatic Defibrillator Implantation Trial Investigators.," *The New England Journal of Medicine*, vol. 335, pp. 1933–40, Dec. 1996.

[66] Rohde, L. E., Bertoldi, E. G., Goldraich, L., and Polanczyk, C. a., "Cost-effectiveness of heart failure therapies.," *Nature Reviews. Cardiology*, vol. 10, pp. 338–54, June 2013.

[67] Russo, A. M., Stainback, R. F., Epstein, A. E., and Stevenson, L. W., "Appropriate Use Criteria for Implantable Cardioverter-Defibrillators and Cardiac Resynchronization Therapy," *Heart Rhythm*, vol. 10, no. 4, pp. 1–47, 2013.

[68] Abraham, W. T., Fisher, W. G., Smith, A. L., Delurgio, D. B., Leon, A. R., Loh, E., Kocovic, D. Z., Packer, M., Clavell, A. L., Hayes, D. L., Ellestad, M., Trupp, R. J., Underwood, J., Pickering, F., Truex, C., McAtee, P., and Messenger, J., "Cardiac resynchronization in chronic heart failure.," *The New England Journal of Medicine*, vol. 346, no. 24, pp. 1845–53, 2002.

[69] Bristow, M. R., Feldman, A. M., and Saxon, L. A., "Heart failure management using implantable devices for ventricular resynchronization: Comparison of Medical Therapy, Pacing, and Defibrillation in Chronic Heart Failure (COMPANION) trial. COMPANION Steering Committee and COMPANION Clinical Investigators.," *Journal of Cardiac Failure*, vol. 6, no. 3, pp. 276–85, 2000.

[70] Cleland, J. G. F., Daubert, J.-C., Erdmann, E., Freemantle, N., Gras, D., Kappenberger, L., and Tavazzi, L., "The effect of cardiac resynchronization on morbidity and mortality in heart failure.," *The New England Journal of Medicine*, vol. 352, pp. 1539–49, Apr. 2005.

[71] Abraham, W. T., "Cardiac resynchronization therapy: a review of clinical trials and criteria for identifying the appropriate patient.," *Reviews in Cardiovascular Medicine*, vol. 4 Suppl 2, pp. S30–7, 2003.

[72] Abraham, W. T., "Cardiac resynchronization therapy for heart failure: biventricular pacing and beyond.," *Current Opinion in Cardiology*, vol. 17, no. 4, pp. 346–52, 2002.

[73] Auricchio, A., Stellbrink, C., Sack, S., Block, M., Vogt, J., Bakker, P., Mortensen, P., and Klein, H., "The Pacing Therapies for Congestive Heart Failure (PATH-CHF) study: rationale, design, and endpoints of a prospective randomized multicenter study.," *The American Journal of Cardiology*, vol. 83, no. 5B, pp. 130D–135D, 1999.

[74] Auricchio, A., Stellbrink, C., Sack, S., Block, M., Vogt, J., Bakker, P., Huth, C., Schöndube, F., Wolfhard, U., Böcker, D., Krahnefeld, O., and Kirkels, H., "Long-term clinical effect of hemodynamically optimized cardiac resynchronization therapy in patients with heart failure and ventricular conduction delay.," *Journal of the American College of Cardiology*, vol. 39, no. 12, pp. 2026–33, 2002.

[75] Cazeau, S., Gras, D., Lazarus, A., Ritter, P., and Mugica, J., "Multisite stimulation for correction of cardiac asynchrony.," *Heart*, vol. 84, no. 6, pp. 579–81, 2000.

[76] Lunati, M., Paolucci, M., Oliva, F., Frigerio, M., Magenta, G., Cattafi, G., Vecchi, R., Vicini, I., and Cavaglià, S., "Patient selection for biventricular pacing.," *Journal of Cardiovascular Electrophysiology*, vol. 13, no. 1 Suppl, pp. S63–7, 2002.

[77] Ricci, R., Ansalone, G., Toscano, S., Pignalberi, C., Lunati, M., Gasparini, M., Padeletti, L., Disertori, M., Ravazzi, P., and Santini, M., "Cardiac Resynchronization: materials, technique and results. The InSync Italian Registry.," *European Heart Journal Supplements*, vol. 2, no. Supplement J, pp. J6–J15, 2000.

[78] Yu, C.-M., Fung, W.-H., Lin, H., Zhang, Q., Sanderson, J. E., and Lau, C.-P., "Predictors of left ventricular reverse remodeling after cardiac resynchronization therapy for heart failure secondary to idiopathic dilated or ischemic cardiomyopathy.," *The American Journal of Cardiology*, vol. 91, no. 6, pp. 684–8, 2003.

[79] Zardini, M., Tritto, M., Bargiggia, G., Forzani, T., Santini, M., Perego, G., Bocchiardo, M., Raviele, A., and Salerno-Uriarte, J., "The InSync Italian Registry: analysis of clinical outcome and considerations on the selection of candidates to left ventricular resynchronization," *European Heart Journal Supplements*, vol. 2, no. Supplement J, pp. J16–J22, 2000.

[80] Fornwalt, B. K., Sprague, W. W., BeDell, P., Suever, J. D., Gerritse, B., Merlino, J. D., Fyfe, D. A., León, A. R., and Oshinski, J. N., "Agreement is poor among current criteria used to define response to cardiac resynchronization therapy.," *Circulation*, vol. 121, pp. 1985–91, May 2010.

[81] Rector, T. S., Kubo, S. H., and Cohn, J. N., "Validity of the Minnesota Living with Heart Failure questionnaire as a measure of therapeutic response to enalapril or placebo.," *The American Journal of Cardiology*, vol. 71, pp. 1106–7, May 1993.

[82] Notabartolo, D., Merlino, J. D., Smith, A. L., DeLurgio, D. B., Vera, F. V., Easley, K. A., Martin, R. P., and León, A. R., "Usefulness of the peak velocity difference by tissue Doppler imaging technique as an effective predictor of response to cardiac resynchronization therapy.," *The American Journal of Cardiology*, vol. 94, pp. 817–20, Sept. 2004.

[83] Lipkin, D. P., Scriven, a. J., Crake, T., and Poole-Wilson, P. a., "Six minute walking test for assessing exercise capacity in chronic heart failure.," *British Medical Journal (Clinical research ed.)*, vol. 292, pp. 653–5, Mar. 1986.

[84] Díaz-Infante, E., Mont, L., Leal, J., García-Bolao, I., Fernández-Lozano, I., Hernández-Madrid, A., Pérez-Castellano, N., Sitges, M., Pavón-Jiménez, R., Barba, J., Cavero, M. A., Moya, J. L., Pérez-Isla, L., and Brugada, J., "Predictors of lack of response to resynchronization therapy.," *The American Journal of Cardiology*, vol. 95, pp. 1436–40, June 2005.

[85] Bax, J. J., Abraham, T., Barold, S. S., Breithardt, O. A., Fung, J. W. H., Garrigue, S., Gorcsan, J., Hayes, D. L., Kass, D. A., Knuuti, J., Leclercq, C., Linde, C., Mark, D. B., Monaghan, M. J., Nihoyannopoulos, P., Schalij, M. J., Stellbrink, C., and Yu, C.-M., "Cardiac resynchronization therapy: Part 2–issues during and after device implantation and unresolved questions.," *Journal of the American College of Cardiology*, vol. 46, no. 12, pp. 2168–82, 2005.

[86] Noyes, K., Veazie, P., Hall, W. J., Zhao, H., Buttaccio, A., Thevenet-Morrison, K., and Moss, A. J., "Cost-effectiveness of cardiac resynchronization therapy in the MADIT-CRT trial.," *Journal of Cardiovascular Electrophysiology*, vol. 24, pp. 66–74, Jan. 2013.

[87] Gorcsan, J., Yu, C.-M., and Sanderson, J. E., "Ventricular resynchronization is the principle mechanism of benefit with cardiac resynchronization therapy.," *Heart Failure Reviews*, pp. 5–8, July 2011.

[88] Soliman, O., Geleijnse, M., Theuns, D., van Dalen, B., Vletter, W., Jordaens, L., Metawei, A., Al-Amin, A., and ten Cate, F., "Usefulness of left ventricular systolic dyssynchrony by real-time three-dimensional echocardiography to predict long-term response to cardiac resynchronization therapy," *The American Journal of Cardiology*, vol. 103, pp. 1586–1591, June 2009.

[89] Yu, C.-M., "Tissue Doppler Echocardiographic Evidence of Reverse Remodeling and Improved Synchronicity by Simultaneously Delaying Regional Contraction After Biventricular Pacing Therapy in Heart Failure," *Circulation*, vol. 105, pp. 438–445, Jan. 2002.

[90] Bax, J. J., Marwick, T. H., Molhoek, S. G., Bleeker, G. B., van Erven, L., Boersma, E., Steendijk, P., van Der Wall, E. E., and Schalij, M. J., "Left ventricular dyssynchrony predicts benefit of cardiac resynchronization therapy in patients with end-stage heart failure before pacemaker implantation.," *The American Journal of Cardiology*, vol. 92, no. 10, pp. 1238–40, 2003.

[91] Breithardt, O. A., Stellbrink, C., Kramer, A. P., Sinha, A. M., Franke, A., Salo, R., Schiffgens, B., Huvelle, E., and Auricchio, A., "Echocardiographic quantification of left ventricular asynchrony predicts an acute hemodynamic benefit of cardiac resynchronization therapy.," *Journal of the American College of Cardiology*, vol. 40, no. 3, pp. 536–45, 2002.

[92] Yu, C.-M., Fung, J. W.-H., Zhang, Q., Chan, C.-K., Chan, Y.-S., Lin, H., Kum, L. C. C., Kong, S.-L., Zhang, Y., and Sanderson, J. E., "Tissue Doppler imaging is superior to strain rate imaging and postsystolic shortening on the prediction of reverse remodeling in both ischemic and nonischemic heart failure after cardiac resynchronization therapy.," *Circulation*, vol. 110, no. 1, pp. 66–73, 2004.

[93] Adelstein, E. C. and Saba, S., "Scar burden by myocardial perfusion imaging predicts echocardiographic response to cardiac resynchronization therapy in ischemic cardiomyopathy.," *American Heart Journal*, vol. 153, no. 1, pp. 105–12, 2007.

[94] Bleeker, G. B., Kaandorp, T. A. M., Lamb, H. J., Boersma, E., Steendijk, P., de Roos, A., van Der Wall, E. E., Schalij, M. J., and Bax, J. J., "Effect of posterolateral scar tissue on clinical and echocardiographic improvement after cardiac resynchronization therapy.," *Circulation*, vol. 113, no. 7, pp. 969–76, 2006.

[95] Bleeker, G. B., Schalij, M. J., Van Der Wall, E. E., and Bax, J. J., "Posterolateral scar tissue resulting in non-response to cardiac resynchronization therapy.," *Journal of Cardiovascular Electrophysiology*, vol. 17, no. 8, pp. 899–901, 2006.

[96] Duncan, A., Wait, D., Gibson, D., and Daubert, J.-C., "Left ventricular remodelling and haemodynamic effects of multisite biventricular pacing in patients with left ventricular systolic dysfunction and activation disturbances in sinus rhythm: substudy of the MUSTIC (Multisite Stimulationin Cardiomyopathies)," *European Heart Journal*, vol. 24, no. 5, pp. 430–41, 2003.

[97] Reuter, S., Garrigue, S., Barold, S. S., Jais, P., Hocini, M., Haissaguerre, M., and Clementy, J., "Comparison of characteristics in responders versus nonresponders with biventricular pacing for drug-resistant congestive heart failure.," *The American Journal of Cardiology*, vol. 89, no. 3, pp. 346–50, 2002.

[98] White, J. a., Yee, R., Yuan, X., Krahn, A., Skanes, A., Parker, M., Klein, G., and Drangova, M., "Delayed enhancement magnetic resonance imaging predicts response to cardiac resynchronization therapy in patients with intraventricular dyssynchrony.," *Journal of the American College of Cardiology*, vol. 48, no. 10, pp. 1953–60, 2006.

[99] Ypenburg, C., Roes, S. D., Bleeker, G. B., Kaandorp, T. A. M., de Roos, A., Schalij, M. J., van Der Wall, E. E., and Bax, J. J., "Effect of total scar burden on contrast-enhanced magnetic resonance imaging on response to cardiac resynchronization therapy.," *The American Journal of Cardiology*, vol. 99, no. 5, pp. 657–60, 2007.

[100] van Tuyn, J., Pijnappels, D. a., de Vries, A. a. F., de Vries, I., van der Velde-van Dijke, I., Knaän-Shanzer, S., van der Laarse, A., Schalij, M. J., and Atsma, D. E., "Fibroblasts from human postmyocardial infarction scars acquire

properties of cardiomyocytes after transduction with a recombinant myocardin gene.," *Journal of the Federation of American Societies for Experimental Biology*, vol. 21, pp. 3369–79, Oct. 2007.

[101] Butter, C., Auricchio, A., Stellbrink, C., Fleck, E., Ding, J., Yu, Y., Huvelle, E., and Spinelli, J., "Effect of Resynchronization Therapy Stimulation Site on the Systolic Function of Heart Failure Patients," *Circulation*, vol. 104, pp. 3026–3029, Dec. 2001.

[102] Demir, A. D., Alyan, O., and Kacmaz, F., "Successful coronary sinus lead placement after stenting of coronary vein stenosis.," *Europace*, vol. 9, pp. 514–5, July 2007.

[103] Hansky, B., Lamp, B., Minami, K., Heintze, J., Krater, L., Horstkotte, D., Koerfer, R., and Vogt, J., "Coronary vein balloon angioplasty for left ventricular pacemaker lead implantation.," *Journal of the American College of Cardiology*, vol. 40, pp. 2144–9, Dec. 2002.

[104] Morgan, J. M. and Delgado, V., "Lead positioning for cardiac resynchronization therapy: techniques and priorities.," *Europace*, vol. 11 Suppl 5, pp. v22–8, Nov. 2009.

[105] Scheffer, M. and Gelder, B. M. V., "Implantation Techniques of Leads for Left Ventricular Pacing in Cardiac Resynchronization Therapy and Electrocardiographic Consequences of the Stimulation Site," in *Advances in Electrocardiograms - Methods and Analysis*, pp. 53–80, InTech, 2012.

[106] Gassis, S. and León, A. R., "Cardiac resynchronization therapy: strategies for device programming, troubleshooting and follow-up.," *Journal of Interventional Cardiac Electrophysiology*, vol. 13, no. 3, pp. 209–22, 2005.

[107] Mullens, W., Grimm, R. A., Verga, T., Dresing, T., Starling, R. C., Wilkoff, B. L., and Tang, W. H. W., "Insights from a cardiac resynchronization optimization clinic as part of a heart failure disease management program.," *Journal of the American College of Cardiology*, vol. 53, pp. 765–73, Mar. 2009.

[108] Bax, J. J., Abraham, T., Barold, S. S., Breithardt, O. A., Fung, J. W. H., Garrigue, S., Gorcsan, J., Hayes, D. L., Kass, D. A., Knuuti, J., Leclercq, C., Linde, C., Mark, D. B., Monaghan, M. J., Nihoyannopoulos, P., Schalij, M. J., Stellbrink, C., and Yu, C.-M., "Cardiac resynchronization therapy: Part 1–issues before device implantation.," *Journal of the American College of Cardiology*, vol. 46, pp. 2153–67, Dec. 2005.

[109] Breithardt, O.-A. and Breithardt, G., "Quest for the best candidate: how much imaging do we need before prescribing cardiac resynchronization therapy?," *Circulation*, vol. 113, no. 7, pp. 926–8, 2006.

[110] Bistoquet, A., Oshinski, J., and Skrinjar, O., "Myocardial deformation recovery from cine MRI using a nearly incompressible biventricular model.," *Medical Image Analysis*, vol. 12, pp. 69–85, Feb. 2008.

[111] Mischi, M., v D Bosch, H. C. M., Jansen, A. H. M., Aarts, R. M., and Korsten, H. H. M., "Assessment of ventricular mechanical dyssynchrony by short-axis MRI.," *IEEE Engineering in Medicine and Biology Society*, vol. 2007, pp. 6012–5, 2007.

[112] Mischi, M., van Den Bosch, H. M., Jansen, A. M., Sieben, M., Aarts, R. M., and Korsten, H. M., "Quantification of regional left ventricular dyssynchrony by magnetic resonance imaging.," *IEEE Transactions on Biomedical Engineering*, vol. 55, no. 3, pp. 985–95, 2008.

[113] Ordas, S. and Frangi, A., "Automatic Quantitative Analysis of Myocardial Wall Motion and Thickening from Long-and Short-Axis Cine MRI Studies.," *IEEE Engineering in Medicine and Biology Society*, vol. 7, pp. 7028–31, 2005.

[114] Chalil, S., Stegemann, B., Muhyaldeen, S., Khadjooi, K., Smith, R. E. a., Jordan, P. J., and Leyva, F., "Intraventricular dyssynchrony predicts mortality and morbidity after cardiac resynchronization therapy: a study using cardiovascular magnetic resonance tissue synchronization imaging.," *Journal of the American College of Cardiology*, vol. 50, pp. 243–52, July 2007.

[115] Fornwalt, B. K., Gonzales, P. C., Delfino, J. G., Eisner, R., León, A. R., and Oshinski, J. N., "Quantification of left ventricular internal flow from cardiac magnetic resonance images in patients with dyssynchronous heart failure.," *Journal of Magnetic Resonance Imaging*, vol. 28, pp. 375–81, Aug. 2008.

[116] Axel, L. and Dougherty, L., "MR imaging of motion with spatial modulation of magnetization.," *Radiology*, vol. 171, no. 3, pp. 841–5, 1989.

[117] Osman, N. F., Kerwin, W. S., McVeigh, E. R., and Prince, J. L., "Cardiac motion tracking using CINE harmonic phase (HARP) magnetic resonance imaging.," *Magnetic Resonance in Medicine*, vol. 42, pp. 1048–60, Dec. 1999.

[118] Delfino, J. G., Bhasin, M., Cole, R., Eisner, R. L., Merlino, J., Leon, A. R., and Oshinski, J. N., "Comparison of myocardial velocities obtained with magnetic resonance phase velocity mapping and tissue Doppler imaging in normal subjects and patients with left ventricular dyssynchrony.," *Journal of Magnetic Resonance Imaging*, vol. 24, no. 2, pp. 304–11, 2006.

[119] Delfino, J. G., Fornwalt, B. K., Oshinski, J. N., and Lerakis, S., "Role of MRI in patient selection for CRT.," *Echocardiography*, vol. 25, pp. 1176–85, Nov. 2008.

[120] Aletras, A. H., Ding, S., Balaban, R. S., and Wen, H., "DENSE: displacement encoding with stimulated echoes in cardiac functional MRI.," *Journal of Magnetic Resonance*, vol. 137, pp. 247–52, Mar. 1999.

[121] Wesbey, G. E., Higgins, C. B., McNamara, M. T., Engelstad, B. L., Lipton, M. J., Sievers, R., Ehman, R. L., Lovin, J., and Brasch, R. C., "Effect of gadolinium-DTPA on the magnetic relaxation times of normal and infarcted myocardium.," *Radiology*, vol. 153, pp. 165–9, Oct. 1984.

[122] Arai, A. E., "The cardiac magnetic resonance (CMR) approach to assessing myocardial viability.," *Journal of Nuclear Cardiology*, vol. 18, pp. 1095–102, Dec. 2011.

[123] Simonetti, O. P., Kim, R. J., Fieno, D. S., Hillenbrand, H. B., Wu, E., Bundy, J. M., Finn, J. P., and Judd, R. M., "An improved MR imaging technique for the visualization of myocardial infarction.," *Radiology*, vol. 218, pp. 215–23, Jan. 2001.

[124] Bilchick, K. C., Dimaano, V., Wu, K. C., Helm, R. H., Weiss, R. G., Lima, J. A., Berger, R. D., Tomaselli, G. F., Bluemke, D. A., Halperin, H. R., Kass, D. A., Abraham, T., and Lardo, A. C., "Cardiac magnetic resonance assessment of dyssynchrony and myocardial scar predicts function class improvement following cardiac resynchronization therapy.," *Journal of the American College of Cardiology. Cardiovascular Imaging*, vol. 1, no. 5, pp. 561–8, 2008.

[125] Duckett, S. G., Chiribiri, A., Ginks, M. R., Sinclair, S., Knowles, B. R., Botnar, R., Carr-White, G. S., Rinaldi, C. a., Nagel, E., Razavi, R., and Schaeffter, T., "Cardiac MRI to investigate myocardial scar and coronary venous anatomy using a slow infusion of dimeglumine gadobenate in patients undergoing assessment for cardiac resynchronization therapy.," *Journal of Magnetic Resonance Imaging*, vol. 33, pp. 87–95, Jan. 2011.

[126] Chiribiri, A., Kelle, S., Götze, S., Kriatselis, C., Thouet, T., Tangcharoen, T., Paetsch, I., Schnackenburg, B., Fleck, E., and Nagel, E., "Visualization of the cardiac venous system using cardiac magnetic resonance.," *The American Journal of Cardiology*, vol. 101, pp. 407–12, Feb. 2008.

[127] Nezafat, R., Han, Y., Peters, D. C., Herzka, D. A., Wylie, J. V., Goddu, B., Kissinger, K. K., Yeon, S. B., Zimetbaum, P. J., and Manning, W. J., "Coronary magnetic resonance vein imaging: imaging contrast, sequence, and timing.," *Magnetic Resonance in Medicine*, vol. 58, pp. 1196–206, Dec. 2007.

[128] Rasche, V., Binner, L., Cavagna, F., Hombach, V., Kunze, M., Spiess, J., Stuber, M., and Merkle, N., "Whole-heart coronary vein imaging: a comparison between non-contrast-agent- and contrast-agent-enhanced visualization of the coronary venous system.," *Magnetic Resonance in Medicine*, vol. 57, pp. 1019–26, June 2007.

[129] Singh, J. P., Houser, S., Heist, E. K., and Ruskin, J. N., "The coronary venous anatomy: a segmental approach to aid cardiac resynchronization therapy.," *Journal of the American College of Cardiology*, vol. 46, pp. 68–74, July 2005.

[130] Stoeck, C. T., Han, Y., Peters, D. C., Hu, P., Yeon, S. B., Kissinger, K. V., Goddu, B., Goepfert, L., Manning, W. J., Kozerke, S., and Nezafat, R., "Whole heart magnetization-prepared steady-state free precession coronary vein MRI.," *Journal of Magnetic Resonance Imaging*, vol. 29, pp. 1293–9, June 2009.

[131] Goldfarb, J. W. and Edelman, R. R., "Coronary arteries: breath-hold, gadolinium-enhanced, three-dimensional MR angiography.," *Radiology*, vol. 206, pp. 830–4, Mar. 1998.

[132] Hofman, M. B., Henson, R. E., Kovács, S. J., Fischer, S. E., Lauffer, R. B., Adzamli, K., De Becker, J., Wickline, S. A., and Lorenz, C. H., "Blood pool agent strongly improves 3D magnetic resonance coronary angiography using an inversion pre-pulse.," *Magnetic Resonance in Medicine*, vol. 41, pp. 360–7, Feb. 1999.

[133] Huber, M. E., Paetsch, I., Schnackenburg, B., Bornstedt, A., Nagel, E., Fleck, E., Boesiger, P., Maggioni, F., Cavagna, F. M., and Stuber, M.,

"Performance of a new gadolinium-based intravascular contrast agent in free-breathing inversion-recovery 3D coronary MRA.," *Magnetic Resonance in Medicine*, vol. 49, pp. 115–21, Jan. 2003.

[134] Huber, M. E., Paetsch, I., Schnackenburg, B., Bornstedt, A., Nagel, E., Fleck, E., Boesiger, P., Maggioni, F., Cavagna, F. M., and Stuber, M., "Performance of a new gadolinium-based intravascular contrast agent in free-breathing inversion-recovery 3D coronary MRA.," *Magnetic Resonance in Medicine*, vol. 49, pp. 115–21, Jan. 2003.

[135] Lewis, M., Yanny, S., and Malcolm, P. N., "Advantages of blood pool contrast agents in MR angiography: a pictorial review.," *Journal of Medical Imaging and Radiation Oncology*, vol. 56, pp. 187–91, Apr. 2012.

[136] Bi, X., Carr, J. C., and Li, D., "Whole-heart coronary magnetic resonance angiography at 3 Tesla in 5 minutes with slow infusion of Gd-BOPTA, a high-relaxivity clinical contrast agent.," *Magnetic Resonance in Medicine*, vol. 58, pp. 1–7, July 2007.

[137] Liu, X., Bi, X., Huang, J., Jerecic, R., Carr, J., and Li, D., "Contrast-enhanced whole-heart coronary magnetic resonance angiography at 3.0 T: comparison with steady-state free precession technique at 1.5 T.," *Investigative Radiology*, vol. 43, pp. 663–8, Sept. 2008.

[138] Knopp, M. V., Schoenberg, S. O., Rehm, C., Floemer, F., von Tengg-Kobligk, H., Bock, M., and Hentrich, H. R., "Assessment of gadobenate dimeglumine for magnetic resonance angiography: phase I studies.," *Investigative Radiology*, vol. 37, pp. 706–15, Dec. 2002.

[139] Giroletti, E. and Corbucci, G., "Cardiac magnetic resonance imaging: patient safety considerations.," *Physica Medica*, vol. 21, no. 1, pp. 5–13, 2005.

[140] Roguin, A., Schwitter, J., Vahlhaus, C., Lombardi, M., Brugada, J., Vardas, P., Auricchio, A., Priori, S., and Sommer, T., "Magnetic resonance imaging in individuals with cardiovascular implantable electronic devices.," *Europace*, vol. 10, pp. 336–46, Mar. 2008.

[141] Roguin, A., Zviman, M. M., Meininger, G. R., Rodrigues, E. R., Dickfeld, T. M., Bluemke, D. A., Lardo, A., Berger, R. D., Calkins, H., and Halperin, H. R., "Modern pacemaker and implantable cardioverter/defibrillator systems can be magnetic resonance imaging safe: in vitro and in vivo assessment of safety and function at 1.5 T.," *Circulation*, vol. 110, pp. 475–82, Aug. 2004.

[142] Sommer, T., Vahlhaus, C., Lauck, G., von Smekal, A., Reinke, M., Hofer, U., Block, W., Träber, F., Schneider, C., Gieseke, J., Jung, W., and Schild, H., "MR imaging and cardiac pacemakers: in-vitro evaluation and in-vivo studies in 51 patients at 0.5 T.," *Radiology*, vol. 215, pp. 869–79, June 2000.

[143] Bushberg, J. T., Seibert, J. A., Leidholdt, E. M., and Boone, J. M., *The Essential Physics of Medical Imaging*. Lippincott Williams & Wilkins, 2 ed., 2001.

[144] Mortensen, P. T., Sogaard, P., Jensen, H. K., Kim, W. Y., Hansen, P. S., Egeblad, E., and Pedersen, A. K., "A left ventricular pacing site at three o'clock

or later in the left anterior oblique view: An easy way to predict responders to cardiac resynchronization with biventricular pacing. (abstract)," *Pacing and Clinical Electrophysiology*, vol. 24, no. Part 11, p. 552, 2001.

[145] Chen, L., Tiongson, J. E., Obrzut, S., McDaniel, M. B., Chang, H.-Y., Patel, J., Friedman, P. J., Feld, G. K., and Birgersdotter-Green, U. M., "Standard chest radiograph predicts left ventricular lead location in chronic resynchronization therapy patients more accurately than intraoperative fluoroscopy.," *Journal of Interventional Cardiac Electrophysiology*, July 2012.

[146] Kumar, P., Blendea, D., Nandigam, V., Moore, S. a., Heist, E. K., and Singh, J. P., "Assessment of the post-implant final left ventricular lead position: a comparative study between radiographic and angiographic modalities.," *Journal of Interventional Cardiac Electrophysiology*, vol. 29, pp. 17–22, Oct. 2010.

[147] Cerqueira, M. D., "Standardized Myocardial Segmentation and Nomenclature for Tomographic Imaging of the Heart: A Statement for Healthcare Professionals From the Cardiac Imaging Committee of the Council on Clinical Cardiology of the American Heart Association," *Circulation*, vol. 105, pp. 539–542, Jan. 2002.

[148] Birnie, D. H. and Tang, A. S., "The problem of non-response to cardiac resynchronization therapy.," *Current Opinion in Cardiology*, vol. 21, pp. 20–6, Jan. 2006.

[149] Tang, A. S. L. and Ellenbogen, K. a., "A futuristic perspective on clinical studies of cardiac resynchronization therapy for heart failure patients.," *Current Opinion in Cardiology*, vol. 21, pp. 78–82, Mar. 2006.

[150] Gorcsan, J., Tanabe, M., Bleeker, G. B., Suffoletto, M. S., Thomas, N. C., Saba, S., Tops, L. F., Schalij, M. J., and Bax, J. J., "Combined longitudinal and radial dyssynchrony predicts ventricular response after resynchronization therapy.," *Journal of the American College of Cardiology*, vol. 50, pp. 1476–83, Oct. 2007.

[151] Kapetanakis, S., Kearney, M. T., Siva, a., Gall, N., Cooklin, M., and Monaghan, M. J., "Real-time three-dimensional echocardiography: a novel technique to quantify global left ventricular mechanical dyssynchrony.," *Circulation*, vol. 112, pp. 992–1000, Aug. 2005.

[152] Chung, E. S., Leon, A. R., Tavazzi, L., Sun, J.-P., Nihoyannopoulos, P., Merlino, J., Abraham, W. T., Ghio, S., Leclercq, C., Bax, J. J., Yu, C.-M., Gorcsan, J., St John Sutton, M., De Sutter, J., and Murillo, J., "Results of the Predictors of Response to CRT (PROSPECT) trial.," *Circulation*, vol. 117, pp. 2608–16, May 2008.

[153] Bogaard, M. D., Doevendans, P. a., Leenders, G. E., Loh, P., Hauer, R. N. W., van Wessel, H., and Meine, M., "Can optimization of pacing settings compensate for a non-optimal left ventricular pacing site?," *Europace*, vol. 12, pp. 1262–9, Sept. 2010.

[154] Zerhouni, E. A., Parish, D. M., Rogers, W. J., Yang, A., and Shapiro, E. P., "Human heart: tagging with MR imaging–a method for noninvasive assessment of myocardial motion.," *Radiology*, vol. 169, pp. 59–63, Oct. 1988.

[155] Xu, C., Pilla, J. J., Isaac, G., Gorman, J. H., Blom, A. S., Gorman, R. C., Ling, Z., and Dougherty, L., "Deformation analysis of 3D tagged cardiac images using an optical flow method.," *Journal of Cardiovascular Magnetic Resonance*, vol. 12, p. 19, Jan. 2010.

[156] Epstein, F. H., "MRI of left ventricular function.," *Journal of Nuclear Cardiology*, vol. 14, no. 5, pp. 729–44, 2007.

[157] Gilson, W. D., Yang, Z., French, B. a., and Epstein, F. H., "Measurement of myocardial mechanics in mice before and after infarction using multislice displacement-encoded MRI with 3D motion encoding.," *American Journal of Physiology. Heart and Circulatory Physiology*, vol. 288, pp. H1491–7, Mar. 2005.

[158] Pan, L., Stuber, M., Kraitchman, D. L., Fritzges, D. L., Gilson, W. D., and Osman, N. F., "Real-time imaging of regional myocardial function using fast-SENC.," *Magnetic Resonance in Medicine*, vol. 55, pp. 386–95, Feb. 2006.

[159] Rüssel, I. K., Zwanenburg, J. J. M., Germans, T., Marcus, J. T., Allaart, C. P., de Cock, C. C., Götte, M. J. W., and van Rossum, A. C., "Mechanical dyssynchrony or myocardial shortening as MRI predictor of response to biventricular pacing?," *Journal of Magnetic Resonance Imaging*, vol. 26, pp. 1452–60, Dec. 2007.

[160] Boyer, K., Gotardo, P., Saltz, J., and Raman, S., "On the Detection of Intra-Ventricular Dyssynchrony in the Left Ventricle from Routine Cardiac MRI," in *3rd IEEE International Symposium on Biomedical Imaging: Macro to Nano, 2006.*, pp. 169–172, IEEE, 2006.

[161] Uzümcü, M., van der Geest, R. J., Swingen, C., Reiber, J. H. C., and Lelieveldt, B. P. F., "Time continuous tracking and segmentation of cardiovascular magnetic resonance images using multidimensional dynamic programming.," *Investigative Radiology*, vol. 41, pp. 52–62, Jan. 2006.

[162] van der Geest, R. J., Lelieveldt, B. P. F., Angelié, E., Danilouchkine, M., Swingen, C., Sonka, M., and Reiber, J. H. C., "Evaluation of a new method for automated detection of left ventricular boundaries in time series of magnetic resonance images using an Active Appearance Motion Model.," *Journal of Cardiovascular Magnetic Resonance*, vol. 6, pp. 609–17, Jan. 2004.

[163] Azhari, H., Sideman, S., Weiss, J. L., Shapiro, E. P., Weisfeldt, M. L., Graves, W. L., Rogers, W. J., and Beyar, R., "Three-dimensional mapping of acute ischemic regions using MRI: wall thickening versus motion analysis.," *The American Journal of Physiology*, vol. 259, pp. H1492–503, Nov. 1990.

[164] Pearlman, J. D., Hogan, R. D., Wiske, P. S., Franklin, T. D., and Weyman, A. E., "Echocardiographic definition of the left ventricular centroid. I. Analysis of methods for centroid calculation from a single tomogram," *Journal of the American College of Cardiology*, vol. 16, pp. 986–992, Oct. 1990.

[165] Heyer, L. J., "Exploring Expression Data: Identification and Analysis of Coexpressed Genes," *Genome Research*, vol. 9, pp. 1106–1115, Nov. 1999.

[166] Oppenheim, A. V., Schafer, R. W., and Buck, J. R., *Discrete-Time Signal Processing*. Prentice Hall, 2nd ed., 1999.

[167] Bland, J. M. and Altman, D., "Statistical methods for assessing agreement between two methods of clinical measurement," *The Lancet*, vol. 47, pp. 931–6, Aug. 1986.

[168] Hulley, S. B., Cummings, S. R., Browner, W. S., Grady, D., Hearst, N., and Newman, T. B., *Designing Clinical Research*. Philadelphia: Lippincott Williams & Wilkins, 2 ed., 2001.

[169] Tanaka, H., Hara, H., Saba, S., and III, J. G., "Usefulness of three-dimensional speckle tracking strain to quantify dyssynchrony and the site of latest mechanical activation," *The American Journal of Cardiology*, vol. 105, pp. 235–42, Jan. 2009.

[170] Ansalone, G., Giannantoni, P., Ricci, R., Trambaiolo, P., Fedele, F., and Santini, M., "Doppler myocardial imaging to evaluate the effectiveness of pacing sites in patients receiving biventricular pacing.," *Journal of the American College of Cardiology*, vol. 39, pp. 489–99, Feb. 2002.

[171] van Bommel, R. J., Ypenburg, C., Mollema, S. a., Borleffs, C. J. W., Delgado, V., Bertini, M., Marsan, N. A., van der Wall, E. E., Schalij, M. J., and Bax, J. J., "Site of latest activation in patients eligible for cardiac resynchronization therapy: Patterns of dyssynchrony among different QRS configurations and impact of heart failure etiology.," *American Heart Journal*, vol. 161, pp. 1060–6, June 2011.

[172] Duckett, S. G., Camara, O., Ginks, M. R., Bostock, J., Chinchapatnam, P., Sermesant, M., Pashaei, A., Lambiase, P. D., Gill, J. S., Carr-White, G. S., Frangi, A. F., Razavi, R., Bijnens, B. H., and Rinaldi, C. A., "Relationship between endocardial activation sequences defined by high-density mapping to early septal contraction (septal flash) in patients with left bundle branch block undergoing cardiac resynchronization therapy.," *Europace*, vol. 14, pp. 99–106, Jan. 2012.

[173] Khan, F. Z., Virdee, M. S., Palmer, C. R., Pugh, P. J., O'Halloran, D., Elsik, M., Read, P. a., Begley, D., Fynn, S. P., and Dutka, D. P., "Targeted left ventricular lead placement to guide cardiac resynchronization therapy: the TARGET study: a randomized, controlled trial.," *Journal of the American College of Cardiology*, vol. 59, pp. 1509–18, Apr. 2012.

[174] Duan, Q., Angelini, E., Homma, S., and Laine, A., "Tracking endocardium using optical flow along iso-value curve.," *IEEE Engineering in Medicine and Biology*, vol. 1, pp. 707–10, Jan. 2006.

[175] Li, Y., Garson, C. D., Xu, Y., French, B. a., and Hossack, J. a., "High frequency ultrasound imaging detects cardiac dyssynchrony in noninfarcted regions of the murine left ventricle late after reperfused myocardial infarction.," *Ultrasound in Medicine & Biology*, vol. 34, pp. 1063–75, July 2008.

[176] Ortega, M., Triedman, J. K., Geva, T., and Harrild, D. M., "Relation of left ventricular dyssynchrony measured by cardiac magnetic resonance tissue tracking

in repaired tetralogy of fallot to ventricular tachycardia and death.," *The American Journal of Cardiology*, vol. 107, pp. 1535–40, May 2011.

[177] Gerber, T. C., Schmermund, a., Reed, J. E., Rumberger, J. a., Sheedy, P. F., Gibbons, R. J., Holmes, D. R., and Behrenbeck, T., "Use of a new myocardial centroid for measurement of regional myocardial dysfunction by electron beam computed tomography: comparison with technetium-99m sestamibi infarct size quantification.," *Investigative Radiology*, vol. 36, pp. 193–203, Apr. 2001.

[178] Skulstad, H., "Postsystolic Shortening in Ischemic Myocardium: Active Contraction or Passive Recoil?," *Circulation*, vol. 106, pp. 718–724, July 2002.

[179] Termeer, M., Bescós, J., Breeuwer, M., Vilanova, A., Gerritsen, F., and Gröller, E., "1104 The volumetric bull's eye plot," *Journal of Cardiovascular Magnetic Resonance*, vol. 10, no. Suppl 1, p. A229, 2008.

[180] Helm, R. H., Leclercq, C., Faris, O. P., Ozturk, C., McVeigh, E., Lardo, A. C., and Kass, D. a., "Cardiac dyssynchrony analysis using circumferential versus longitudinal strain: implications for assessing cardiac resynchronization.," *Circulation*, vol. 111, pp. 2760–7, May 2005.

[181] Sade, L. E., Demir, O., Atar, I., Müderrisoglu, H., and Ozin, B., "Effect of mechanical dyssynchrony and cardiac resynchronization therapy on left ventricular rotational mechanics.," *The American Journal of Cardiology*, vol. 101, pp. 1163–9, Apr. 2008.

[182] Derval, N., Steendijk, P., Gula, L. J., Deplagne, A., Laborderie, J., Sacher, F., Knecht, S., Wright, M., Nault, I., Ploux, S., Ritter, P., Bordachar, P., Lafitte, S., Réant, P., Klein, G. J., Narayan, S. M., Garrigue, S., Hocini, M., Haissaguerre, M., Clementy, J., and Jaïs, P., "Optimizing hemodynamics in heart failure patients by systematic screening of left ventricular pacing sites: the lateral left ventricular wall and the coronary sinus are rarely the best sites.," *Journal of the American College of Cardiology*, vol. 55, pp. 566–75, Feb. 2010.

[183] Tse, H.-F., Lee, K. L., Wan, S.-H., Yu, Y., Hoersch, W., Pastore, J., Zhu, Q., Kenknight, B., Spinelli, J., and Lau, C.-P., "Area of left ventricular regional conduction delay and preserved myocardium predict responses to cardiac resynchronization therapy.," *Journal of Cardiovascular Electrophysiology*, vol. 16, pp. 690–5, July 2005.

[184] Vo Thang, T.-T., Thibault, B., Finnerty, V., Pelletier-Galarneau, M., Khairy, P., Grégoire, J., and Harel, F., "Canine left ventricle electromechanical behavior under different pacing modes.," *Journal of Interventional Cardiac Electrophysiology*, vol. 35, pp. 11–7, Oct. 2012.

[185] Russell, K., Smiseth, O. a., Gjesdal, O., Qvigstad, E., Norseng, P. A., Sjaastad, I., Opdahl, A., Skulstad, H., Edvardsen, T., and Remme, E. W., "Mechanism of Prolonged Electro-Mechanical Delay in Late Activated Myocardium during Left Bundle Branch Block.," *American Journal of Physiology. Heart and Circulatory Physiology*, Oct. 2011.

[186] Dou, J., Xia, L., Deng, D., Zang, Y., Shou, G., Bustos, C., Tu, W., Liu, F., and Crozier, S., "A study of mechanical optimization strategy for cardiac resynchronization therapy based on an electromechanical model.," *Computational and Mathematical Methods in Medicine*, vol. 2012, p. 948781, Jan. 2012.

[187] Klemm, H. U., Krause, K. T., Ventura, R., Schneider, C., Aydin, M. a., Johnsen, C., Boczor, S., Meinertz, T., Morillo, C. a., and Kuck, K.-H., "Slow wall motion rather than electrical conduction delay underlies mechanical dyssynchrony in postinfarction patients with narrow QRS complex.," *Journal of Cardiovascular Electrophysiology*, vol. 21, pp. 70–7, Jan. 2010.

[188] Hampton, J. R., *The ECG In Practice*. Churchill Livingstone, 5th ed., 2008.

[189] Suever, J., Fornwalt, B. K., Lloyd, M., and Oshinski, J. N., "A method to determine regional mechanical left ventricular dyssynchrony based on high temporal resolution short axis SSFP cine images," *Journal of Cardiovascular Magnetic Resonance*, vol. 14, no. Suppl 1, p. W18, 2012.

[190] Gurev, V., Constantino, J., Rice, J. J., and Trayanova, N. a., "Distribution of electromechanical delay in the heart: insights from a three-dimensional electromechanical model.," *Biophysical Journal*, vol. 99, pp. 745–54, Aug. 2010.

[191] Usyk, T. P. and McCULLOCH, A. D., "Relationship Between Regional Shortening and Asynchronous Electrical Activation in a Three-Dimensional Model of Ventricular Electromechanics," *Journal of Cardiovascular Electrophysiology*, vol. 14, pp. S196–S202, Oct. 2003.

[192] Bleeker, G. B., Bax, J. J., Fung, J. W.-H., van Der Wall, E. E., Zhang, Q., Schalij, M. J., Chan, J. Y.-S., and Yu, C.-M., "Clinical versus echocardiographic parameters to assess response to cardiac resynchronization therapy.," *The American Journal of Cardiology*, vol. 97, pp. 260–3, Jan. 2006.

[193] Bleeker, G. B., Kaandorp, T. a. M., Lamb, H. J., Boersma, E., Steendijk, P., de Roos, A., van der Wall, E. E., Schalij, M. J., and Bax, J. J., "Effect of posterolateral scar tissue on clinical and echocardiographic improvement after cardiac resynchronization therapy.," *Circulation*, vol. 113, no. 7, pp. 969–76, 2006.

[194] Lu, B., Mao, S. S., Zhuang, N., Bakhsheshi, H., Yamamoto, H., Takasu, J., Liu, S. C., and Budoff, M. J., "Coronary artery motion during the cardiac cycle and optimal ECG triggering for coronary artery imaging.," *Investigative Radiology*, vol. 36, pp. 250–6, May 2001.

[195] Li, D., Paschal, C. B., Haacke, E. M., and Adler, L. P., "Coronary arteries: three-dimensional MR imaging with fat saturation and magnetization transfer contrast.," *Radiology*, vol. 187, pp. 401–6, May 1993.

[196] Wolff, S. D. and Balaban, R. S., "Magnetization transfer contrast (MTC) and tissue water proton relaxation in vivo.," *Magnetic Resonance in Medicine*, vol. 10, pp. 135–44, Apr. 1989.

[197] Bhat, H., Lai, P., and Li, D., "Self-tracking of contrast kinetics for automatic triggering of contrast-enhanced whole-heart coronary magnetic resonance angiography.," *Journal of Magnetic Resonance Imaging*, vol. 29, pp. 809–16, Apr. 2009.

[198] Plein, S., Jones, T. R., Ridgway, J. P., and Sivananthan, M. U., "Three-dimensional coronary MR angiography performed with subject-specific cardiac acquisition windows and motion-adapted respiratory gating.," *American Journal of Roentgenology*, vol. 180, pp. 505–12, Feb. 2003.

[199] Wang, Y., Vidan, E., and Bergman, G. W., "Cardiac motion of coronary arteries: variability in the rest period and implications for coronary MR angiography.," *Radiology*, vol. 213, pp. 751–8, Dec. 1999.

[200] Jongbloed, M. R. M., Lamb, H. J., Bax, J. J., Schuijf, J. D., de Roos, A., van Der Wall, E. E., and Schalij, M. J., "Noninvasive visualization of the cardiac venous system using multislice computed tomography.," *Journal of the American College of Cardiology*, vol. 45, pp. 749–53, Mar. 2005.

[201] Ehman, R. L. and Felmlee, J. P., "Adaptive technique for high-definition MR imaging of moving structures.," *Radiology*, vol. 173, pp. 255–63, Oct. 1989.

[202] McConnell, M. V., Khasgiwala, V. C., Savord, B. J., Chen, M. H., Chuang, M. L., Edelman, R. R., and Manning, W. J., "Comparison of respiratory suppression methods and navigator locations for MR coronary angiography.," *American Journal of Roentgenology*, vol. 168, pp. 1369–75, May 1997.

[203] Edelsbrunner, H. and Mücke, E. P., "Three-dimensional alpha shapes," *ACM Transactions on Graphics*, vol. 13, pp. 43–72, Jan. 1994.

[204] Desbrun, M., Meyer, M., Schröder, P., and Barr, A., "Implicit fairing of irregular meshes using diffusion and curvature flow," *Proceedings of the 26th annual conference on Computer graphics and interactive techniques*, 1999.

[205] Loukas, M., Bilinsky, S., Bilinsky, E., El-Sedfy, A., and Anderson, R. H., "Cardiac veins: a review of the literature.," *Clinical Anatomy*, vol. 22, pp. 129–45, Jan. 2009.

[206] Isaacs, D., Hazany, S., Gamst, A., Stark, P., and Mahmud, E., "Evaluation of the coronary sinus on chest computed tomography in patients with and without pulmonary artery hypertension.," *Journal of Computer Assisted Tomography*, vol. 33, no. 4, pp. 513–6, 2009.

[207] Schwitter, J., DeMarco, T., Kneifel, S., von Schulthess, G. K., Jörg, M. C., Arheden, H., Rühm, S., Stumpe, K., Buck, A., Parmley, W. W., Lüscher, T. F., and Higgins, C. B., "Magnetic resonance-based assessment of global coronary flow and flow reserve and its relation to left ventricular functional parameters: a comparison with positron emission tomography.," *Circulation*, vol. 101, pp. 2696–702, June 2000.

[208] Cazals, F., Giesen, J., Pauly, M., and Zomorodian, a., "Conformal alpha shapes," *Proceedings Eurographics/IEEE VGTC Symposium Point-Based Graphics, 2005.*, pp. 55–61, 2005.

[209] Abraham, W. T., Fisher, W. G., Smith, A. L., Delurgio, D. B., Leon, A. R., Loh, E., Kocovic, D. Z., Packer, M., Clavell, A. L., Hayes, D. L., Ellestad, M., Trupp, R. J., Underwood, J., Pickering, F., Truex, C., McAtee, P.,

and Messenger, J., "Cardiac resynchronization in chronic heart failure.," *The New England Journal of Medicine*, vol. 346, pp. 1845–53, June 2002.

[210] Linde, C., Leclercq, C., Rex, S., Garrigue, S., Lavergne, T., Cazeau, S., McKenna, W., Fitzgerald, M., Deharo, J.-C., Alonso, C., Walker, S., Braunschweig, F., Bailleul, C., and Daubert, J.-C., "Long-term benefits of biventricular pacing in congestive heart failure: results from the MUltisite STimulation in cardiomyopathy (MUSTIC) study.," *Journal of the American College of Cardiology*, vol. 40, pp. 111–8, July 2002.

[211] St John Sutton, M. G., Plappert, T., Abraham, W. T., Smith, A. L., DeLurgio, D. B., Leon, A. R., Loh, E., Kocovic, D. Z., Fisher, W. G., Ellestad, M., Messenger, J., Kruger, K., Hilpisch, K. E., and Hill, M. R. S., "Effect of cardiac resynchronization therapy on left ventricular size and function in chronic heart failure.," *Circulation*, vol. 107, no. 15, pp. 1985–90, 2003.

[212] Wong, J. a., Yee, R., Stirrat, J., Scholl, D., Krahn, a. D., Gula, L. J., Skanes, a. C., Leong-Sit, P., Klein, G. J., McCarty, D., Fine, N., Goela, a., Islam, a., Thompson, T., Drangova, M., and White, J. a., "Influence of Pacing Site Characteristics on Response to Cardiac Resynchronization Therapy," *Circulation: Cardiovascular Imaging*, June 2013.

[213] Suffoletto, M. S., Dohi, K., Cannesson, M., Saba, S., and Gorcsan, J., "Novel speckle-tracking radial strain from routine black-and-white echocardiographic images to quantify dyssynchrony and predict response to cardiac resynchronization therapy.," *Circulation*, vol. 113, pp. 960–8, Feb. 2006.

[214] Chen, L., Tiongson, J. E., Obrzut, S., McDaniel, M. B., Chang, H.-Y., Patel, J., Friedman, P. J., Feld, G. K., and Birgersdotter-Green, U. M., "Standard chest radiograph predicts left ventricular lead location in chronic resynchronization therapy patients more accurately than intraoperative fluoroscopy.," *Journal of Interventional Cardiac Electrophysiology*, vol. 35, pp. 323–30, Dec. 2012.

[215] Sasaki, T., Hansford, R., Zviman, M. M., Kolandaivelu, A., Bluemke, D. a., Berger, R. D., Calkins, H., Halperin, H. R., and Nazarian, S., "Quantitative assessment of artifacts on cardiac magnetic resonance imaging of patients with pacemakers and implantable cardioverter-defibrillators.," *Circulation. Cardiovascular imaging*, vol. 4, pp. 662–70, Nov. 2011.

[216] Huizar, J. F., Kaszala, K., Koneru, J. N., Thacker, L. R., and Ellenbogen, K. a., "Comparison of Different Pacing Strategies to Minimize Phrenic Nerve Stimulation in Cardiac Resynchronization Therapy.," *Journal of Cardiovascular Electrophysiology*, pp. 1–7, Apr. 2013.

[217] Noheria, A., Desimone, C. V., Lachman, N., Edwards, W. D., Gami, A. S., Maleszewski, J. J., Friedman, P. a., Munger, T. M., Hammill, S. C., Hayes, D. L., Packer, D. L., and Asirvatham, S. J., "Anatomy of the coronary sinus and epicardial coronary venous system in 620 hearts: an electrophysiology perspective.," *Journal of Cardiovascular Electrophysiology*, vol. 24, pp. 1–6, Jan. 2013.

[218] Frangi, A., Niessen, W., Vincken, K., and Viergever, M., "Multiscale vessel enhancement filtering," *Lecture Notes in Computer Science*, vol. 1496, pp. 130–137, 1998.

[219] Fitzpatrick, J. M. and Sonka, M., eds., *Handbook of Medical Imaging, Volume 2: Medical Image Processing and Analysis*. SPIE Publications, 2009.

[220] Knackstedt, C., Mühlenbruch, G., Mischke, K., Schummers, G., Becker, M., Kühl, H., Franke, A., Schmid, M., Spuentrup, E., Mahnken, A., Lang, R. M., Kelm, M., Günther, R. W., and Schauerte, P., "Registration of coronary venous anatomy to the site of the latest mechanical contraction.," *Acta Cardiologica*, vol. 65, pp. 161–70, Apr. 2010.

[221] Chen, L., Tiongson, J. E., Obrzut, S., McDaniel, M. B., Chang, H.-Y., Patel, J., Friedman, P. J., Feld, G. K., and Birgersdotter-Green, U. M., "Standard chest radiograph predicts left ventricular lead location in chronic resynchronization therapy patients more accurately than intraoperative fluoroscopy.," *Journal of Interventional Cardiac Electrophysiology*, July 2012.

[222] Truong, Q. A., Hoffmann, U., and Singh, J. P., "Potential uses of computed tomography for management of heart failure patients with dyssynchrony.," *Critical Pathways in Cardiology*, vol. 7, pp. 185–90, Sept. 2008.

[223] Cubuk, R., Aydin, A., Tasali, N., Yilmazer, S., Celik, L., Dagdeviren, B., and Guney, S., "Non-invasive evaluation of the coronary venous system in patients with chronic systolic heart failure by 64-detector computed tomography.," *Acta Radiologica*, vol. 52, pp. 372–7, May 2011.

[224] Doganay, S., Karaman, A., Gündogdu, F., Duran, C., Yalcin, A., and Kantarci, M., "Usefulness of multidetector computed tomography coronary venous angiography examination before cardiac resynchronization therapy.," *Japanese Journal of Radiology*, vol. 29, pp. 342–7, June 2011.

[225] Van de Veire, N. R., Schuijf, J. D., De Sutter, J., Devos, D., Bleeker, G. B., de Roos, A., van der Wall, E. E., Schalij, M. J., and Bax, J. J., "Non-invasive visualization of the cardiac venous system in coronary artery disease patients using 64-slice computed tomography.," *Journal of the American College of Cardiology*, vol. 48, pp. 1832–8, Nov. 2006.

[226] Heiberg, E., Sjögren, J., Ugander, M., Carlsson, M., Engblom, H., and Arheden, H. k., "Design and validation of Segment–freely available software for cardiovascular image analysis.," *BMC Medical Imaging*, vol. 10, p. 1, Jan. 2010.

[227] Zhou, H., Yuan, Y., Lin, F., and Liu, T., "Level set image segmentation with Bayesian analysis," *Neurocomputing*, vol. 71, pp. 1994–2000, June 2008.

[228] Kydd, A. C., McCormick, L. M., and Dutka, D. P., "Optimizing benefit from CRT: role of speckle tracking echocardiography, the importance of LV lead position and scar.," *Expert Review of Medical Devices*, vol. 9, pp. 521–36, Sept. 2012.

[229] Notabartolo, D., Merlino, J. D., Smith, A. L., DeLurgio, D. B., Vera, F. V., Easley, K. A., Martin, R. P., and León, A. R., "Usefulness of the peak

velocity difference by tissue Doppler imaging technique as an effective predictor of response to cardiac resynchronization therapy.," *The American Journal of Cardiology*, vol. 94, no. 6, pp. 817–20, 2004.

[230] Yu, C.-M., Fung, J. W.-H., Chan, C.-K., Chan, Y.-S., Zhang, Q., Lin, H., Yip, G. W. K., Kum, L. C. C., Kong, S.-L., Zhang, Y., and Sanderson, J. E., "Comparison of efficacy of reverse remodeling and clinical improvement for relatively narrow and wide QRS complexes after cardiac resynchronization therapy for heart failure.," *Journal of Cardiovascular Electrophysiology*, vol. 15, pp. 1058–65, Sept. 2004.

[231] Auger, D., Ducharme, a., Harel, F., Thibault, B., and O'Meara, E., "Patient assessment for cardiac resynchronization therapy: Past, present and future of imaging techniques.," *The Canadian Journal of Cardiology*, vol. 26, pp. 27–34, Jan. 2010.

[232] Macías, A., Gavira, J.-J., Castaño, S., Alegría, E., and García-Bolao, I., "Left ventricular pacing site in cardiac resynchronization therapy: clinical follow-up and predictors of failed lateral implant.," *European Journal of Heart Failure*, vol. 10, pp. 421–7, Apr. 2008.

[233] Fung, J. W. H., Lam, Y.-Y., Zhang, Q., Yip, G. W. K., Chan, W. W. L., Chan, G. C. P., Chan, J. Y. S., and Yu, C.-M., "Effect of left ventricular lead concordance to the delayed contraction segment on echocardiographic and clinical outcomes after cardiac resynchronization therapy.," *Journal of Cardiovascular Electrophysiology*, vol. 20, pp. 530–5, May 2009.

[234] Deplagne, A., Lafitte, S., Reuter, S., Reant, P., Ploux, S., Mokrani, B., Roudaut, R., Jais, P., Haissaguerre, M., Clementy, J., DosSantos, P., and Bordachar, P., "Absence of additional improvement in outcome of patients receiving cardiac resynchronization therapy paced at the most delayed left ventricular region.," *Archives of Cardiovascular Diseases*, vol. 102, no. 8-9, pp. 641–9, 2009.

[235] Molhoek, S. G., Bax, J. J., Bleeker, G. B., Boersma, E., van Erven, L., Steendijk, P., van der Wall, E. E., and Schalij, M. J., "Comparison of response to cardiac resynchronization therapy in patients with sinus rhythm versus chronic atrial fibrillation.," *The American Journal of Cardiology*, vol. 94, pp. 1506–9, Dec. 2004.

[236] Molhoek, S. G., Bax, J. J., van Erven, L., Bootsma, M., Boersma, E., Steendijk, P., van der Wall, E. E., and Schalij, M. J., "Comparison of benefits from cardiac resynchronization therapy in patients with ischemic cardiomyopathy versus idiopathic dilated cardiomyopathy.," *The American Journal of Cardiology*, vol. 93, pp. 860–3, Apr. 2004.

[237] Molhoek, S. G., VAN Erven, L., Bootsma, M., Steendijk, P., Van Der Wall, E. E., and Schalij, M. J., "QRS duration and shortening to predict clinical response to cardiac resynchronization therapy in patients with end-stage heart failure.," *Pacing and Clinical Electrophysiology*, vol. 27, pp. 308–13, Mar. 2004.

[238] Duchateau, N., De Craene, M., Piella, G., Silva, E., Doltra, A., Sitges, M., Bijnens, B. H., and Frangi, A. F., "A spatiotemporal statistical atlas of

motion for the quantification of abnormal myocardial tissue velocities.," *Medical Image Analysis*, vol. 15, pp. 316–28, June 2011.

[239] Kashani, A. and Barold, S. S., "Significance of QRS complex duration in patients with heart failure.," *Journal of the American College of Cardiology*, vol. 46, pp. 2183–92, Dec. 2005.

[240] Aranda, J. M., Conti, J. B., Johnson, J. W., Petersen-Stejskal, S., and Curtis, A. B., "Cardiac resynchronization therapy in patients with heart failure and conduction abnormalities other than left bundle-branch block: analysis of the Multicenter InSync Randomized Clinical Evaluation (MIRACLE).," *Clinical Cardiology*, vol. 27, pp. 678–82, Dec. 2004.

[241] Rickard, J., Kumbhani, D. J., Gorodeski, E. Z., Baranowski, B., Wazni, O., Martin, D. O., Grimm, R., and Wilkoff, B. L., "Cardiac resynchronization therapy in non-left bundle branch block morphologies.," *Pacing and Clinical Electrophysiology*, vol. 33, pp. 590–5, May 2010.

[242] Merchant, F. M., Heist, E. K., McCarty, D., Kumar, P., Das, S., Blendea, D., Ellinor, P. T., Mela, T., Picard, M. H., Ruskin, J. N., and Singh, J. P., "Impact of segmental left ventricle lead position on cardiac resynchronization therapy outcomes.," *Heart Rhythm*, vol. 7, pp. 639–44, May 2010.

[243] Mele, D., Toselli, T., Capasso, F., Stabile, G., Piacenti, M., Piepoli, M., Giatti, S., Klersy, C., Sallusti, L., and Ferrari, R., "Comparison of myocardial deformation and velocity dyssynchrony for identification of responders to cardiac resynchronization therapy.," *European Journal of Heart Failure*, vol. 11, pp. 391–9, Apr. 2009.

[244] Prutkin, J., Chen, M., and Rho, R., "Echocardiographic Assessment of Dyssynchrony for Predicting a Favorable Response to Cardiac Resynchronization Therapy," *The New England Journal of Medicine*, pp. 57–59, 2005.

[245] Budge, L. P., Helms, A. S., Salerno, M., Kramer, C. M., Epstein, F. H., and Bilchick, K. C., "MR cine DENSE dyssynchrony parameters for the evaluation of heart failure: comparison with myocardial tissue tagging.," *Journal of the American College of Cardiology. Cardiovascular Imaging*, vol. 5, pp. 789–97, Aug. 2012.

[246] Task, A., Members, F., Mcmurray, J. J. V., Uk, C., Germany, S. D. A., Auricchio, A., Bo, M., Denmark, L. K. b., Uk, G. Y. H. L., Pietro, A., Popescu, B. A., and Rutten, F. H., "ESC GUIDELINES ESC Guidelines for the diagnosis and treatment of acute and chronic heart failure 2012 The Task Force for the Diagnosis and Treatment of Acute and Chronic Heart Failure 2012 of the European Society of Cardiology . Developed in collaboration," pp. 1787–1847, 2012.

[247] *Digital Imaging and Communications In Medicine (DICOM).* National Electrical Manufacturers Association, 2011.

[248] Sato, Y., Nakajima, S., Atsumi, H., and Koller, T., "3D Multi-scale line filter for segmentation and visualization of curvilinear structures in medical images," *Medical Image Analysis*, vol. 2, no. 2, pp. 143–168, 1998.

[249] Troccaz, J., Grimson, E., and Mosges, R., eds., *Multi-scale line segmentation with automatic estimation of width, contrast and tangential direction in 2D and 3D medical images*, CVRMed-MRCAS, 1997.

[250] de Berg, M., Cheong, O., van Kreveld, M., and Overmars, M., *Computational Geometry: Algorithms and Applications*. Springer-Verlag, 2008.